NUREG/CR-5023
WHC-EP-0081
RM

HIGH-LEVEL SEISMIC RESPONSE AND FAILURE PREDICTION METHODS FOR PIPING

NUREG/CR--5023

TI88 005178

L.K. Severud
M.J. Anderson
M.R. Lindquist
S.E. Wagner
E.O. Weiner

Manuscript Completed: September 1987
Date Published: January 1988

Westinghouse Hanford Company
P.O. Box 1970 Richland, WA 99352
A Subsidiary of Westinghouse Electric Corporation

Prepared for Division of Engineering
Office of Nuclear Regulatory Research
U.S. Nuclear Regulatory Commission
Washington, DC 20555
NRC FIN D1611

HIGH-LEVEL SEISMIC RESPONSE AND FAILURE PREDICTION METHODS FOR PIPING

L. K. Severud
M. J. Anderson
M. R. Lindquist
S. E. Wagner
E. O. Weiner

ABSTRACT

Seismic response and failure analyses were performed for four piping systems that were shake-tested to high level nonlinear and inelastic response levels. Both pre- and post-test analyses were accomplished. A number of simplified elastic, elasto-plastic, and inelastic transient dynamic analysis methods were utilized. Descriptions of these methods, with their special structural parameters and comparisons of predictions using each method to test data, are provided. Reasonably useful, but conservative, methods were found for predicting the high-level inelastic response and the failure modes.

ACKNOWLEDGMENTS

The authors wish to thank A. T. Onesto, Advanced Planning, Nuclear Programs, Energy Technology Engineering Center, Rockwell International for willingly providing technical details of the 6-inch and 3-inch diameter piping test article configurations and loading environment. Additionally, the direction and support of D. J. Guzy and J. E. Richardson, Mechanical/Structural Engineering Branch, Division of Engineering Safety, U.S. Nuclear Regulatory Commission are very much appreciated.

CONTENTS

CONTENTS (CONT'D)

CONTENTS (CONT'D)

CONTENTS (CONT'D)

CONTENTS (CONT'D)

CONTENTS (CON'T)

TABLES

TABLES (CONT'D)

FIGURES

FIGURES (Cont'd)

FIGURES (CONT'D)

FIGURES (CONT'D)

FIGURES (CONT'D)

FIGURES (CONT'D)

FIGURES (CONT'D)

ACRONYMS

ASCE	American Society of Civil Engineers
ASME	American Society of Mechanical Engineers
EPRI	Electric Power Research Institute
ETEC	Energy Technology Engineering Center
FFTF	Fast Flux Test Facility
HDR	Heissdampfreaktor
KWU	Kraftwerk Union AG
LMR	Liquid Metal Reactor
NRC	Nuclear Regulatory Commission
NUPEC	Nuclear Power Engineering Test Center
OBE	Operational Basis Earthquake
PRA	Probabilistic Risk Assessment
PVRC	Pressure Vessel Research Committee
SMIRT	Structural Mechanics in Reactor Technology
SRSS	Square Root of the Sum of the Squares
SSE	Safe Shutdown Earthquake
SSMRP	Seismic Safety Margins Research Program
WHC	Westinghouse Hanford Company
ZPA	Zero Period Acceleration

HIGH-LEVEL SEISMIC RESPONSE AND FAILURE PREDUCTION METHODS FOR PIPING

1.0 INTRODUCTION

Nuclear power plant piping systems are currently designed to resist the low cycle, high-level loading of dynamic events such as earthquakes by generally considering the structural materials to behave in a linear, elastic fashion. Current American Society of Mechanical Engineers (ASME) Level D service stress limits provide assurance of adequacy by limiting loads on individual components such that their collapse capability is not exceeded. This design approach fails to consider the redundancy potential in most piping systems which requires the collapse of several components before system integrity is compromised. Current design rules also do not account for the favorable effects of energy absorption caused by material ductility, load redistributions, and frequency shifts that occur in piping systems loaded beyond the material elastic limits.

Dynamic restraint of nuclear power plant piping has often been provided by the use of mechanical snubbers. Laboratory tests of prototypic piping systems, such as reported herein and in References 1 through 5, have shown strong evidence that the number of restraints and snubbers used to support piping is excessive. With the establishment of an adequate data base that demonstrates that piping systems have capabilities beyond those of current design criteria, the number of restraints and snubbers used to support piping in nuclear power plants could be reduced resulting in significant cost reduction and increased reliability of the piping system when subjected to thermal cycling.

The U.S. Nuclear Regulatory Commission (NRC) has contracted with the Energy Technology Engineering Center (ETEC) to perform seismic fragility demonstration tests on a prototypic nuclear power plant test loop under high-level seismic dynamic loading. NRC has also contracted with Westinghouse Hanford Company (WHC) for nonlinear piping response predictions.
The objective of the WHC program is:

> "To provide the bases for recommending pseudo-linear-elastic methods and procedures to be used in predicting the high-level seismic response and failure of piping systems."

The WHC analytic program specifically includes the following tasks:

1. Perform response/failure analyses on the following dynamic test articles:

   . WHC 1-inch diameter piping test (Reference 6)

- ETEC 6-inch diameter seismic fragility demonstration test (Reference 7)
- Kraftwerk Union (KWU) 2 and 4-inch diameter pipe system test (Reference 8)
- ETEC 3-inch piping test

Using the following various simplified elastic and elasto-plastic methods and a simplified nonlinear method:

- Standard ASME Code Class 1 and 2 design analyses
- Newmark modified spectra method (Reference 9)
- Campbell/Kennedy/Thrasher dynamic/static (D/S) margin ratio method (Reference 10)
- Progressive hinge simplified limit analysis method by Jaquay (Reference 11)
- Nonlinear transient dynamic inelastic analysis using the NONPIPE computer code (Reference 12)
- Seismic probabilistic risk assessment (PRA)-type piping fragility estimations using the procedures of References 13 and 14.

2. Compare the results of the above analyses with each other, and with the results of dynamic tests.

3. Perform analyses of damping energy distribution in four pipe systems excited to high-level response to determine how much of the total systems damping is due to:

   - Plastic hinges
   - Snubbers and supports
   - Rest of pipe system exclusive of two above items.

2.0 SUMMARY

A series of analyses were performed for predicting elastic and nonlinear inelastic dynamic response and collapse failure levels for a one-inch diameter pipe test article tested at the Westinghouse Hanford Company (WHC), for a six-inch diameter seismic fragility piping test article tested at the Energy Technology Engineering Center (ETEC), for a combination two-inch and four-inch diameter pipe test article tested by the German Kraftwerk Union AG (KWU), and for a three-inch diameter test article tested at ETEC. These analyses include (1) standard ASME Code Class 1 and 2 elastic methods, (2) the Newmark modified plastic spectra method, (3) the D/S margin ratio method, (4) a progressive hinge simplified limit analysis method, and (5) a nonlinear inelastic method.

Methods 2, 3, and 4 require special parameters that are not easy to quantify. They include the system ductility ratio, the D/S margin ratio, and the dynamic magnification factor. More comparisons of analytical and experimental data are needed to clarify appropriate values.

The predictions of piping collapse and test findings are shown in Table 2-1. The WHC one-inch diameter pipe system withstood 2.8 g zero period acceleration (ZPA) sinusoidal load input which did not fail the pressure boundary of the pipe although gross deformation did occur. The ETEC six-inch diameter system withstood 30 g ZPA testing without collapse but eventually failed because of incremental ratcheting. The failure mode was described as a local ratchet-fatigue rupture subsequent to local wall thinning and diametral bulging at one pipe leg anchor location. The KWU test article withstood 5.5 g ZPA acceleration during test without collapse. Testing was stopped at this level before any failure occurred. The ETEC three-inch diameter pipe system withstood 30 g ZPA acceleration during testing without collapse. Failure eventually occurred as a result of fatigue in a tee. As can be seen from Table 2-1, all analytical methods (except the probability risk assessment for the KWU test article) substantially underpredict the collapse capacity of the piping system. Moreover, ASME code allowable design levels, based upon linear elastic analyses, are a factor of approximately 2 to 10 times less than maximum test levels.

A ratchet-fatigue failure mode analysis was performed on the ETEC six-inch system and compared well with the test findings. However, further development of procedures and limits are recommended.

Analyses using a simplified approach of damping energy distributions have been made for four pipe systems that have been excited to high-level response. The purpose of the studies was to determine damping attributable to plastic hinges, snubbers and supports, and to the remainder of the pipe system. A number of correlations of the calculated damping values have been

made to piping experimental findings. These comparisons of calculated and experimental data of numerous piping systems at multiple levels of response show good correlations. The simple methods provide a useful tool in assessing the extent plasticity and snubbers add to piping system damping during high-level inelastic response.

It appears that the simplified inelastic methods and acceptance criteria referred to above have very good potential for becoming reliable conservative design tools. Before simple design-oriented methods are endorsed by NRC, however, the authors think that additional test data and analytical correlations are needed to provide adequate confidence in the procedures and code limits.

TABLE 2-1

SUMMARY OF ANALYTICAL PREDICTIONS* AND TEST FINDINGS

ANALYTIC METHOD	HEDL 1-IN DIA. PIPING	KWU 2-IN/4-IN DIA. PIPING	ETEC 3-IN DIA. PIPING	ETEC 6-IN DIA PIPING
A. ASME CLASS 1, $3S_M$ LEVEL D, G'S	0.36 SINE	1.9 ZPA	1.4 ZPA	2.0 ZPA
B. ASME CLASS 2, $3S_H$, G'S	0.34	1.7	1.0	1.4
C. NEWMARK METHOD, G'S	1.55	4.8	10.2	10.0
D. DYNAMIC/STATIC MARGIN RATIO, G'S	1.58	4.5	10.0	9.7
E. PROGRESSIVE HINGE, STATIC LOAD, G'S				
() = DYN. MAGNIF. FACTOR	1.50 (1.8)	4.2 (5.0)	9.5 (2.0)	8.1 (2.0)
	2.70 (1.0)	21.0 (1.0)	19.0 (1.0)	16.2 (1.0)
F. PRA-TYPE FRAGILITY				
ZION METHOD, G'S	--	7.8	4.4	4.4
SSMRP METHOD, G'S	--	11.5	5.2	8.8
G. NONLINEAR INELASTIC DYNAMIC				
LOAD LEVEL, G'S	2.5	4.0 SINE	30.0	30.0
STRAIN RANGE, PERCENT	2.5	1.6	14.0	4.1
TEST FINDINGS				
A. MAX. BASE INPUT, G'S	2.8 SINE, 2 H_Z	4.0 SINE, 8.9 H_Z	30.0 ZPA	30.0 ZPA
	0:5 ZPA	5.5 ZPA	25.0 SINE, 6 H_Z	18.7 SINE, 5H_Z
B. NO FAILURES FOR ALL ZPA'S				
C. FAILURE MODE	RATCHETING-GROSS DEFORMATION	NONE	FATIGUE	RATCHET/FATIGUE OR DUCTILITY EXHAUSTION

* See Section 10.0 for discussion of conservatisms not included.

NUREG/CR-5023
WHC-EP-0081

3.0 ANALYSIS METHODS FOR RESPONSE/COLLAPSE FAILURE PREDICTION

A number of piping analysis methods are available to calculate response and failure levels and to establish margins to failure of a piping system under dynamic loading. These methods include the simplified techniques of (1) linear elastic analyses, (2) the Newmark plastic spectra method, (3) the D/S margin ratio method, and (4) the static progressive hinge formation method. Additionally direct, detailed nonlinear methods are also available. Failure predictions addressed in this report were primarily associated with excessive plastic deformation and collapse of the piping system. Post-test analyses also include local fatigue and ratchet-fatigue failure modes.

3.1 SIMPLIFIED ELASTIC AND ELASTO-PLASTIC METHODS

Several simplified methods available for piping failure predictions are discussed below.

3.1.1 Linear Elastic Dynamic Analysis Method

Conventional linear elastic analysis methods are available for response assessment of piping systems under dynamic loading. Standard procedures use finite element computer programs, with a number of suitable programs available. The PIPESD program (Reference 15) was used to assess piping systems subjected to high-level dynamic testing at WHC and ETEC. PIPESD is a verified code and it uses the ASME Code, Section III, NB-3600, and Reference NC-3600 equations and stress indices.

Linear Elastic dynamic analyses are performed using the response spectrum method with the modal responses combined using the methods of Regulatory Guide 1.92 (Reference 16). The piping stresses of a response spectrum analysis are normally compared with allowable limits such as the ASME allowable for an operational basis earthquake (OBE) or a safe shutdown earthquake (SSE). ASME allowable limits are set much lower than failure conditions to ensure safety during operating conditions. Current elastic seismic allowables are judged by many investigators to be very conservative.

Linear elastic results are useful for assessment not only by themselves but they also form the basis on which many other simplified analysis methods are implemented.

3.1.2 Newmark Plastic Spectra Method

The Newmark plastic spectra method, Reference 9, uses a procedure that involves the construction of an elasto-plastic response spectra. This spectra is developed by reducing the elastic spectra by an energy absorption factor that is related to the system ductility. The system ductility is that

ratio determined from the resistance-displacement relationship for the structure as a whole. This system ductility ratio, u', is further discussed in Section 4.0. The spectral reduction varies within the spectrum. In the amplified spectral acceleration region of the response spectrum (approximately 2 to 8 hertz for a Newmark-type spectrum), the spectrum is reduced by a factor $\sqrt{2u'-1}$. For higher frequencies, above 20 hertz, no reduction is used while, between the two above regions, a transition from the amplified spectral acceleration factor is used.

Campbell et al., Reference 10, demonstrated that, for a number of simple piping configurations, the system ductility ratio is substantially lower than that for the material itself. A similar conclusion has been expressed for piping systems by Stevenson (Reference 17), Newmark (Reference 9), and others. The analyses presented herein also demonstrated system ductility to be much less than material ductility.

The major feature of the Newmark method, therefore, is that of reducing the elastic response spectra by a factor relating to ductility. Conventional linear, elastic analyses are, in turn, performed using the reduced response spectrum. The resulting piping stresses are assessed against an allowable related to material yield strength such as Fy' (discussed in Section 4.0). The estimated collapse failure loading is determined by reduced-spectra pipe primary stresses (at any location in the piping system) having magnitudes sufficient to develop a fully plastic pipe section (plastic hinge).

3.1.3 Dynamic/Static (D/S) Margin Ratio Method

The D/S margin ratio method, Reference 10, is a method that modifies linear elastic dynamic analysis results by a D/S factor. The D/S factor is a ratio of the dynamic margin divided by the static margin and is a direct measure of the factor of conservatism inherent in designing equipment subjected to dynamic load to static load criteria. The dynamic margin is defined as the dynamic load to cause failure divided by the dynamic load that results in a predicted elastic response equal to a specified stress acceptance criteria. The static margin is the static failure load divided by the static load that results in a predicted elastic response equal to the stress acceptance criteria.

The D/S factor is a function of the frequency content and duration of the dynamic load and the frequency of the structure. A relationship also exists between the D/S factor and the system ductility of an elasto-plastic or bilinear resistance structure. Reference 10 established a method to evaluate the D/S factor for single-degree-of-freedom models and approximate methods for multi-degree-of-freedom systems.

The D/S method, like the Newmark method, recognizes the system ductility ratio as a major parameter for structural response to dynamic loading. The

D/S method, however, uses the system ductility ratio to develop the D/S factor rather than to reduce the spectra. The D/S method is implemented by performing a conventional linear elastic analysis using the full elastic response spectrum. The results of the analysis are then divided by the appropriate D/S factor to obtain the final system piping stresses. The resulting stresses are compared with an equivalent yield strength, such as shown in Figure 3-1 and discussed in Section 4.0, or with an ASME Code allowable stress. As is the case using the Newmark plastic spectra method, the equivalent yield strength is factored also to account for the development of a fully plastic pipe section (plastic hinge).

3.1.4 Static Progressive Hinge Formation Method

The static progressive hinge formation method, Reference 11, is an assessment based on equivalent static loading combined with material yielding and plastic hinges forming at specific locations. The method recognizes that load redistributions and redundancy in piping systems prevent system collapse until enough individual components are loaded past their collapse loads to form a mechanism and an unstable structural system results.

The analysis procedure consists of a series of static analyses. The first analysis is performed to determine the equivalent static-g loading to cause the first plastic hinge to develop. Then, the piping model is modified by inserting a "pin-type" joint at the plastic hinge location. This allows freedom of rotation and does not transmit any moment across the joint. A second equivalent static-g load analysis of the modified model is then performed to determine the increment of load needed to develop a second plastic hinge in the system. This procedure is repeated until the number of plastic hinges in the model lead to a static instability (collapse mechanism) of the system. By summing the initial and incremented loads, the static limit load carrying capacity of the piping system is determined.

As in the Newmark and the D/S methods, the assessment of the collapse loading capability (plastic hinge strength) of the various system components is important. Jaquay, Reference 8, suggested that test data justify using collapse loading capacities 50% and 70% higher than predicted by normal elasto-plastic limit load capacities of elbows and straight pipe, respectively. This was done in the progressive hinge analyses reported herein. However, the Newmark and D/S analyses did not include the 50% and 70% increases.

An advantage of the progressive hinge method is that it allows visualization of the probable failure sequence of the structure thus giving an indication of the final failed shape. However, this method of Reference 8 predicts failure based on pipe accelerations. To fully develop the method, procedures need to be developed to determine the factor that relates pipe dynamic accelerations to base static acceleration (magnification factor). One

suggestion is to use magnification factors from the Newmark plastic spectrum method.

3.2 SYSTEM DUCTILITY RATIO AND EQUIVALENT YIELD POINT STRENGTH

The Newmark and D/S simplified methods, discussed previously in Section 3.1, utilize the concept of reduced system response as a result of inelastic action. This is based upon the premise that even a slight amount of inelastic action reduces the response of the structure significantly because of nonlinear behavior. The inelastic action is accounted for in these methods by the introduction of parameters called the system ductility ratio and the equivalent yield point strength.

3.2.1 System Ductility Ratio

For impulse and impact loads in nuclear plant facilities, the AISC guidelines of Reference 25 suggest allowable ductility ratios. For structural steel structures, beams with local and lateral buckling prevented, allowable ductility ratio of 20 is recommended. For axial tensile members, the ratio is half the material total elongation divided by the material yield strain. However, it is noted in Reference 25 that the NRC requires specific justification for allowable ratios in excess of 10 in most cases.

The system ductility ratio is a measure of the elastic plus inelastic capability of the structure, see Figure 3-1. It is important to recognize that the system ductility ratio is based upon the ductility that is determined from the resistance-displacement relationship of the structural system as a whole rather than from, for example, the moment-rotation capacity of a particular joint or the ductility of a particular element or component of the structure. Since the system ductility ratio represents the energy absorption capacity of the structure as a whole, it is generally substantially lower than the material ductility by itself because of strain concentrations.

For the seismic collapse failure levels being predicted in this report, appropriate maximum ductility ratios are needed for each piping multi-degree-of-freedom system.

If an elasto-plastic response is assumed, Reference 7 states that, for any structural system, the system ductility developed in response to loading can be approximated by the weighted mass displacement of the elastic-plastic system divided by the weighted mass displacement at first yield of the elastic system, i.e.,

$$u' = \frac{\Sigma M_i \, \delta i_p}{\Sigma M_i \, \delta i_e}$$

where:

u'	=	System ductility
M_i	=	Ith mass
δi_e	=	Displacement of the ith mass in the elastic material model solution at first yield
δi_p	=	Displacement of the ith mass in the elastic-plastic material model solution at a given system inelastic response (strain) level.

It is important to note that the system ductility, u', is a variable dependent on the level of inelastic response and the deformation shape. For a single degree-of-freedom system, the δi_p would correspond to the material strain and the u' would simply equal the ratio of the material response total strain to the yield strain.

For a multi-degree-of-freedom system, the change in deformed shape of the system (because of strain localization) after first yield can limit the u' significantly.

The equation described above was used to estimate the system ductility for the WHC one-inch diameter pipe loop and the configuration proposed for the ETEC seismic fragility demonstration test.

3.2.2 Equivalent Yield Point Strength

A simple elasto-plastic model of the system inelastic response is employed. To adjust for strain hardening and for section limit-load capacities relative to first local yielding, an equivalent yield point strength concept was adapted. Figure 3-1 depicts these relationships.

3.3 NONLINEAR INELASTIC TRANSIENT DYNAMIC ANALYSES

Nonlinear, inelastic analysis provides more accurate predictions of the structural response of a system under time-varying dynamic loads. These analyses typically require specialized computer programs to implement the analyses. The NONPIPE program, Reference 9, was used for inelastic analyses of the piping systems involved in high-level dynamic testing at WHC and that planned for ETEC.

The NONPIPE computer code provides a relatively inexpensive means of inelastic dynamic analysis of piping systems by the uncoupling of bending, torsion and axial responses. Nonlinearities include those caused by material inelastic response. By uncoupling the moment and axial responses, bending definition in the plastic range may be specified by trilinear load-deflection curves of bending and torsion components. NONPIPE analysis utilizes the direct stiffness method, with viscous damping proportional to the mass and tangential stiffness matrices.

3.4 STRESS INDICES

The piping stress analyses have been based on Equation 9 of the ASME Code (Reference 18). Equation 9 calculates primary stresses as follows:

$$S = \frac{B_1 P D_o}{2t} + \frac{B_2 D_o M_i}{2I}$$

where:

B_1, B_2 = Primary stress indices for the specific component under investigation
P = Pressure
D_o = Outside pipe diameter
t = Nominal wall thickness
I = Moment of inertia
M_i = Resultant moment because of mechanical loads.

The B_1 stress index addresses pressure stresses; the B_2 stress index calculates stresses caused by moments from dead weight and dynamic loading effects. More recent editions of the ASME Code were used for the stress indices since the later editions remove some of the conservatisms in earlier versions of the Code (see Reference 20).

3.4.1 Straight Pipe

The following terms were used for straight pipe stress indices:

$B_1 = 0.50$
$B_2 = 1.00$

3.4.2 Elbows

The pressure term, B_1, for elbows was taken as:

$$B_1 = -0.1 + 0.4h, \text{ but not } < 0 \text{ nor } > 0.5$$

where:

$$h = \frac{tR}{r_m^2}$$

and

t = Nominal wall thickness
R = Nominal bend radius
r_m = Mean pipe radius.

The moment term, B_2, for elbows was taken as:

$$B_2 = \frac{2}{3} \times \frac{(1.95)}{h^{2/3}}$$

3.4.3 Tees

The pressure term, B_1, for tees was taken as:

$$B_1 = 0.5$$

The tee moment terms, B_{2b} and B_{2r}, for the branch and the run were taken as:

$$B_{2b} = 0.4\ (Rm/Tr)^{2/3}$$
$$B_{2r} = 0.5\ (Rm/Tr)^{2/3}$$

where:

R_m = Mean radius of run pipe
T_r = Nominal wall thickness of run pipe.

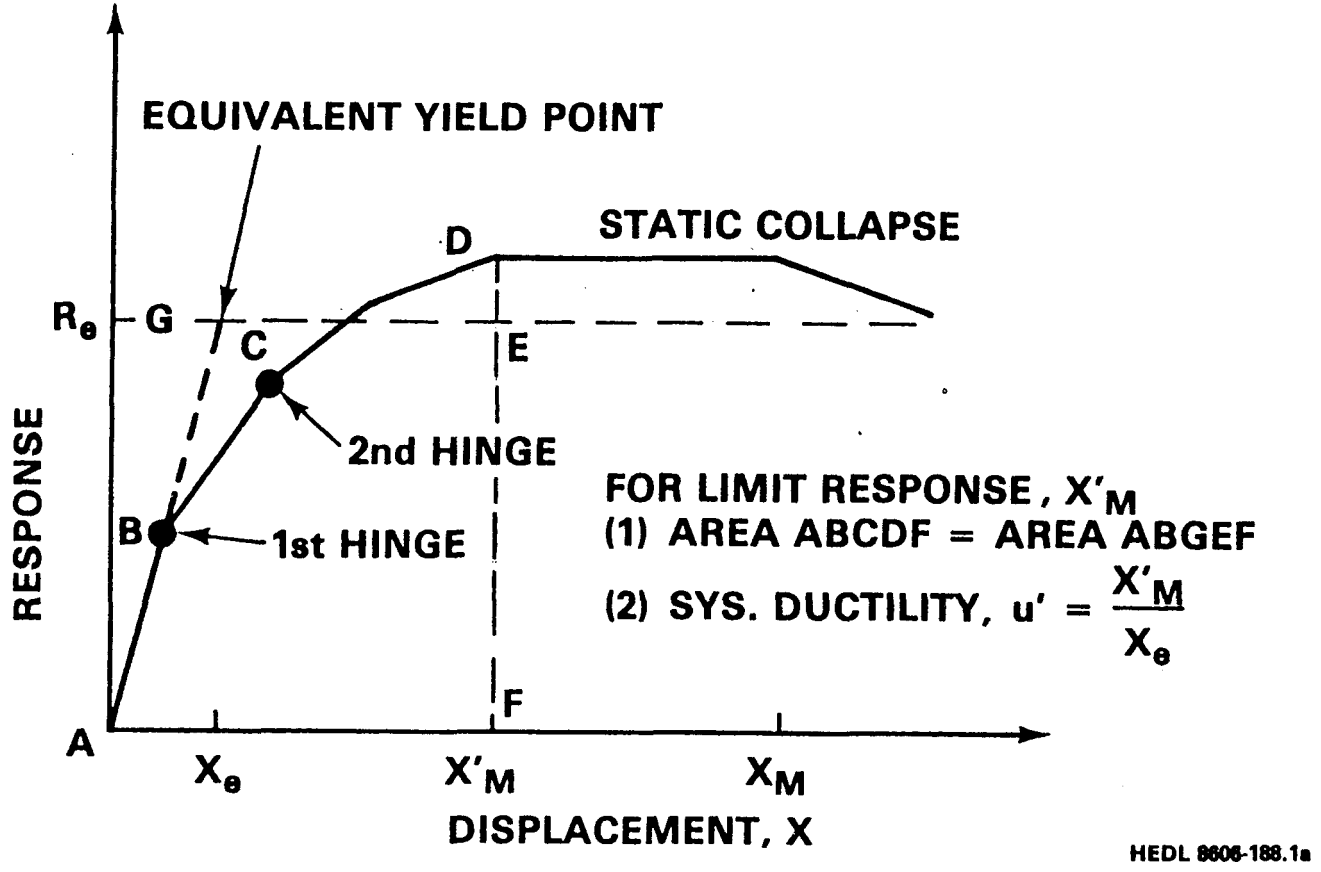

FIGURE 3-1. Typical System Response Showing Definition of System Ductility Ratio and Equivalent Yield Point Strength.

4.0 COMPARISON OF RESPONSE/FAILURE PREDICTION METHODS

A number of simplified elastic and elasto-plastic methods and a nonlinear method for piping system collapse failure under dynamic loading have been described. Each of the methods require estimation or calculation of structural parameters unique to the particular method. Table 4-1 shows the features of each method, the significant parameters considered in the analysis, the analysis approach, and the limit criteria.

Table 4-1 lists the methods in ascending order of detail, complexity, cost, and degree of accuracy and information. All methods are practical and not unduly costly. Except for the ASME Code-type linear elastic method, the key input parameters include choice of: (1) damping or dynamic amplification factors, (2) effective yield strength of material, (3) component limit load factors, (4) system ductility (maximum strain) and effective yield point, and (5) a criteria of failure such as collapse and/or fatigue, etc.

The methods described above were used for pretest predictions of seismic load levels needed to initiate collapse of the piping systems. Other failure modes such as fatigue and ratchet-fatigue were not assessed initially; however, post-test analyses discussed in Section 6.8 do address these failure modes.

TABLE 4-1

COMPARISON OF PIPING RESPONSE/FAILURE PREDICTION METHODS

Method	Significant Parameters	Analysis Approach	Limiting Criteria
Linear Elastic	. Response Spectra . Damping Ratio	Dynamic Analysis with Elastic Spectra	$3S_M$, $3S_H$ of ASME Code, Class 1 or 2 for Level D
Newmark (Reference 9)	. Response Spectra . Damping Ratio . Effective Yield Point . System Ductility	1) Reduce Spectra 2) Dynamic Analysis with Plastic Spectra	1) Effective Yield Point 2) System Ductility Ratio (Max Strain)
Dynamic/Static Margin Ratio (Reference 10)	. Response Spectra . Damping Ratio . D/S Factor (Sys Ductility) . Effective Yield Point	1) Dynamic Analysis with Elastic Spectra 2) Reduce Results by D/S Factor	1) Effective Yield Point 2) System Ductility Ratio (Max Strain)
Static Progressive Hinge (Reference 11)	. Component Hinge Strengths . System Collapse (Limit Load)	1) Static Analyses for g Loads and Plastic Hinges 2) Reduce Results by Effective Dynamic Amplification Factor	1) Enough Plastic Hinges to Cause System Instability and Collapse 2) Dynamic Amplification Factor
Nonlinear, Inelastic (Reference 12)	. Time History Input . Damping . Elbow Inelastic Stiffness	Time-History Dynamic Analysis	1) System Instability 2) Max Strain and Strain Range

5.0 WHC ONE-INCH DIAMETER PIPE SYSTEM TESTS

A series of high-level dynamic tests were performed on a one-inch diameter piping system at WHC. The piping was tested until gross deformation occurred and a number of analytical prediction methods (both pre-test and post-test) were used to assess the results.

5.1 TEST ARTICLE/STRUCTURAL MODEL

The WHC one-inch piping system consisted of a one-inch diameter, 304 stainless steel, Schedule 40 pipe approximately 35 feet long. The piping system contained nine elbows and/or bends along with risers and one liquid metal valve. The pipe was insulated with Fast Flux Test Facility (FFTF) stand-off insulation with an inner heater annulus and outer metal cover similar to that planned for liquid metal reactor (LMR) pipe systems. Typical insulation details are shown in Figure 5-1. The pipe was supported from a strongback by insulated pipe clamps connected with prototypic rigid struts or mechanical snubbers with the pipe ends being fixed. A sketch of the piping configuration tested is shown in Figure 5-2, with the structural model shown in Figure 5-3.

The pipe loop was mounted to a "rigid" strongback support structure that was, in turn, installed on a base mass. Loading was applied horizontally to the system through the strongback by a hydraulic load thruster actuator (see Figure 5-4). The line was not pressurized (0 psig).

5.2 TEST LOADING/FAILURE MODE

High-level testing of the various pipe loop configurations was accomplished by introducing acceleration loads into the support strongback by means of the hydraulic actuator system. Loading was in the horizontal (Z) direction and consisted of response spectrum and sinusoidal loading. The multi-frequency response spectrum loading was applied by means of a time-history that was synthesized to match the specified shape. Since the response spectrum loading did not fail the test system, the loading was changed to sinusoidal with a frequency that matched the first mode natural frequency of the system. The sinusoidal loading was applied at a frequency of 2 hertz in steps of increasing acceleration levels until failure occurred, as described below. A typical sinusoidal loading is shown in Figure 5-5.

During the progressively increasing sinusoidal load steps, gross deformation of the test piping system occurred. This deformation resulted from the formation of plastic hinges at specific locations. The sequence of system deformation is described below. For node identification, see Figure 5-3.

Permanent local deformation of the pipe wall (see Figures 5-6 and 5-7) was first noted near the vertical support at Node 99 and a plastic hinge subsequently developed at this location. Pipe plastic bending started at a base input load level between 0.2 g and 0.5 g. As the load steps increased, permanent deformation also increased with the vertical portion of the pipe system (Nodes 22-24) gradually rotating (with the top moving in a positive Z direction). A second increase in the deformation rate of this vertical portion initiated at about 1.5 g base load input implying that a second plastic hinge was operative. Testing continued up to 2.8 g where it was terminated. Progressive gross deformation (ratcheting) led to very near collapse of the piping system. After the test was completed and the insulation was removed, a second region of plastic deformation was found on the pipe section between Nodes 35 and 36. Despite the gross deformations that occurred as a result of the testing, the pressure boundary of the piping system remained intact.

The photographs in Figures 5-6 through 5-8 were taken after testing was completed and show the permanent deformation that occurred during testing. Figure 5-6 shows the overall condition of the pipe system at the end of testing. Figure 5-7 shows the local region near Node 99 where the first plastic hinge developed while Figure 5-8 shows the local region between Nodes 35 and 36 where the second plastic hinge developed.

5.3 LOCAL STRAIN/EQUIVALENT DAMPING

Post-test calculations were made to determine the amount of local strain that had developed in the region of the first hinge (Node 99) during the test. The calculations were based on pipe accelerations measured during testing combined with elastic static bending analysis under lateral loading. The maximum local strain at Node 99 was estimated to be about 0.5% amplitude (1.0% range).

Accelerations at various locations were measured during the WHC high-level dynamic tests of the one-inch pipe loop. The relationship between the measured strongback base acceleration and pipe acceleration is shown in Figure 5-9 for positive and negative response. The acceleration on the pipe represents the location (Figure 5-3, near Node 27) with maximum displacement during the test. The magnification factor (pipe acceleration divided by base input acceleration) is also shown on Figure 5-9.

As the test load level increased, the increase in piping response was not proportional because of plasticity and other mitigating effects. This is seen as a decrease in the magnification factor and may be expressed as an increase in equivalent system damping. For a steady-state sinusoidal excitation resonance, equivalent damping may be expressed as:

$$\text{Equivalent Damping } * = \frac{1}{2 \times \text{Magnification Factor}}$$

Figures 5-9 and 5-10 present the equivalent damping as a function of base load input using the above equation and the test-determined magnification factors shown in Figure 5-9. The equivalent damping is near 10% initially (when the structure is elastic) and increases to approach 50% as large deformations occur (pipe hinge strain range of about 1% or more).

5.4 WHC TEST ARTICLE PARAMETERS

As discussed in Section 3, implementation of the Newmark and D/S methods requires that the parameters of system ductility and effective yield point be defined. These parameters are unique to a given piping configuration support system, response level, deformation shapes, and material. Calculations to estimate these for the specific piping configuration of the WHC one-inch diameter pipe loop are discussed below.

5.4.1 System Ductility Calculations

A series of calculations were performed to estimate the system ductility for the WHC one-inch diameter pipe system tested during the high-level dynamic tests. The calculations (as discussed below) used the formula discussed in Section 3.2.1 to obtain the system ductility results. Local strains were also calculated.

The system ductility, u', was calculated using the previously discussed formula:

$$u' = \frac{\Sigma M_i \delta_{i_p}}{\Sigma M_i \delta_{i_e}}$$

(Refer to Section 3.2.1)

combined with PIPESD analyses and the following steps:

---

* For seismic random excitation, equivalent damping = $\frac{1}{2(MF)^2}$ approximately, Reference 19.

1. A lateral load (static) of 1 g was applied to the system with stresses and deflections obtained assuming linear, elastic response of the structure.

2. A value of material yield stress was selected and the lateral load factor to cause yield was calculated from stresses obtained in Step 1.

3. The quantity $\Sigma M\delta$ for the system was calculated for the g level corresponding to the selected yield stress.

4. The moment required to develop a plastic hinge for the selected yield stress was calculated, including a plastic shape factor.

5. A constant moment hinge, as calculated in Step 1, was applied to the system at the most highly stressed location and PIPESD analyses were made for several levels of lateral g loading.

6. The quantity M for the lateral load levels of Step 5 was calculated.

7. The system ductility was obtained by dividing the values obtained in Step 6 by that obtained in Step 3.

8. The above steps were repeated for other values of yield stress.

The local effect strain at the hinge location (Node 99) was calculated for the various above-loading conditions based upon analytical results. The calculations are a summation of elastic-plus-plastic strain. The plastic strain is based upon elastic results increased by a strain concentration factor. Reference 12 indicates that a strain concentration factor of approximately 2 is appropriate for the stainless steel piping considered herein.

The results of the system ductility calculations, along with corresponding material yield strength and local strain, are plotted in Figure 5-11. For the 53 ksi yield strength of the pipe material, system ductility ranges from about 3 to 10 for local strains of 0.5 to 1.0% amplitude.

5.4.2 Equivalent Yield Point Calculations

The equivalent yield point, R_e, was estimated using the pipe material tensile test data (see Table 5-1) and factors to account for (a) bending limit load capacity, (b) material strain hardening, and (c) multiple plastic hinges before system collapse.

The bending limit load capacity factors were for plastic hinges located in straight pipe sections. To account for the limit capacity, the elastically calculated stress level at each hinge was divided by a 1.4 factor (analogous to a bending modulus).

To estimate the increase in strength caused by (b) and (c), an equivalent yield point strength equal to $S_y + 1/4\ (S_u - S_y) = 54$ ksi was adapted. This approach was judged reasonable for stainless steel applications. However, it may not serve well for carbon steels with pronounced yielding and little effective strain hardening. Moreover, pipe systems that require many plastic hinges to approach static collapse conditions may have much higher effective yield strengths than the above formula would indicate. Progressive hinge elasto-plastic analyses of the WHC pipe system indicated only two hinges would be needed for static collapse. The second hinge was calculated to develop at piping response loads about 10% higher than required for the first hinge.

5.4.3 Estimate of System Ductility

The results of the one-inch WHC pipe loop general system ductility studies of the previous sections have been assessed to determine a more specific ductility value for the tested system. As stated previously, the value of system ductility is needed to properly utilize and implement the Newmark and the D/S simplified methods.

The data of Figure 5-11 are repeated in Figure 5-12. Identified in Figure 5-12 is the total local strain (0.5%) that was calculated from the elastic calculations based upon measured test accelerations (see Section 5.1.4). Also shown in Figure 5-12 is the strain amplitude calculated by the NONPIPE code over a range of base input accelerations which are typical of those used in the test. Using the range of calculated strain and a material effective yield strength of 40 ksi (per tensile tests) results in a system ductility in the range of 5 to 10. These values are higher than that of Reference 7 in which a system ductility of 3.8 was found for a simple two-elbow stainless steel pipe configuration at load levels permitted by current code rules for Level D Service.

Because the values of system ductility experienced by the WHC pipe system during high-level shaking are not precise, parametric analyses of their effect on collapse load capacity were conducted. The results are provided in the next section.

5.5 SIMPLIFIED ELASTIC AND ELASTO-PLASTIC ANALYSES

The simplified elastic and elasto-plastic methods described in Section 3.1 have been applied to the configuration and loading environment used for the high-level dynamic testing of the one-inch diameter WHC pipe system.

5.5.1 Linear Elastic Analyses

Linear elastic analyses were performed on the pipe system for sinusoidal loadings which were developed into a response spectra for 10% damping as shown in Figure 5-14, with the value of 10% damping obtained from average measured snapback test data. The analyses were accomplished by scaling the spectra to obtain results for various base load levels. The allowable base

input loading was found to be 0.36 g for an ASME Class 1, Level D limit ($3\ S_m$ = 60 ksi) and 0.34 g for an ASME Class 2, Level D limit ($3\ S_H$ = 57 ksi). This limit is shown in Figure 5-13 as "ASME". Margins to failure (second hinge formation) are approximately 4. The dynamic magnification for 10% damping and sinusoidal excitation is 5. This has been verified by the measured test results as shown in Figure 5-9. During initial loading, when the response was in the linear range, the magnification factor is near 5.

5.5.2 Newmark Plastic Spectra Method

As discussed in Section 3.1.2, the Newmark plastic spectra method uses a procedure that involves the construction of an elasto-plastic response spectra. The input spectra are reduced by the factor $\sqrt{2u'-1}$, where u′ is the system ductility ratio.

The allowable limits based upon the Newmark plastic spectra method were calculated for several system ductility values. The elastic spectrum peak and loads were reduced by large factors, 3.3 to 5.0 (See Figure 5-15), and elastic analysis performed. The results are presented in Figure 5-13 for system ductilities ratios of 5, 10, and infinity. A system ductility of 5 was chosen as a conservative value for the one-inch diameter piping loop, as discussed in Section 5.2.3.

As can be seen from Figure 5-13, an effective yield point of 54 ksi (based on material measured properties) and a system ductility ratio of 5 gives a predicted base acceleration limit of approximately 1.5 g for the Newmark plastic spectra method. The corresponding magnification factor was 1.5 based on the peak of the response spectrum.

5.5.3 Dynamic/Static Margin Ratio Method

As discussed in Section 3.1.3, the D/S margin ratio method uses an elastic response spectrum analysis, followed by a reduction of the stress results by means of a D/S factor. This method was used to assess the components of the pipe system under the proposed test loadings.

The allowable limits based on the D/S margin ratio method were calculated for D/S ratios of 1.5 and 3.0 (see Figure 5-13). The D/S value of 3 corresponds to a system ductility of approximately 5. Figure 5-12 shows that an

effective yield point of 54 ksi and a D/S value of 3 gives a predicted based acceleration limit of approximately 1.5 g. The corresponding magnification factor was 1.5.

Location of high calculated stress and hinge formation during testing coincided except for the elbows. At elbows, higher yield strength existed because of cold-forming the elbow bends during pipe system fabrication.

5.5.4 Progressive Hinge Formation Method

As discussed in Section 3.1.4, the static progressive hinge formation method is based on an assessment of system stresses resulting from a static loading analysis which leads to a resulting collapse mechanism.

The static progressive hinge method was used to calculate failure levels for several material yield levels for the WHC one-inch pipe loop. The locations where hinges were predicted to occur agreed with the location and sequence of hinge formation observed during the testing (See Figure 5-16). The static progressive hinge method gives analytical failure predictions on the basis of load levels on the pipe, this being shown in Figure 5-13 as the case with magnification factor = 1.0. To express the results in consistent terms as the other data shown in Figure 5-13, the relationship between pipe acceleration and base acceleration must be known or estimated. Figure 5-9 indicates a measured magnification factor of approximately 1.8 at an acceleration level at which the second hinge formed (1.5 g's). The predicted failure levels are therefore shown in Figure 5-13 for a second case in which the magnification factor = 1.8.

The base input acceleration limit of 1.5 g is not the maximum acceleration withstood by the pipe system. Even though maximum accelerations of about 2.8 g were withstood, it was judged that the degree of progressive deformation after 1.5 g represented unacceptable response. Thus, the conservative 1.5 g limit was selected.

5.6 NONLINEAR TRANSIENT DYNAMIC INELASTIC ANALYSIS

Nonlinear dynamic analyses of the WHC one-inch pipe loop were performed to investigate the capacity of the system on an inelastic basis. The NONPIPE computer code (Reference 12) offered a relatively inexpensive means of analysis by characterizing elbow and pipe behavior through trilinear moment-curvature relations. The code has the capability of including proportional damping in addition to plasticity hysteric damping.

The NONPIPE analysis was performed for a sinusoidal load input at 2 hertz, with load magnitude increased in steps. A base input as high as 2.5 g's did not produce system instability. The analysis did show development of a hinge

at the same location as that developed during test. The local material strain range was calculated as 2.5% for the 2.5 g base input acceleration. Calculated pipe magnification factors agreed well with test data.

5.7 SUMMARY OF TEST RESULTS/COLLAPSE PREDICTIONS, WHC ONE-INCH DIAMETER PIPE SYSTEM

Seismic random input motions to 1.3 times a 0.4 g ZPA typical SSE did not challenge the integrity of the pipe system. As the facility could not impose higher random input, sinusoidal resonant dwell dynamic tests were subsequently performed. A series of tests, each at higher input accelerations, led to a progressive gross deformation (ratcheting) and very near collapse of the pipe system.

Visual observation and recorded data revealed increased deformation with developing of a plastic hinge near the middle of the pipe system during testing in the 0.2 to 0.5 g's base input level. A second hinge and increased deformations resulted at about 1.5 g's load level. Testing was terminated at 2.8 g's input levels. The gross distortion was as depicted in Figures 5-6, 5-7, and 5-8.

Results of the WHC high-level dynamic test and analytical studies are summarized in Figure 5-13. Where a range of failure levels are predicted, the best estimates are shown in Figure 5-13 with a diamond (◆) identification. The effective yield point of 54 ksi for the failure prediction is based on the measured properties of the pipe material (see Table 5-1). The results of Figure 5-13 are also summarized in Table 2-1.

Collapse of the piping system was not fully achieved at levels up to the 2.8 g base input. The ASME Level D allowable (for 10% damping) load level = 0.36 g (Class 1) and 0.34 g (Class 2). Gross deformation occurred at approximately 1.5 g, which is in excess of 4 times the Class 1 and Class 2 allowables.

Piping response inertia test loads were less than calculated. Dynamic magnification drops off (from about 5 to 1) with increased load input. Plastic response causes natural frequencies to shift off of resonance.

The system ductility of a piping system is significantly lower than that of the material itself. Values of 5 to 10 are reasonable.

The Newmark and the D/S methods predicted failure approximately equal to the second plastic hinge load level. Test failure level, however, was somewhat difficult to define and the occurrence of the second hinge probably occurred over a range of test load values.

The static progressive hinge method correctly predicted the sequence of plastic hinge formation. It also closely predicted the load carrying capacity of 2.8 g's, provided a magnification factor of 1.0 consistent with test data, was used.

The NONPIPE analysis correctly predicted the location of initial hinge formation. No collapse was predicted at 2.5 g base input acceleration, with maximum strain calculated as 2.5%. Analytical pipe magnification factors reduced with increasing load level and agreed well with test data.

TABLE 5-1

PIPE MATERIAL PROPERTIES, 304 STAINLESS STEEL

	Yield Strength (ksi)	Ultimate Strength (ksi)	Elongation (e_u) at Failure (%)
Code Minimum	30	75	30
Measured	40	93	78

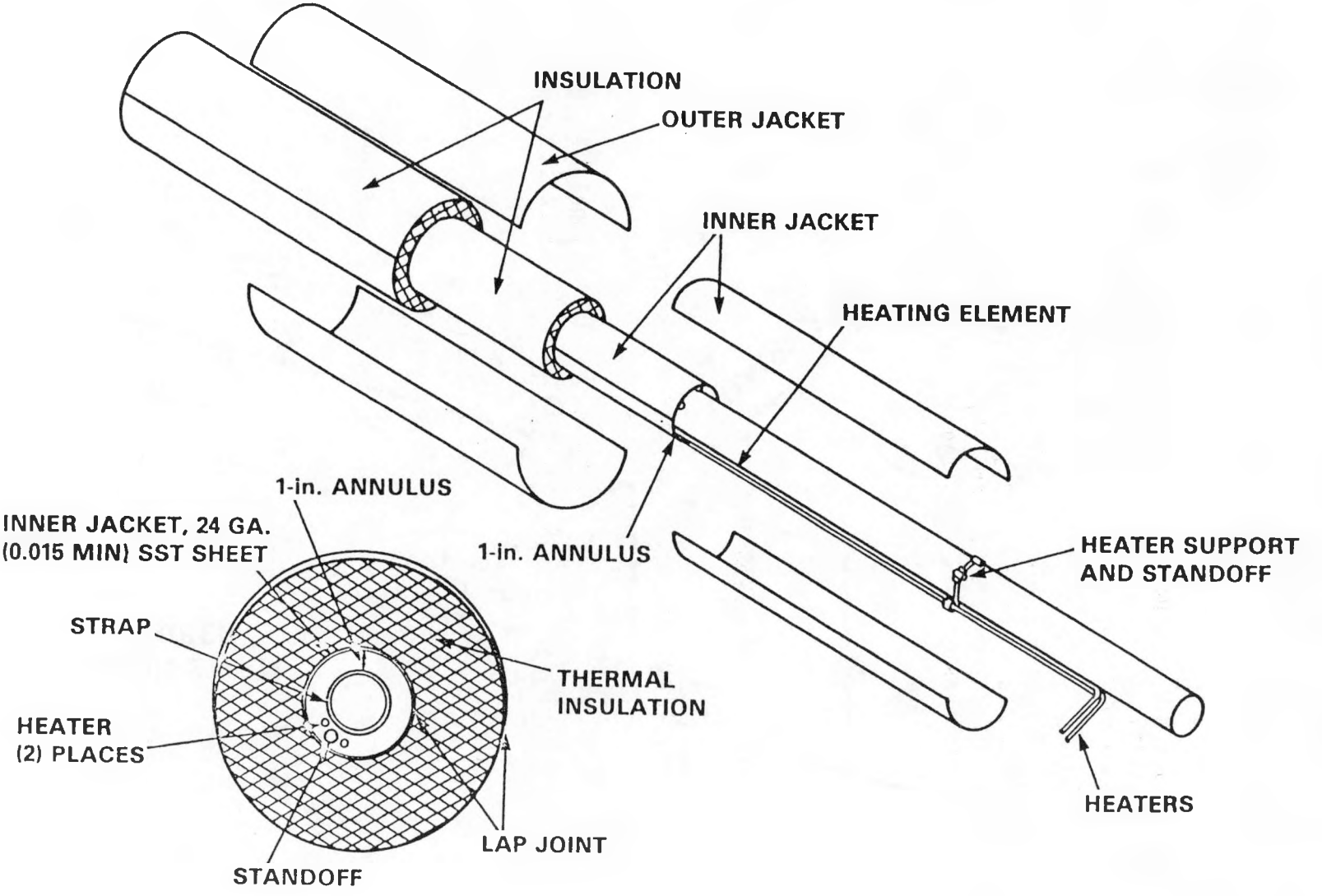

FIGURE 5-1. Typical LMR Insulation and Trace Heat Design.

HEDL 8308-344.5

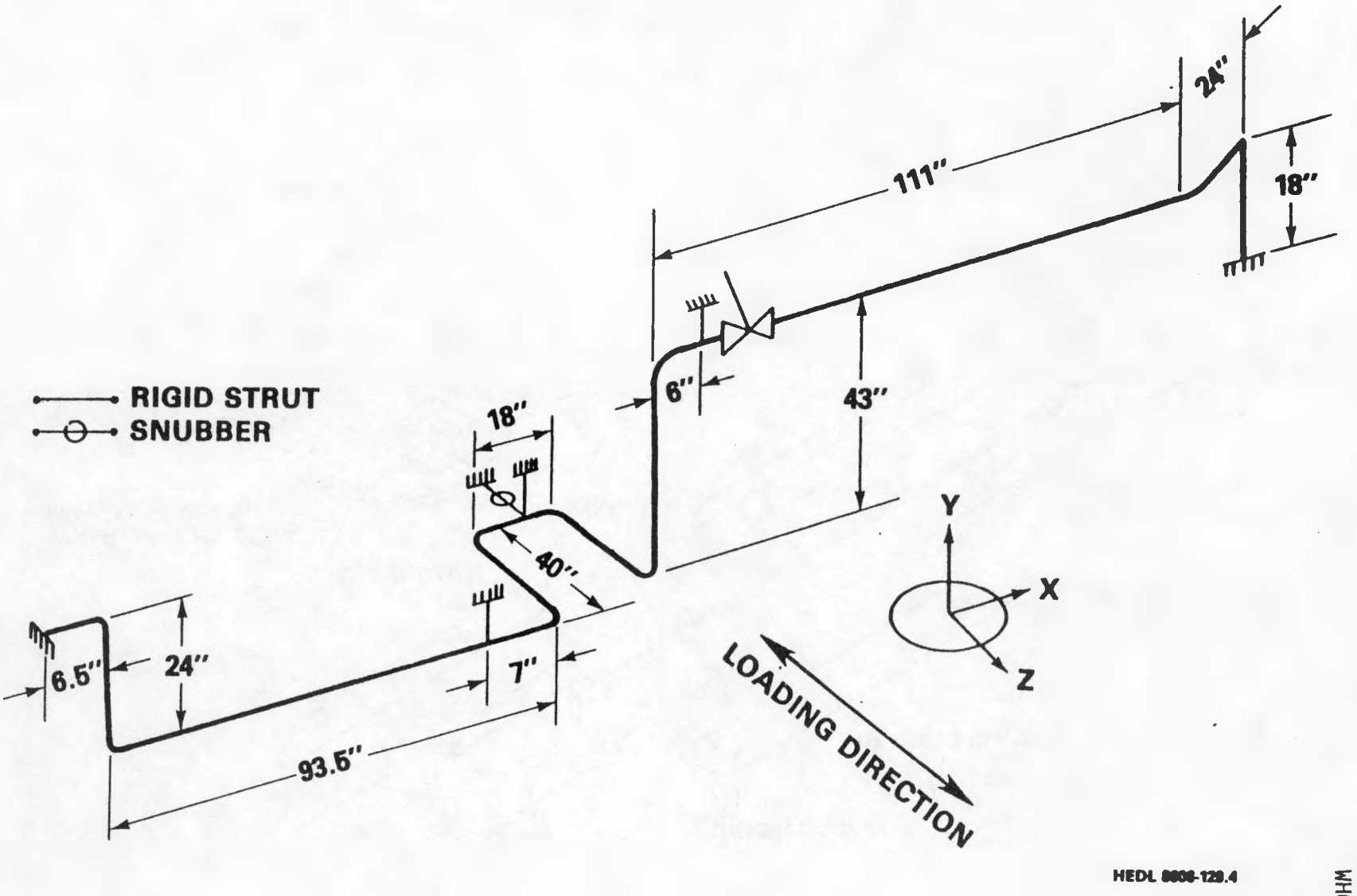

FIGURE 5-2. WHC One-Inch Diameter Pipe Loop, Support Configuration.

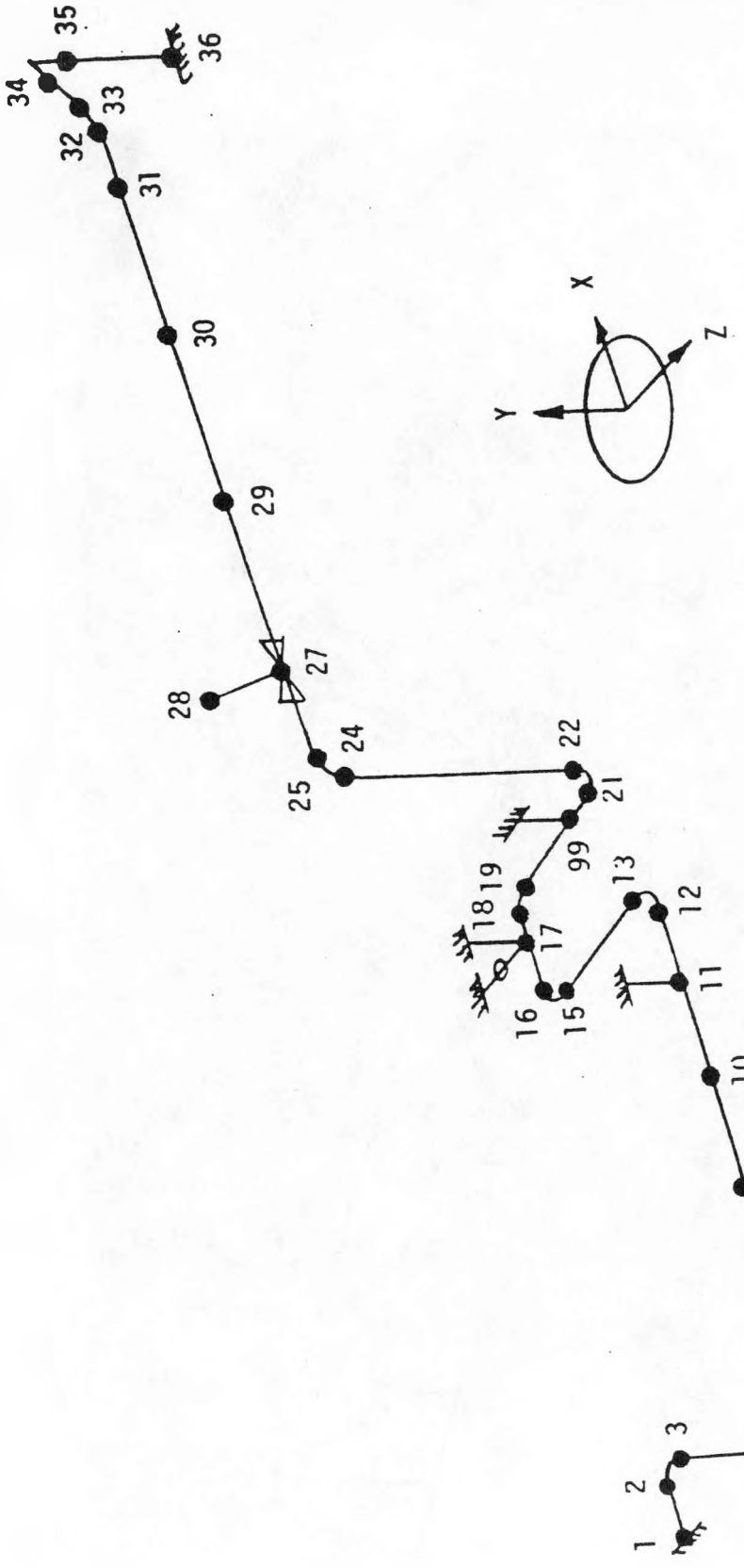

FIGURE 5-3. WHC One-Inch Diameter Pipe Loop, Analysis Model.

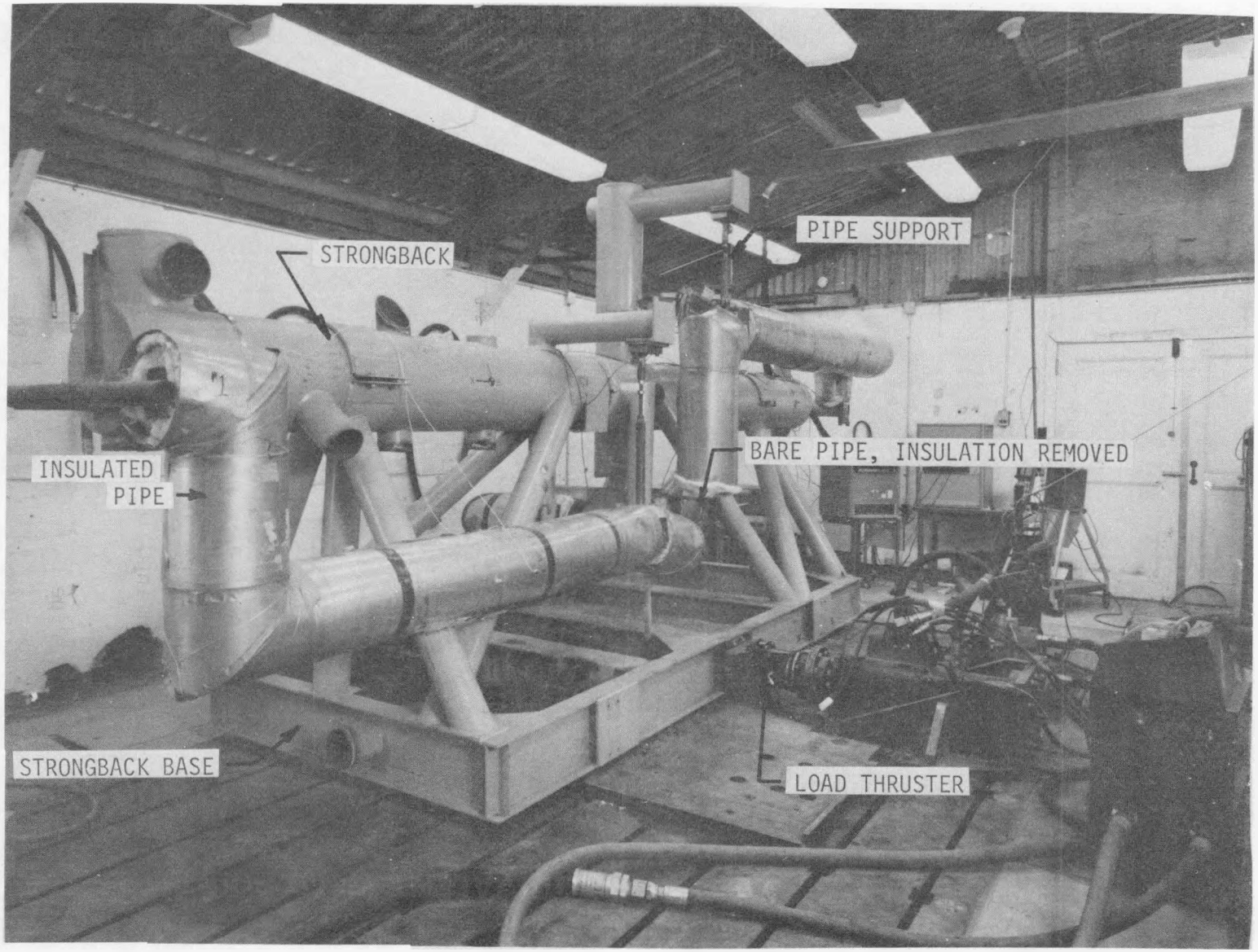

FIGURE 5-4 . WHC One-Inch Diameter Pipe Loop, Overall View. Neg 8502181-1cn

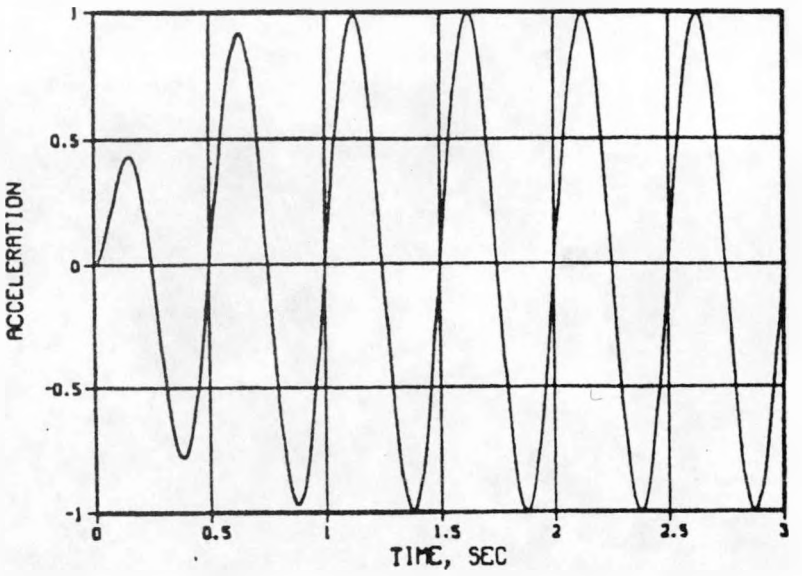

(a) Typical Nominal Exciter Input to Strongback Support Frame.

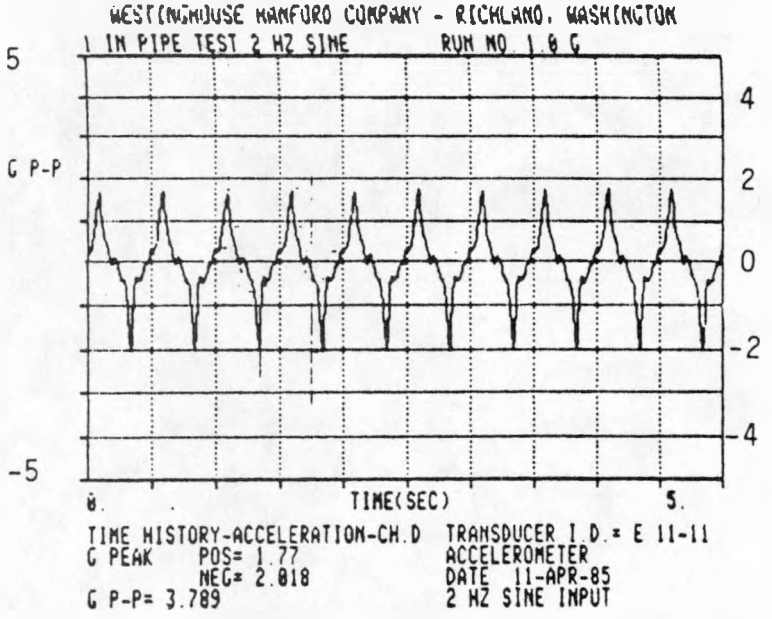

(b) Typical Excitation Input to Pipe System.

FIGURE 5-5. WHC One-Inch Diameter Pipe Loop, Typical Sinusoidal Test Loading.

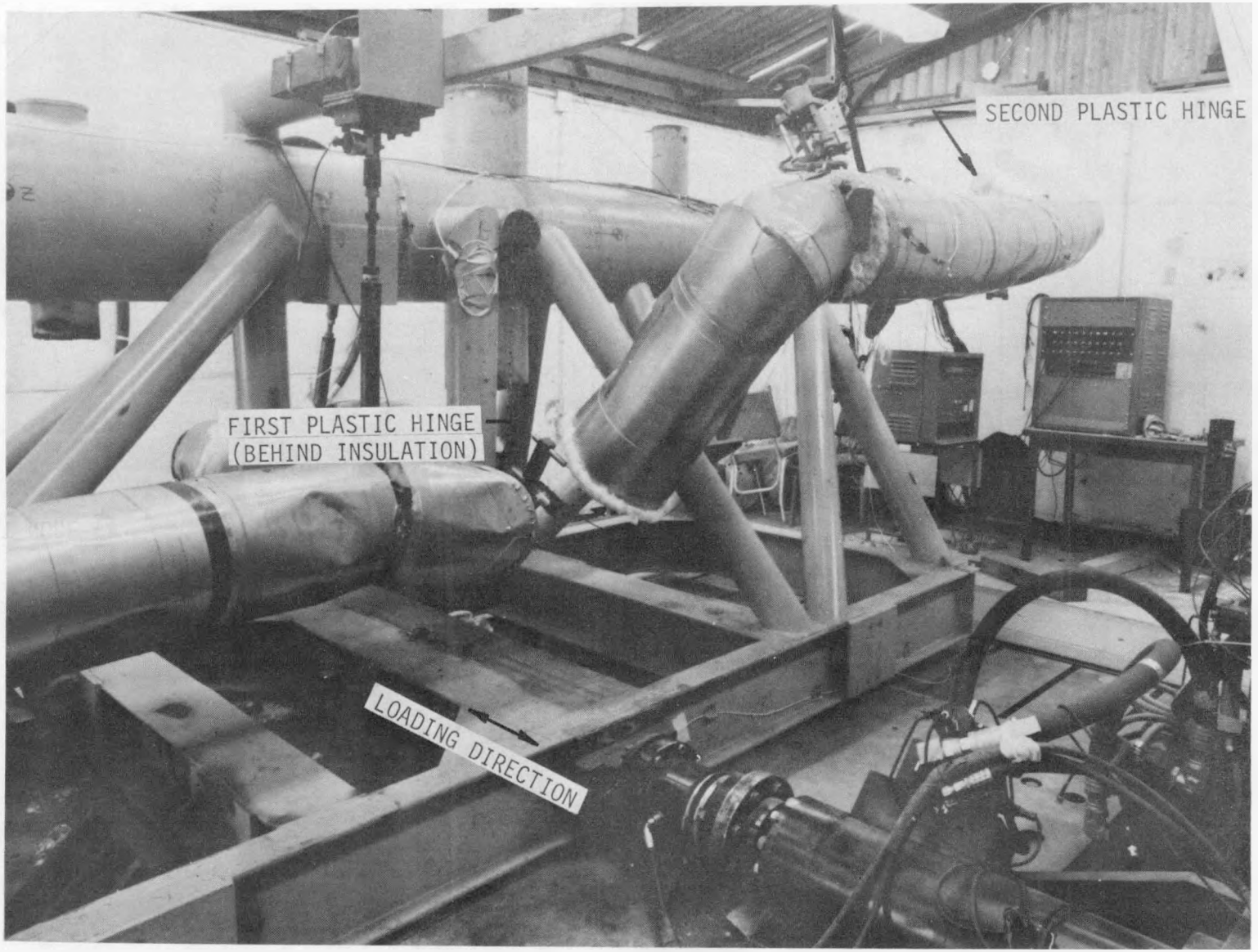

FIGURE 5-6. WHC One-Inch Diameter Pipe Loop, Permanent Displacement of Vertical Leg After High-Level Sinusoidal Testing. Neg 8502357-1cn

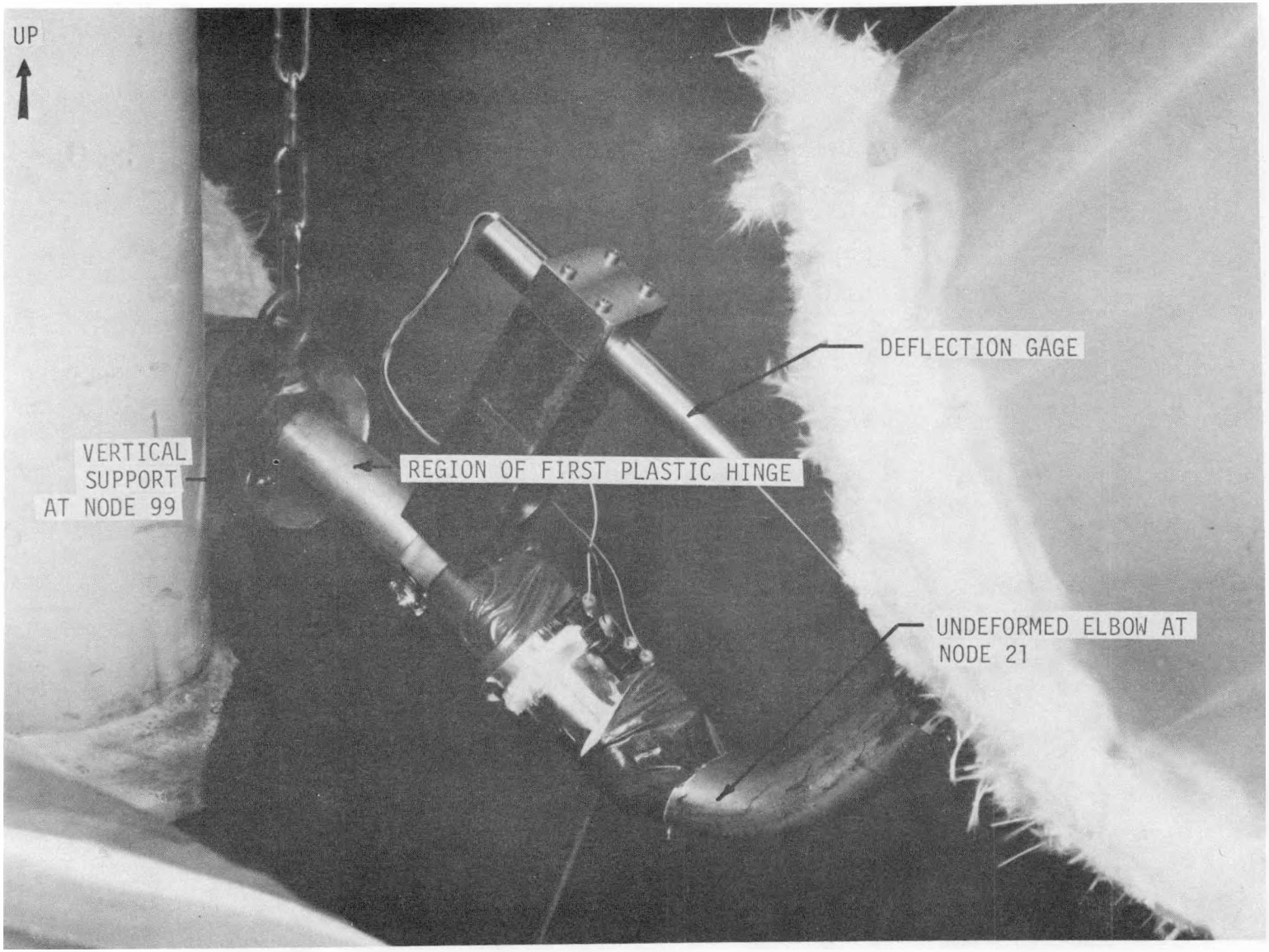

FIGURE 5-7. WHC One-Inch Diameter Pipe Loop After High-Level Sinusoidal Testing, Region of First Plastic Hinge. Neg 8502357-5cn

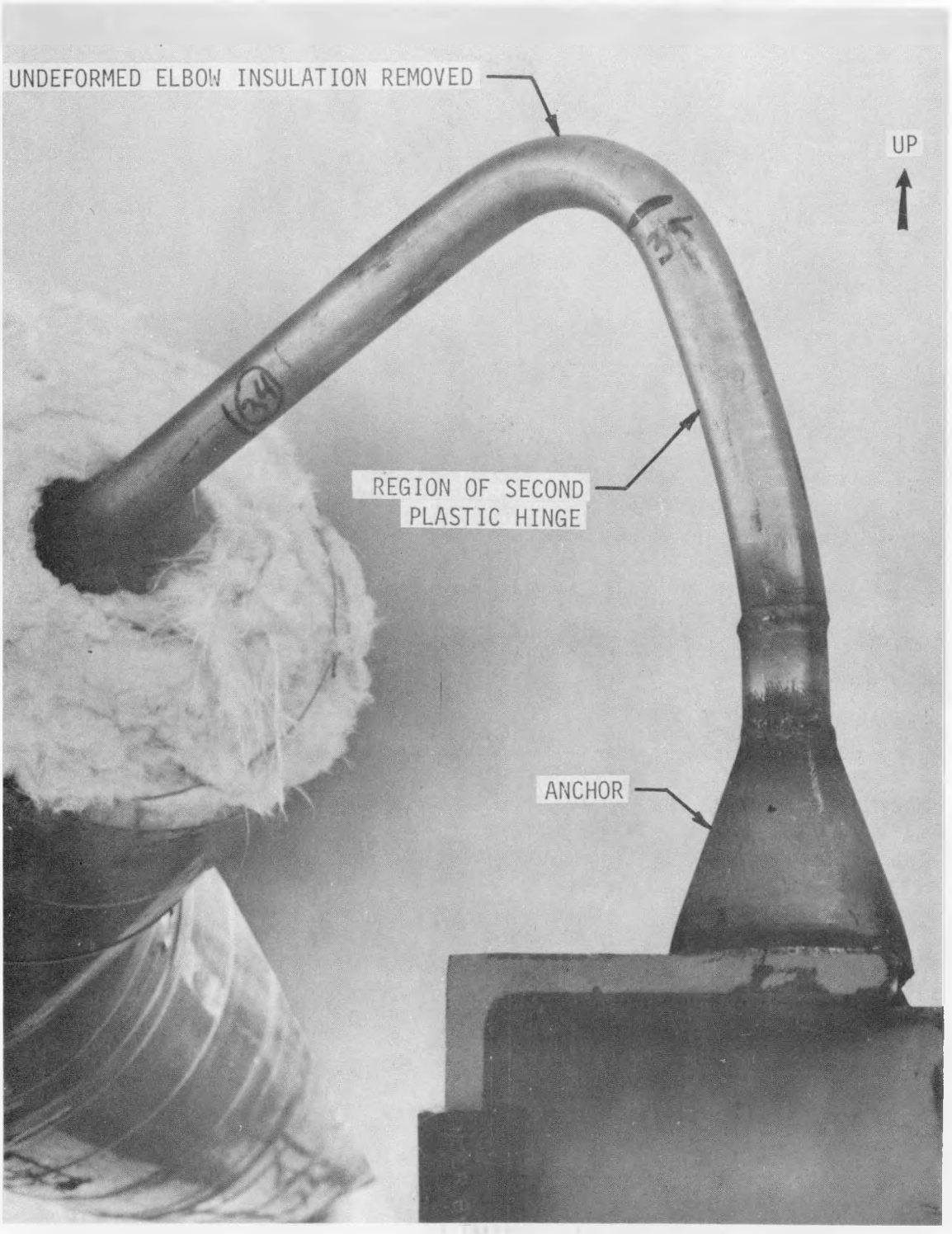

FIGURE 5-8. WHC One-Inch Diameter Pipe Loop After High-Level Sinusoidal Testing, Region of Second Plastic Hinge. Neg 8503019-4cn

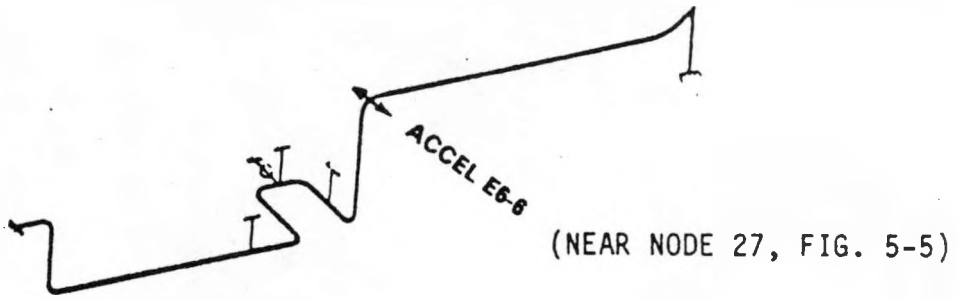

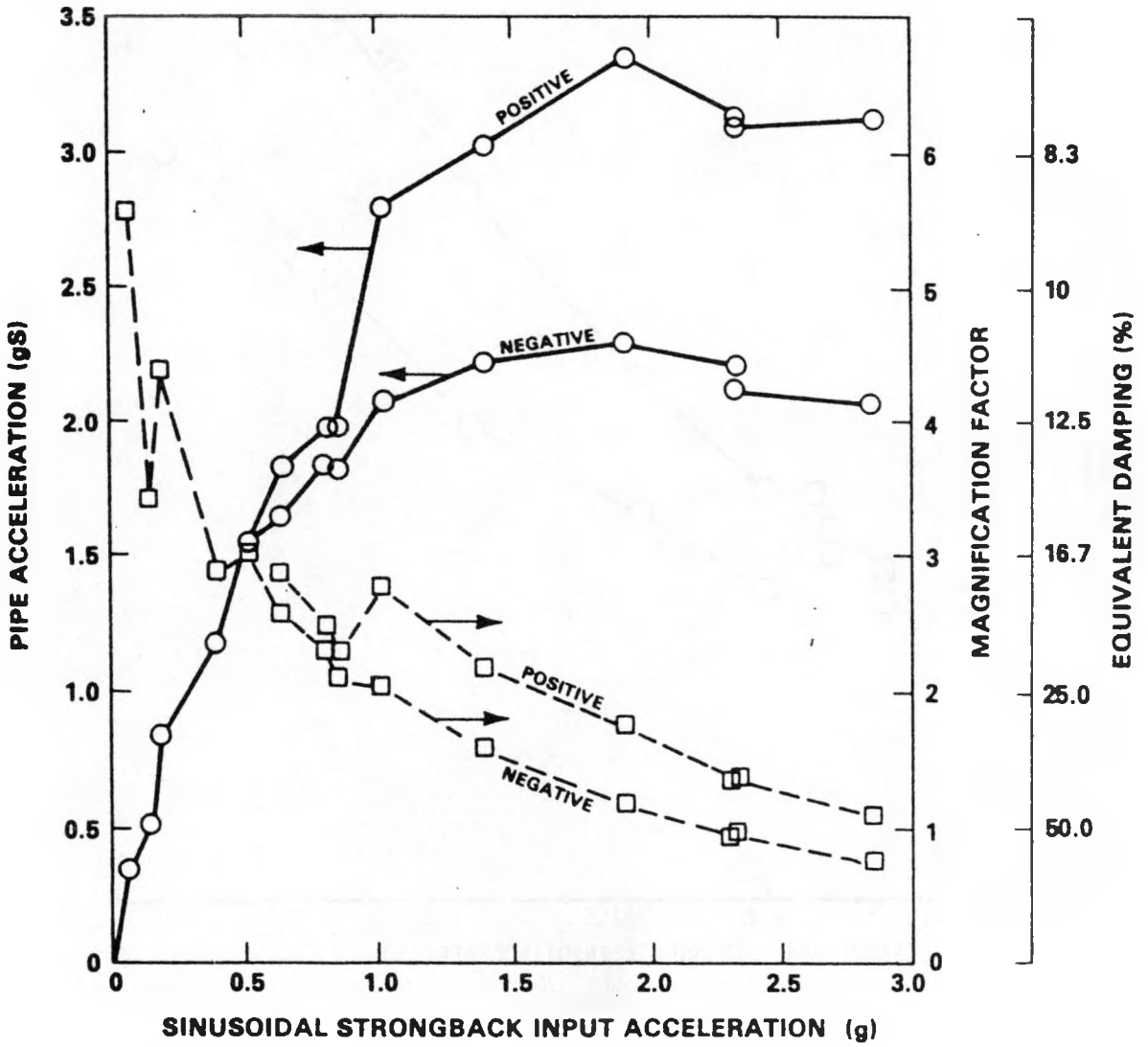

FIGURE 5-9. WHC One-Inch Diameter Pipe Loop High-Level Sinusoidal Test, Piping Response.

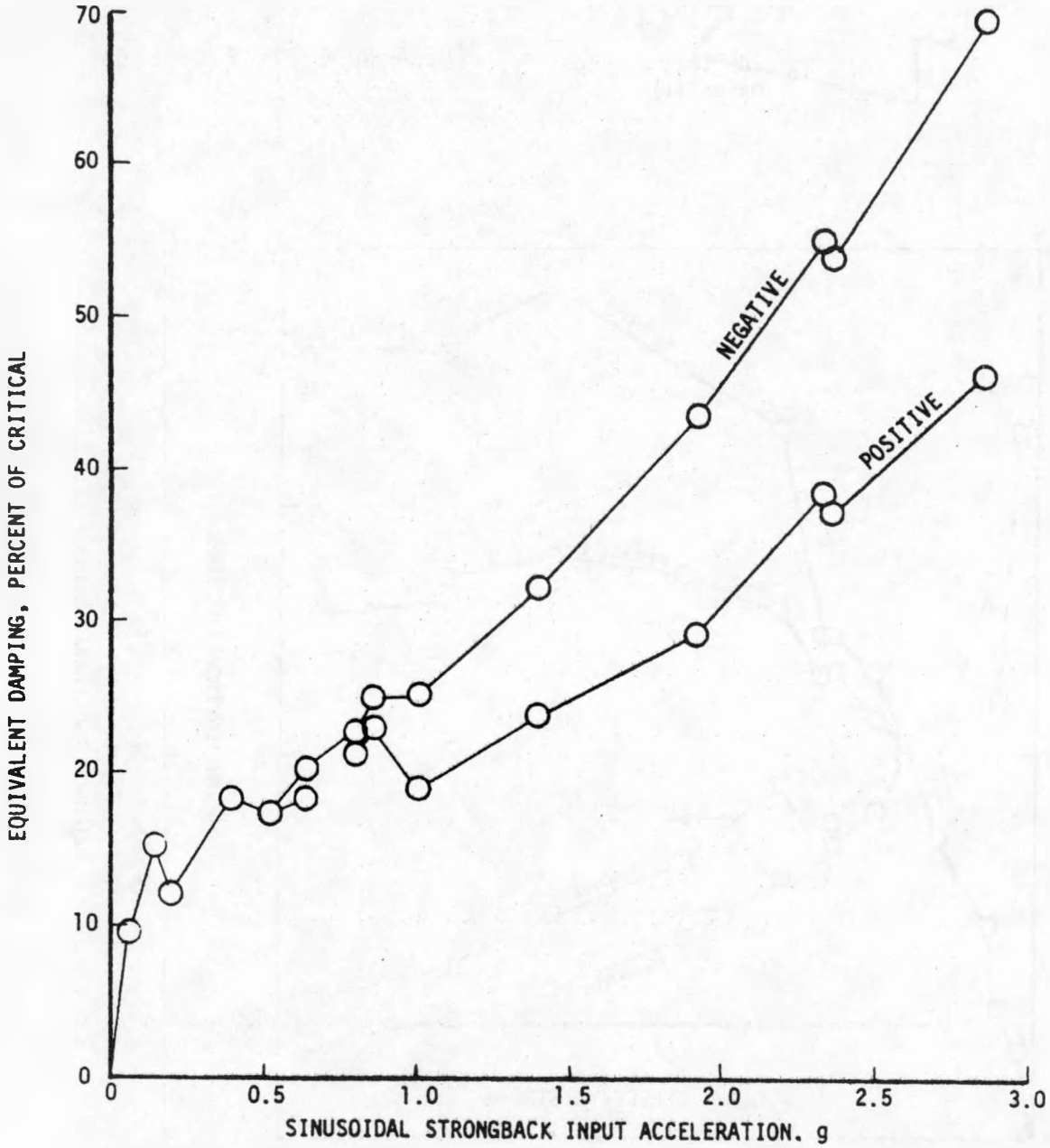

FIGURE 5-10. WHC One-Inch Diameter Pipe Loop High-Level Sinusoidal Test, Equivalent Damping.

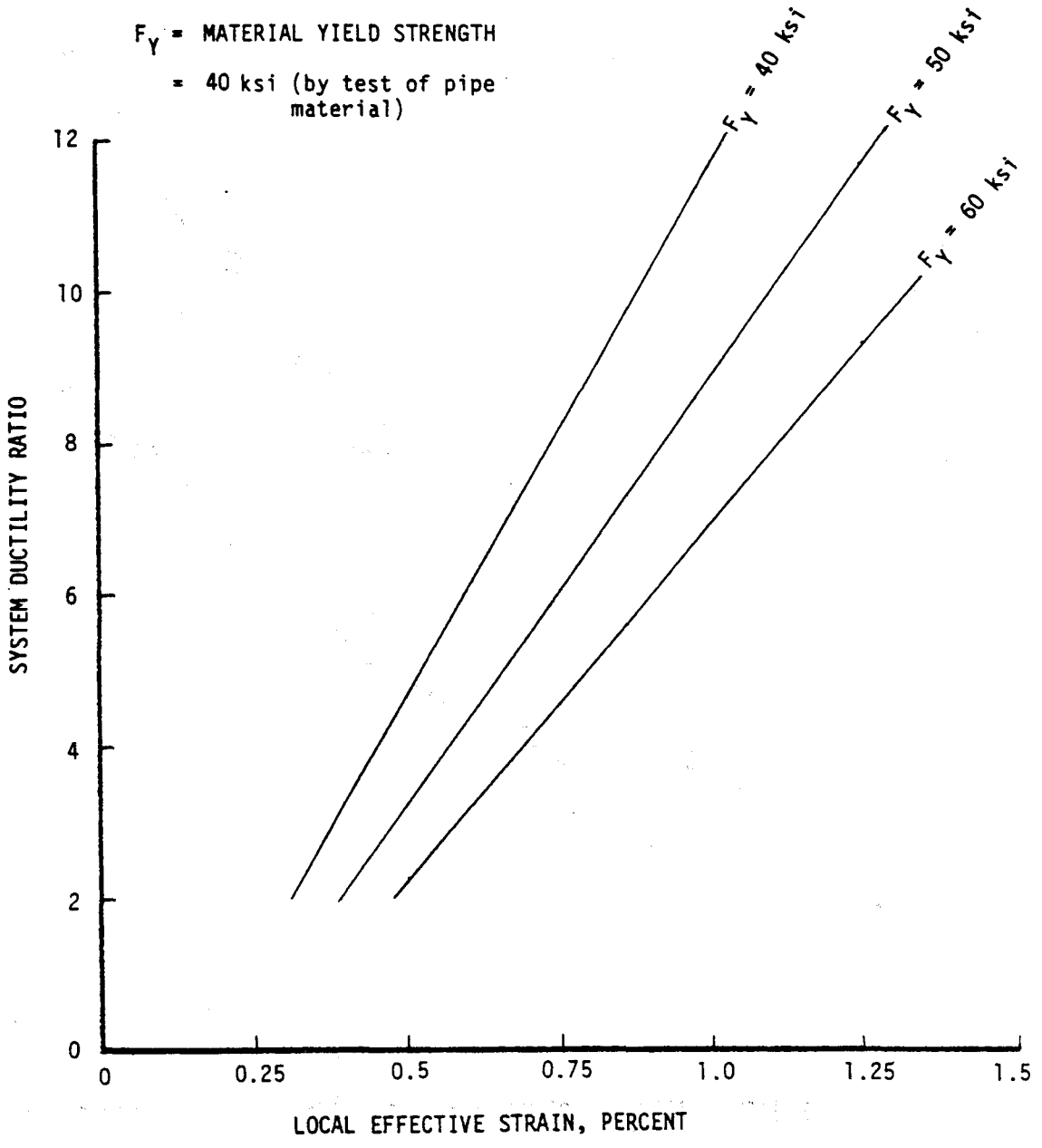

FIGURE 5-11. WHC One-Inch Diameter Pipe Loop, System Ductility Versus Local Strain.

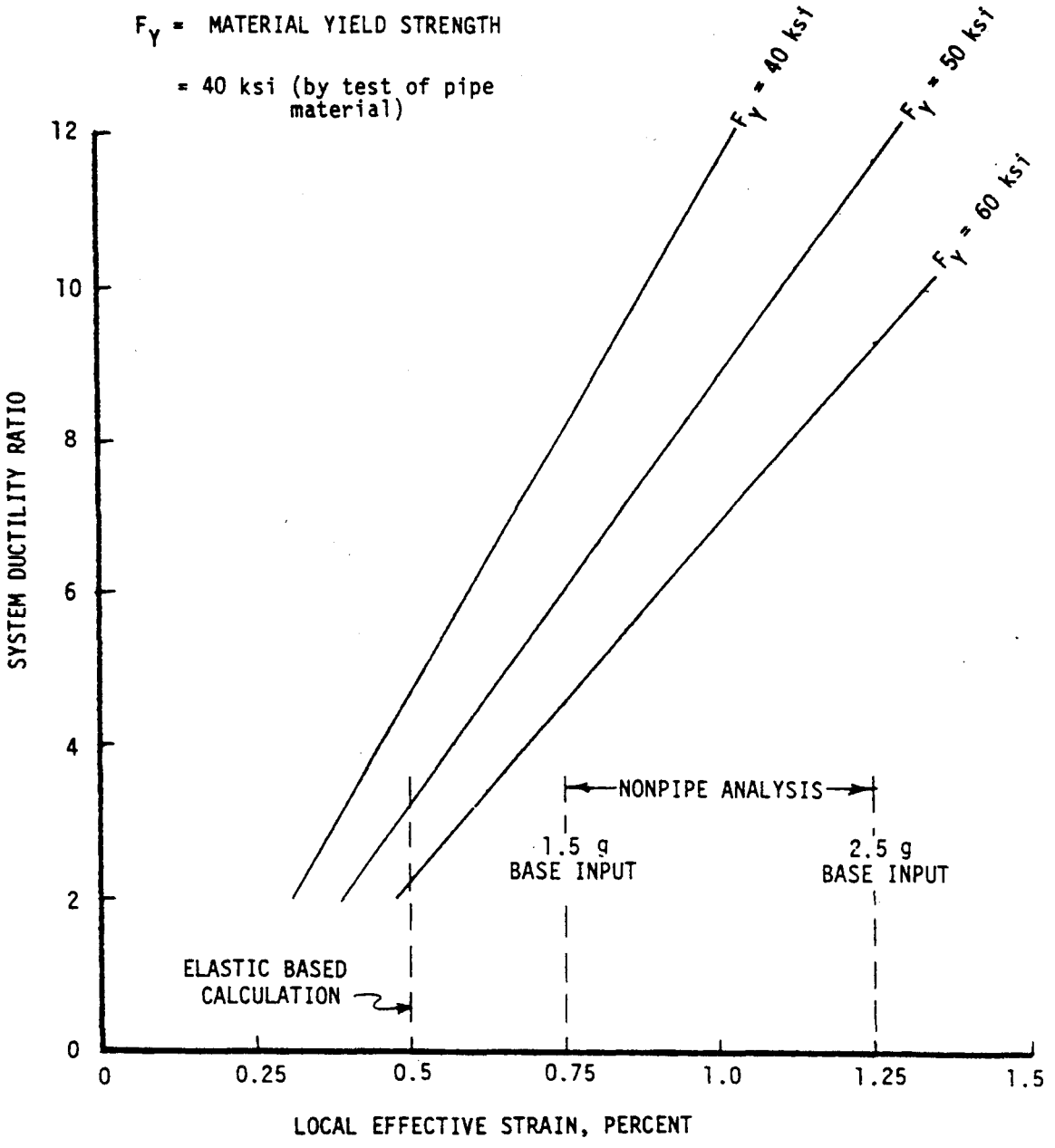

FIGURE 5-12. WHC One-Inch Diameter Pipe Loop, System Ductility Estimation.

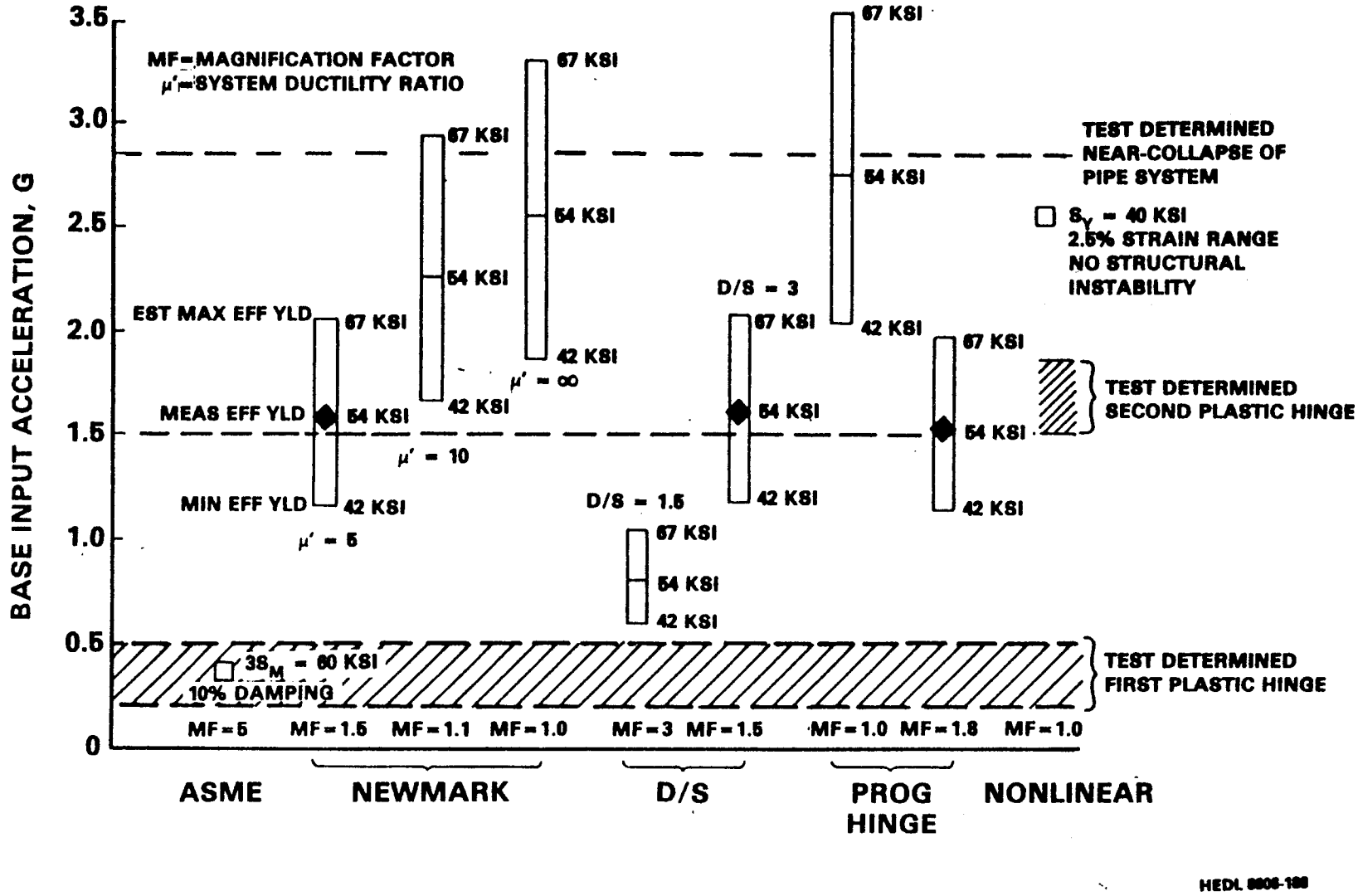

FIGURE 5-13. WHC One-Inch Diameter Pipe Loop, Summary of Failure Predictions and Test Findings.

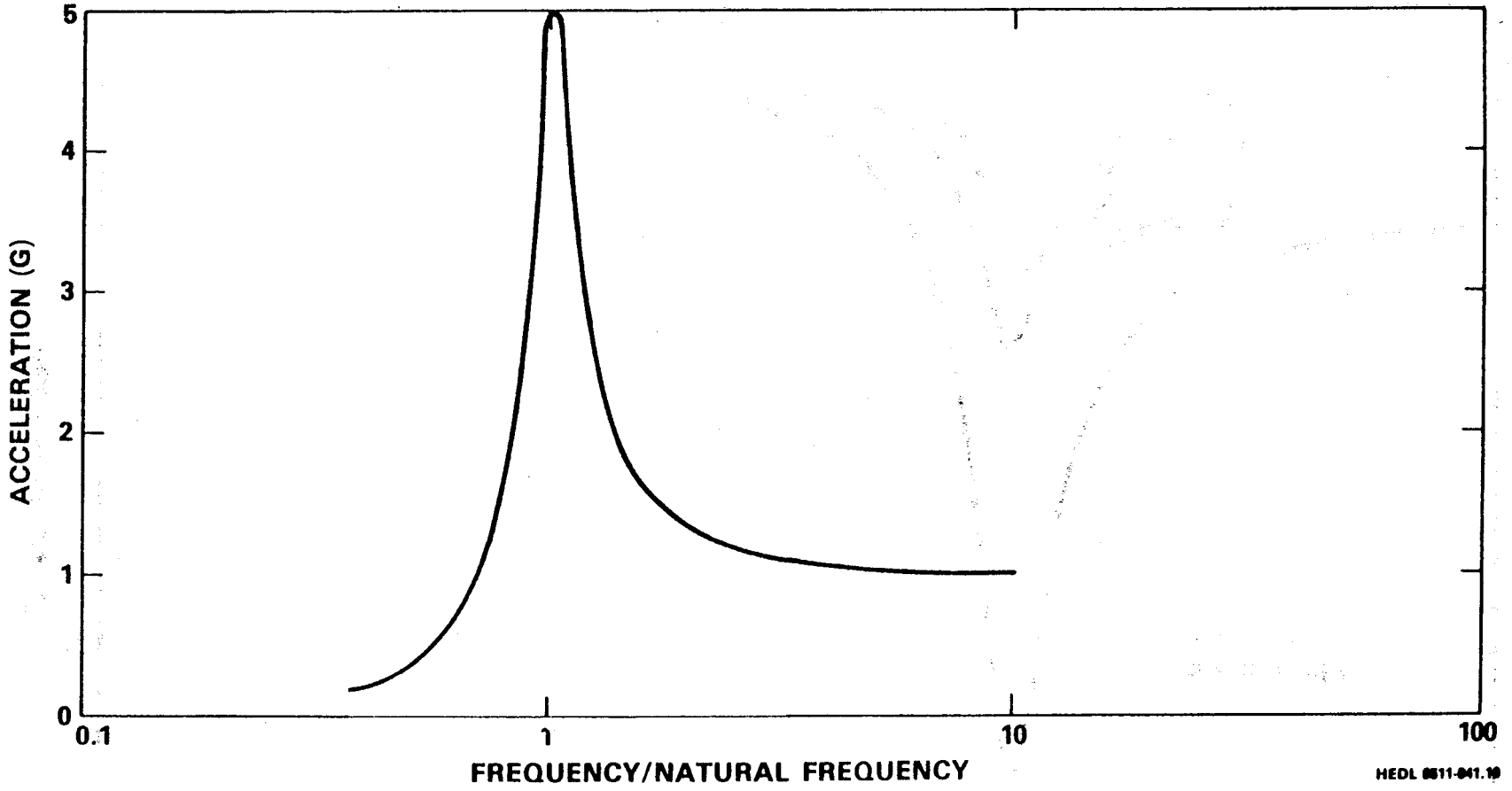

FIGURE 5-14. WHC One-Inch Diameter Pipe Loop, Two-Hertz Response Spectrum, 10% Damping.

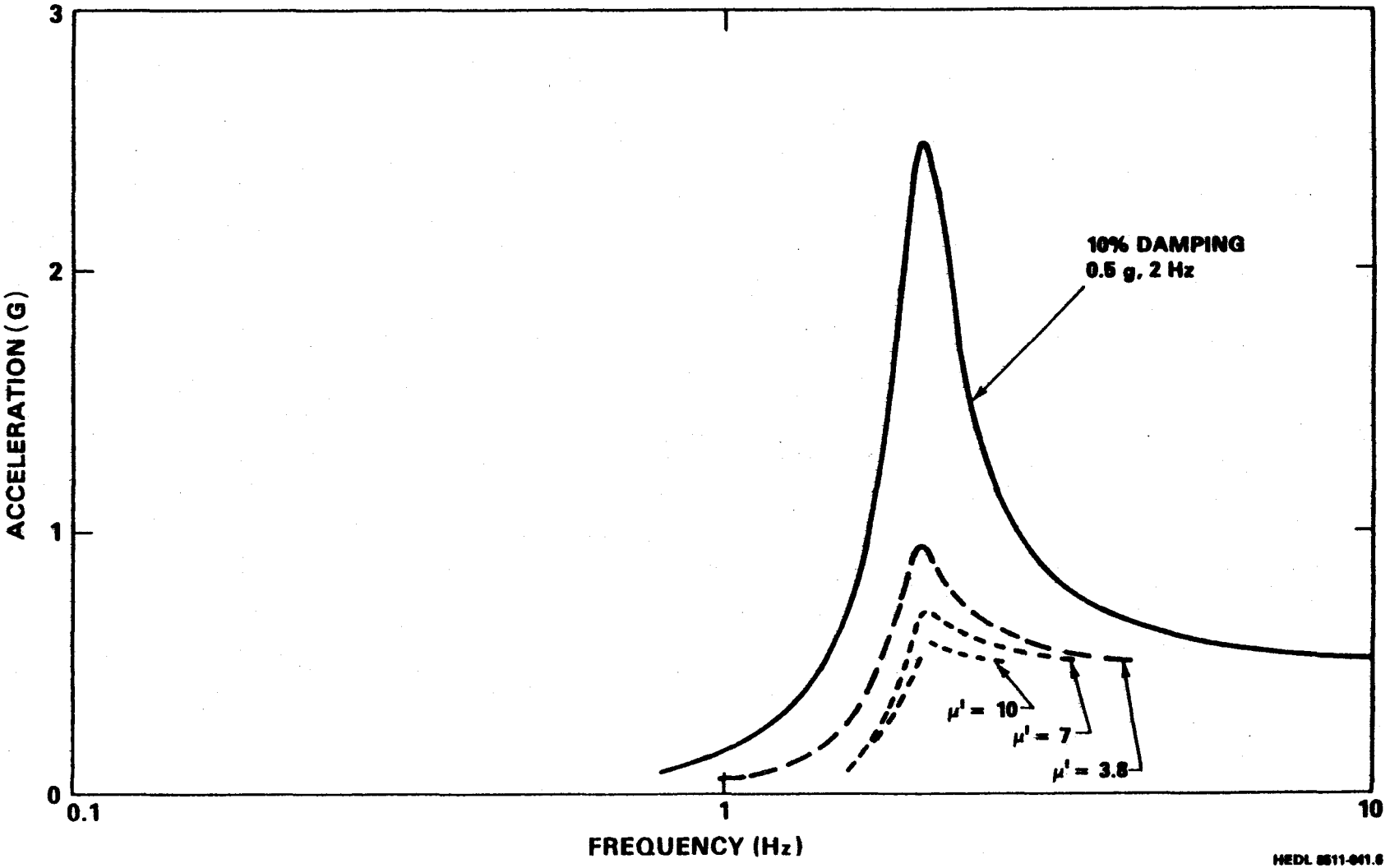

FIGURE 5-15. WHC One-Inch Diameter Pipe Loop, Elasto-Plastic Response Spectrum, Newmark Method.

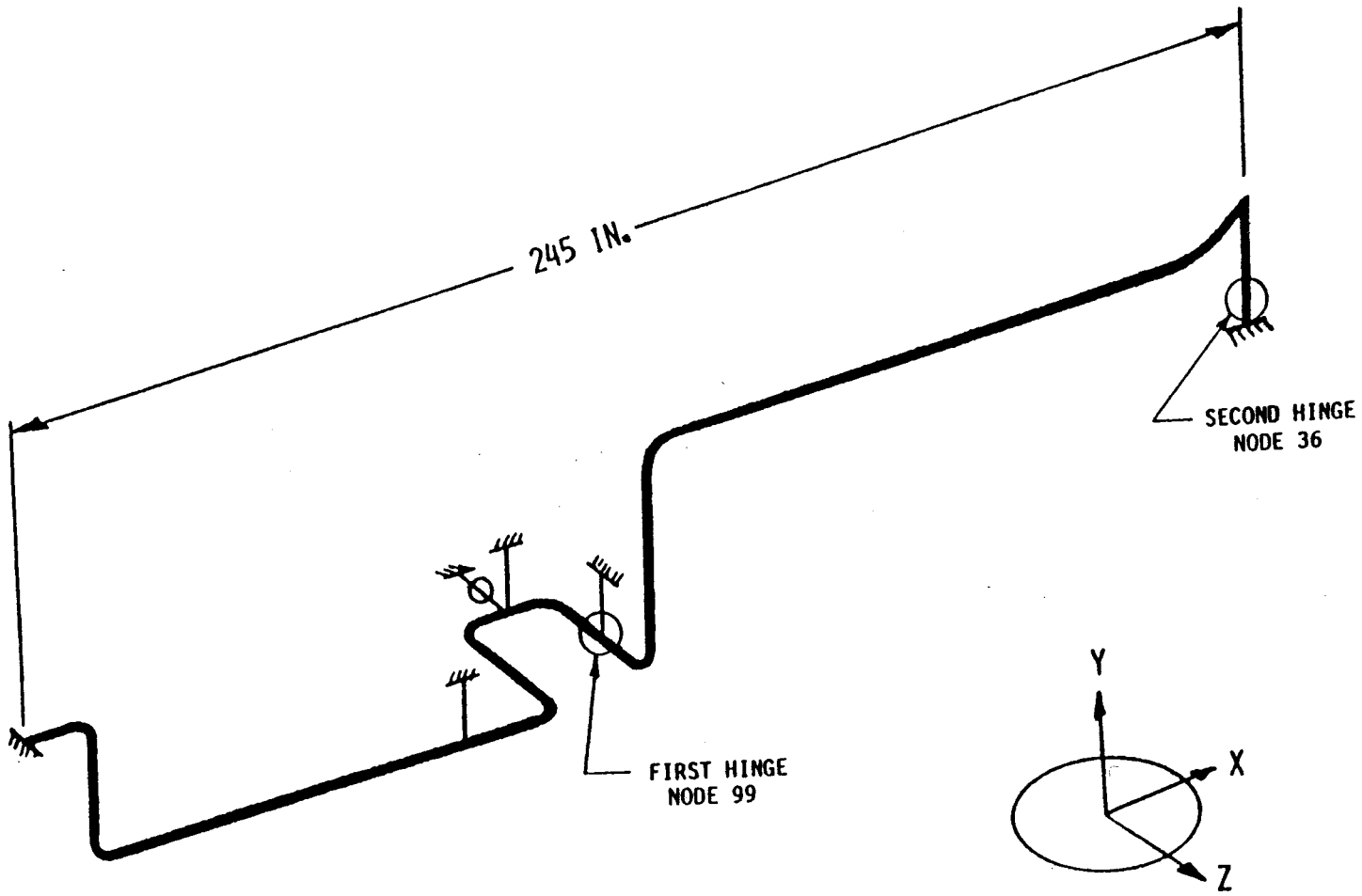

FIGURE 5-16. One-Inch Diameter Pipe Loop, Static Progressive Hinge Method.

6.0 NRC/ETEC SIX-INCH DIAMETER PIPE SYSTEM FRAGILITY TESTS

Pretest analyses were performed on the pipe loop test article configuration tested in the NRC/ETEC high-level pipe seismic test program, Reference 21. Loading for the pipe analyses included time history and response spectrum dynamic loading. Various simplified elastic methods were used to calculate load levels for collapse of the piping system.

6.1 TEST ARTICLE/STRUCTURAL MODEL

A structural model was developed for the analyses of the six-inch diameter pipe system test article used in the NRC/ETEC high-level tests. The pipe system, shown in Figure 6-1, is fabricated of 3-inch and 6-inch diameter Schedule 40 pipe. Long radius elbows are used and a dummy valve is incorporated into the system. The piping material is ASTM A-106, Grade B, with a minimum ASME Code allowable yield strength of 35 ksi and a minimum allowable ultimate strength of 60 ksi. The system was tested at room temperature under 1000 psi internal pressure, with the piping filled with oil (specific gravity = 0.9).

Figure 6-2 presents the model that was developed, based on the above information, for PIPESD computer code finite element analyses. Pressure stiffening (at 1000 psi) of the elbows was assumed to occur.

6.2 TEST LOADING

Baseline test loading for the pretest analyses consisted of the time history dynamic seismic loading base input specified in Reference 13 and shown in Figure 6-3. Response spectra corresponding to the time history are shown in Figure 6-4 for 5% and 15% damping. The ZPA of the spectra is 0.39 g's. The 5% damping value was chosen as a representative average value for low-level loading in consideration of the PVRC test data supporting ASME Code Case N-411. For sensitivity assessments, note that 15% damping significantly reduces spectra peaks in Figure 6-4.

Loading for various tests was to consist of scaled dynamic input based on the time history shape of Figure 6-3.

All elastic analyses use the 5% response spectrum of Figure 6-4, or a scaled condition thereof.

6.3 SIMPLIFIED ELASTIC AND ELASTO-PLASTIC ANALYSES

The simplified elastic methods described in Section 3.1 have been applied to the configuration and loading environment used for the NRC/ETEC six-inch

diameter pipe system high-level seismic tests. These are discussed below. The results in this section will be presented on the basis of several variables, with no failure predictions made. Levels at which failure is predicted to occur will be discussed in Section 6.7.

6.3.1 Linear Elastic Analyses

Linear elastic analyses have been performed using the PIPESD code for the structural model of Figure 6-2 under the response spectrum of Figure 6-4 with 5% damping. Stresses were calculated for the baseline spectrum and multiples thereof. The maximum stresses at several system locations, incorporating the stress indices of Section 3.4, have been plotted in Figure 6-5 with the stresses being the summation of pressure, dead weight, and seismic test loading. On the abscissa, the factor or multiplier on the baseline response spectra loading is shown. Also on the abscissa is the equivalent ZPA.

Figure 6-5 shows that the tee at Node 65 and the elbows at Nodes 71 and 59 have the maximum total stress. These locations are different than the plastic hinge locations identified later in this report. The ASME Code, Class 1, Level D allowable, 3 S_m (60 ksi), and the comparable ASME Code, Class 2 allowable, 3 S_H (45 ksi) are also shown in Figure 6-5. The allowable ZPA loading for the system is 2.0 g for Class 1 allowables and 1.4 g for Class 2 allowables.

6.3.2 Newmark Plastic Spectra Method

As discussed in Section 3.1.2, the Newmark plastic spectra method (Reference 9) uses a procedure that involves the construction of an elasto-plastic response spectra. The spectra are reduced by the factor $\sqrt{2u'-1}$, where u′ is the system ductility ratio. This reduction is applied in the region of approximately 2 hertz to 8 hertz (for a Newmark-type spectrum). Figure 6-6 presents the test baseline spectrum and reduced spectra for several values of u′. Figure 6-6 shows that, as the ductility ratio increases, the incremental change to the response spectrum becomes increasingly small. Analyses were performed using the spectra of Figure 6-6 for various values of u′.

Figure 6-7 presents the summation of NRC/ETEC six-inch diameter pipe test article pressure plus dead weight plus seismic test loading stresses as a function of factored baseline response spectra loading for a system ductility ratio of 10. Also shown is the equivalent ZPA. The tee at Node 65 is critical, with the elbows at Nodes 71 and 59 also relatively highly stressed. Figure 6-8 presents the total stress at the Node 65 tee for several system ductility ratios with similar data for the elbow at Node 71 shown in Figure 6-9. As might be expected from inspection of the spectra in Figure 6-6, the reduction in stress becomes less as higher system ductility ratios are approached.

6.3.3 Dynamic/Static Margin Ratio Method

As discussed in Section 3.1.3, the D/S margin ratio method (Reference 10) used an elastic response spectrum analysis followed by a reduction of the stress results by means of a D/S factor. This method was used to assess the components of the pipe system under the proposed test loadings.

Figure 6-10 presents the summation of NRC/ETEC six-inch diameter test article pressure plus dead weight plus seismic test loading stresses as a function of factored baseline response spectra loading for a typical D/S ratio of 4. Also shown is the equivalent ZPA. The results are similar to the Newmark method in that the tee at Node 65 and the elbows at Nodes 71 and 59 are nearly equally stressed. Figure 6-11 presents the total stress at the Node 65 tee for several D/S ratios, with similar data for the elbow at Node 71 shown in Figure 6-12.

6.3.4 Static Progressive Hinge Formation Method

As discussed in Section 3.1.4, the Reference 11 static progressive hinge formation method is based on an assessment of system stresses resulting from a static loading analysis which leads to a resulting collapse mechanism. An equivalent static loading was applied in the Z direction to the NRC/ETEC six-inch diameter pipe test article with resulting pipe stresses assessed against component capabilities.

The analysis did not consider maximum stresses at the tee (Node 65) since these represent crotch stresses in the branch pipe and not part of the main run. As such the tee does not represent an area of plastic hinge formation that would contribute directly to a collapse mechanism of the main 6-inch pipe. High stresses in the tee crotch area would be expected to cause collapse of the branch piping. The moment capability of the elbows included a factor of 1.5, which resulted from the Reference 22 comparison of limit moments on carbon steel elbows. Additionally, an examination of elbow moment-rotation plots for typical 4.5-inch elbow tests indicated moments at loss of load-carrying capacity are approximately 15% higher than moments at twice the angle at loss of linearity. The elbow moment collapse factor was therefore taken to be: $1.5 \times 1.15 = 1.7$. The 1.5 factor alone was used for straight pipe.

The analysis considered pressure plus dead weight plus seismic test loading and indicated first hinge formation at straight pipe Node 10, with a second hinge forming at elbow 59-61 (see Figure 6-13). Any additional hinge formation beyond these two locations resulted in an unstable system. A

summary of the various g levels at which the hinges formed is shown in Table 6-1 for several assumed yield stress values. The accelerations of Table 6-1 represent loads on the pipe itself and not base input values. To obtain the latter value, the magnification factor for the system must be determined.

6.4 NONLINEAR TRANSIENT DYNAMIC INELASTIC ANALYSES

Detailed nonlinear transient analysis was carried out with the NONPIPE computer program (Reference 12) to provide an estimate of strains occurring at various load levels. Runs with ZPA up to 30 g show a much more gradual increase in strain versus load level than is found in static analysis.

6.4.1 NONPIPE Program Description

The NONPIPE computer program provides a simplified means of inelastic dynamic analysis of piping systems by the uncoupling of bending, torsion and axial responses. Nonlinearities include material plastic response and geometric gap elements. By uncoupling the moment and axial responses, bending definition in the plastic range may be specified by trilinear response of bending and torsion components, and there is no need for the program to track the deformation state at many integration points over the pipe cross section. The trilinear response is displayed in Figure 6-14 in terms of the sum of three parallel components. Cyclic response is described in Reference 23. Essentially, the radius of curvature of the response curve is doubled after initial loading. This is typical of cyclic stress-strain curves.

NONPIPE analysis is carried out by the direct stiffness method with a trapezoidal rule for the time marching algorithm. The tangent stiffness approach is used for nonlinear effects, and the stiffness matrix is modified each time a change of the yield status occurs. Equilibrium errors found after completing a time step are applied as corrective loads in the next step. The piping system analyzed herein is a narrow band structure that results in the structural matrices fitting in core. Viscous damping (alpha-beta damping) is proportional to the mass and tangential stiffness matrices. Energy dissipation caused by plastic work is inherent to the time marching procedure and is a form of dissipation in addition to the viscous damping. Gap elements are available, but they are not used in this analysis.

6.4.2 Line Modelling

The piping system is a six-inch Schedule 40 line with a three-inch branch as shown in Figure 6-1. The minimum ASME Code allowable yield strength of 35 ksi for the ASTM A-106 Grade B material is increased to 44 ksi to represent an average value. The piping is filled with oil at a 0.9 specific gravity and 1000 psi pressure. The modulus of elasticity is 28E6 psi, and the plastic modulus in the bilinear stress-strain curve is 28E4 psi.

The moment-curvature relation for straight pipe sections was calculated using beam theory and the stress-strain curve in a short Fortran program that integrates the forces around the section of the pipe. The result for monotonic loading of six-inch pipe is shown in Figure 6-15, along with the trilinear approximation used in NONPIPE. Torsional response is not as important as bending. The second yield point in torsion was determined from the 0.2% yield stress converted to torsion with the Mises criterion and a plastic section modulus, as shown in Reference 12. Slopes were scaled from bending slopes with the proper elastic slope as reference.

Elbow elements require consideration of ovality and collapse, in accordance with Reference 18 (NB-3680) and Reference 24. Beam elements with appropriate section properties were used. From Reference 18, the stress intensification and flexibility factors are B_2 = 3.69 and k - 6.07, respectively.

Elastic analysis of the system indicates that the worst elbow loading is out-of-plane. Reference 24 provides load-deflection data for a six-inch elbow with similar geometry and material (Specimen PE3). Moment-rotation response is shown in Figure 6-16. Extrapolation to higher rotations and a collapse moment is done with the Southwell method of Reference 25. The trilinear fit shown in Figure 6-16 was scaled to account for minor differences in yield stress and pressure. The torsional relation was the same as the straight pipe.

Pipe nodes used in elastic analysis of the line are shown in Figure 6-2. The same node numbers were used in the NONPIPE analyses, and refinement is provided in critical areas. The refinement resulted in straight pipe spans of 7 in. or less in critical areas, while elbows with significant loads were refined with four segments. The importance of the refinement is based on the tendency of a plastic hinge to localize in the area of a maximum moment. Once refined, the grid was run on NONPIPE with the three 1 g inertial loadings and checked against the PIPESD (Reference 15) results.

Proportional (alpha-beta) damping is based on a minimum fractional damping of 5% at the 4.8-hertz natural frequency of the elastic system.

6.4.3 Loading

Static loading consisted of a fixed 1 g Y gravity loading along with a variable inertial load in the +Z direction. This inertial loading was obtained by assigning very large time steps to a transient run in which the inertial loading was gradually increased. The full transient loading for the test configuration is illustrated in Figure 6-3. Only the first burst of high acceleration data between 3.3 s and 4.8 s is used. The data contains the maximum acceleration in the 25 s excitation and is shown in Figure 6.17. It is applied in the Z direction, and a fixed 1 g Y gravity loading is applied as well. The transient amplitude is scaled in a series of runs to

determine the response of increasing levels of horizontal excitation. Each load level starts with an unreformed system contrary to the testing. Table 6-3 gives load levels, time step data, and durations. The very small steps required in the higher load levels are associated with the equilibrium corrections. Spurious results were found at the 0.001 time step as soon as the upper My2 yield point was exceeded.

6.4.4 Results

Results of the static horizontal inertial loading for the two worst points are shown in Figure 6-18. Load levels at which yielding takes place are easily detected by sudden convex turns. Strain increase is rapid after 9.6 g where a near-failure mechanism has formed with hinges at Nodes 10 and 59.

Maximum strains during transient loading are shown in Figure 6-19 for the two worst points in the line. Load levels at which yielding takes place are shown by the node number and yield point number 1 or 2 (see Figure 6-14). Although the elbow and straight pipe sections start yielding at nearly the same load level, the elbow shows substantially less response at the higher excitation levels. Figure 6-20 shows a similar plot but with strain range on the ordinate. The range is the largest accumulation in the history without reversal, e.g., from 0.92 s to 0.98 s in the strain-time plot of Figure 6-21. At the highest level of excitation, the range is almost the same as the maximum value.

6.5 NRC/ETEC TEST ARTICLE PARAMETERS

As discussed in Section 3.0 and calculated in Section 5.2, implementation of the Newmark and D/S methods requires that the parameters of system ductility and effective yield point be defined. Calculations of these for the NRC/ETEC six-inch diameter test article are discussed below.

6.5.1 System Ductility Calculations

A series of calculations were performed to estimate the system ductility for the NRC/ETEC six-inch diameter test article. The calculations used the formula discussed in Section 4.0 to obtain the system ductility results. Local strains were also calculated.

A 1 g lateral load was applied to the structural model of Figure 6-2 to obtain stresses and deflections assuming linear, elastic response of the structure. The most highly stressed location (Node 10) was identified and a plastic moment hinge was assumed to occur at this point. Additional static analyses were made with the moment hinge at Node 10 to approximate elasto-plastic response of the system.

The weighted mass displacement parameters and the steps discussed in Section 5.2.1 were used to calculate system ductility of the NRC/ETEC six-inch diameter test article.

The local effective strain at the hinge location was calculated for the various loading conditions based on analytical results. The calculations used a summation of elastic-plus-plastic strain as discussed in Section 5.1.

A strain concentration factor of 2 was used to calculate the strain in the plastic region, as suggested in Reference 16.

The results of the system ductility calculations, along with corresponding local strain, are plotted in Figure 6-22. The significance of Figure 6-22 will be discussed in Section 6.5.3.

6.5.2 Equivalent Yield Point Calculations

The equivalent yield point, R_e, based upon the equivalent elasto-plastic response of a material (as discussed in Section 3-2), has been calculated for the NRC/ETEC test article.

The test article is fabricated from ASTM A-106 Grade B carbon steel. This material has a minimum ASME Code allowable yield strength of 35 ksi, a corresponding minimum ultimate strength of 60 ksi, and expected elongation at failure of 22%. An average yield value would be expected to be approximately 43 ksi, an average ultimate to be 30%. The equivalent yield point was calculated using the approximate formula of $R_e = S_y + 0.25$ $(S_u - S_y) = 53$ ksi, using the properties shown in Table 6-2.

A $\pm$25% variation on yield strength was assumed to estimate maximum and minimum yield points.

6.5.3 Estimate of System Ductility

The results of the general system ductility calculations and the equivalent yield point structural material calculations can be used to estimate the system ductility for the NRC/ETEC test article. As shown previously, the value of system ductility is needed to properly utilize and implement the Newmark and the D/S simplified methods.

In comparing the calculated system ductility for the NRC/ETEC test article (Figure 6-22), it is seen that, for a calculated local strain of 1.8% corresponding to a 20 g shake test given strain, the system ductility for the NRC/ETEC test article is approximately 10. The WHC one-inch test system ductility was calculated to be in the 5 to 10 range. Since the NRC/ETEC test article has more areas of equal stress, it would be expected that the system ductility would be higher than for the WHC one-inch test loop. For purposes

of collapse prediction, then, the system ductility of the NRC/ETEC test article will be chosen to be 10, which is twice that used in the collapse evaluation of the WHC one-inch high-level dynamic test results (Section 5.3).

Additional considerations follow from the inelastic analyses results described in Section 6.4. The maximum strain amplitude calculated dynamically (Figure 6-19) was 3.5% for base input accelerations above 20 g's. Taking the yield strain equal to 53 ksi/E = 0.2% leads to a ductility ratio of 17.5. If one considers the static inelastic analyses results (Figure 6-18), the strain for initial yield (first hinge) was 0.2% and the strain grew to 3.0% when the second hinge developed. This corresponds to a ductility ratio of 15.0.

6.6 PROBABILISTIC RISK ASSESSMENT-TYPE FRAGILITY ESTIMATES

Probabilistic risk assessments of the test article are made using the methods described in References 13 and 14. Reference 13, referred to by the author as the Zion method, determines the fragility of a piping system by estimating the median safety factor and logarithmic standard deviation. The latter are determined from analysis of a number of typical piping systems. Reference 14, the SSMRP method, is similar except that analysis of the piping system under consideration is used.

6.6.1 Test Article Fragility Using the Zion Method

The Zion method considers the capacity of the piping, supports, anchors, equipment, and structure response factors. These are expressed in terms of a median safety factor, $\bar{F}$, and logarithmic standard deviations of randomness, β_R, and uncertainty, δ_U. Reference 10 has been used extensively to obtain typical values of various parameters.

6.6.1.1 Piping Capacity Factor

The piping capacity factor consists of a strength factor, inelastic energy absorption factor and a three-hinge factor.

Strength Factor ($\bar{F}_S$) -- Two extreme conditions are considered. A two-logarithmic standard deviation ($+2\beta$) upper bound assumes the entire pipe cross section is at the flow stress level which is defined as the midpoint between yield strength and ultimate strength. The lower bound (-2β) considers a piece of straight pipe with a circumferential flaw of length equal to six times the wall thickness which is considered to bound the possible flaws occurring at a butt welded joint. This results in a median collapse load of 3.11 times the ASME Code yield with an estimated of 0.16. It is assumed that the median yield is 1.25 times the Code yield.

An estimation of the relative magnitudes of sustained stress and seismic stress in terms of Code allowable are made assuming a Class 2 piping system with the upset condition governing (Pressure + Dead Weight + OBE).

This results in a median strength factor of safety, F_2 of 8.04 and a β of 0.36 which is considered to be all uncertainty, i.e., $\beta_R = 0$ and $\beta_U = 0.36$.

For thin-walled pipe (Schedule 40 and Schedule 80), Reference 13 states that buckling will occur before flow stress is reached. For this case the median pipe capacity is taken at 1.5 times the yield moment. An analysis similar to the above results in an F_S of 4.3.9 with $\beta_R = 0$ and $\beta_U = 0.36$.

The ETEC test piping consists of 6-inch and 3-inch Schedule 40 pipe with an internal pressure of 1000 lb-in^2. The internal pressure, in addition to reducing the compression stress, has a stiffening effect; therefore, the prediction will be based on F_S of 8.04.

The design response spectra (0.4 g) is taken as the SSE. It is assumed that the OBE is 1/2 x SSE or 0.2 g.

Inelastic Energy Absorption Factor ($\overline{F}\mu$) -- Based on Newmark's recommendation of a ductility ratio of 1.5 to 3.0 for design, a median factor, $\overline{F}\mu$, of 2.24 with $\beta_R = 0.16$ and $\beta_U = 0.16$ is derived. This is based on the ductility ratio of 3.0 being a median value and 1.5 being a lower bound (-2β). $\overline{F}\mu$ is calculated from $F\mu = \sqrt{2\mu - 1}$, where μ is the ductility ratio.

Three-Hinge Factor ($\overline{F}$ sys) -- For a piping system to completely collapse, usually more than one plastic hinge must form. An upper threshold ($+2\beta$) is likened to a fixed-fixed beam where three hinges must form, and the elastically calculated maximum moment would be 1.5 times the pipe element collapse moment. The lower threshold (-2β) is like a simple beam where only one hinge is required for collapse. This results in F_{sys} of 1.22, $\beta_R = 0$ and $\beta_U = 0.10$.

6.6.1.2 Support Capacity Factor

The support capacity factor consists of a strength factor and an inelastic energy absorption factor.

Strength Factor ($\overline{F}s$) -- This is derived based on the upset condition and assumes that a fillet weld is the most critical item. Assumptions are also made as to the magnitudes of sustained and seismic stresses relative to Code allowable, The resulting F_S is 3.26 with $\beta_R = 0$ and $\beta_U = 0.29$.

For the ETEC test, it will be assumed that the one support is stronger than the piping system.

Inelastic Energy Absorption Factor ($\bar{F}_\mu$) -- This is based on some inelastic energy absorption in yielding of the fillet welds. $\bar{F}_\mu$ is estimated to be 1.50 with β_R = 0 and β_U = 0.16.

6.6.1.3 **Anchor Capacity Factor**

The anchor capacity factor consists of a strength factor and an inelastic energy absorption factor.

Strength Factor ($\bar{F}_s$) -- Wedge-type anchors are required to have a factor of safety of 4.0 based on median ultimate capacity. It is estimated that the median load is 70% of the design allowable. This results in F_s of 5.70, with β_R taken as 0 and β_U as 0.30.

This is not considered for the ETEC test since no wedge-type anchors are used.

Inelastic Energy Absorption Factor (F_μ) -- If the wedge anchor fails while the piping is still elastic, the failure mode is brittle and $\bar{F}$ = 1.00. If the piping is highly inelastic, the calculated support load would not develop and the value of F_μ for the piping, 2.24, is appropriate. If these are considered $\pm 2\beta$ values, the resulting $F_\mu$is 1.50 with β_R = 0.15 and β_U = 0.15.

6.6.1.4 **Equipment Response Factor**

This factor consists of a number of items, which are discussed below.

Qualification Method Factor -- Piping is currently qualified by response spectrum analysis, and is considered to provide a median centered estimate of piping response. Thus a median factor of 1.0 with zero variability is considered appropriate.

Spectral Shape Factor ($\bar{F}SA$) -- This accounts for the conservatism involved in developing the floor response spectra from the ground response spectra. It includes the effects of peak broadening and smoothing ($\bar{F}_{PS}$) and generation of artificial time-history ($\bar{F}_{ATH}$) that envelopes the applicable ground spectra.

Comparison of a large number of floor response spectra before and after peak broadening and smoothing results in a value of $\bar{F}_{PS}$ of 1.26 with β_R = 0 and β_U = 0.13.

Studies (Reference 13) estimate the conservatism to generate an artificial time-history to be 10%; therefore, an $\bar{F}_{ATH}$ of 1.10 is used. It was also observed that different artificial time-histories that adequately envelope the ground response spectra can lead to floor spectra, which may differ by a factor of 2. Values of β_R of 0.20 and β_U of 0 are considered appropriate.

The combined factors are $\bar{F}_{SA}$ of 1.39, β_R of 0.20 and β_U of 0.13.

These do not apply to the ETEC test since the response spectra used in the analysis was unbroadened, unsmoothed and was derived from the time-history used in the test.

Modelling Factor ($\bar{F}m$) -- This accounts for assumptions made in modelling the piping system, boundary conditions and material behavior. If it is assumed that the analytical model is accurate, F_m can be taken as 1.0. For moderately complex models β_R is taken as 0 and β_U as 0.15.

Damping Factor ($\bar{F}\delta$) -- This accounts for the damping used in design being lower than the median value of damping of 5% at or near failure. It is assumed that the design damping is 2%. This results in $F\delta$ of 1.34 β_R of 0.03 and β_U of 0.17.

For the ETEC test the design damping was 5%. Therefore, $\bar{F}\delta$ of 1.0 will be used. Values of β_R and β_U above will be used, however.

Mode Combination Factor ($\bar{F}mc$) -- It is assumed that modes are combined by the square root of the sum of the squares (SRSS), which is considered median centered. Therefore, $\bar{F}_{mc}$ is 1.0. It is recommended that β_R of 0.15 and β_U of 0 be used.

Earthquake Component Combination Factor ($\bar{F}ECC$) -- It is assumed that the three components are combined by SRSS. This is considered median centered with an F_{ECC} of 1.0. Considering different phasing between components, it is estimated that a β_R of 0.12 and β_U of 0.10 should be used.

In the ETEC test and in the analysis only one component is applied. Therefore, β_R and β_U of 0 are appropriate.

6.6.1.5 Structural Response Factor ($\bar{F}RS$)

This factor considers the variables pertinent to the structural response analyses used to generate floor spectra for equipment design. These variables are spectral shape, damping, modelling and soil-structure interaction. Resulting values are $\bar{F}_{RS}$ of 1.11, β_R of 0.25 and β_U of 0.18.

These values do not apply to the ETEC test/analysis since the seismic input is applied directly to the pipe.

6.6.1.6 Summary

A summary of the above factors is shown in Table 6-4. The factors used to predict the fragility of the test article are shown in Table 6-5. The median

acceleration based on a 0.2 g OBE is 21.97 x 0.2 or 4.39 g. Probability of failure curves for 0.05, 0.50 and 0.95 non-exceedence probabilities are shown in Figure 6-23.

6.6.2 Test Article Fragility Using the SSMRP Method

Reference 14 describes a probabilistic computational procedure for the seismic risk assessment of nuclear power plants. In this procedure, seismic input, soil-structure interaction, structure response, subsystem response and fragilities are considered on a probabilistic basis. Volume 7 of Reference 14 describes the methods used in determining fragilities.

For a piping system, the fragility calculations consider material strength, pipe capacity and ductility. Median strength is taken as 25% above specified code strength which is considered to be a 95% nonexceedence value.

An upper value of moment capacity is determined by assuming the outer fibers to be at the material ultimate strength with the neutral axis at the material yield strength. This value is considered to be one logarithmic standard deviation above the median. A lower bound value is derived based on a through-wall flaw of length equal to six times the wall thickness. This is considered a minus 3 logarithmic standard deviation value.

Ductility is considered to range from 1 to 5 where the low value of 1 represents the flawed condition and the value of 5 corresponds to about 1% primary strain. The associated ductility factors are 1.0 and 3.0 as assumed in the Zion method. These factors are assumed to represent a plus or minus two logarithmic standard deviation range.

Calculations of the above for the test article show a median acceleration of 8.82 g with β_R = 0.17 and β_U = 0.30. Probability of failure curves for the 0.05, 0.50 and 0.95 non-exceedence probabilities are shown in Figure 6-24.

6.7 SUMMARY OF COLLAPSE FAILURE PREDICTIONS, NRC/ETEC TEST

A summary of the pretest analysis results performed on the NRC/ETEC test article are presented herein and, based upon experience gained from the WHC one-inch pipe loop tests and analyses, test collapse levels are predicted. Figure 6-25 (which is further discussed below) presents a summary of the analytical results for the NRC/ETEC test article using various simplified elastic methods. In all cases shown, the analytical results consider the summation of pressure plus dead weight plus dynamic test load stresses. The pretest estimates of collapse loads for the various assessments are indicated in Figure 6-25 with a diamond (◆), which represents effective yield point (53 ksi) corresponding to an average material value. The results of Figure 6-25 are also summarized in Table 2-1.

The limits discussed below for the Newmark, D/S, and static progressive hinge methods are 41 ksi, 53 ksi, and 66 ksi. These represent a minimum, average, and maximum expected effective yield point for carbon steel material (see Section 6.5.2).

Linear elastic analyses were performed on the pipe system for a baseline response spectra loading intended for the tests. The analyses were accomplished by scaling the spectra to obtain results for various base load levels. The allowable base input loading was found to be 2.0 g's for an ASME Class 1, Level D limit (3 S_m=60 ksi) and 1.4 g's for an ASME Class 2, Level D limit (3 S_h=45 ksi). This limit is shown on Figure 6-15 as "ASME."

Resulting stresses from a Newmark analysis have been previously developed for several system components and system ductility ratios, as shown in Figures 6-7 through 6-9. The base acceleration limits for the elbow at Node 71 are presented in Figure 26 for several effective yield stresses and system ductilities. As stated previously, the nearly equally stressed tee at Node 65 was not considered critical since failure in the crotch area of the tee would not contribute a mechanism hinge for overall collapse of the pipe system but rather a collapse of the branch piping. The results of the Newmark analysis are presented in Figure 6-25 for system ductility ratios of 5 to 10 and infinity. A system ductility ratio of 10 has been previously estimated which, along with an average effective yield value of 53 ksi, gives a failure level of 10.0 g's base acceleration.

The allowable limits based upon the D/S margin ratio method were calculated for the elbow at Node 71 for D/S ratios of 2 and 4, shown in Figure 6-25. The D/S value of 4 corresponds to a system ductility of approximately 10. It is seen in Figure 6-25 that an effective yield point of 53 ksi and a D/S value of 4 gives a predicted base acceleration limit of 9.7 g's.

The results of the static progressive hinge method are shown in Figure 6-15 for yield values of 42, 53, and 66 ksi. An average effective yield stress of 53 ksi gives a predicted failure level of approximately 16 g's. It should be noted that this represents the acceleration of the pipe itself and is related to the base input acceleration by the magnification factor. If one assumes a magnification factor of 2 (as suggested by Reference 8 and also by the results of the WHC one-inch high level tests), the predicted based acceleration at failure would be approximately 8 g's for a yield point of 53 ksi.

The inelastic dynamic analyses predicted the pipe system first plastic hinge at about 5 to 8 g's ZPA and a second plastic hinge to develop between 14 to 20 g's ZPA. However, no dynamic instability or pipe system collapse is indicated.

The PRA-type fragility estimates of Section 6.6 gave collapse loads, at 50% probability and 50% nonexceedence, of 4.4 g's per the "Zion" method and 8.8 g's per the SSMRP method.

6.8 POST-TEST ANALYSES AND COMPARISONS, ETEC SIX-INCH DIAMETER TEST ARTICLE

6.8.1 Overview of Test Results and Failure Mode

The tests were conducted by ETEC for the U.S. NRC, Division of Engineering Technology. Test details and results are contained in an ETEC report to NRC by Onesto, Chen, and DeVita (Reference 7).

A sketch of the 6-inch diameter piping and the locations of accelerometers and strain gages are provided in Figure 6-27. The pipe system was excited by using four synchronous motion sliding tables. The Schedule 40 piping was made of ASTM A-106 Grade B ferritic steel and pressurized to 1000 psi with oil.

The test sequence consisted of three seismic motion tests of 7.5 g, 13 g and 30 g ZPA inputs at the slide tables in the X-direction. Each seismic test had about 10 seconds of strong motion. Figure 6-28 shows typical table input motions for the 30 g test. Following the seismic tests, two sinusoidal burst tests were carried out. The first test was at 4-hertz frequency and 10 cycles long. The second test, at 5-hertz frequency, terminated in a rupture of the piping after about 6 cycles.

Response maximum values of acceleration, displacements, and strains are provided in Tables 6-6 and 6-7. Strain gages were located on the piping about 8 inches above the sliding table. These gages measured longitudinal strains. Figures 6-29, 6-30, and 6-31 show strain levels typical of the test series. Figure 6-32 depicts the pipe rupture location, just above Table #3, and shows a significant hoop ratchet/bulge deformation.

The strain gages near the failure location failed before the sinusoidal tests. However, strain ranges up to about 3.5% were measured during the seismic tests. Using plots and extrapolation it was concluded that strains between 3.5% and 8% were experienced by the pipe at the rupture location during the sinusoidal dwell tests.

The failure mode (see Figure 6-32) had the appearance of an "elephant foot" bulge. This could have been brought on by the hoop ratchet from internal pressure and cyclic longitudinal plastic straining. Gross deformation collapse or structural instability of the piping system did not occur. Rather, the failure was by local crack and rupture. More discussion on the failure mode and mechanism will be given later in the report.

6.8.2 Comparison of Analyses and Test Response Data

Five analysis methods were used to predict the pipe system response before the tests. Assuming the tests would not involve enough cycles of loading to induce fatigue cracking, the failure mode by collapse or gross deformation was considered the limiting condition. All of the elastic or simplified elastic-plastic methods underpredicted the test-demonstrated piping collapse capacity of over 30 g.

As shown in Table 2-1, the ASME Class 2 design method predicted a design allowable of about 1.4 g seismic loading. The Newmark plastic-spectra and the Reference 10 D/S ratio methods predicted about 10 g. The Reference 11 progressive hinge method gave collapse load estimates of 8 to 16 g depending on the dynamic magnification factor taken as 2 or 1, respectively.

The ASME method also did not predict the correct failure location. The tee (see Figure 6-5) had higher calculated primary stress than the straight pipe failure area. Use of the ASME Code B_2 index for a tee (or branch) may result in an overly conservative primary stress.

The nonlinear transient dynamic inelastic analysis accomplished with the NONPIPE computer program (refer to Section 6.4) did not predict a dynamic instability or system collapse mode. Both static and dynamic inelastic solutions were obtained. Figure 6-33 shows that the maximum strains under dynamic loading are dynamically magnified relative to static response. However, the formation of plastic hinges in the piping system at high-level loading does not induce a dynamic instability like it does under static loading. Thus, the static analysis underpredicts response at low-level loading but it overpredicts response at high-level loading.

The nonlinear transient dynamic inelastic analysis predicted about 3.5% strain range (see Figure 6-34) for the 15 to 20 g seismic loading. This compares very well with the test data of Figure 6-30.

Another comparison of the inelastic analysis prediction is shown in Figure 6-35. The displacement calculated for 15 g of about the 14-inch range compares well with the 14 g test value of 13 inches.

In general, the linear analysis ASME Code method underpredicted the test-demonstrated load capacity by more than an order of magnitude. The simplified elastic-plastic response spectra methods underpredicted by about a factor of 3 and the static progressive hinge underpredicted the collapse capacity by about a factor of 2.

The controlling failure mode, however, was not system collapse. Rather, it was a local cracking/rupture induced by hoop ratcheting from the combined sustained pressure stresses and cyclic dynamic stresses. This is called a ratchet-fatigue failure mode.

6.8.3 Ratchet-Fatigue Failure Mode

The failure of the pipe system occurred when the straight pipe section just above sliding Table #3 ruptured. A circumferential through-wall crack, extending over 180 degrees around the pipe, was developed during the cycle that leaking occurred.

A post-test standard fatigue analysis was performed for the ruptured pipe location. The pretest nonlinear inelastic analysis (Section 6.4) used a seismic time history that was about one quarter as long as the test history motion. Two major strain ranges of 2.8% and 3.5% (see Figure 6-36) were computed for the 15 g input test. Because the response is nonlinear with input level, the computed maximum strain for each test was deduced using the data in Figure 6-34. Each major strain range, according to the analysis, would repeat about four times during each total test duration. The values are:

Test Input ZPA	Major Strain Ranges, %	
	1st	2nd
5 g	0.4	0.5
14 g	2.8	3.5
25 g	3.0	3.6

The strain ranges for the sinusoidal tests were estimated as follows. The 4-hertz test had an input motion of 12 g maximum acceleration for 10 cycles. The 5-hertz test withstood about 6 cycles of 18 g input before gross rupture of the piping. Based on earlier analyses of Section 6.4, it was estimated that the pipe maximum strain range for the 4-hertz test was about 3.4%; the 5-hertz test experienced strains between 3.5% and 8.0%.

To predict the fatigue usage of the total test series, a "best fit" fatigue curve (see Figure 6-37) for carbon steels, given in the ASME criteria document (Reference 26) and represented in equation form by Harvey (Reference 27), was used. Figure 6-38 presents the fatigue analysis details.

The standard fatigue analysis calculated a cumulative usage factor of 0.13 to 0.27 for the entire test series. Because a usage factor of unity indicates fatigue failure, the standard fatigue analysis overpredicted the pipe cyclic life.

The pipe failure mode, depicted in Figure 6-32, suggests that the hoop ratchet strain could have exhausted the material ductility and reduced the pipe cycle life capacity. To assess the ratchet mode of failure by ductility exhaustion, an analysis (using the ratchet strain per cycle formula from Reference 28) was accomplished and is summarized in Figure 6-40. Since tensile tests indicated the material elongation was about 35%, about 30 to 40 cycles of 3% to 4% strain range superposed on the sustained hoop stress appear sufficient to exhaust the ductility.

The ductility reduction caused by the ratchet strain accumulation has an interaction with the cyclic fatigue life. Figure 6-41 depicts an approximate analysis of the ratchet-fatigue interaction. Using this approximate interaction method, the ratchet-fatigue usage factors were computed as shown in Figure 6-39. The cumulative usage factor reaches unity and indicates failure as it happened during the last test.

The ratchet-fatigue conditions need the sustained internal pressurization. It appears that the noncycling pressure loading, normally not included in ASME Code fatigue assessments, may be an important parameter -- especially for low-cycle fatigue from strain ranges above a few per cent.

TABLE 6-1

NRC/ETEC TEST ARTICLE, PREDICTED HINGE FORMATION LOAD LEVELS, STATIC PROGRESSIVE HINGE METHOD

Yield Stress (ksi)	First Hinge formation (g)	Second Hinge Formation (g)
30	8.3	8.9
40	11.4	12.1
50	14.5	15.3
60	17.6	18.5
70	20.7	21.8

Note: Loads shown represent loads on pipe, not base input loads.

TABLE 6-2

MATERIAL PROPERTIES, ASTM A-106 GRADE B CARBON STEEL

Property	Yield Strength (ksi)	Ultimate Strength (ksi)	Elongation (e_u) at Failure (%)
Minimum Properties	35	60	22
Average Properties	43	80	30
Measured Properties*	54	78	34

Equivalent Yield Point Assumed = $S_y + 1/4\ (S_u - S_y)$

$= 43 + 1/4\ (80 - 43) = 53$ ksi

*From pipe material samples, after pretest analyses were completed. Corresponding Equivalent Yield Point = 54 + 1/4 (78 - 54) = 60 ksi.

TABLE 6-3

TRANSIENT LOAD SUMMARY

Maximum Z Acceleration (g)	Time Step (s)	Duration (s)
3.52	0.0025	1.5
4.89	0.0025	1.5
5.87	0.001	1.5
10.2	0.0001	0.55
15.6	0.0001	1.25
19.9	0.0001	0.55

TABLE 6-4

FRAGILITY PARAMETERS FOR CLASS 2 PIPING
(ZION METHOD)

Factors	Median Safety Factor	Randomness R	Uncertainty U
CAPACITY FACTOR			
PIPING			
Strength - Thick Wall	8.04	0	0.36
- Thin Wall	4.39	0	0.36
Inelastic Energy Absorption	2.24	0.16	0.16
Three-Hinge Factor	1.22	0	0.10
SUPPORTS			
Strength	3.26	0	0.29
Inelastic Energy Absorption	1.50	0.16	0.16
ANCHOR (WEDGE)			
Strength	5.70	0	0.30
Inelastic Energy Absorption	1.50	0.15	0.15
EQUIPMENT RESPONSE FACTOR			
Qualification Method	1.00	0	0
Spectral Shape	1.39	0.20	0.13
Modelling	1.00	0	0.15
Damping	1.34	0.03	0.17
Mode Combination	1.00	0.15	0
Earthquake Component Combination	1.00	0.12	0.10
STRUCTURAL RESPONSE FACTOR	1.11	0.25	0.18

TABLE 6-5

FRAGILITY PARAMETERS FOR TEST ARTICLE
(ZION METHOD)

Factors	Median Safety Factor	Randomness R	Uncertainty U
CAPACITY FACTOR			
PIPING			
Strength	8.04	0	0.36
Inelastic Energy Absorption	2.24	0.16	0.16
Three-Hinge Factor	1.22	0	0.10
EQUIPMENT RESPONSE FACTOR			
Qualification Method	1.00	0	0
Spectral Shape	1.00	0	0
Modelling	1.00	0	0.15
Damping	1.00	0.03	0.17
Mode Combination	1.00	0.15	0
Earthquake Component Combination	1.00	0	0
STRUCTURAL RESPONSE FACTOR	1.00	0	0
TOTAL	21.97	0.22	0.47

TABLE 6-6

6-INCH DIAMETER ETEC PIPE TESTS

Measurements			Test Values 5 g	14 g	25 g	Sine Burst		Remarks
A	A	Y,g	±13	±15	+25	+18-13	+28-22	Failure @ 7.8 s of Sine Bursts
	B	Z	±18-12	±22-18	±35-32	+18	+38-32	
	C	X	±16	+17-20	±23	+18	+23-28	
	D	X	±44-25	+42	±52	+50	-57+66	
	E	Y	+14-12	±14-12	±17	±12-14	±17	
	F	Y	+11-13	+12-14	±17-15	±9	±15	
T3	X, g		±7	±12	±30	±18	+46-42	
T1	X		±7-5	±12	±25	±18	+40-35	
T2	X		±6.5	±15	±30-35	±18	±48	
D1	X, in.		+2-1.5	+4	+7	+7	+7	
D2	X		±1.5	±4	±7	±6.5	±8	
D3	X		±2	±4	±7	±7	±7.5	
ϵ3N, %			+0.8-0.4R	+1-0.6?	+1.7-1.8	?	?	SG* Failed
ϵ3E			+0.25-0.22	+0.9-0.4R	+0.8-0.9	+1.4-1.0	?	SG* Failed
ϵ3S			±0.6	-1.5-1.2?	-0.9+1.2?	-0.8+1.3?	?	SG* Failed
ϵBN			+0.14	+0.15	+0.15	+0.15	+0.15	
ϵBE			±0.006	±0.006	±0.007	?	?	SG* Failed
ϵBS			±0.014	±0.15	±0.16	+0.16	±0.16	
ϵ2N			±0.1	±0.1	±0.15	±0.15-0.1	±0.15	
ϵDS-CIRC (EL.)			+0.15-0.07	+0.15	+0.24	+0.2-0.26	+0.35-0.40	
ϵDN-CIRC (EL.)			±0.12-0.08	±0.2-0.13	±0.47-0.18R	+0.45-0.2R	+0.45-0.38R	
No. Strong Cycles			8-12	13	6-9	10-12	4	41-50 TOTAL CYCLES

*Strain Gage Failure.

NUREG/CR-5023
WHC-EP-0081

TABLE 6-7

MAXIMUM RESPONSES

Input	Peak $g_{in.}$	Acceleration Data (g) A Y	B Z	C X	D X	E Y	F Y	Amplification X	Y	Z	Strain Range (%) N	S	E
5 g Seismic	7.5	13	15	15	35	10	12	6.7	1.5	2.0	1.2	1.2	0.5
14 g Seismic	13	14	20	17	40	13	14	4.4	1.0	1.5	1.6*	2.8*	1.2
25 g Seismic	30	22	32	22	55	16	17	2.5	0.6	1.1	3.5	1.8*	1.8
**12 g 4 Hz SINE	18	15	18	17	34	13	8	2.1	--	--	5.0*	2.1*	2.4*
**18 g 5 Hz SINE	30	25	35	25	45	15	15	1.9	--	--	*	*	*

*Strain Gage Failure.
**±7-in. Stroke.

NUREG/CR-5023
MHC-EP-0081

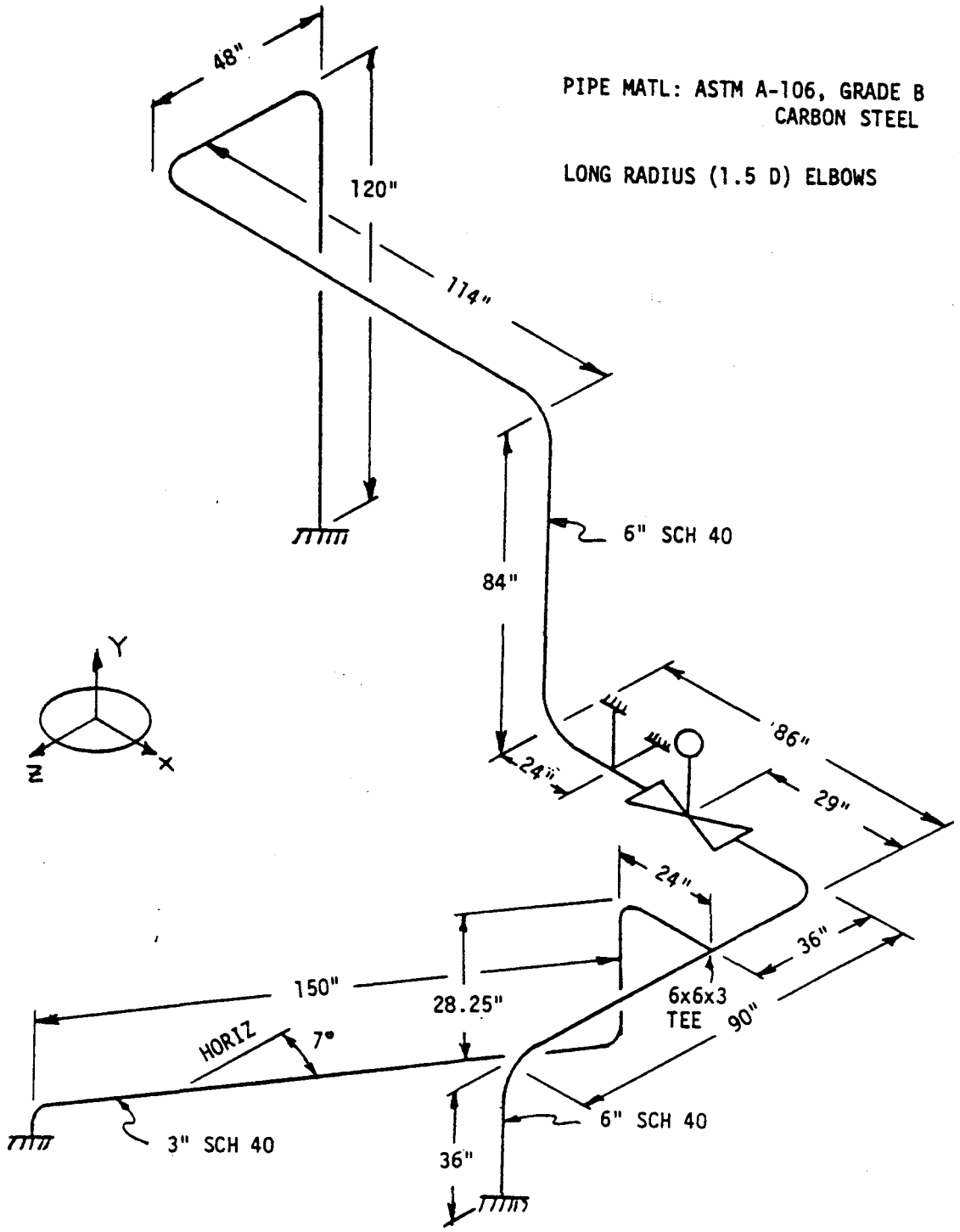

FIGURE 6-1. NRC/ETEC Test Article, System Configuration.

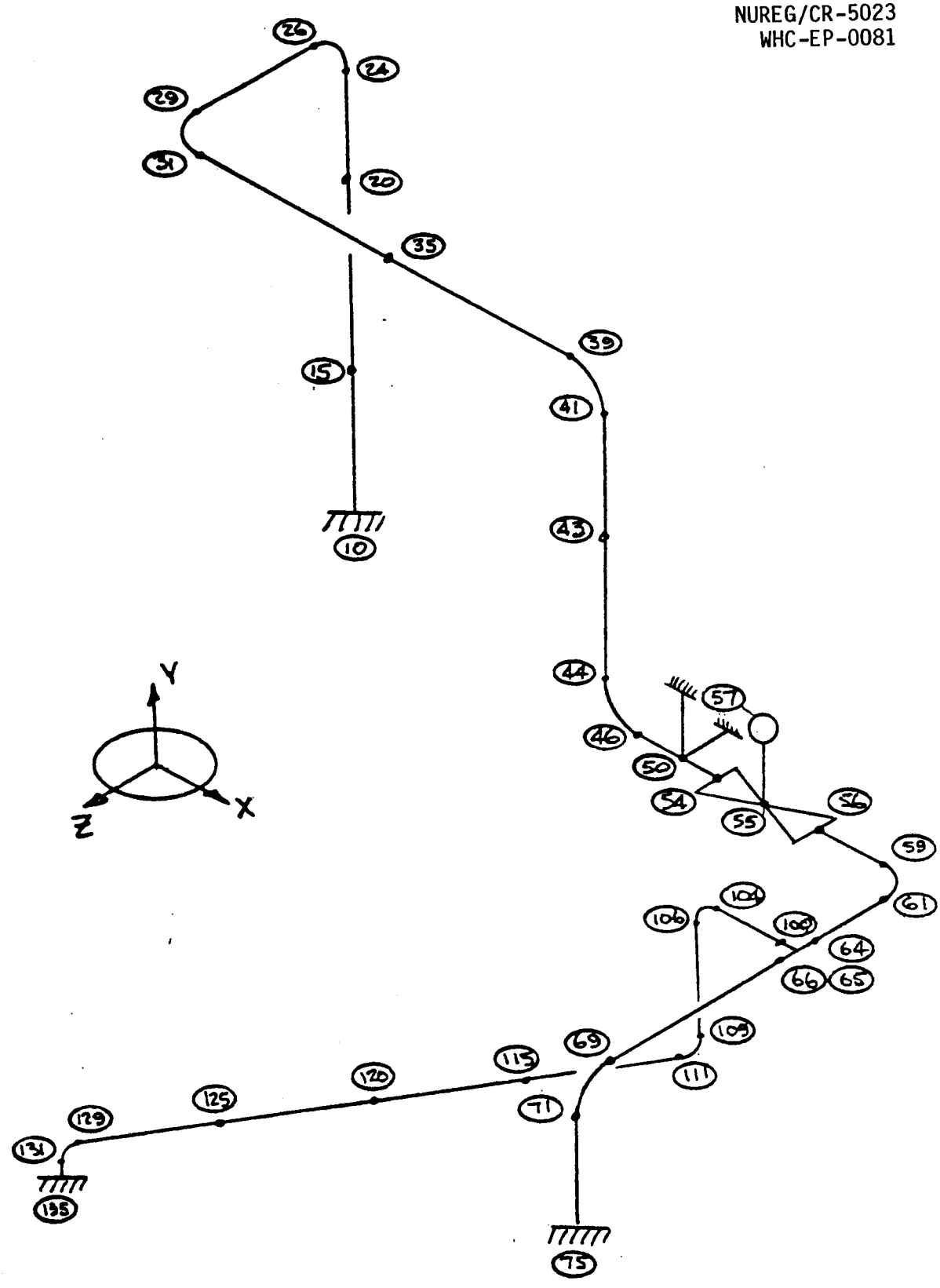

FIGURE 6-2. NRC/ETEC Test Article, Analysis Model.

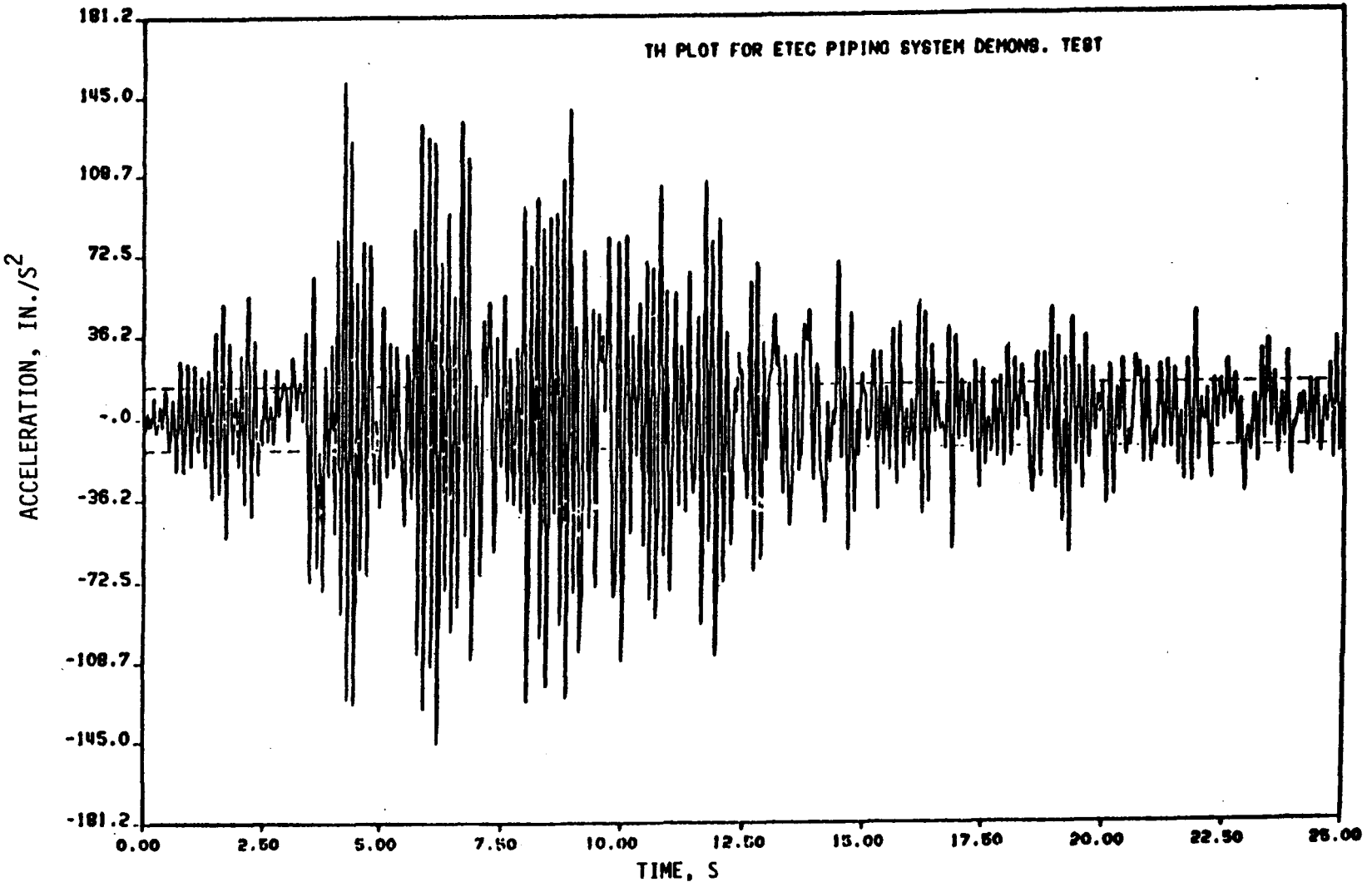

FIGURE 6-3. NRC/ETEC Test Article, Acceleration Time History.

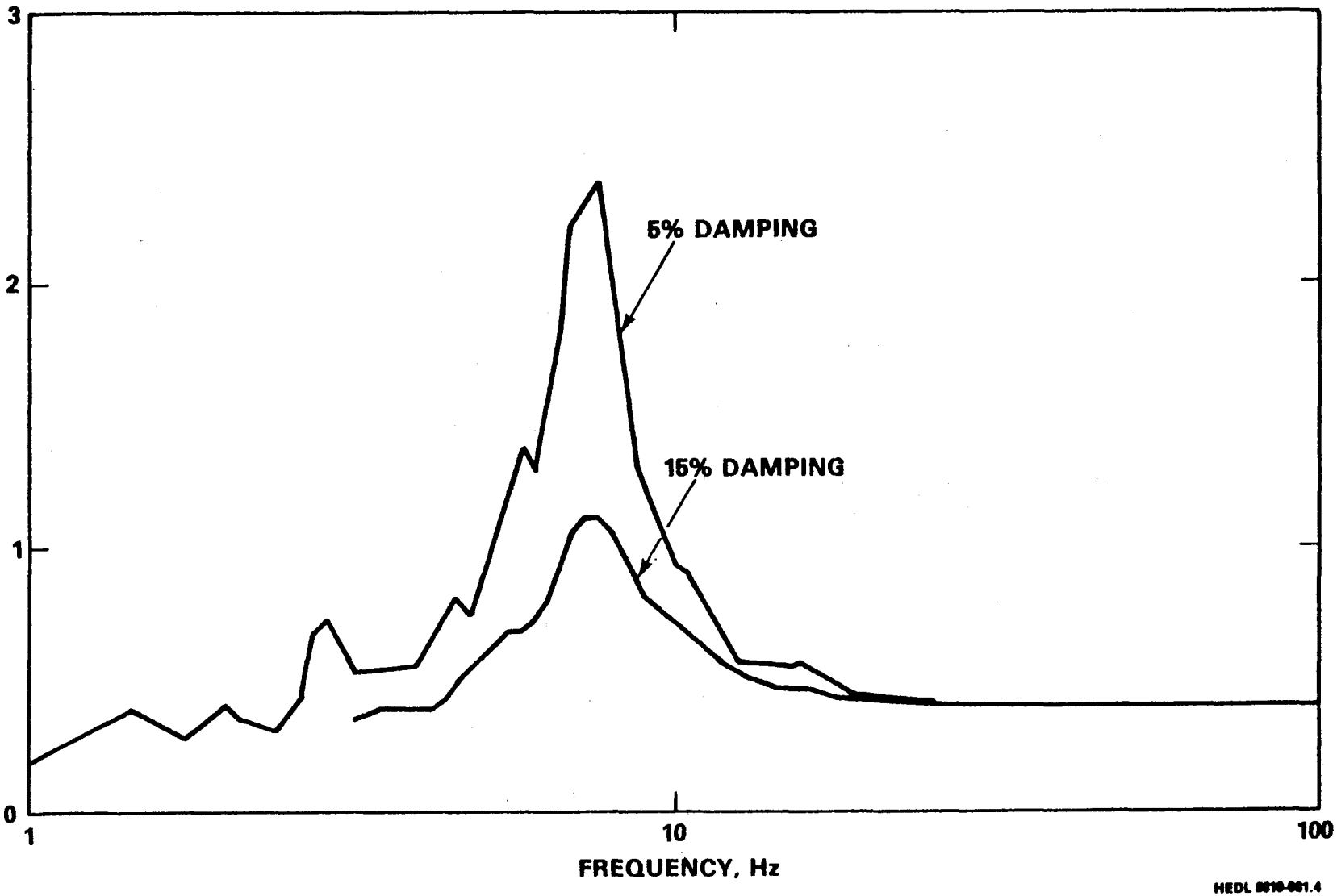

FIGURE 6-4. NRC/ETEC Test Article, Baseline Response Spectrum.

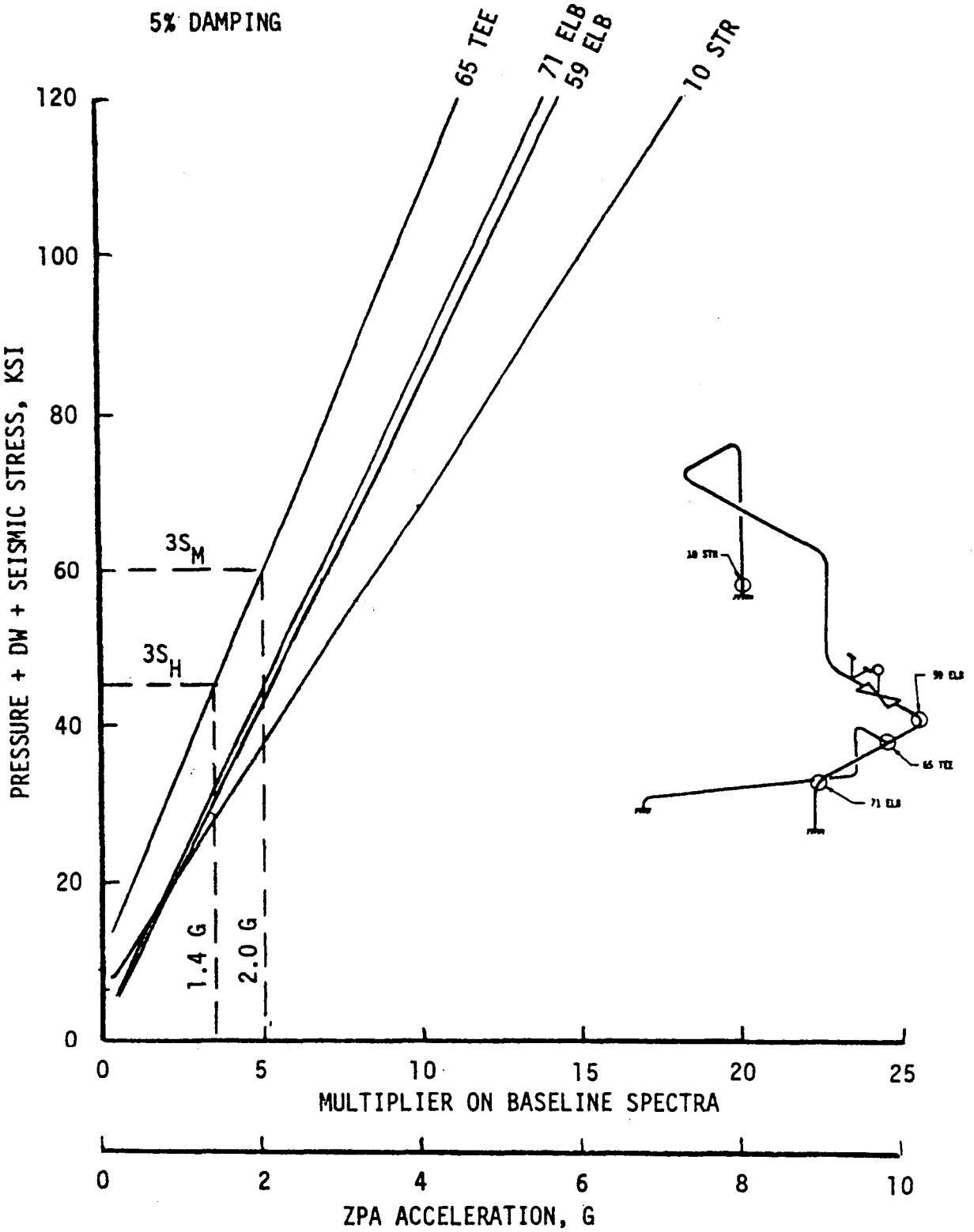

FIGURE 6-5. NRC/ETEC Test Article, Elastic Analysis.

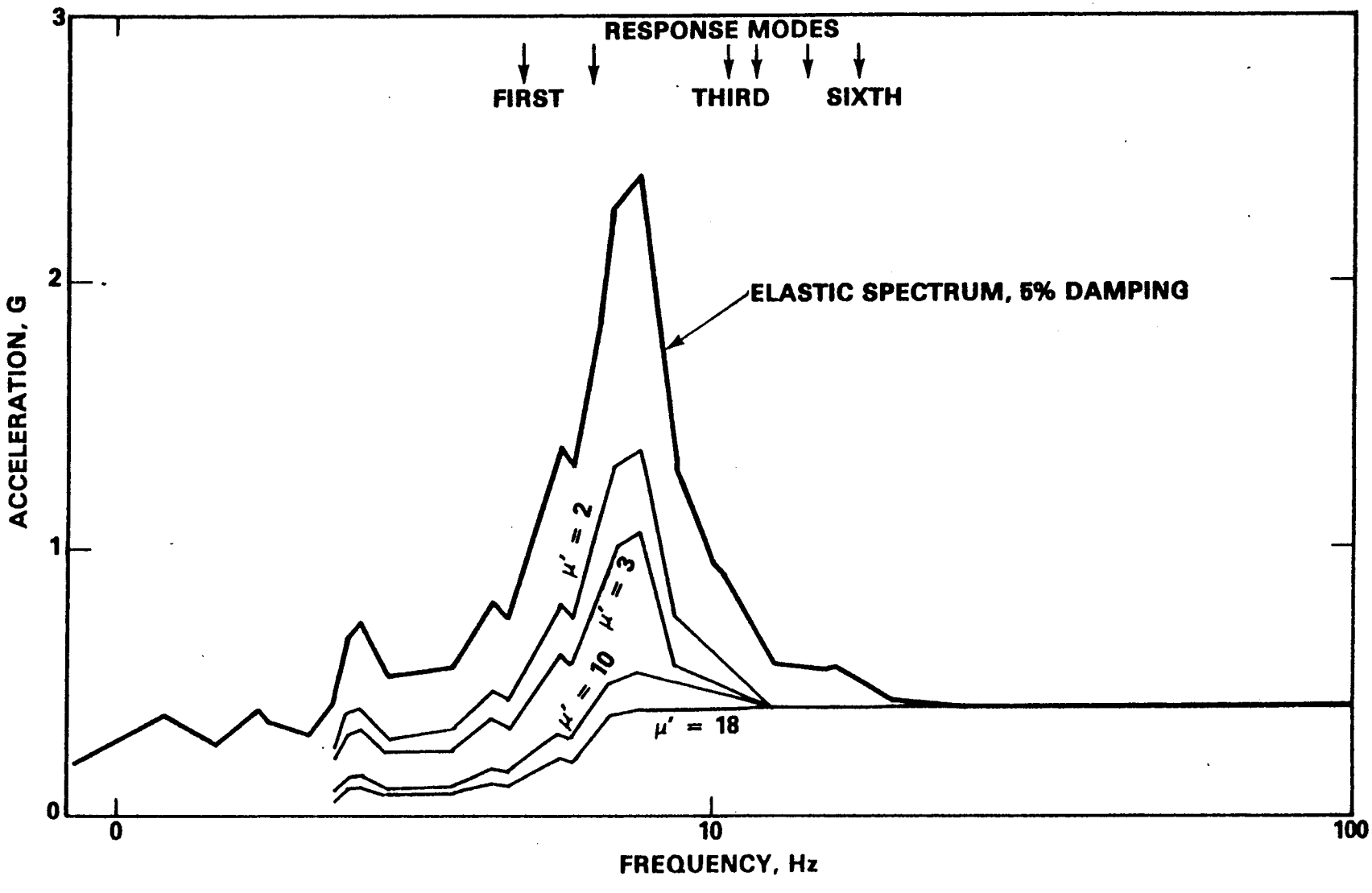

FIGURE 6-6. NRC/ETEC Test Article, Elasto-Plastic Response Spectra, Newmark Method.

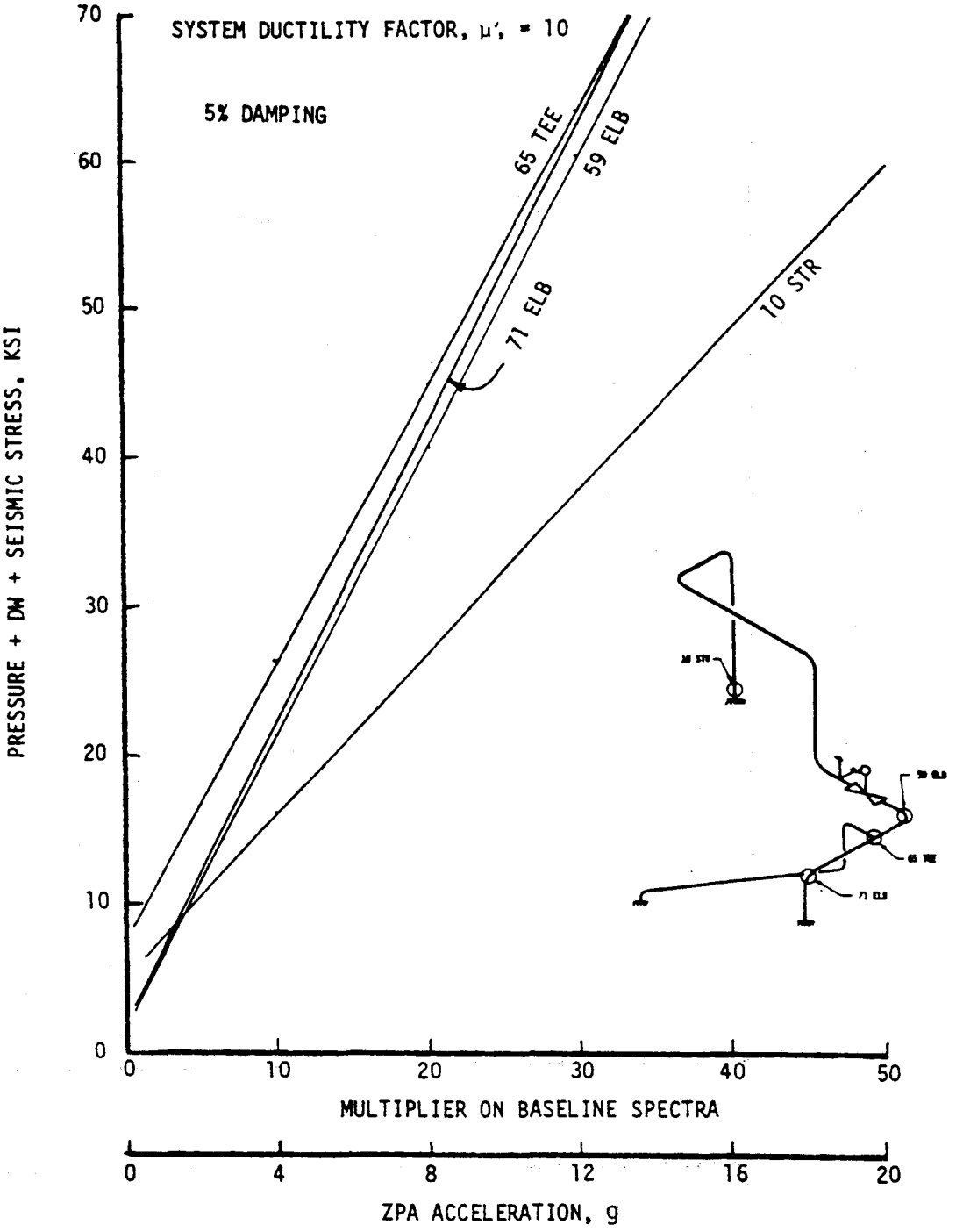

FIGURE 6-7. NRC/ETEC Test Article, Newmark Method.

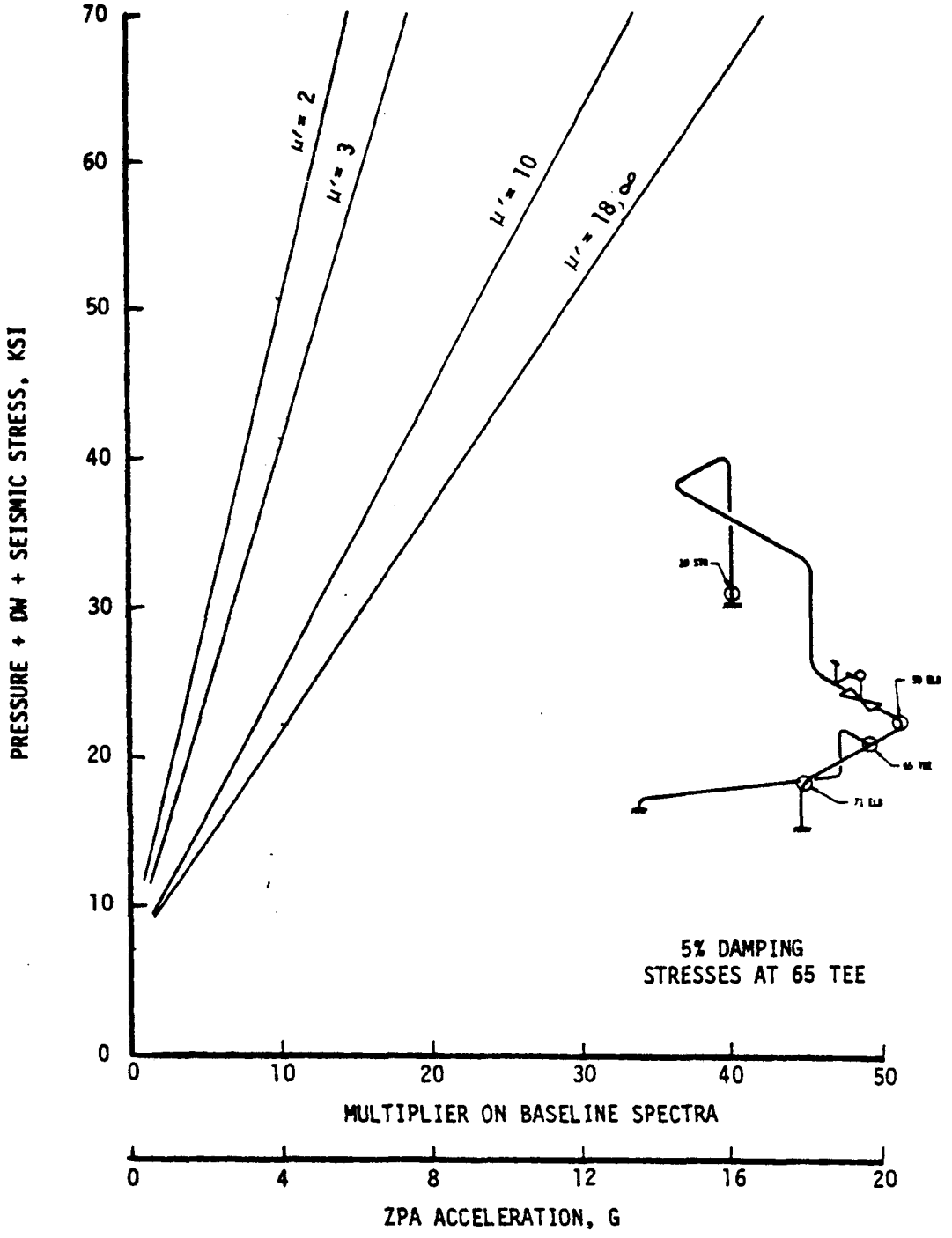

FIGURE 6-8. NRC/ETEC Test Article, Newmark Method, Tee Stresses.

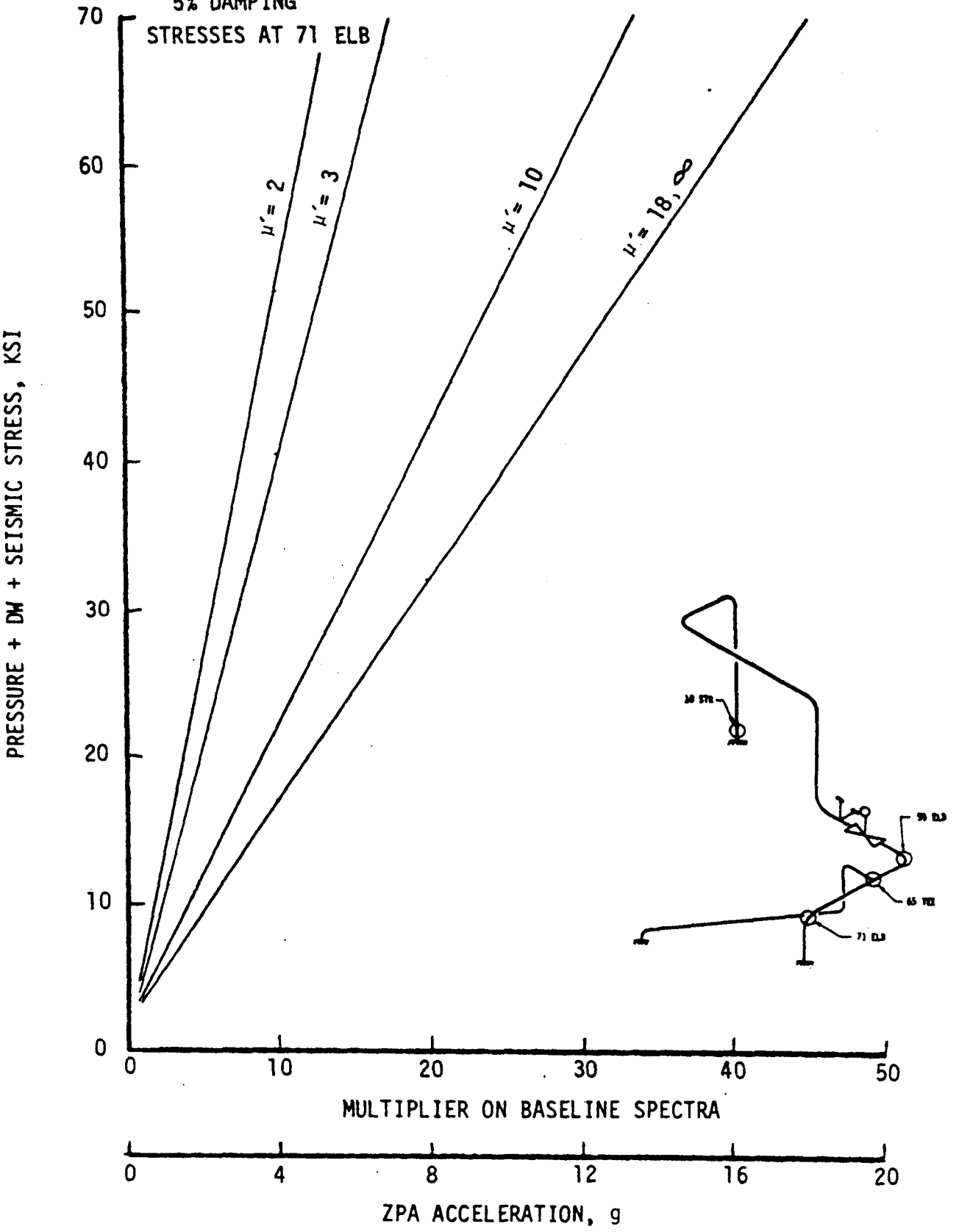

FIGURE 6-9. NRC/ETEC Test Article, Newmark Method, Elbow Stresses.

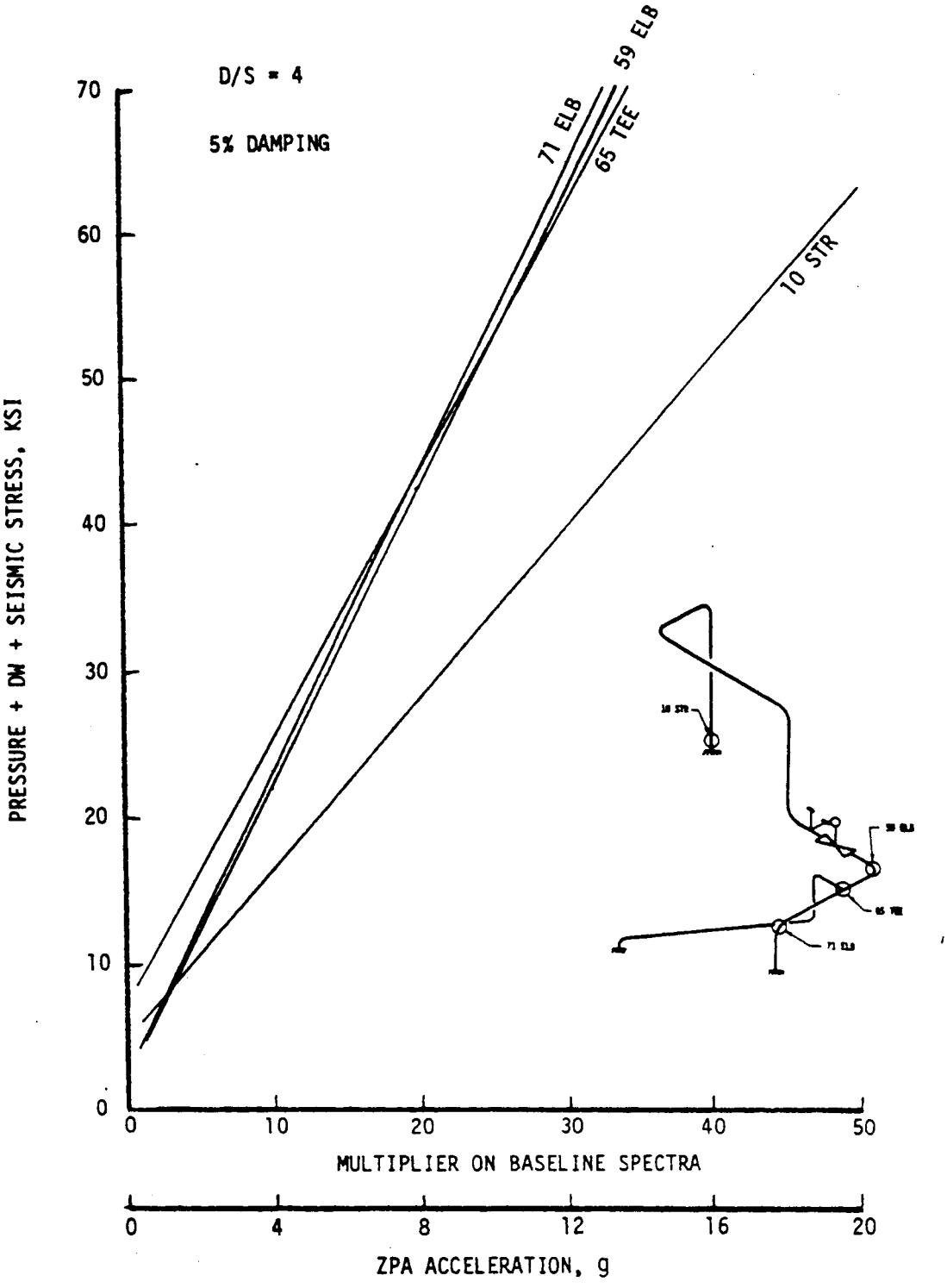

FIGURE 6-10. NRC/ETEC Test Article, D/S Method.

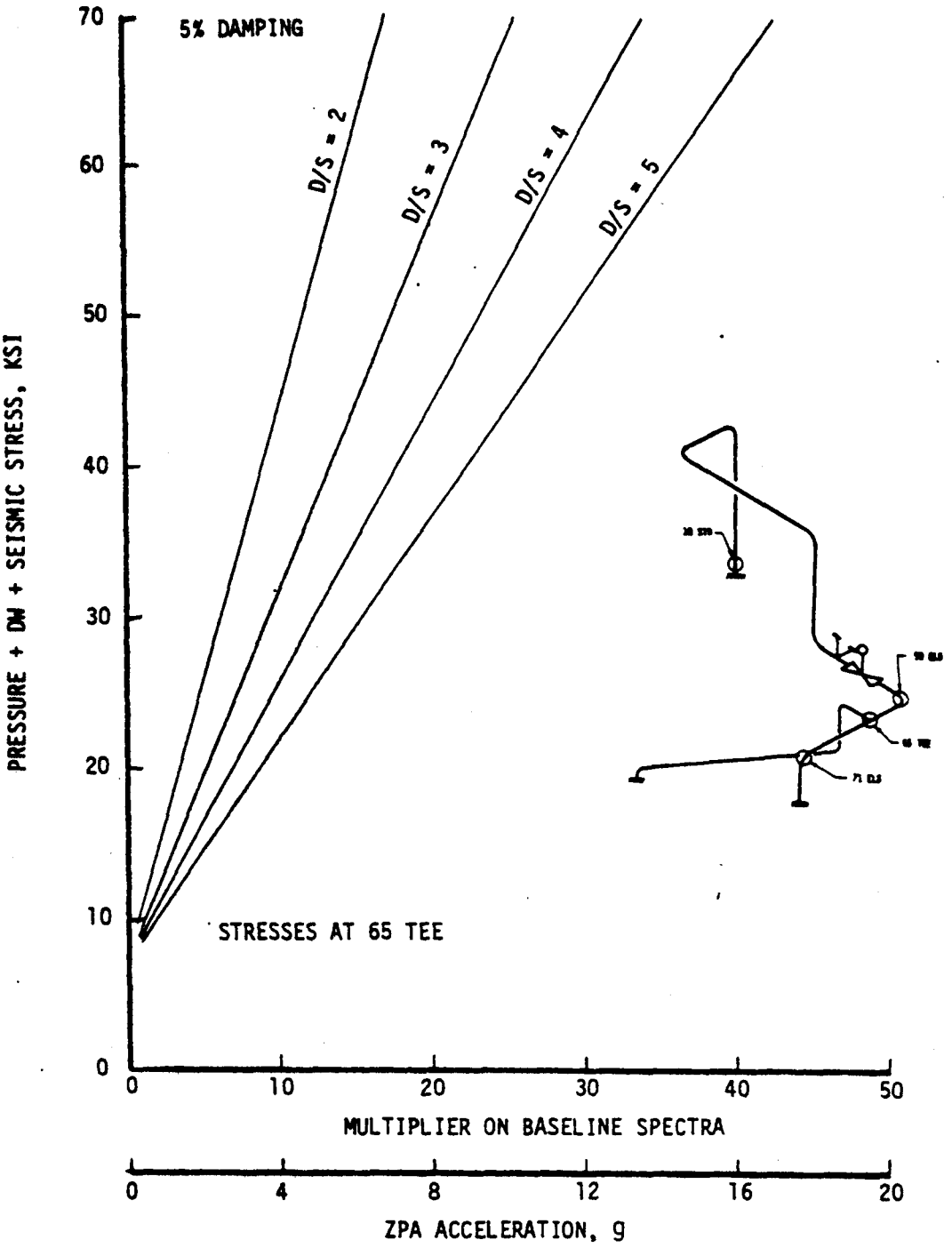

FIGURE 6-11. NRC/ETEC Test Article, D/S Method, Tee Stresses.

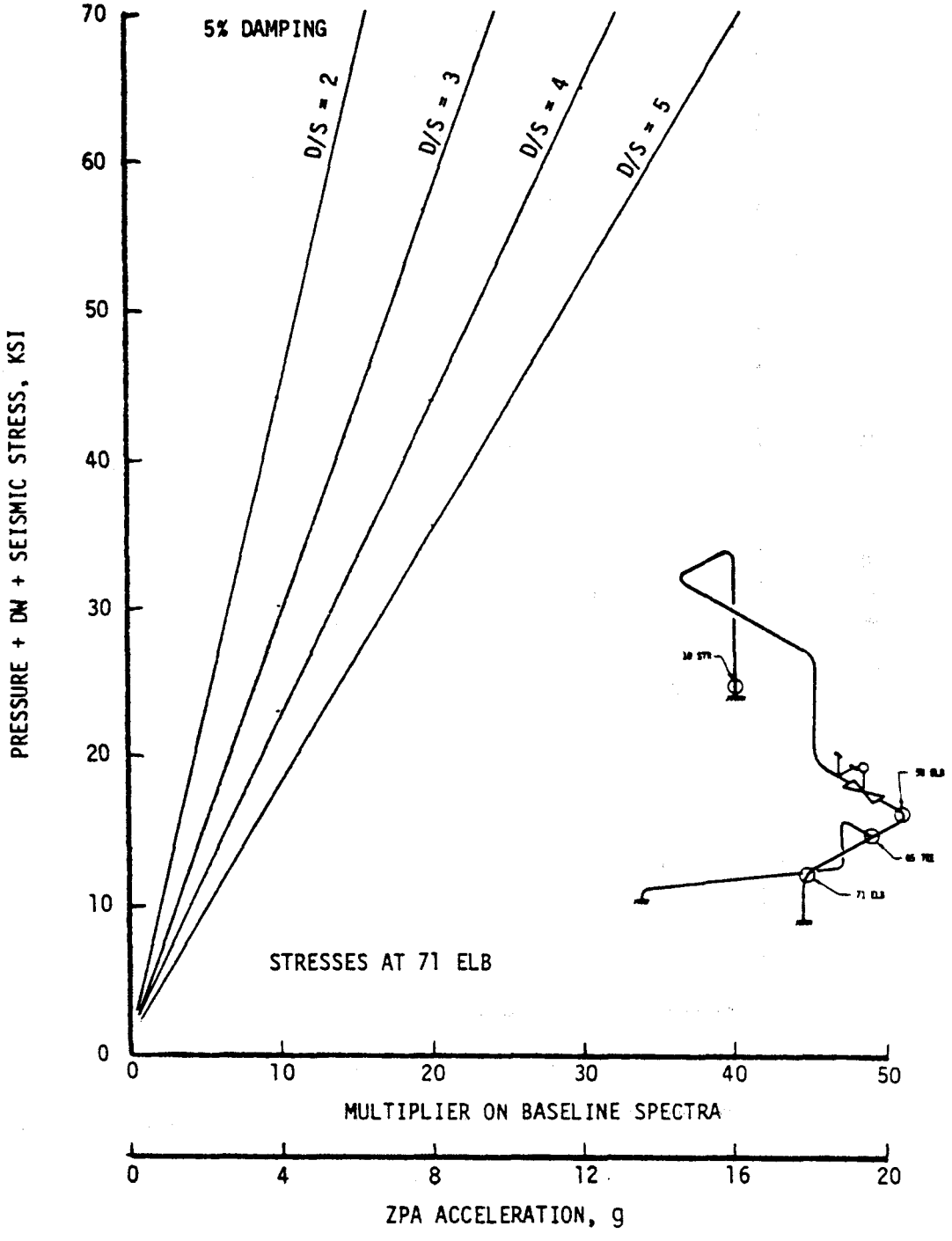

FIGURE 6-12. NRC/ETEC Test Article, D/S Method, Elbow Stresses.

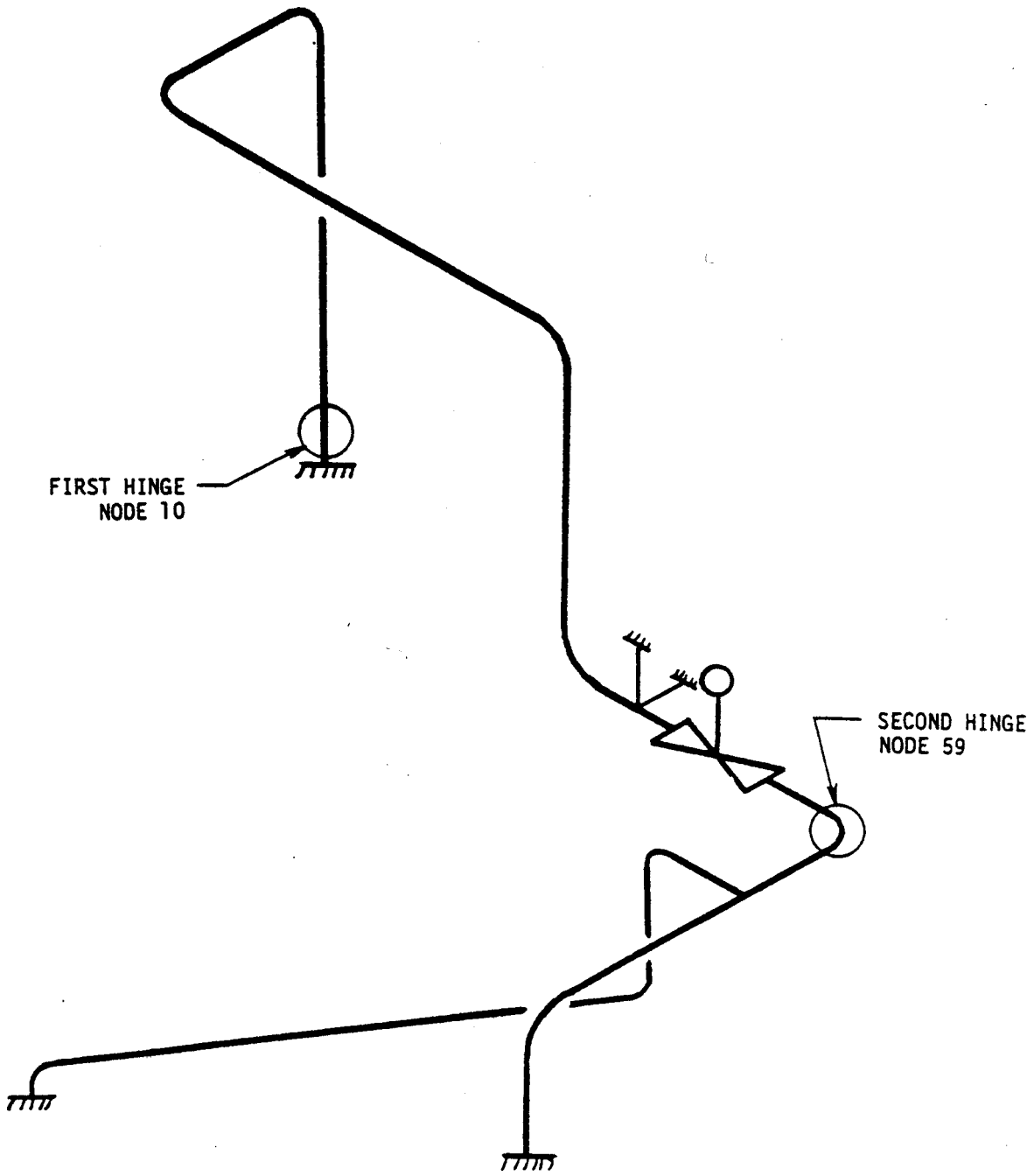

FIGURE 6-13. NRC/ETEC Test Article, Static Progressive Hinge Method.

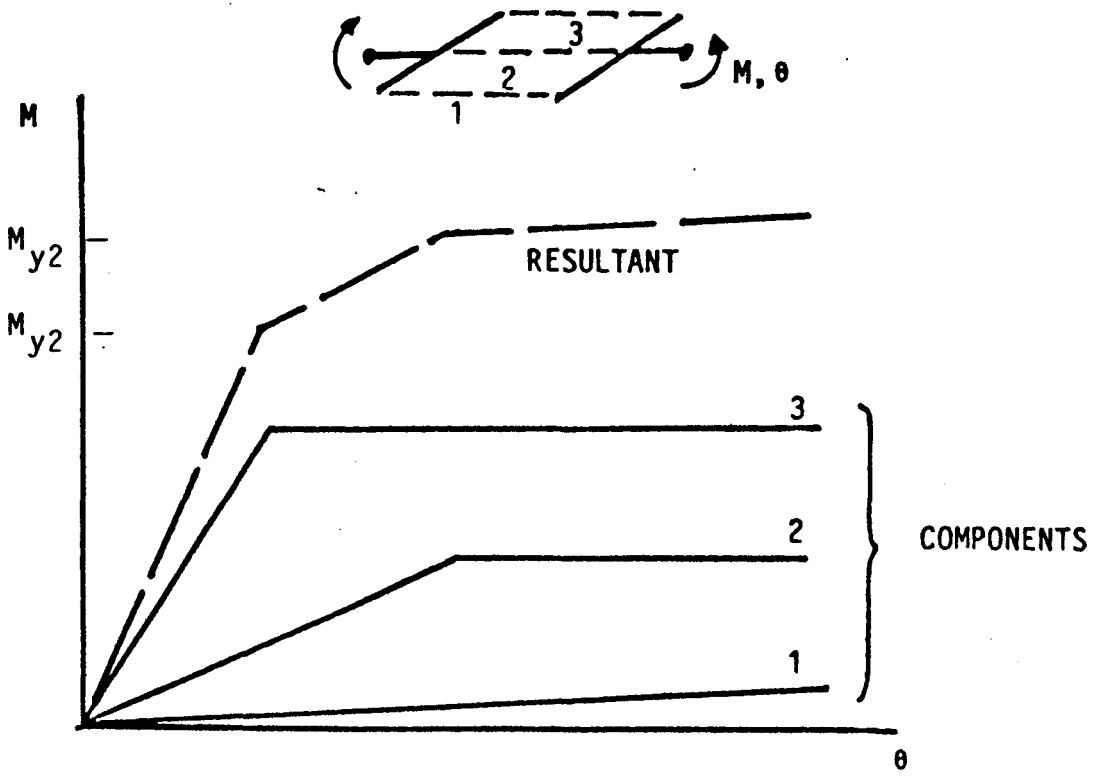

FIGURE 6-14. Trilinear Moment-Curvature Relation of Parallel Components.

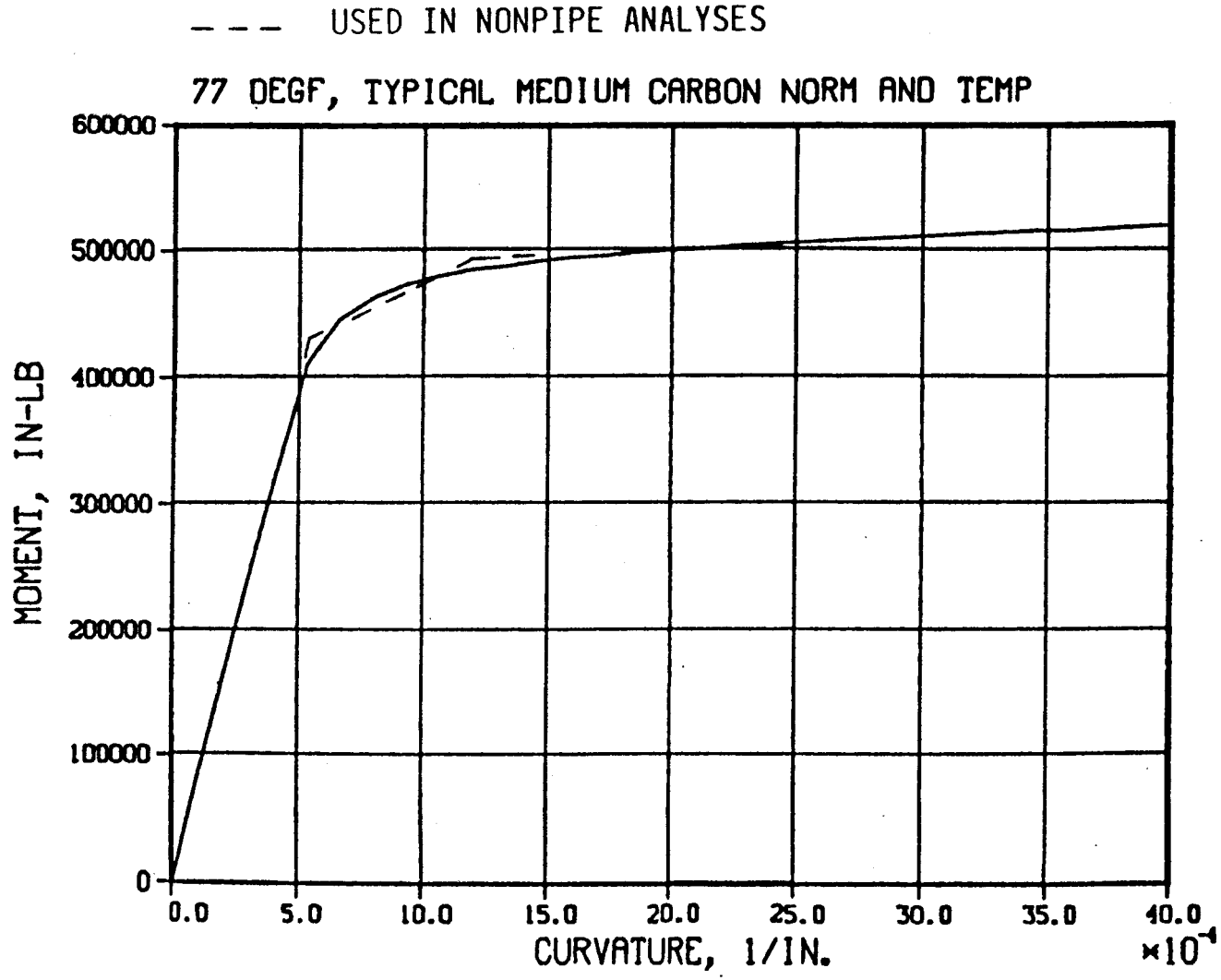

FIGURE 6-15. Six-Inch Straight Pipe Moment-Curvature.

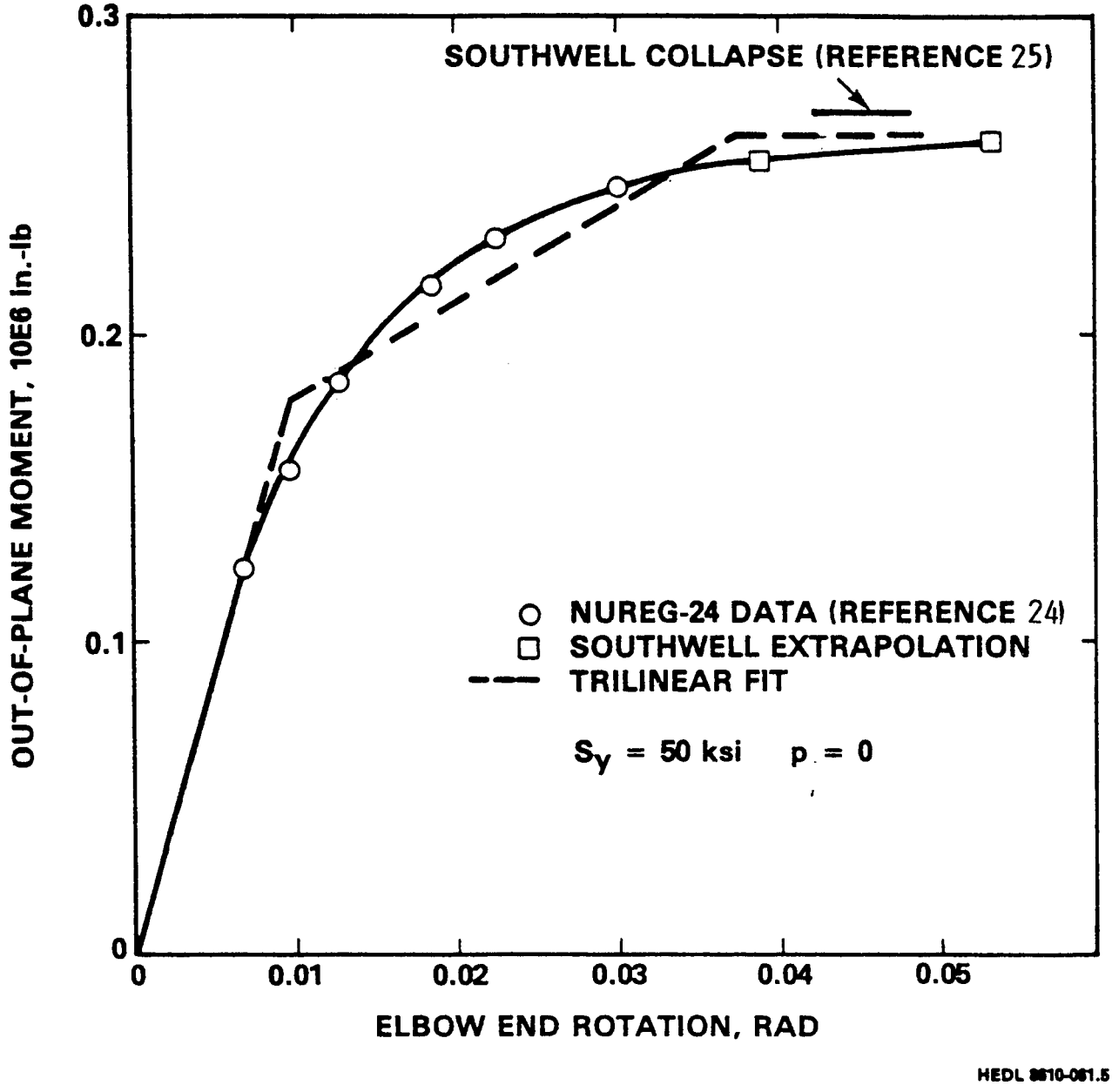

FIGURE 6-16. Six-Inch Elbow Response (Reference 24).

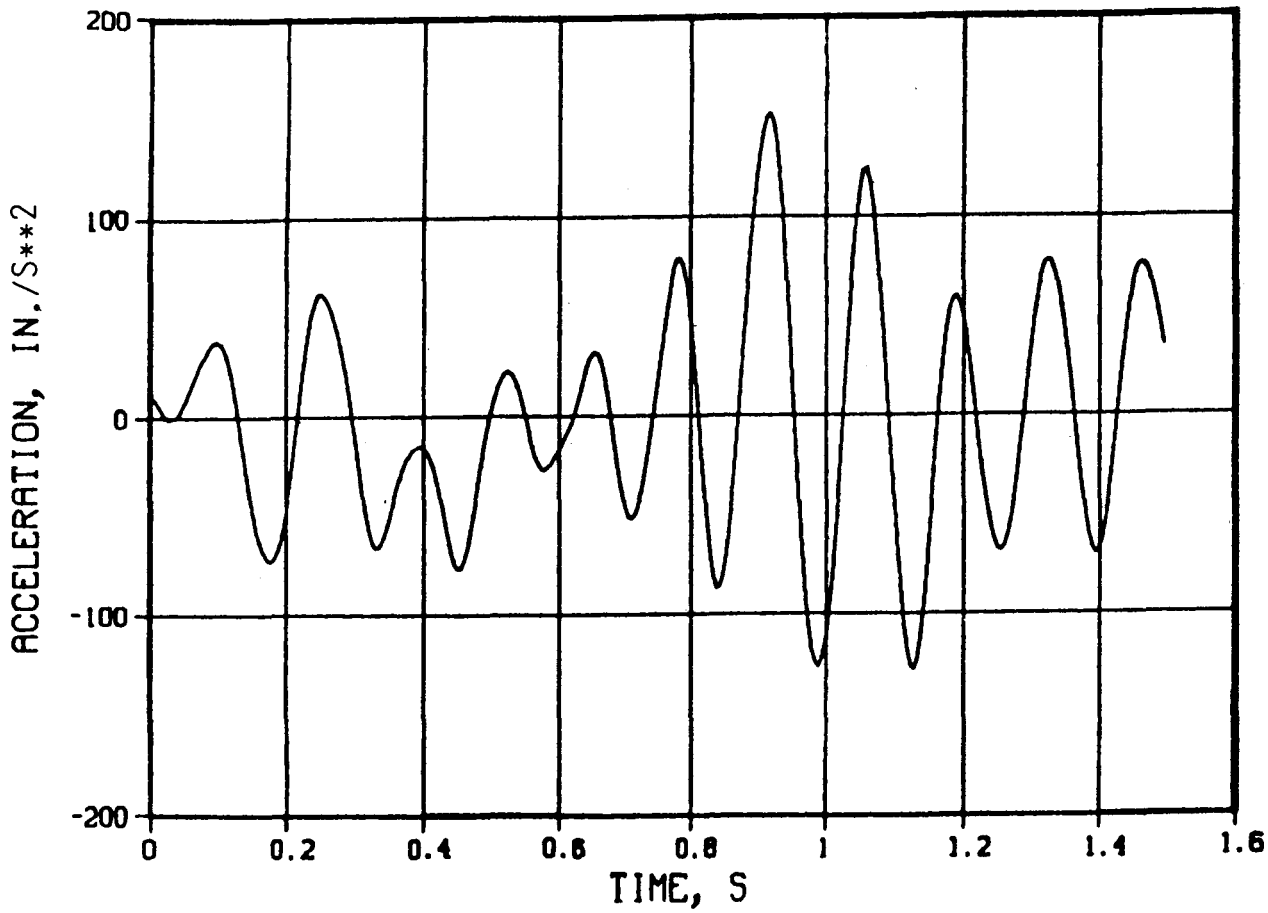

FIGURE 6-17. Nominal 1.5 s Excitation.

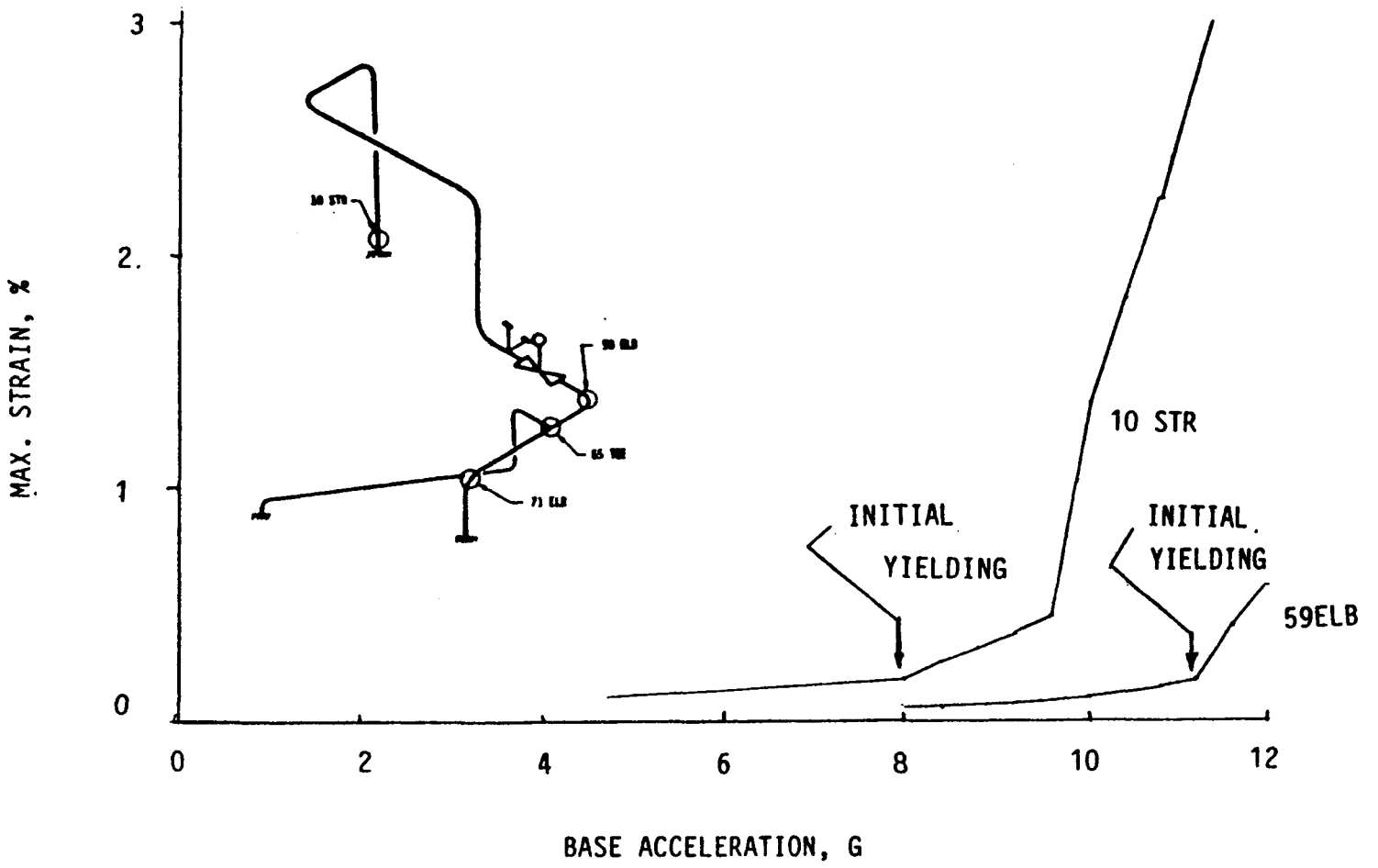

FIGURE 6-18. Response to Static Loading.

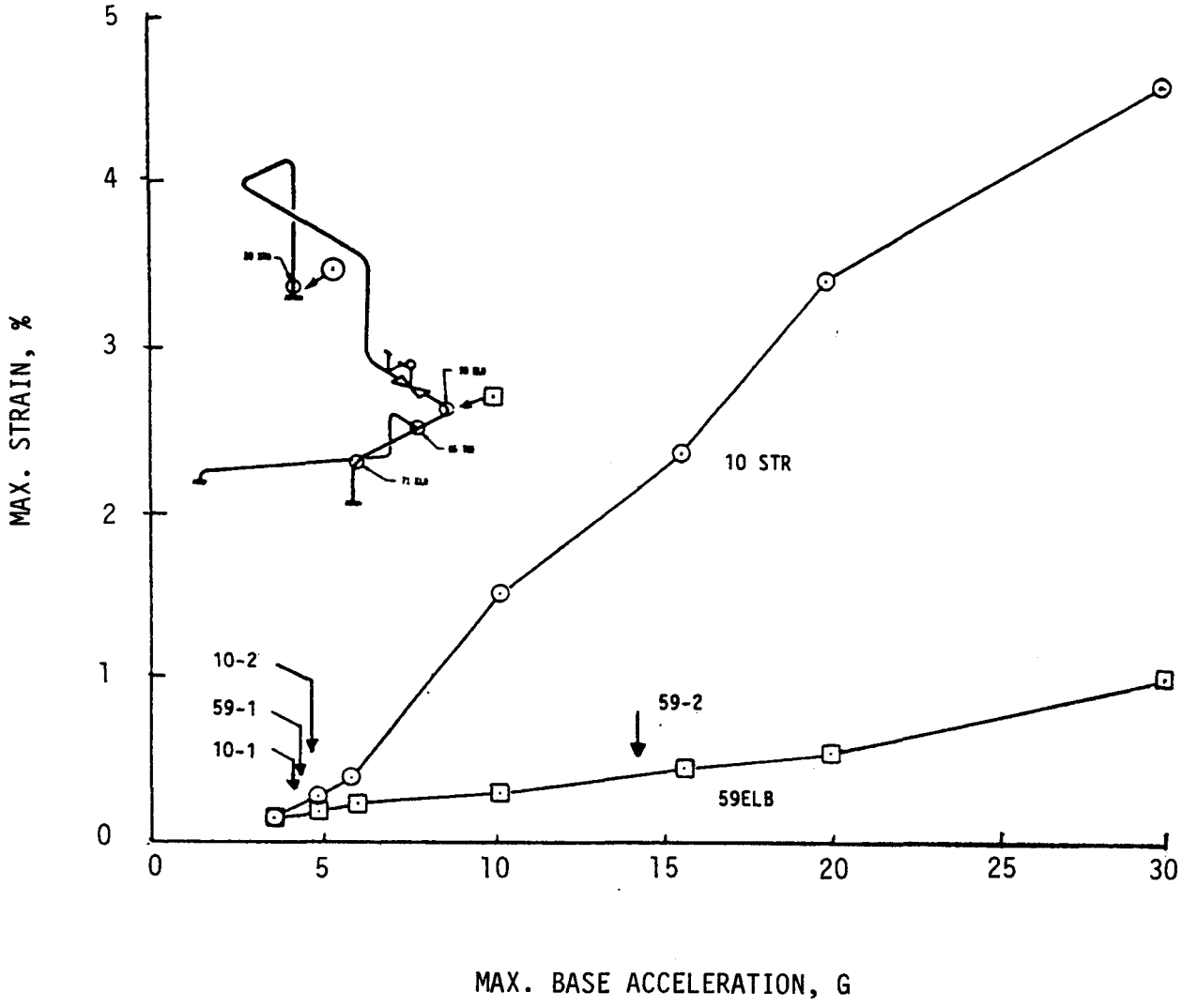

FIGURE 6-19. Transient Response - Maximum Strain.

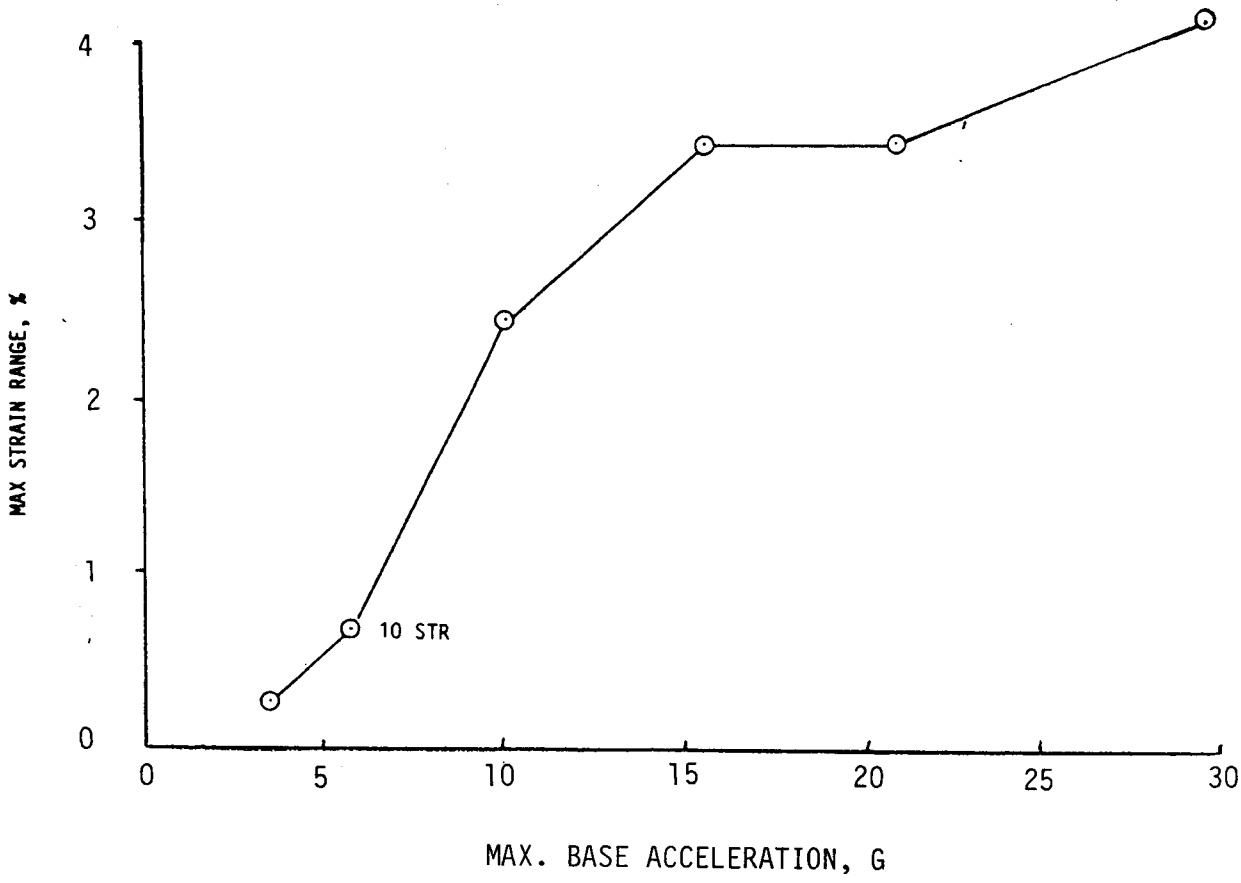

FIGURE 6-20. Transient Response - Maximum Strain Range .

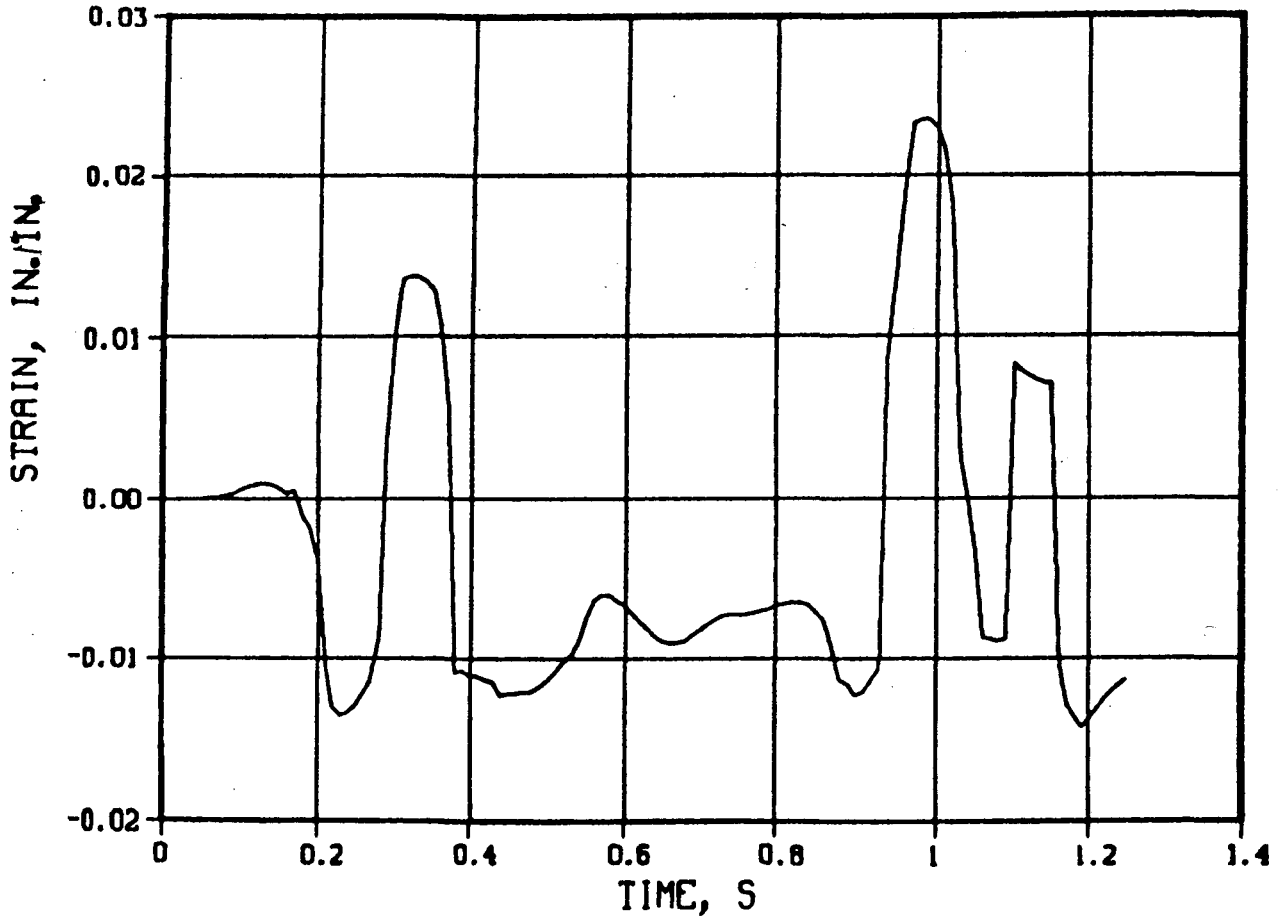

FIGURE 6-21. 15 g Excitation, Point 10 Strain History.

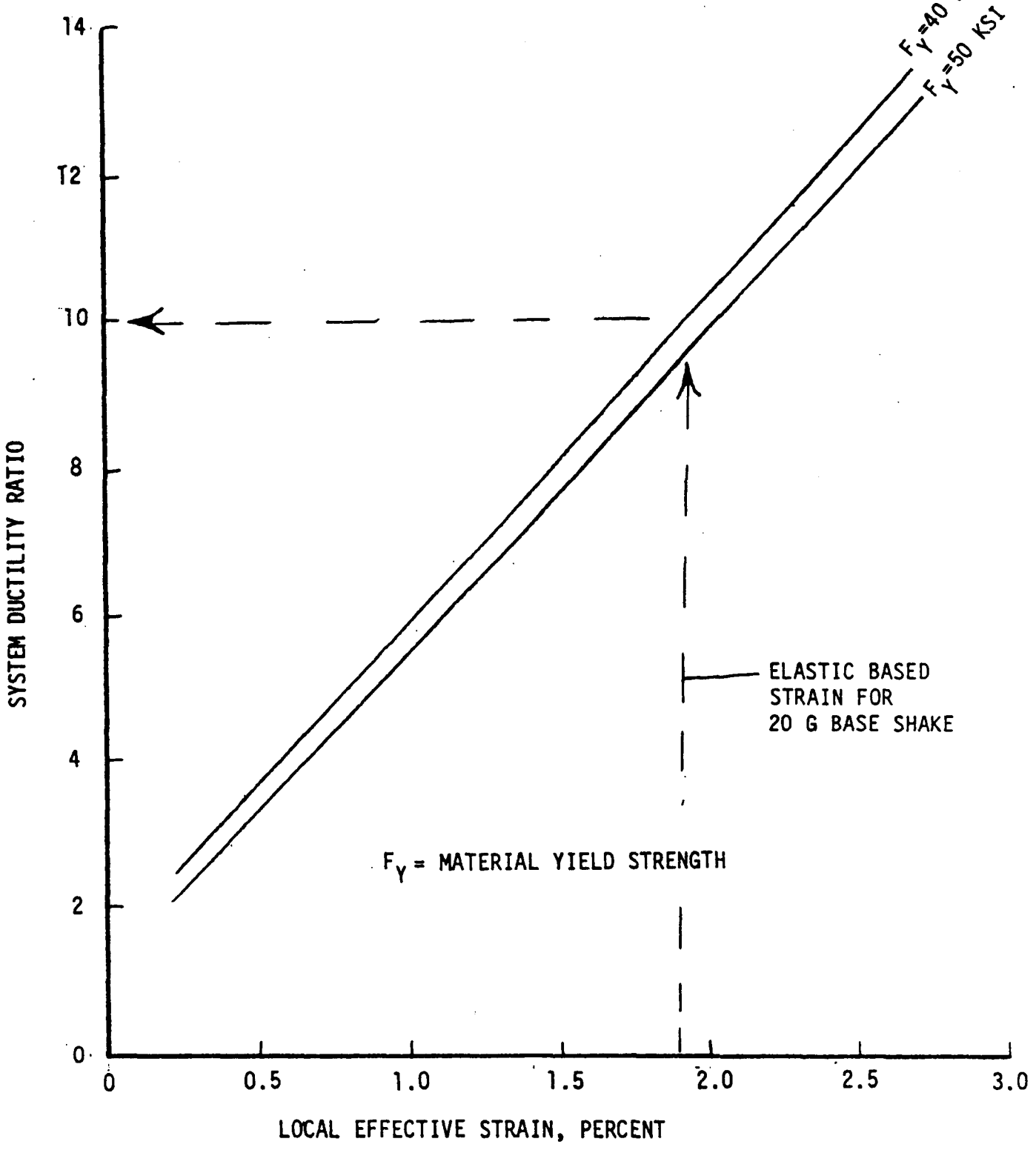

FIGURE 6-22. NRC/ETEC Test Article, System Ductility Versus Local Strain.

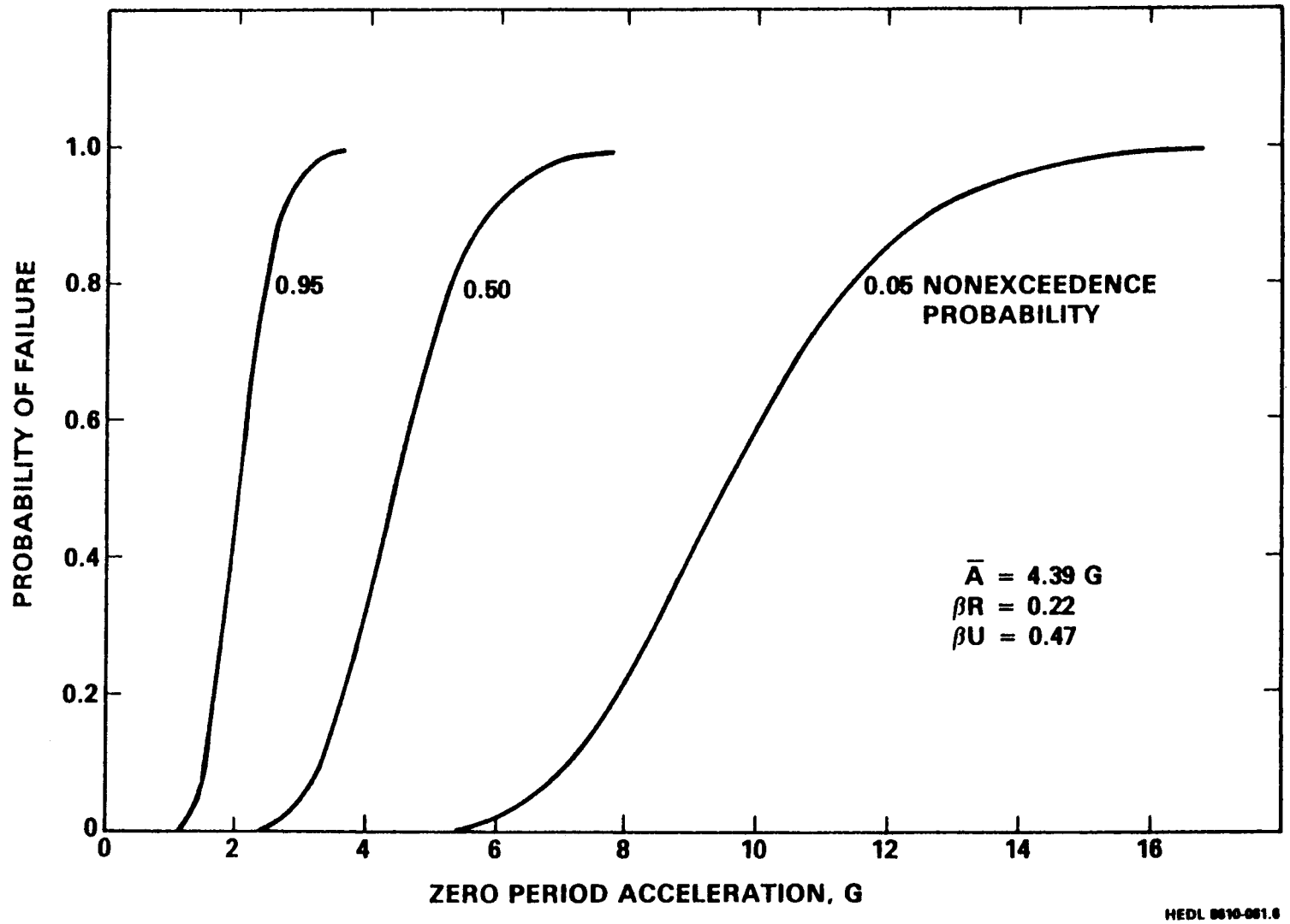

FIGURE 6-23. Seismic Fragility of Test Article by Zion Method.

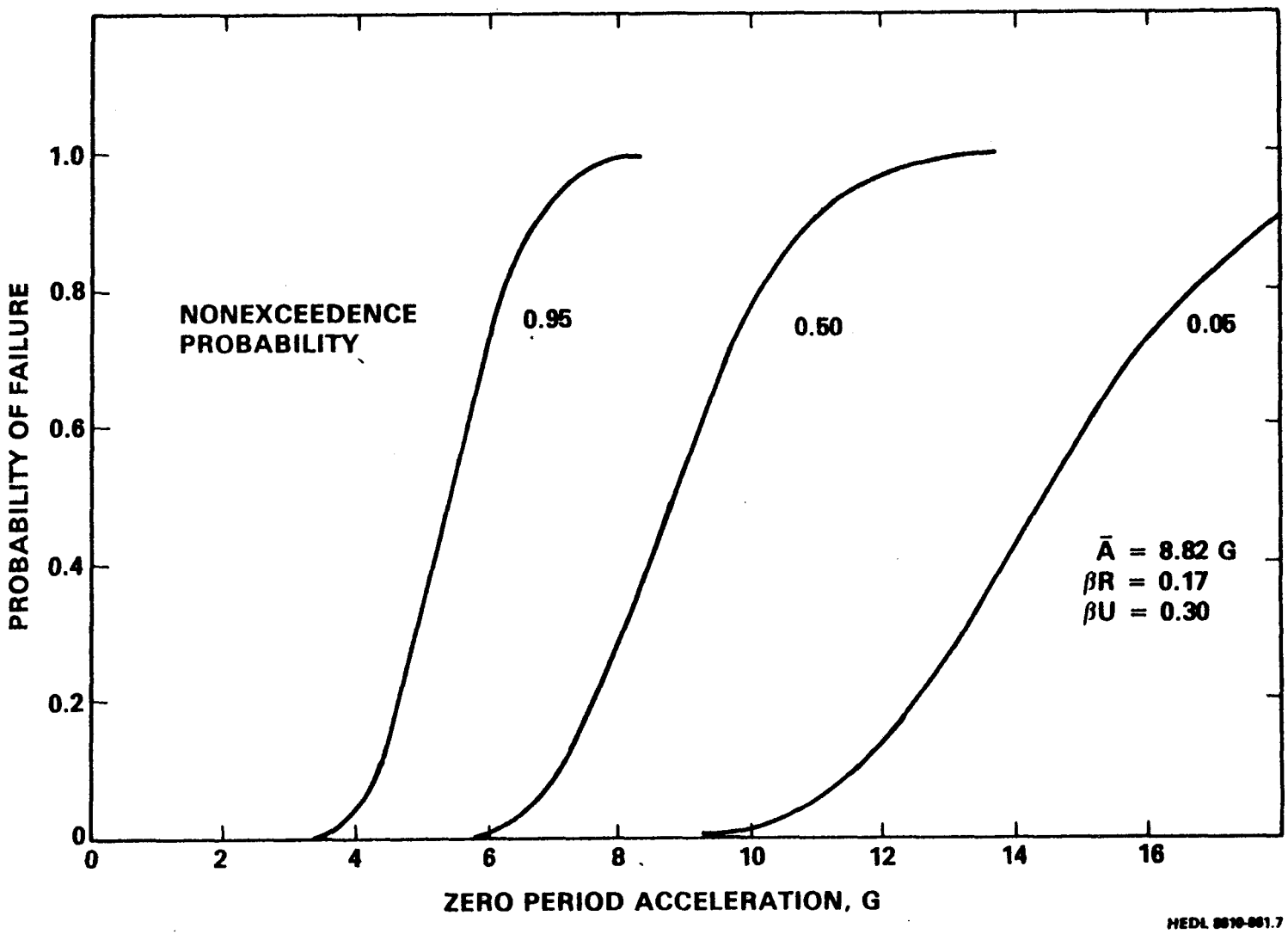

FIGURE 6-24. Seismic Fragility of Test Article by SSMRP Method.

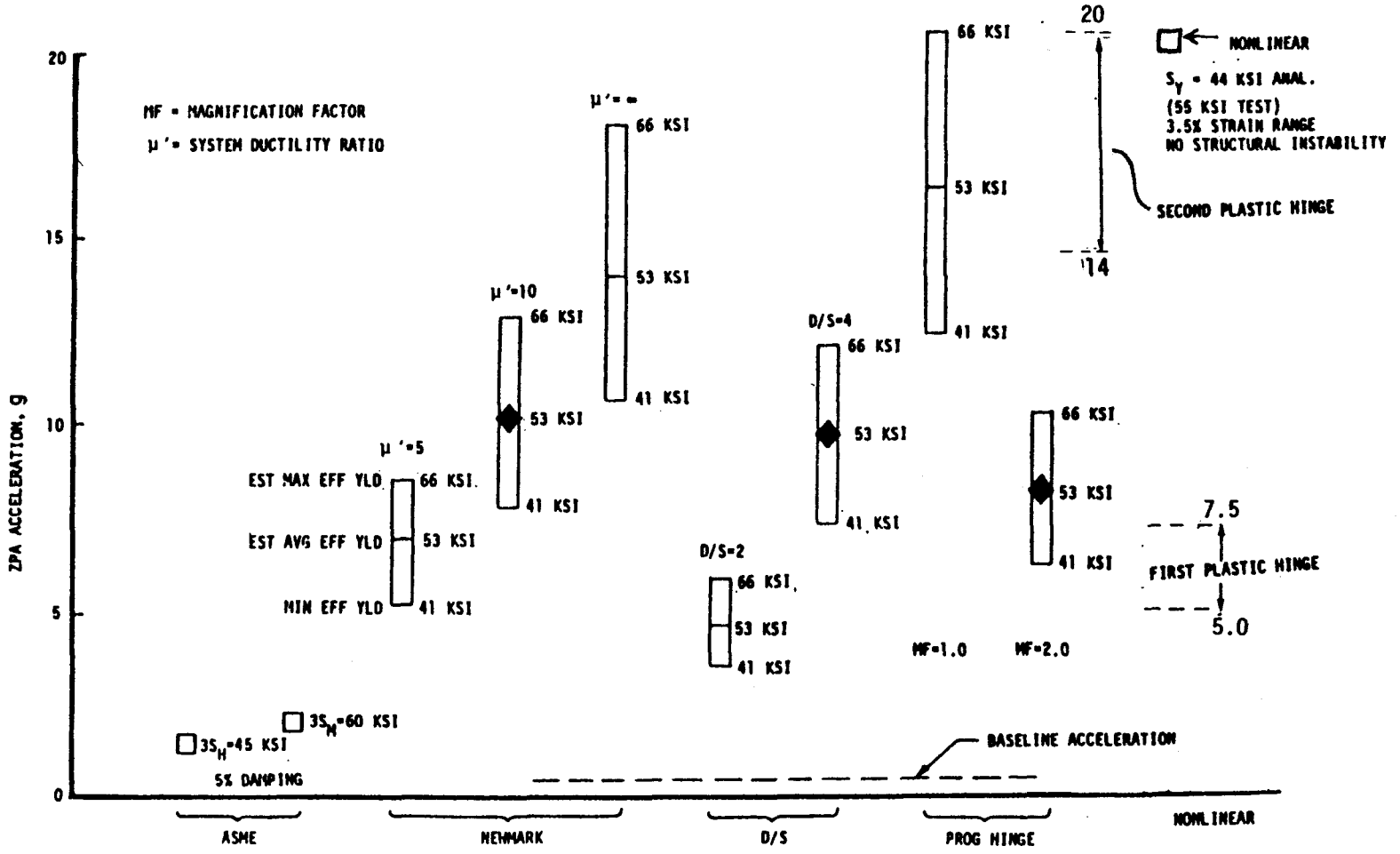

FIGURE 6-25. NRC/ETEC Test Article, Summary of Failure Predictions.

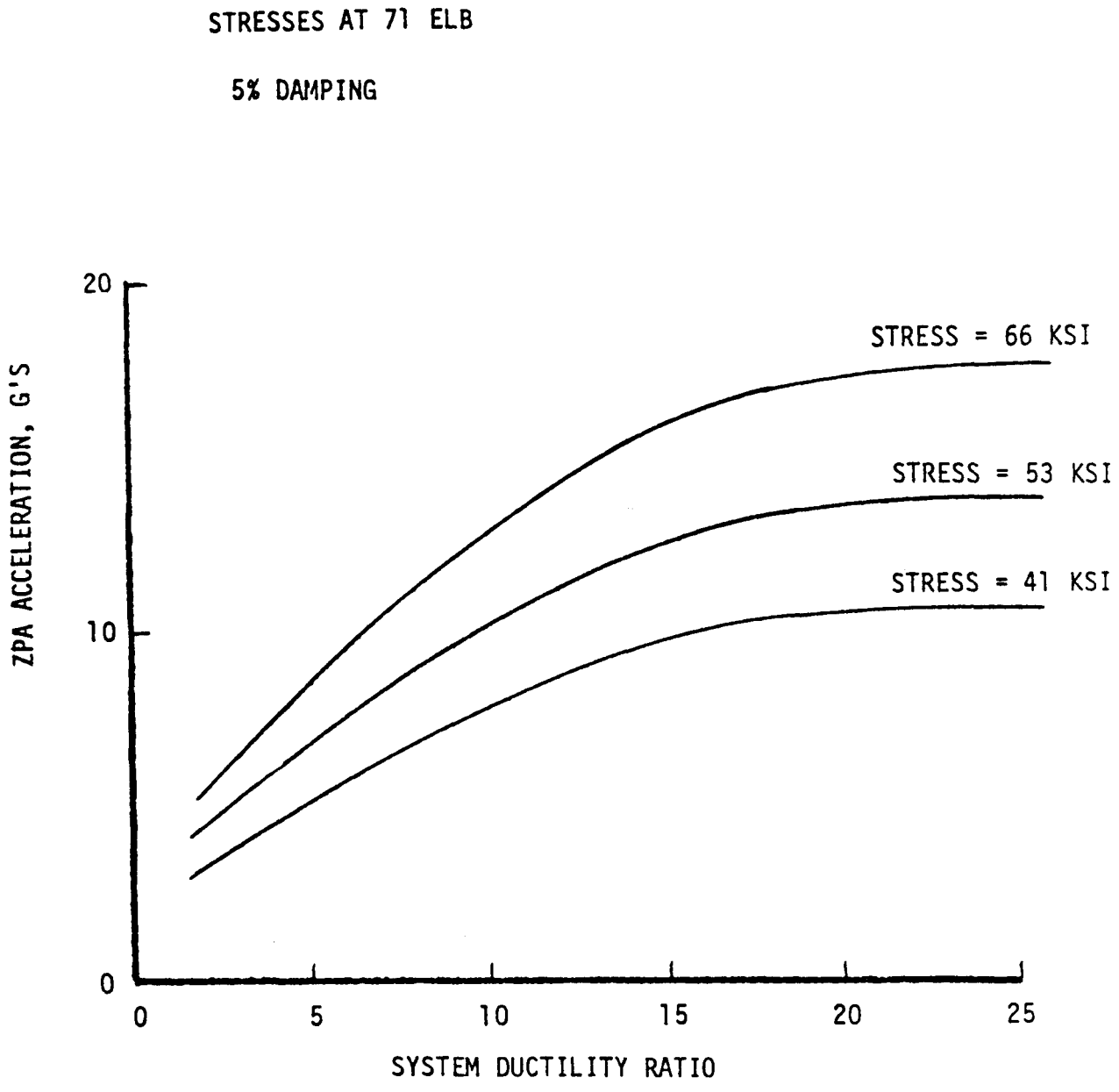

FIGURE 6-26. NRC/ETEC Test Article, Newmark Method, Effect of Changing Ductility Ratio.

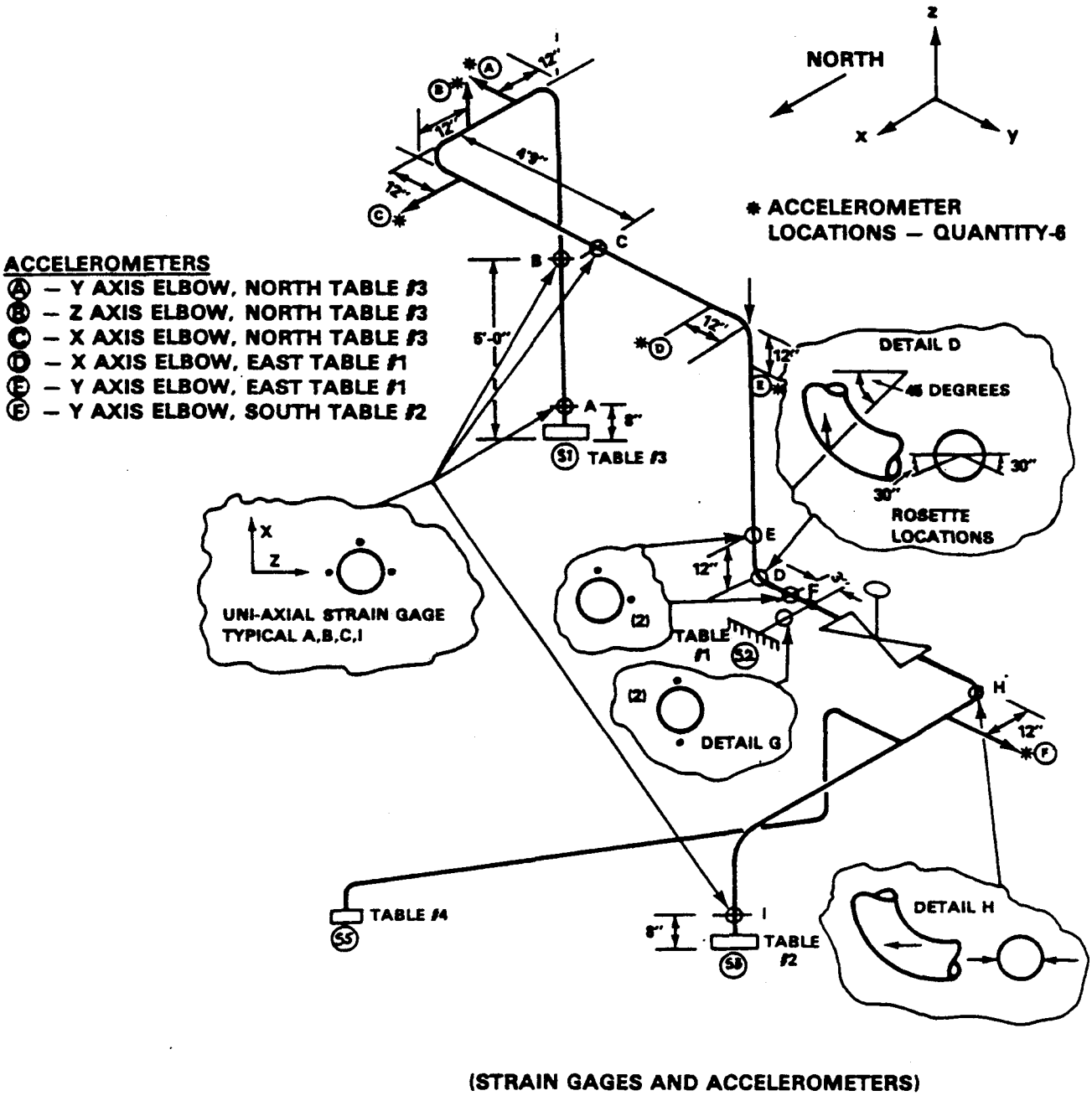

(STRAIN GAGES AND ACCELEROMETERS)

HEDL 8610-061.1

FIGURE 6-27. Instrument Locations.

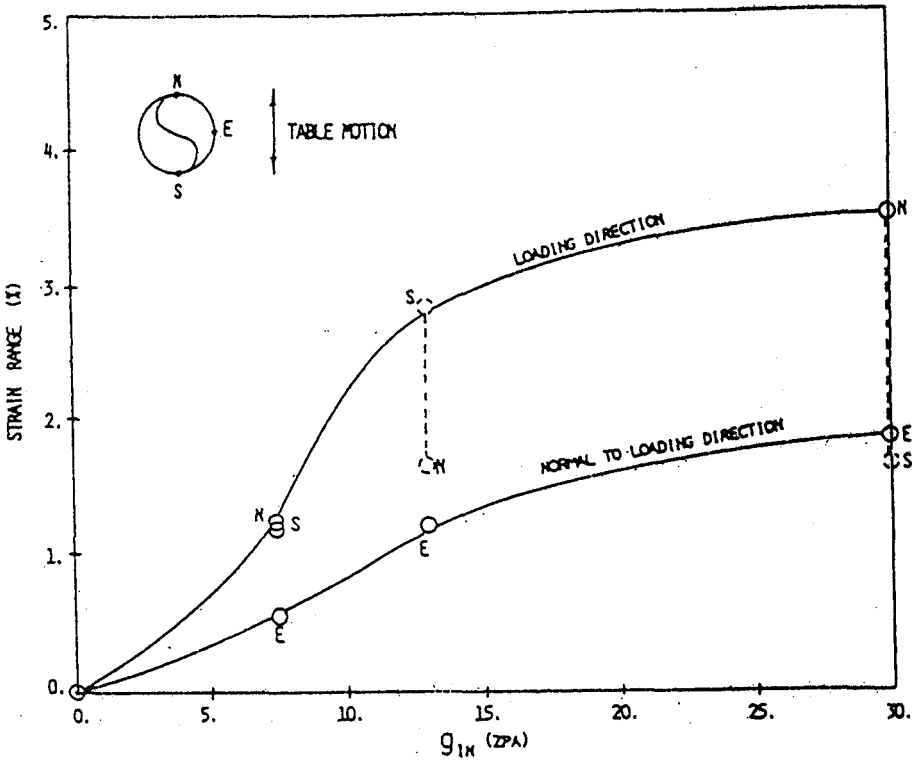

FIGURE 6-30. Test-Determined Strain Range.

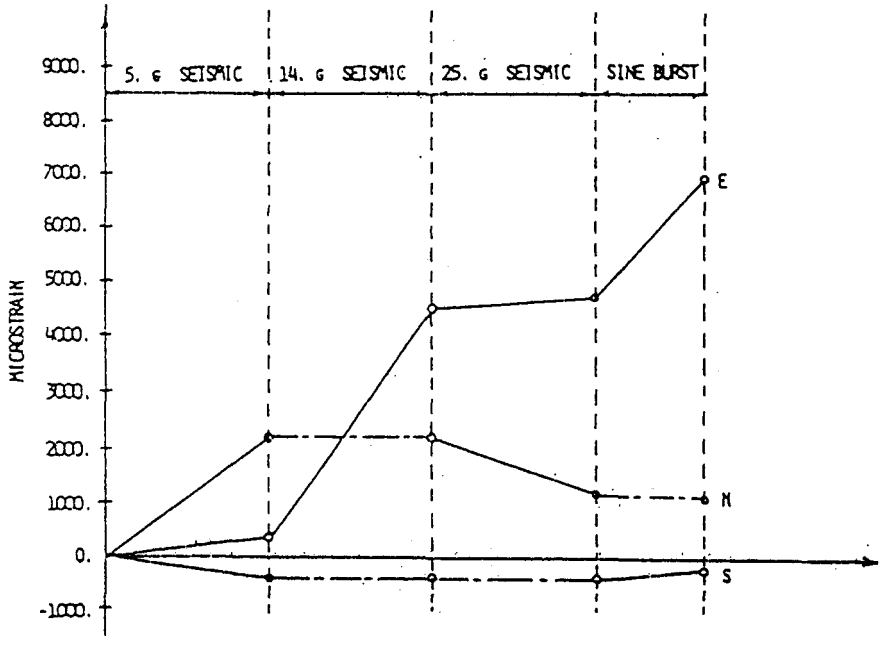

FIGURE 6-31. Longitudinal Strain Ratchet at Failure Location.

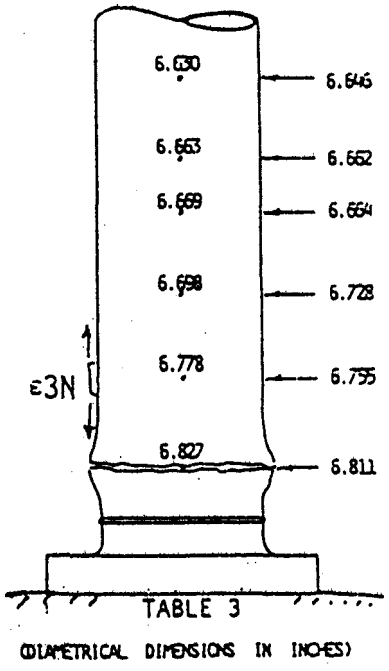

FIGURE 6-32. Pipe Failure Area.

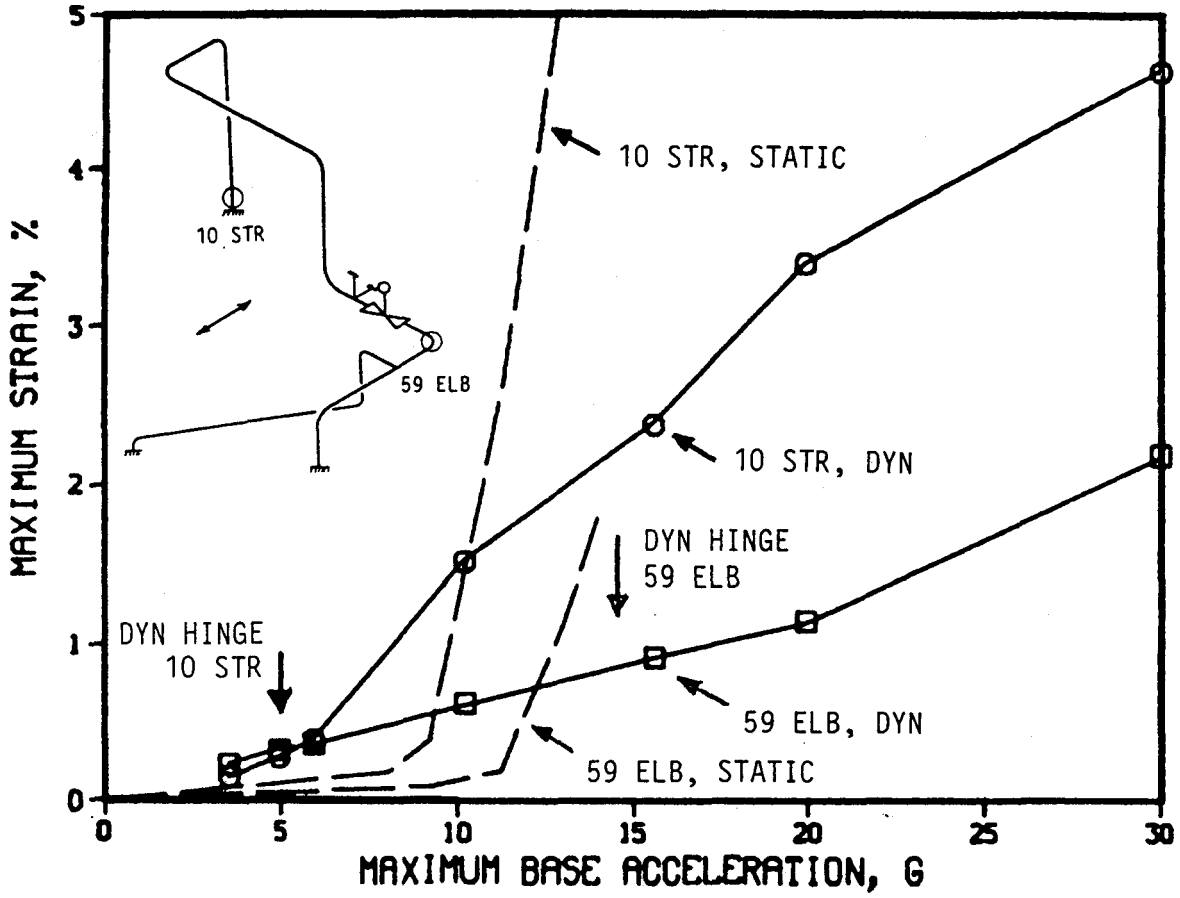

FIGURE 6-33. Transient Response - Maximum Strain.

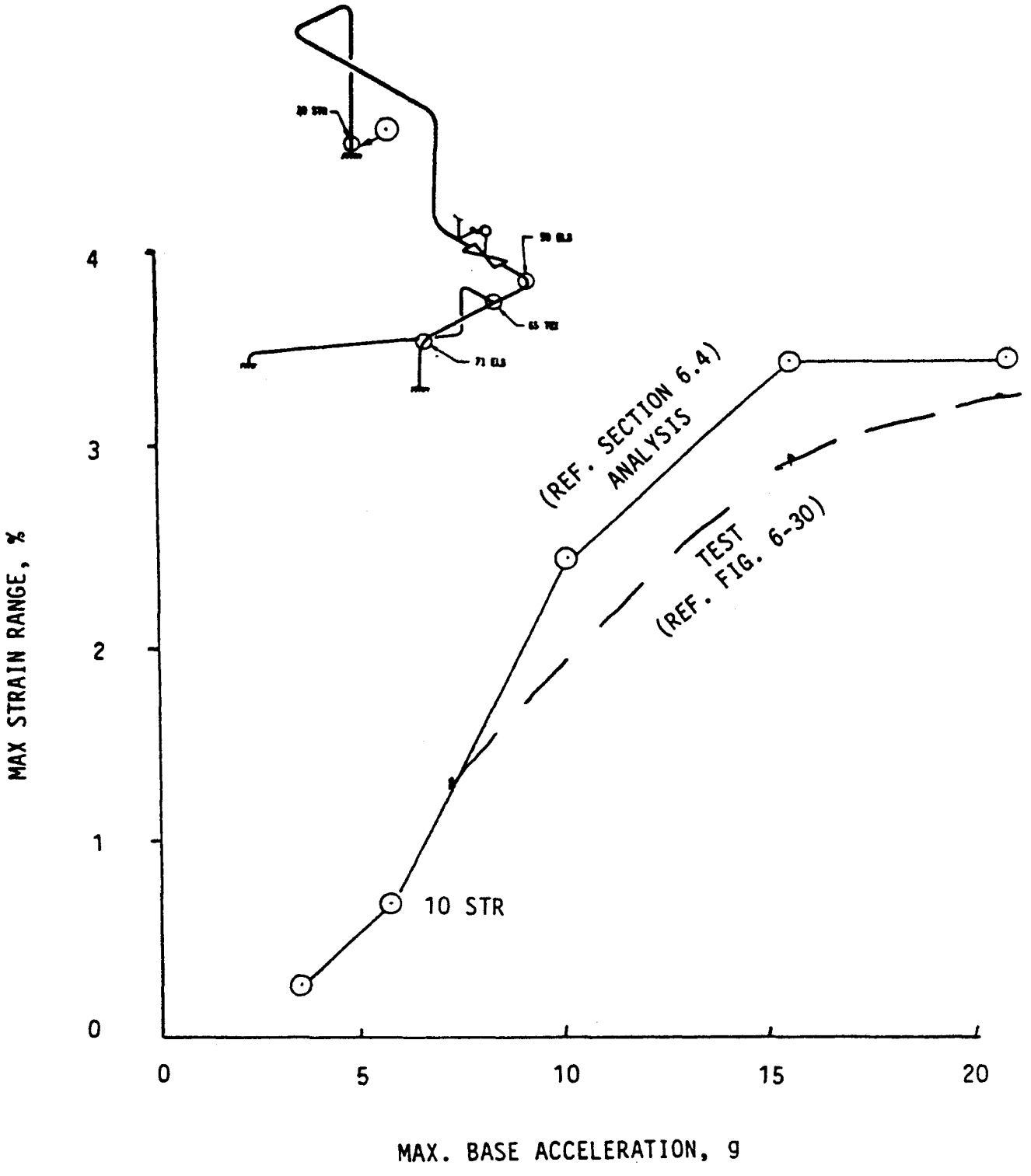

FIGURE 6-34. Transient Response - Maximum Strain Range.

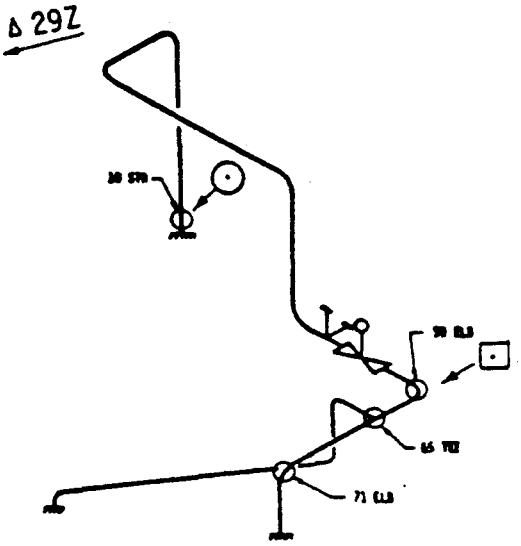

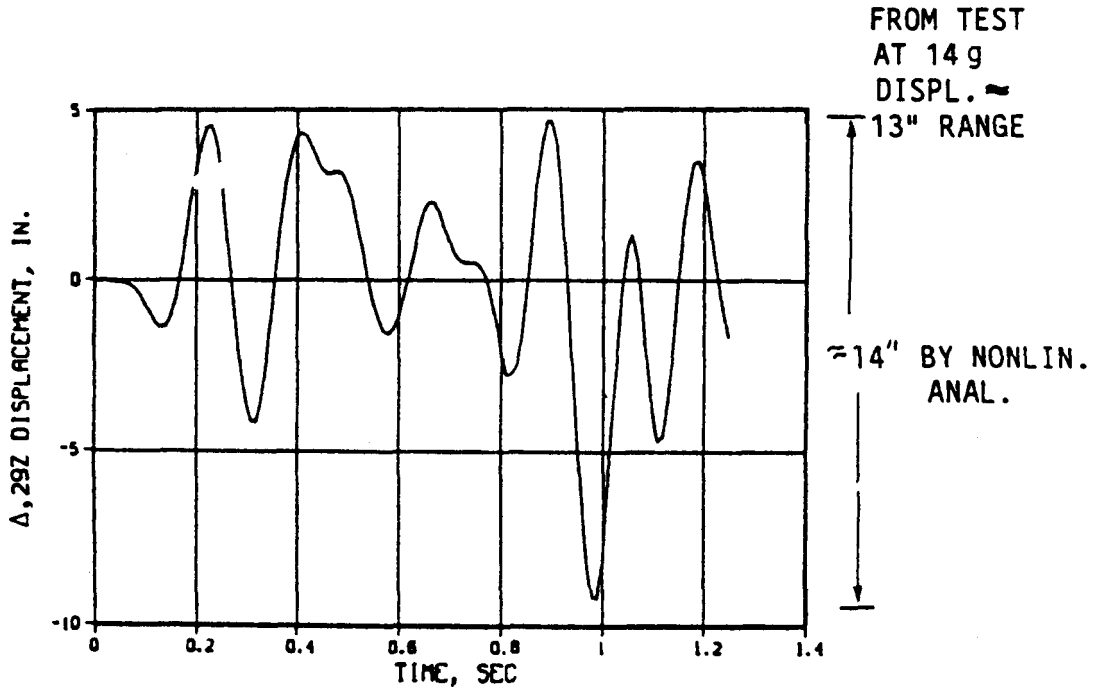

FIGURE 6-35. Comparison of Predicted and Test Displacements.

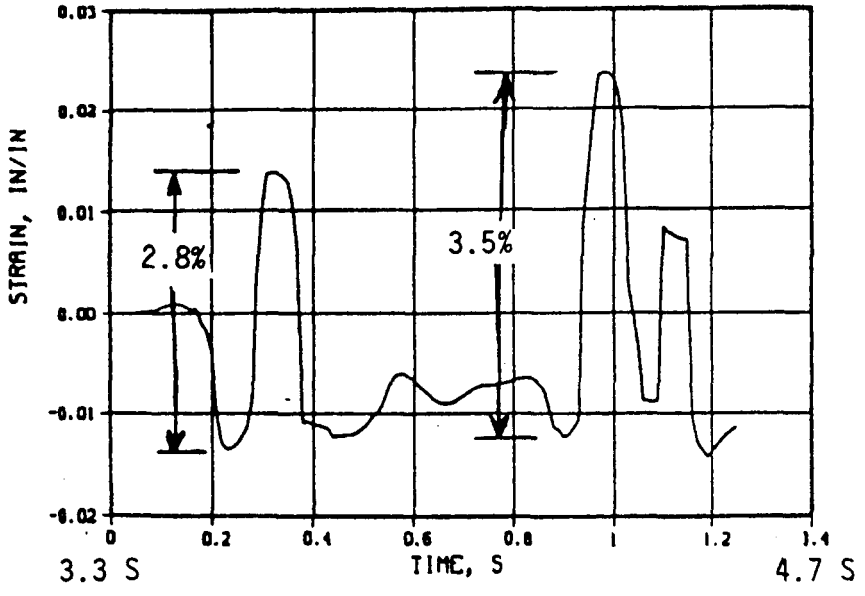

15 g Excitation, Point 10 Strain History

FIGURE 6-36. Predicted Maximum Strains.

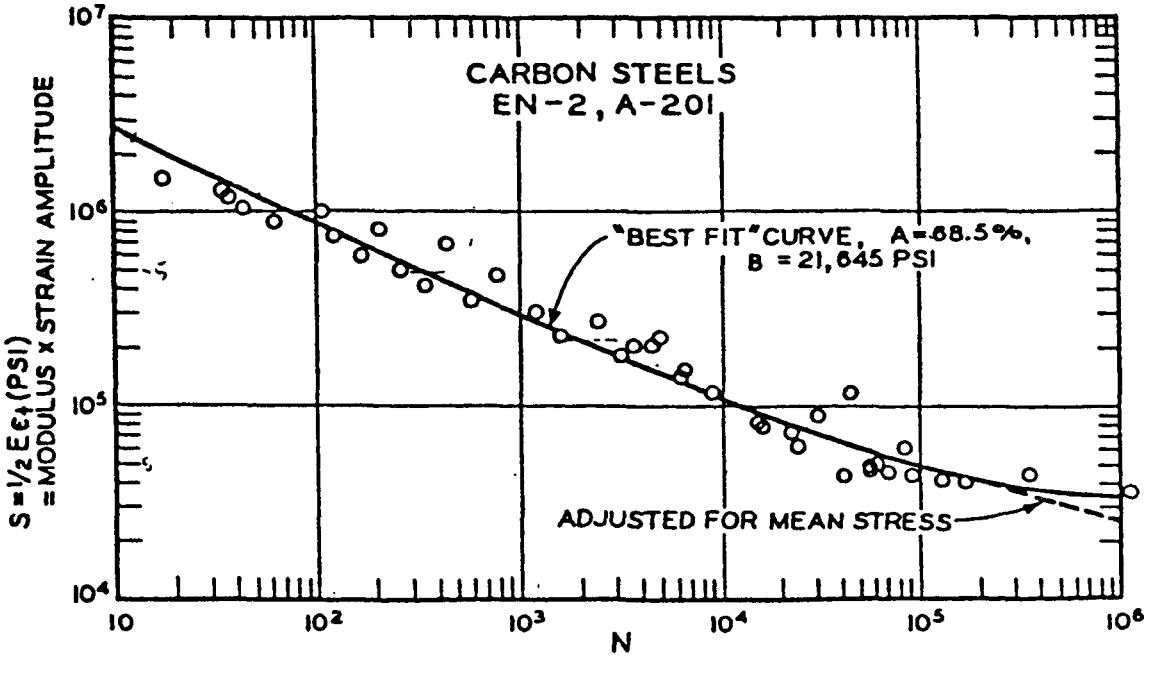

FIGURE 6-37. Material Fatigue Data.

6" DIAM ETEC PIPE TESTS
CYCLES TO FAILURE FOR EACH STRAIN RANGE

REF: HARVEY, PRESSURE VESSEL DESIGN, VAN NOSTRAND, 1963
W/O HOOP RATCHET & DUCTILITY EXHAUSTION.

$$N_f = \left[\frac{0.46}{\Delta \epsilon_t - 0.0037} \right]^2$$

ZPA	$\Delta \epsilon_t$	N_f	N	N/N_f
5	0.4%	$(10)^6$ CYCLE	4	0
	0.5%	$(10)^4$ CYCLE	4	0
15	2.8%	358	4	.011
	3.5%	215	4	.019
25	3.0%	305	4	.013
	3.6%	202	4	.020
12@ 4 H_3	3.4%	230	10	.043
18.7@ 5 H_3	3.5-8%	215-36	6 Σ 40	.028-.167 0.13-.27

- STANDARD FATIGUE CUMULATIVE DAMAGE ANALYSIS DOES NOT PREDICT FAILURE.
- TEST RESULTED IN FAILURE.
- STANDARD FATIGUE ANALYSIS UNDERPREDICTS TEST DATA.

FIGURE 6-38. Six-inch Diameter ETEC Pipe Tests--Cycles to Failure for Each Strain Range.

6" DIAM. ETEC PIPE TESTS
RATCHET/FATIGUE LIFE APPROXIMATIONS - ACCOUNTING FOR DUCTILITY EXHAUSTION

ZPA	$\Delta \epsilon_t$, %	N	ϵ_R, %	$N\epsilon_R$	$\Sigma N\epsilon_R$	N_{RF}	N/N_{RF}	$\Sigma N/N_{RF}$
5	0.4	4	.022	0.09%	0.09%	10^6	0	
	0.5	4	.05	0.20	.29	10^4	0	
15	2.8	4	0.81	3.23	3.52	350	.01	.01
	3.5	4	1.03	4.15	7.67	210	.02	.03
25	3.0	4	0.88	3.52	11.19	197	.02	.05
	3.6	4	1.07	4.28	15.49	104	.04	.09
12@ 4 H_3	3.4	10	1.00	10.00	25.00	73	.14	.23
18.7@ 5 H_3	3.5-8	6-4	1.03-2.3	6.22-9.2	31.22-34 $< e_\mu = 35\%$	7-4	.86-1.0	1.09-1.23 >1.0

- CUMULATIVE DAMAGE PREDICTS FAILURE IN LAST TEST WHICH MATCHES THE TEST RESULTS.
- RATCHETING IN HOOP DIRECTION DUE TO INTERNAL PRESSURE AND CYCLIC BENDING ON PIPE LEADS TO DUCTILITY EXHAUSTION AND RUPTURE.

FIGURE 6-39. Six-inch Diameter ETEC Pipe Tests--Ratchet/Fatigue Life Approximations - Accounting for Ductility Exhaustion.

RATCHETING OF PIPE SUBJECTED TO:

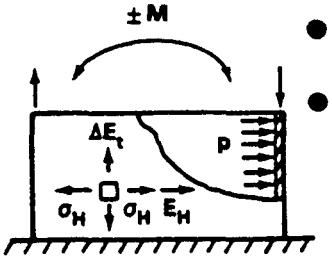

- SUSTAINED INTERNAL PRESSURE AND
- CYCLIC END MOMENT LOADING

$$\text{HOOP RATCHET STRAIN/CYCLE} = \frac{3\sigma_H}{2\sigma_y - \sigma_H}\left(\Delta\varepsilon_t - \frac{2\sigma_y - \sigma_H}{E}\right) = \varepsilon_R$$

RATCHET CALCULATIONS FOR 6 INCH DIAMETER ETEC/NRC PIPE TESTS

σ_y = 55 ksi, e_u = 35% ASTM A-106, GRADE B $S_{y\ min}$ = 35 ksi
σ_H = 10.8 ksi FOR p = 1000 psi
ε_R = 0.327 ($\Delta\varepsilon_t$ - 0.003) PER CYCLE

- DUCTILITY EXHAUSTED WHEN:

$\varepsilon_R \cdot N = e_u$

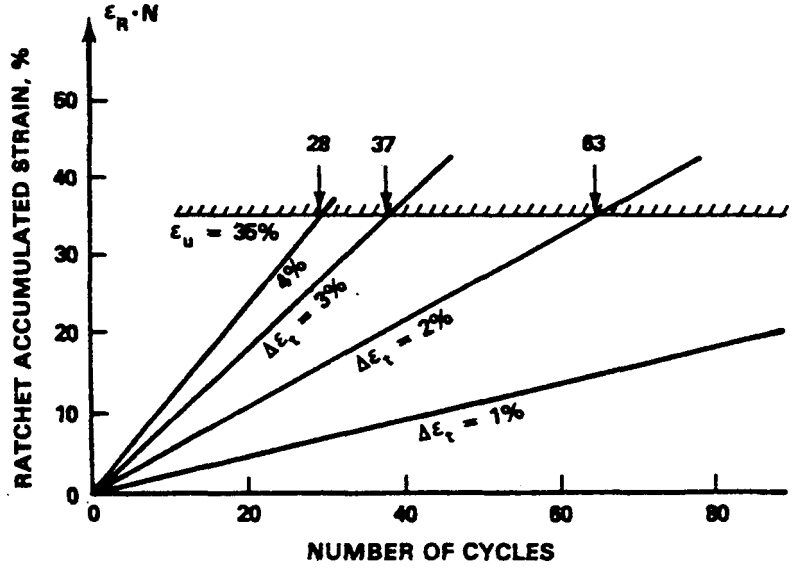

HEDL 8610-061.3

FIGURE 6-40. Ratchet Analysis.

- COFFIN FATIGUE EQ., $N_F = \left(\frac{C}{\Delta\varepsilon_P}\right)^2$
- RATCHETING $\varepsilon_R \cdot N$ REDUCES C
- RATCHET-FATIGUE EQ., $N_{RF} = \left(\frac{C - \varepsilon_R \cdot N}{\Delta\varepsilon_P}\right)^2 = \left[\frac{0.46 - \varepsilon_R \cdot N}{\Delta\varepsilon_t - 0.0037}\right]^2$
- INTERACTION FACTOR

$$N_{RF}/N_F = \left[1 - \frac{\varepsilon_R \cdot N}{C}\right]^2$$

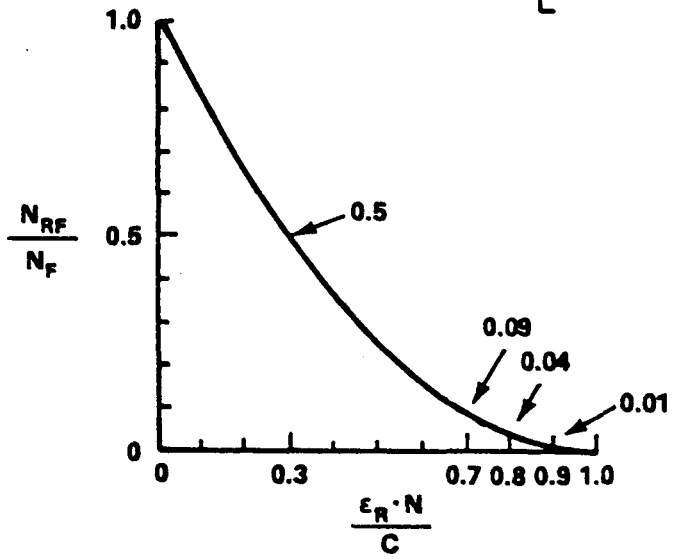

HEDL 8610-061.2

FIGURE 6-41. Approximate Ratchet-Fatigue Interaction.

7.0 KWU FOUR-INCH/TWO-INCH DIAMETER PIPE SYSTEM TEST

A series of high-level dynamic tests have been performed on a combination four-inch and two-inch diameter pipe system by the KWU. The testing is reported in Reference 8.

7.1 TEST ARTICLE/STRUCTURAL MODEL

The KWU test system consisted of a four-inch diameter main pipe line approximately 41 feet in length with a two-inch diameter branch line approximately 17 feet in length (Figure 7-1). Wall thickness of the piping was 0.165 inch and 0.114 inch, respectively. Pipe material was austenitic stainless steel, with 3 S_m of 60 ksi and 3 S_H of 56 ksi. A structural analytical model was developed as shown in Figure 7-2.

7.2 TEST LOADING/FAILURE MODE

Test loading consisted of two time-history load inputs and a harmonic excitation. The time histories represented (1) a standard-type broadened and enveloped floor earthquake response spectrum and (2) a "natural" free field time history. Multiples of the time histories were also run. The maximum time-history test response spectrum, provided by KWU through INTERATOM to WHC, is shown in Figure 7.3. Shown in the Figure is the actual spectrum and the broadened spectrum used for analyses.

Although local distortion occurred, failure of the piping test article did not occur as a result of the test load inputs. The greatest measured distortion was approximately 1% local strain near the anchor on the two-inch diameter branch line for the sinusoidal testing and slightly less for seismic testing. Maximum test acceleration levels are estimated to be 4.0 ZPA for sinusoidal input and 5.5 ZPA for time-history input.

7.3 SIMPLIFIED ELASTIC AND ELASTO-PLASTIC ANALYSES

In a manner similar to that discussed in Section 3.1, simplified elastic and elasto-plastic methods have been applied to the configuration and loading environment used for the KWU pipe test system. These are discussed below.

7.3.1 Linear Elastic Analysis

Linear elastic analyses have been performed using the PIPESD code for the structural model of Figure 7-2 under the magnified response spectrum of Figure 7-3. Stresses were calculated for the above spectrum and multiples thereof. The maximum stresses at several system locations have been plotted in Figure 7-4, with the stresses being the summation of dead weight and seismic test loading. On the abscissa, the equivalent ZPA is shown.

Figure 7-4 shows that the tee at Node 24, the straight section at Node 120 and the elbow at Node 117 have the maximum total stress. The ASME Code, Class 1, Level D allowable, 3 S_m of 60 ksi, and the comparable ASME Code, Class 2 allowable, 3 S_H (56 ksi) are also shown in Figure 7-4. The allowable ZPA loading for the system is 1.9 g for Class 2 allowables and 1.7 g for Class 2 allowables.

7.3.2 Newmark Plastic Spectra Method

Figure 7-5 presents the reduced spectra incorporating several values of system ductility ratio that was used for Newmark method analyses.

Figure 7-6 presents the summation of KWU pipe test article dead weight plus seismic test loading stresses as a function of response spectra ZPA loading for a system ductility ratio of 3. Location at elbow Node 117 is seen to be critical.

7.3.3 Dynamic/Static Margin Ratio Method

Figure 7-7 presents the summation of KWU test article dead weight plus seismic test loading stresses as a function of response spectra ZPA loading for typical D/S ratios of 2 and 3. The elbow at Node 117 and the straight section at Node 120 are seen to be nearly equally stressed.

7.3.4 System Ductility and Equivalent Yield Point

The KWU four-inch/two-inch diameter test article was fabricated from a material (austenitic stainless steel) similar to that of the WHC one-inch diameter pipe loop (Reference 6). On the basis of the results of analytic studies and an assessment of test results, a system ductility ratio of 5 was chosen for the WHC one-inch diameter test article. A somewhat more conservative system ductility ratio of 3 was chosen for the KWU test article. Corresponding dynamic/static margin ratio is approximately 2.

A yield point equivalent to that of the WHC one-inch diameter test loop was chosen for the KWU test article. This effective yield value is 54 ksi. Maximum and minimum yield points were taken at 67 ksi and 42 ksi, respectively.

7.3.5 Progressive Hinge Formation Method

As in previous studies, the progressive hinge formation method was implemented by applying a constant lateral load to the system and assessing the resulting stresses against component capabilities.

The four-inch diameter mainline portion of the system formed the first collapse mechanism under static lateral loading. Plastic hinges formed at two locations of straight pipe as shown in Figure 7-8.

Application of a constant dynamic load (response spectrum) caused a branch line mode involving vertical response to be critical. Two plastic hinges in this line result in a collapse mechanism as shown in Figure 7-9. Since the dynamic case causes response of a different portion of the system the resulting failure levels do not correlate between the dynamic case and the static case.

Table 7-1 summarizes results of progressive hinge studies for three levels of effective yield strength.

7.3.6 PRA-Type Methods

PRAs of the piping systems were made using the methods described in References 13 and 14. Reference 13, referred to by the author as the "Zion Method," determines the fragility of a piping system by estimating the median safety factor and logarithmic standard deviation. The latter are determined from analysis of a number of typical piping systems. Reference 14, the "SSMRP Method," is similar except that analysis of the specific piping system under consideration is utilized.

Both of these methods and their application to the KWU four-inch/two-inch diameter test article are described in the following sections.

7.3.6.1 Test Article Fragility Using the "Zion Method"

Since this method considers the capacity of the piping, supports, and other factors based on typical systems, the individual capacity factors for the KWU test article are quite similar to that of the ETEC three-inch diameter test system, Section 8.3.6. The only difference is the % damping for the design response spectrum. The "Konvoi" spectrum (Reference 8) with 7% damping is assumed for the KWU system. This affects the "damping factor" used in the Zion Method. The factors used in predicting the fragility of the test article are shown in Table 7-2. The median acceleration based on a 0.42 g OBE is 18.46 x 0.42 or 7.75 g. Probability of failure curves for 0.05, 0.50 and 0.95 nonexceedence probabilities are shown in Figure 7-10.

7.3.6.2 Test Article Fragility Using the "SSMRP Method"

The methods used for the SSMRP are those previously discussed in Section 6.6. The results show a median acceleration $\bar{A}$ = 11.48 g with β_R = 0.17 and β_U = 0.30. Probability of failure curves for 0.05, 0.50, and 0.95 nonexceedence probabilities are shown in Figure 7.11.

7.4 NONLINEAR TRANSIENT DYNAMIC INELASTIC ANALYSIS

Modelling of the KWU test article is based on Reference 8. The methods employed were similar to those described in Section 6.4. Figure 7-12 shows the grid before refinement, and Table 7-4 has other modelling information. Mode 3 with a frequency of 9.8 Hz is characterized by branch deformation (Figure 7-13). The 8.9 Hz excitation frequency appears to concentrate on the branch by anticipating a frequency shift caused by plastic softening.

The results of the 4 g excitation are summarized in Table 7-3. The maximum strain range at the branch anchor compares well with the test results, but the other analysis results run about half. The analysis strain record at the branch anchor is shown in Figure 7-14. The shift is not reflected in the displacement record at Node 82 (Figure 7-15). The two-inch length element at the branch anchor is the only one exceeding the M_{y2} moment. Thus, the system barely went plastic, and this may explain the large magnification (6.2) found in the analysis.

7.5 SUMMARY OF COLLAPSE PREDICTIONS, KWU FOUR-INCH/TWO-INCH SYSTEM

A summary of the analysis results performed on the KWU test system is presented below with collapse levels predicted, Figure 7-16. Most likely collapse loads are shown for an effective yield point of 54 ksi. The results shown in Figure 7-16 are also summarized in Table 2-1.

The limits discussed below for the Newmark, D/S, and static progressive hinge methods are 42 ksi, 54 ksi, and 67 ksi. These represent a minimum, average, and maximum expected effective yield point for austenitic steel material.

Linear elastic analyses were performed on the pipe system for a broadened response spectra loading used for the tests. The analyses were accomplished by scaling the spectra to obtain results for various base load levels. The allowable base input loading was found to be 1.9 g for an ASME Class 1, Level D limit ($3\ S_m$ = 60 ksi) and 1.7 g for an ASME Class 2, Level D limit ($3\ S_H$ of 56 ksi). This limit is shown on Figure 7-16 as "ASME."

The results of the Newmark analysis are presented in Figure 7-16 for system ductility ratios of 3, 5, and infinity. A system ductility ratio of 3 has been previously estimated which, along with an average effective yield value of 54 ksi, results in a failure level of 4.8 g base acceleration.

The allowable limits based upon the D/S margin ratio method were calculated for D/S ratios of 2 and 3, with these shown in Figure 7-16. The D/S value of 2 corresponds to a system ductility of approximately 3. It is seen in Figure 7-16 that an effective yield point of 54 ksi and a D/S value of 2 gives a predicted base acceleration limit of 4.5 g.

The results of the static progressive hinge method are shown in Figure 7-16 for yield values of 42, 54, and 67 ksi. An average effective yield stress of 54 ksi gives a predicted failure level of approximately 21 g and 11.2 g for the static and dynamic analyses using the progressive hinge method. It should be noted that this represents the acceleration of the pipe itself and is related to the base input acceleration by the magnification factor. If one assumes a magnification factor of 5, the predicted based acceleration at failure would be approximately 4.2 g and 2.2 g for the assumed yield point of 54 ksi.

The PRA-type fragility estimates gave collapse loads, at 50% probability and 50% nonexceedence, of 7.8 g for the "Zion" method and 11.5 g for the SSMRP method. These are shown in Figure 7-16.

The nonlinear transient analysis showed no indication of system collapse at a 4 g load level. Maximum calculated strain at this load level was 1.6%, which agreed well with test data.

TABLE 7-1

KWU TEST ARTICLE, PREDICTED

HINGE FORMATION LOAD LEVELS, PROGRESSIVE HINGE METHOD

Yield Stress (KSI)	Static Load Application		Dynamic Load Application	
	Collapse (G)	No. of Hinges	Collapse (G)	No. of Hinges
42	16.2	2	8.6	2
54	21.0	2	11.2	2
67	26.4	2	13.9	2

TABLE 7-2

FRAGILITY PARAMETERS FOR KWU TEST ARTICLE
(ZION METHOD)

FACTORS	MEDIAN SAFETY FACTOR	RANDOMNESS β_R	UNCERTAINTY β_U
CAPACITY FACTOR			
PIPING			
Strength	8.04	0	0.36
Inelastic Energy Absorption	2.24	0.16	0.16
Three Hinge Factor	1.22	0	0.10
EQUIPMENT RESPONSE FACTOR			
Qualification Method	1.00	0	0
Spectral Shape	1.00	0	0
Modeling	1.00	0	0.15
Damping	0.84	0.03	0.17
Mode Combination	1.00	0.15	0
Earthquake Component Combination	1.00	0	0
STRUCTURAL RESPONSE FACTOR	1.00	0	0
TOTAL	18.46	0.22	0.47

TABLE 7-3

TRANSIENT ANALYSIS SUMMARY
KWU TEST ARTICLE

	ANALYSIS	TEST
STRAIN RANGE, % NODE 94	1.6	1.7
STRAIN RANGE, % NODE 10	0.4	0.8
STRAIN, % ELBOW 88-90	0.11	0.21
STRAIN, % ELBOW 20-22	0.16	0.28
MAGNIFICATION NODE 82	6.2	-
PHASE, DEGR NODE 82 vs BASE	86	-

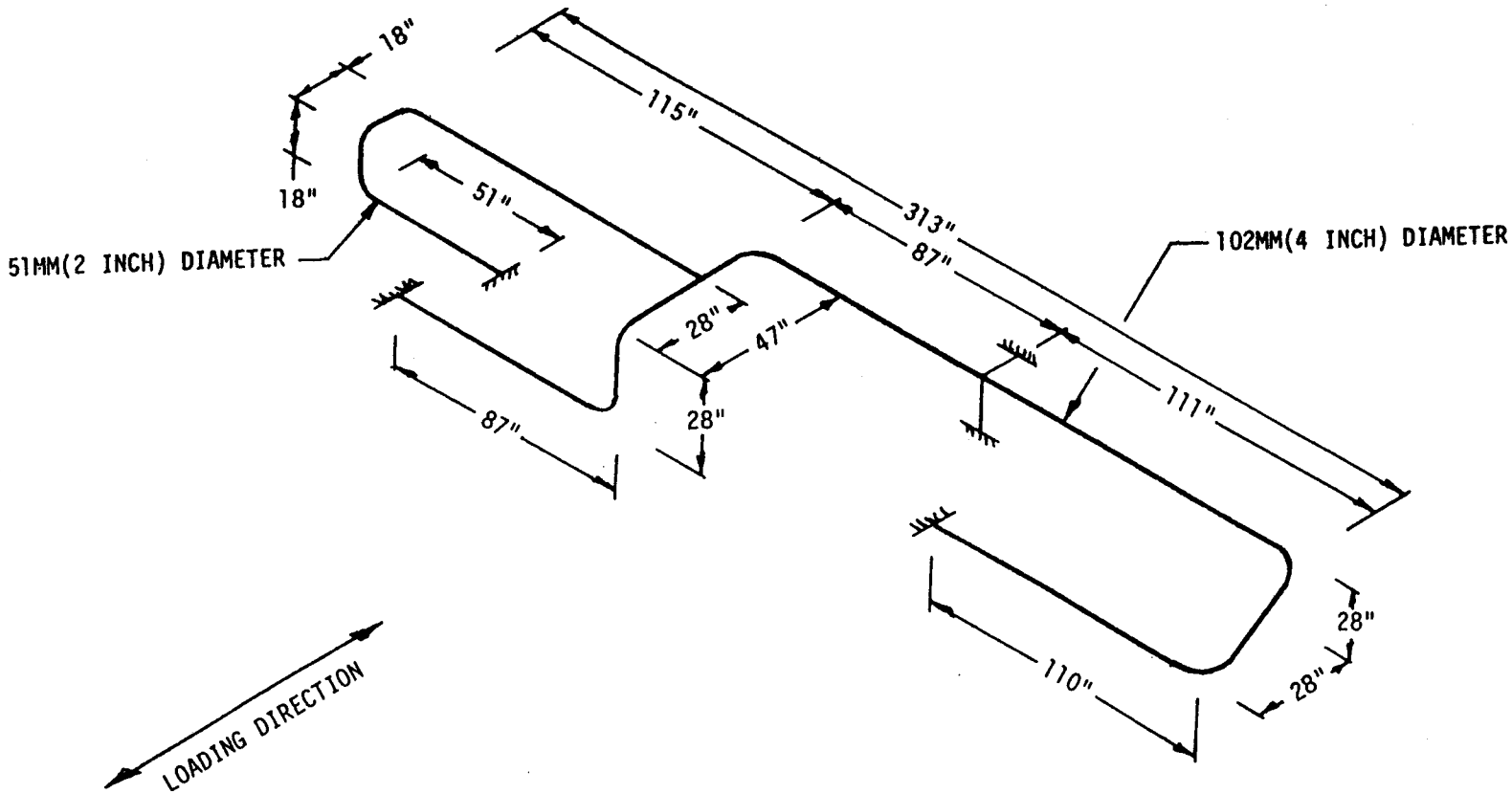

FIGURE 7-1. KWU Test Article.

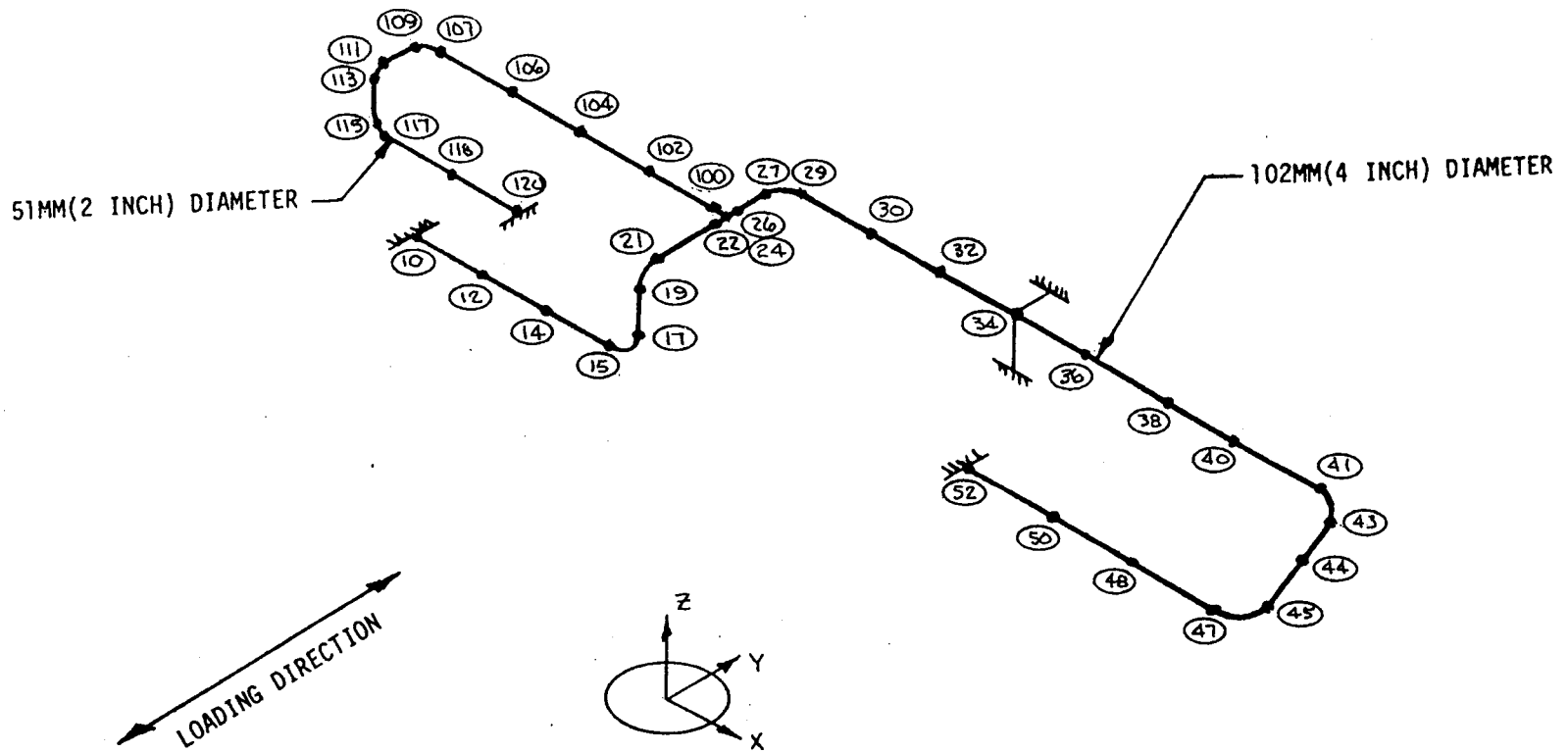

FIGURE 7-2. KWU Test Article, Analytical Model.

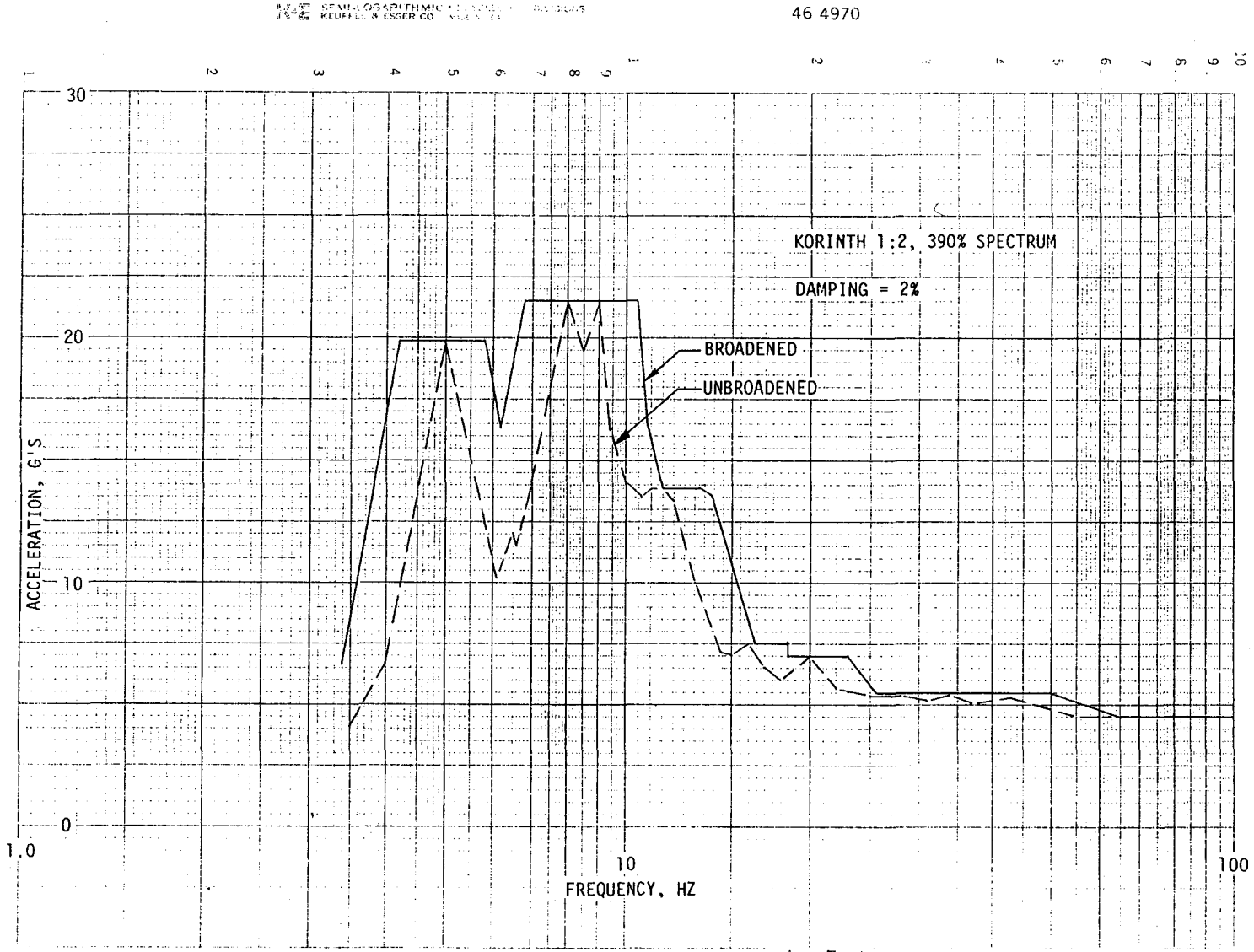

FIGURE 7-3. KWU Test Article, Response Spectrum Used During Test.

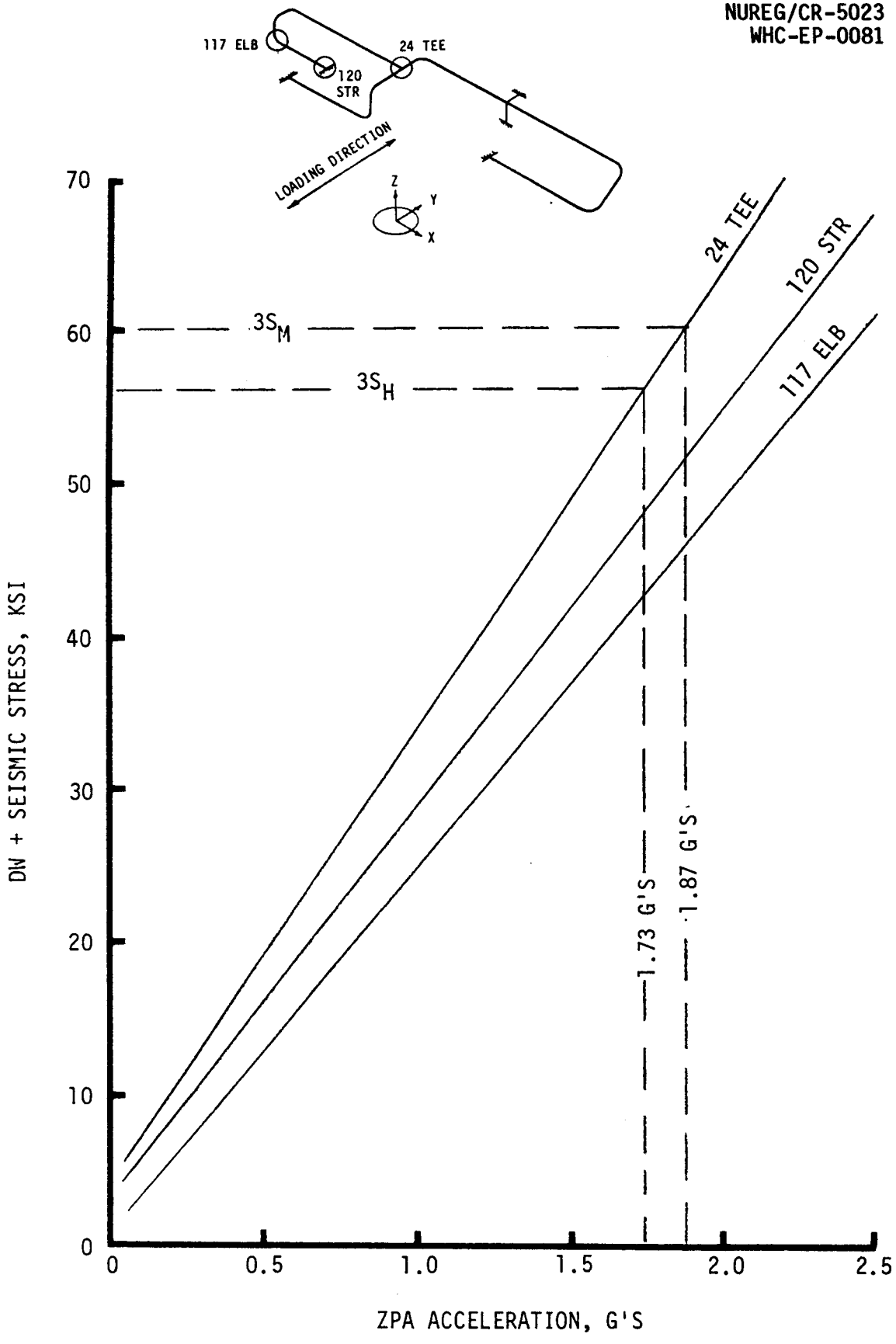

FIGURE 7-4. KWU Test Article, Elastic Analysis.

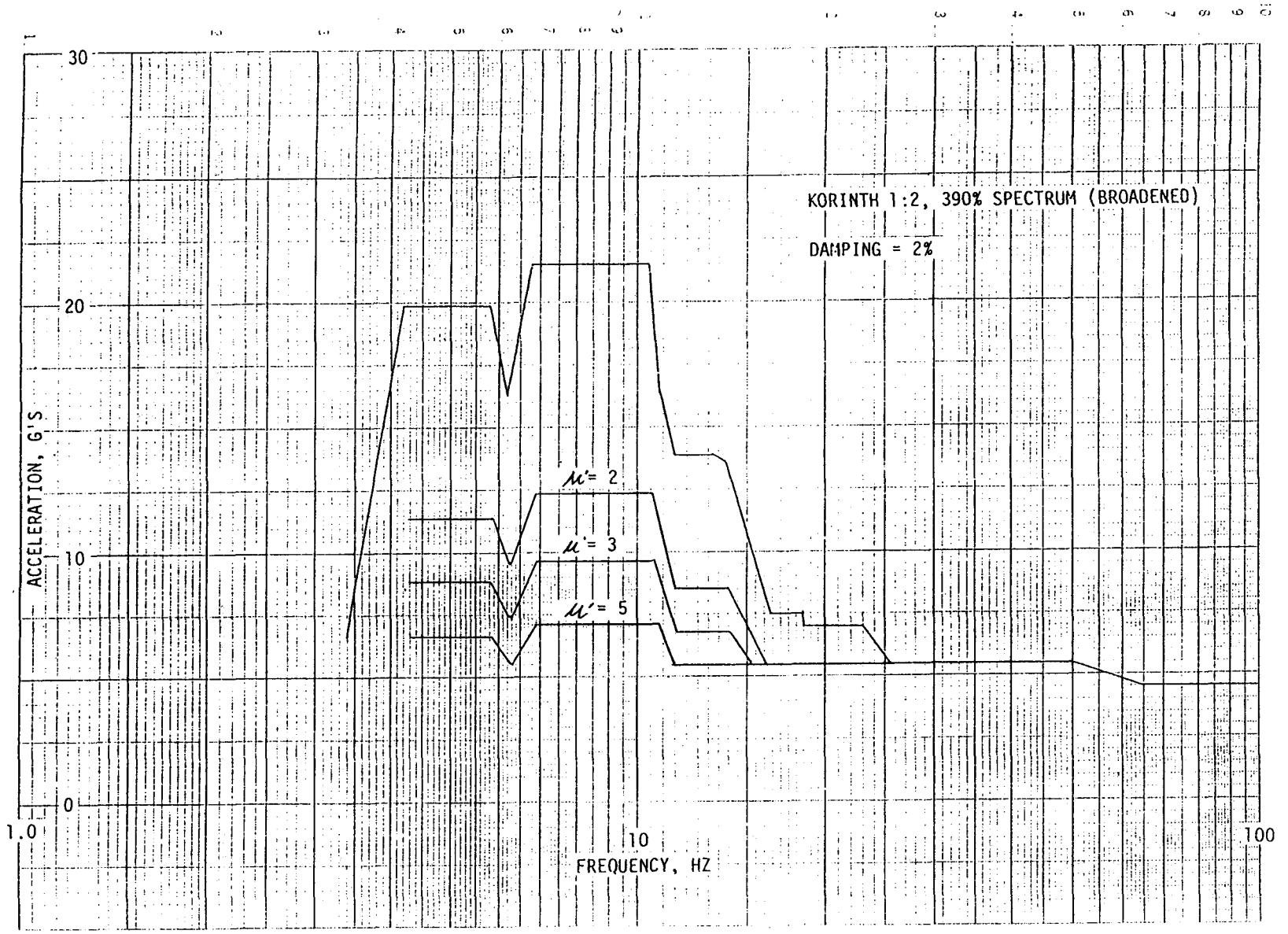

FIGURE 7-5. KWU Test Article, Elasto-Plastic Response Spectrum, Newmark Method.

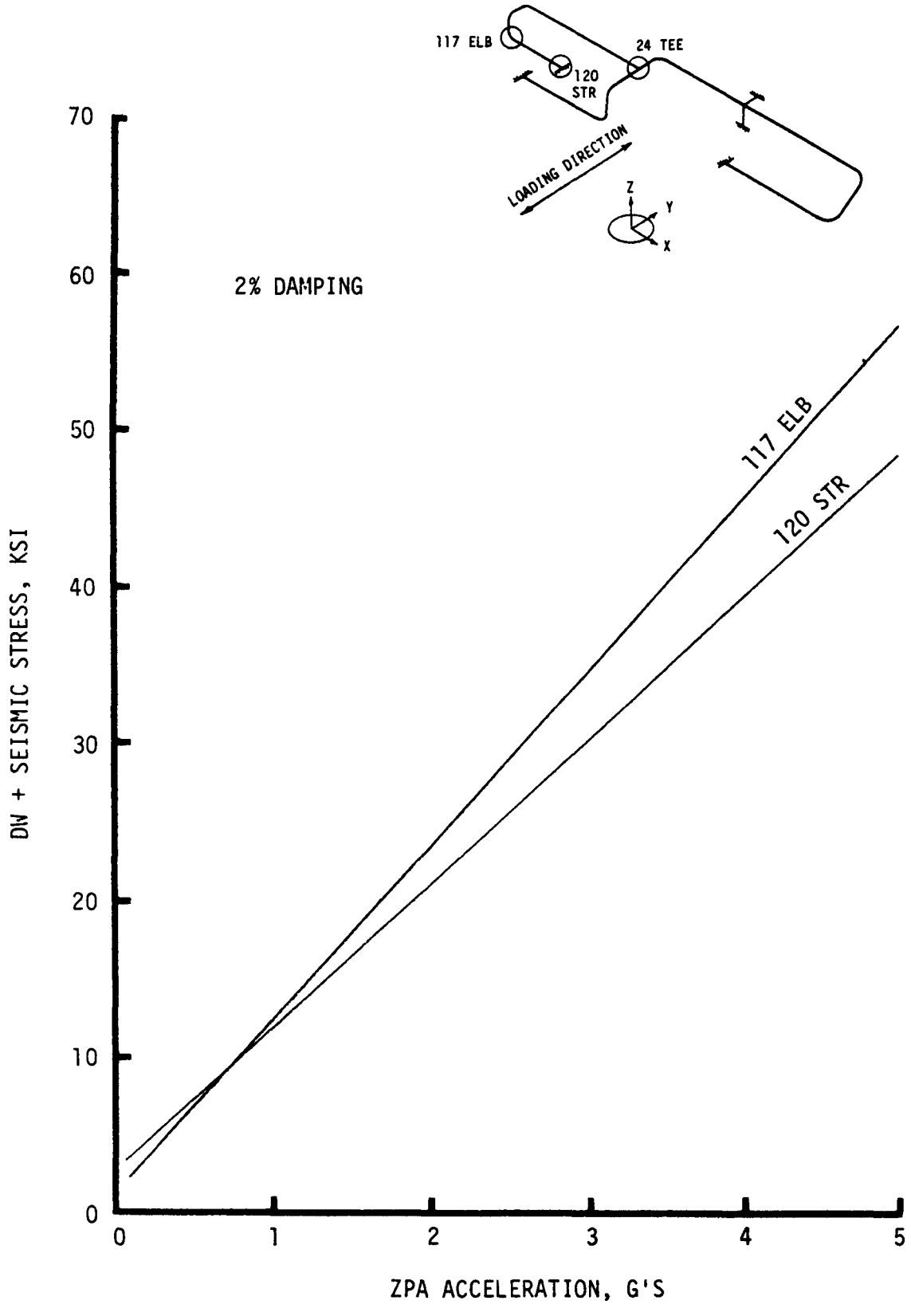

FIGURE 7-6. KWU Test Article, Newmark Method.

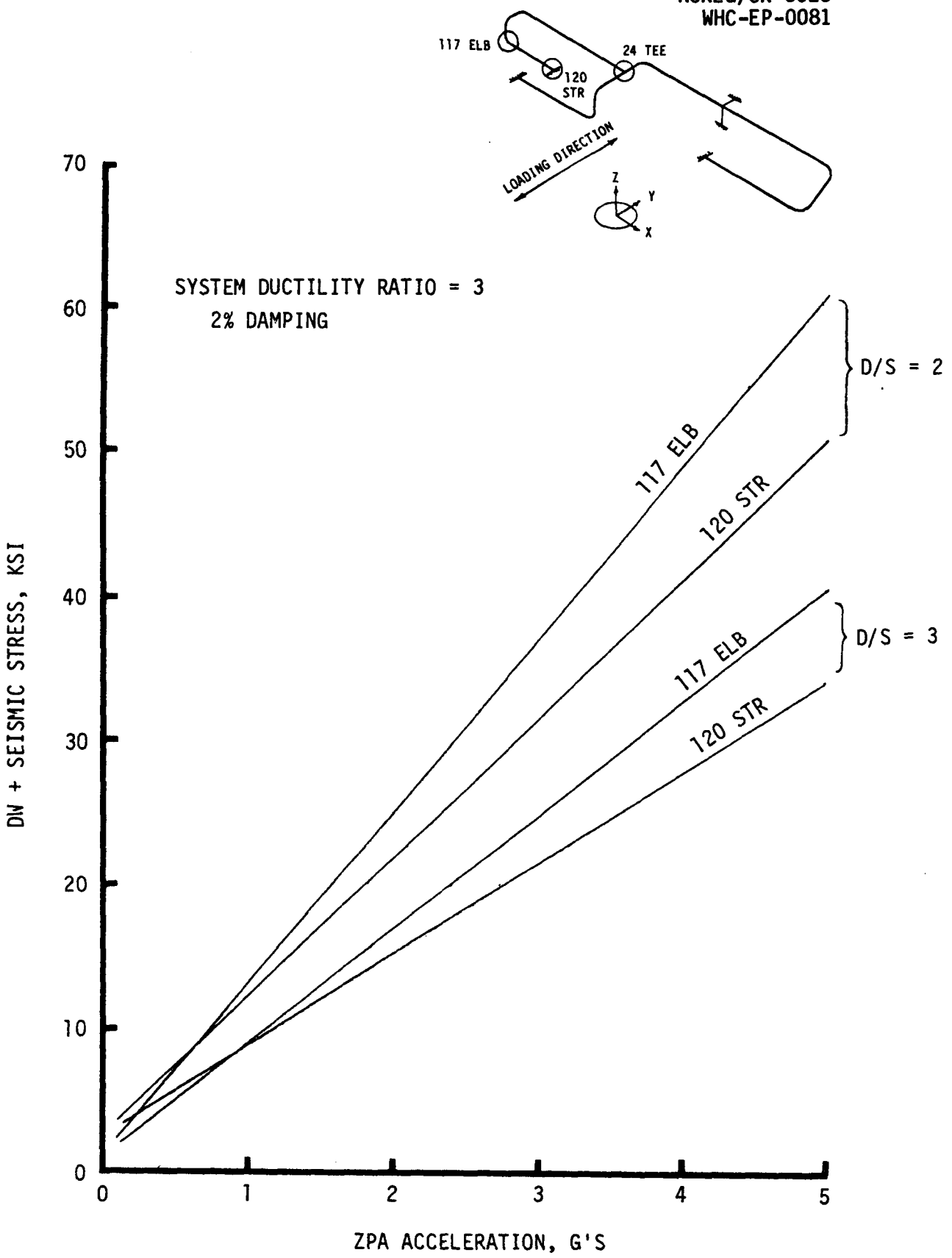

FIGURE 7-7. KWU Test Article, D/S Method.

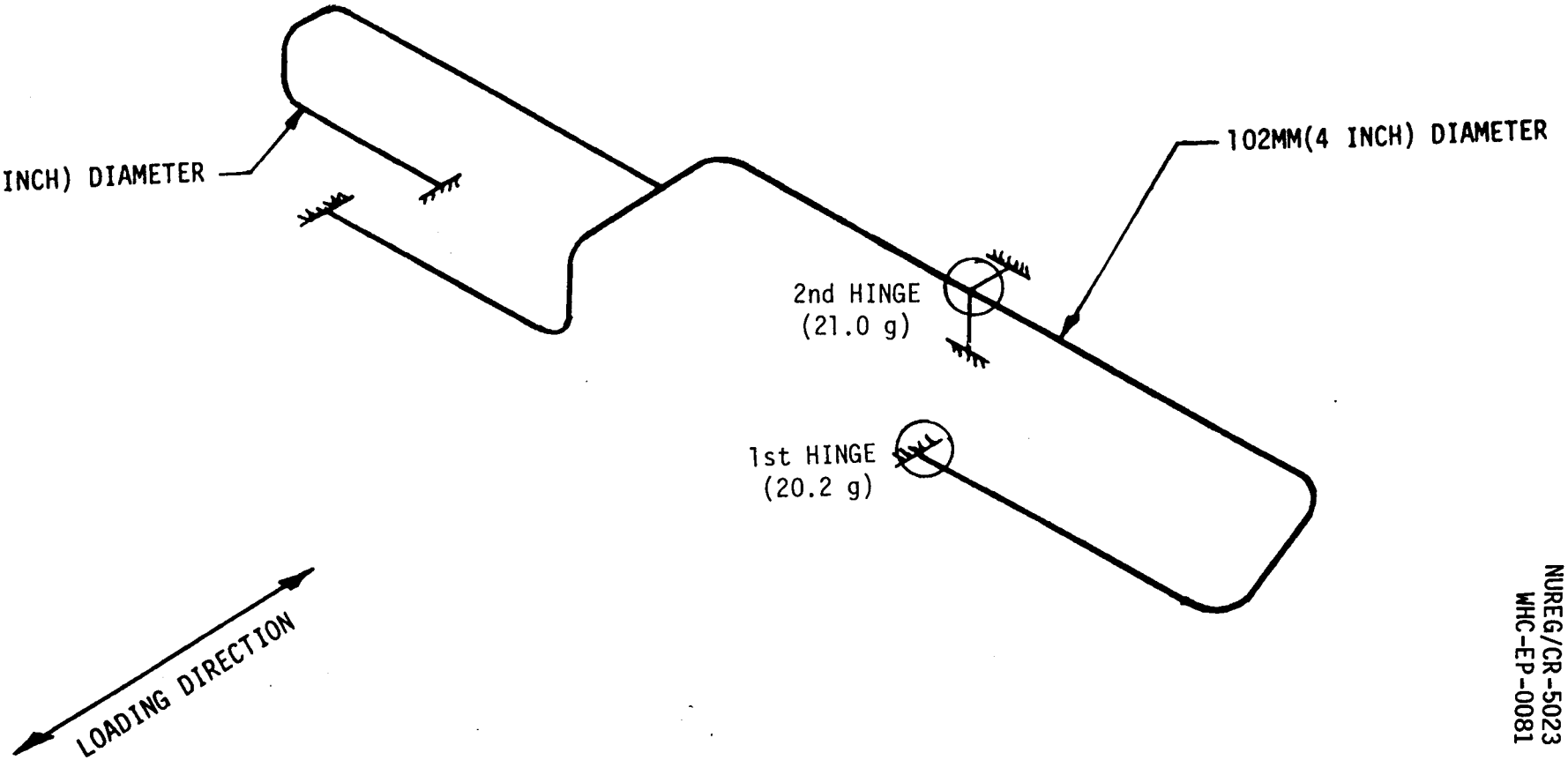

FIGURE 7-8. KWU Test Article, Progressive Hinge Method, Static Load Application.

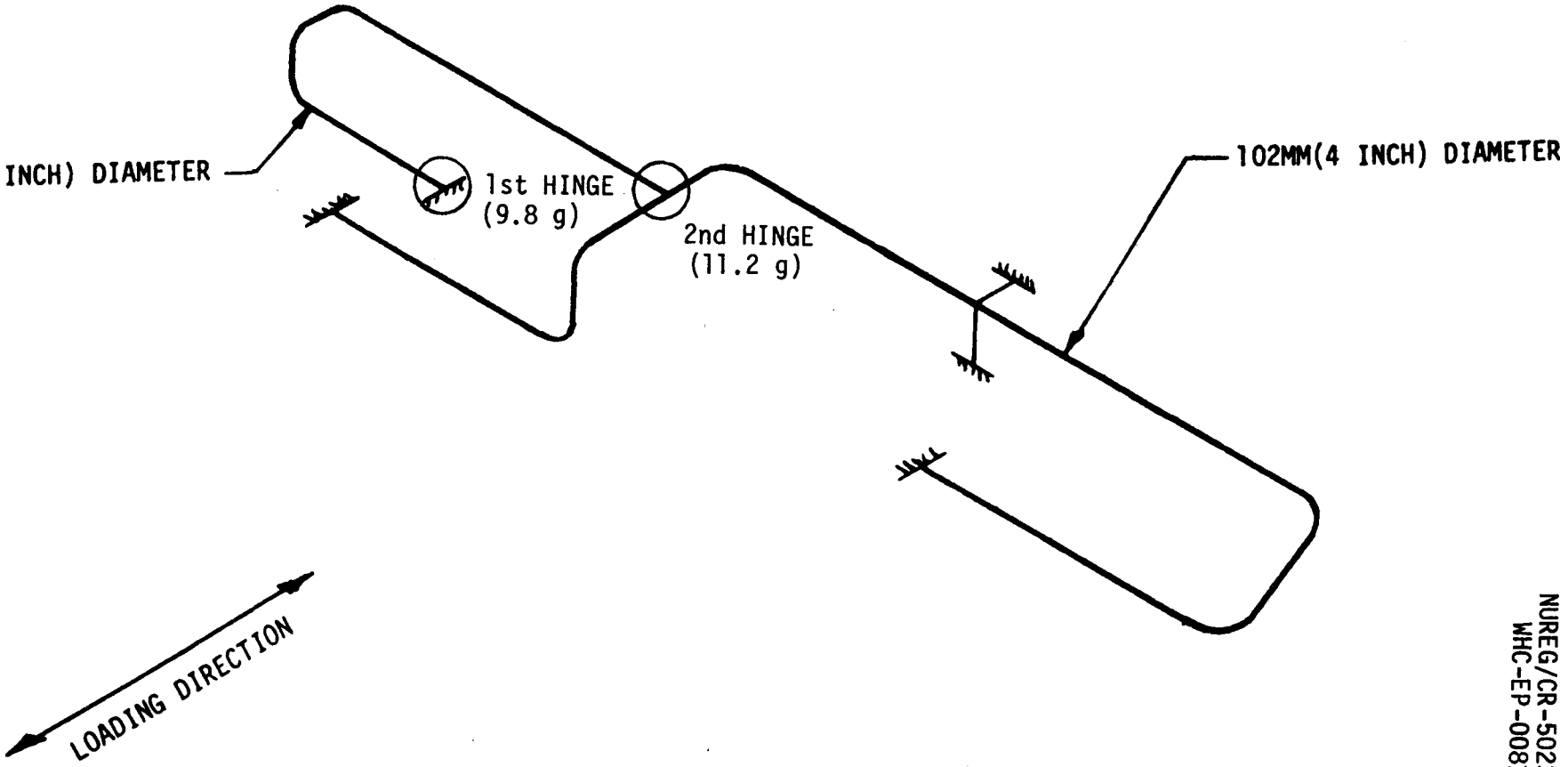

FIGURE 7-9. KWU Test Article, Progressive Hinge Method, Dynamic Load Application.

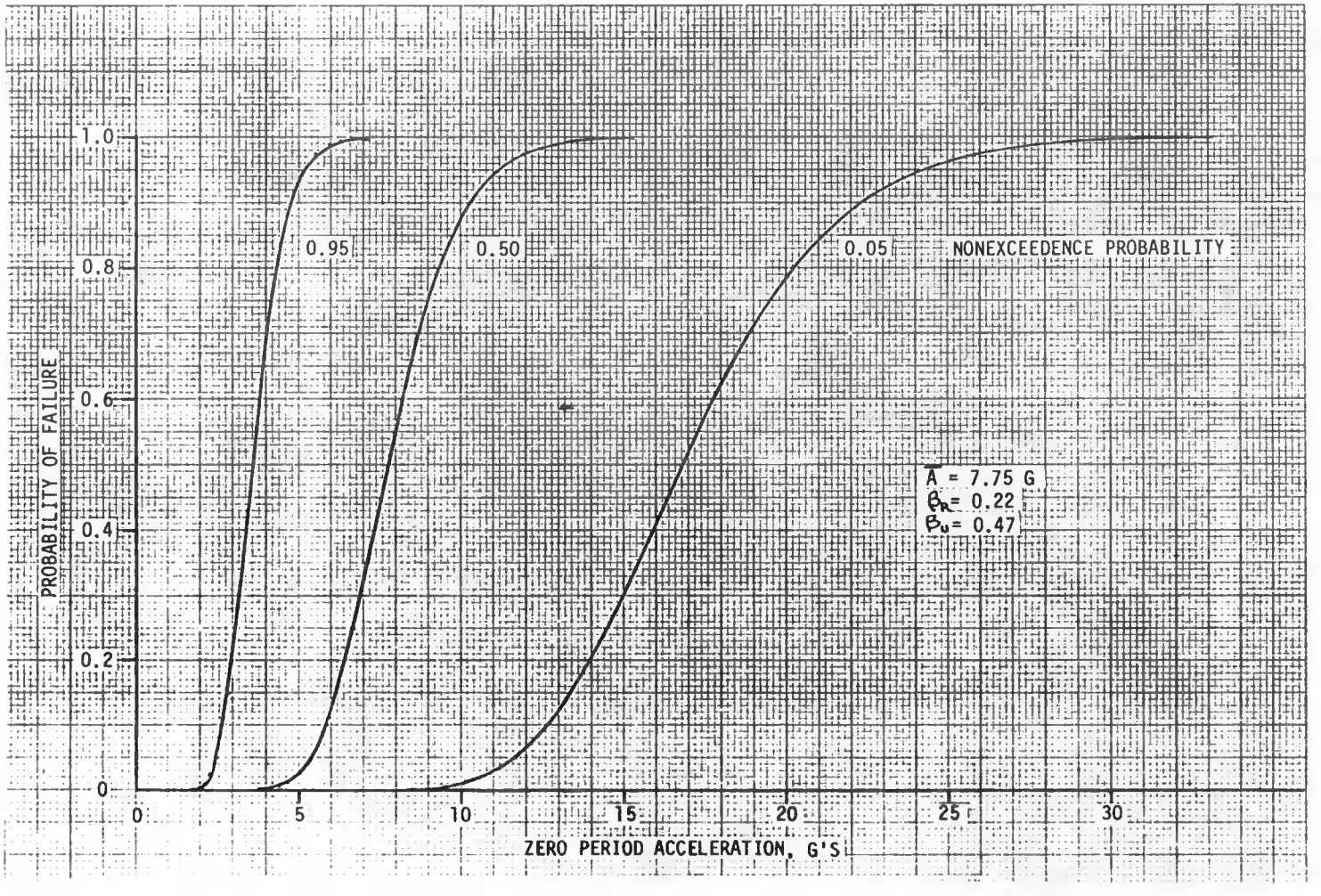

FIGURE 7-10. KWU Test Article, Seismic Fragility by the "Zion Method."

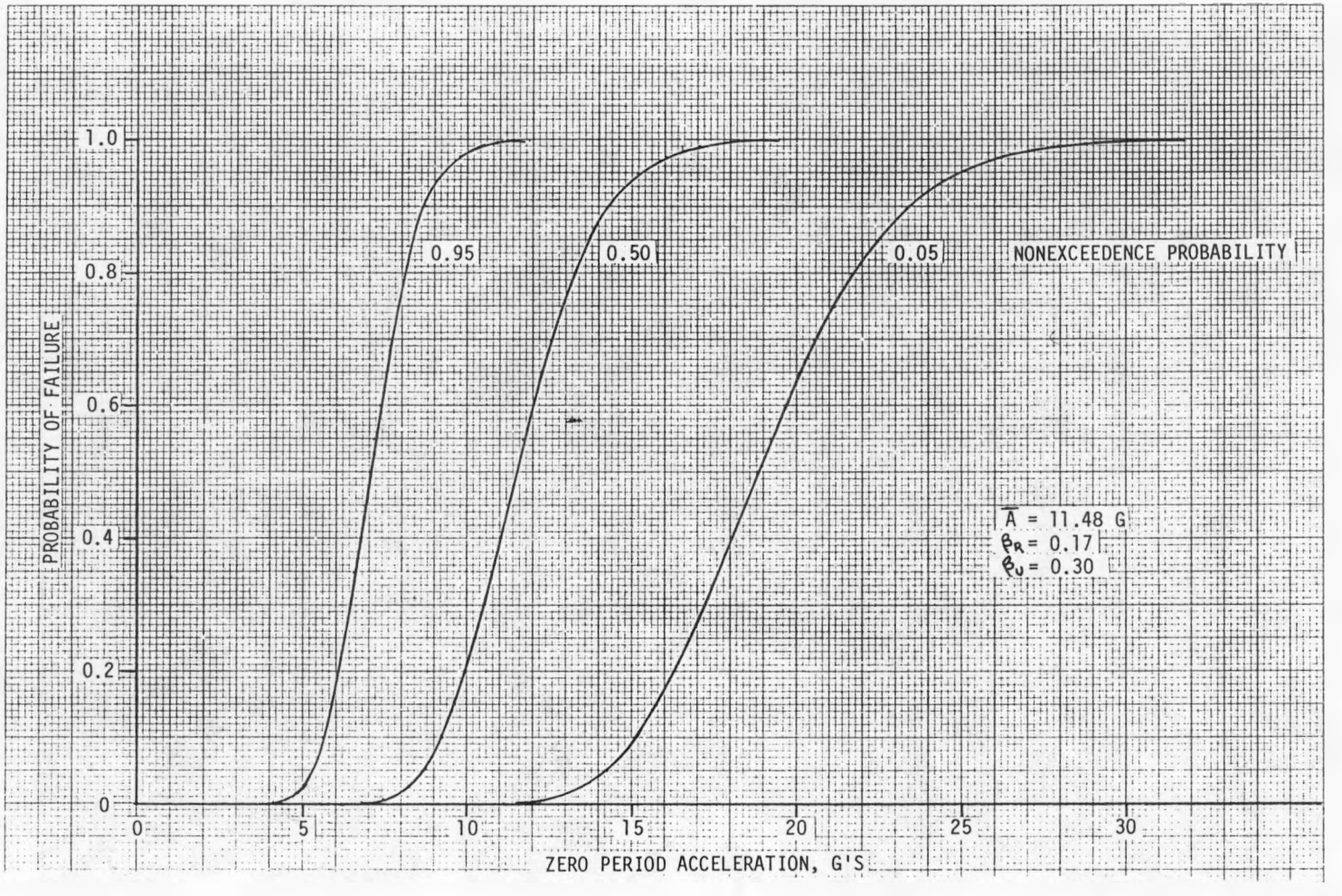

FIGURE 7-11. KWU Test Article, Seismic Fragility by the "SSMRP Method".

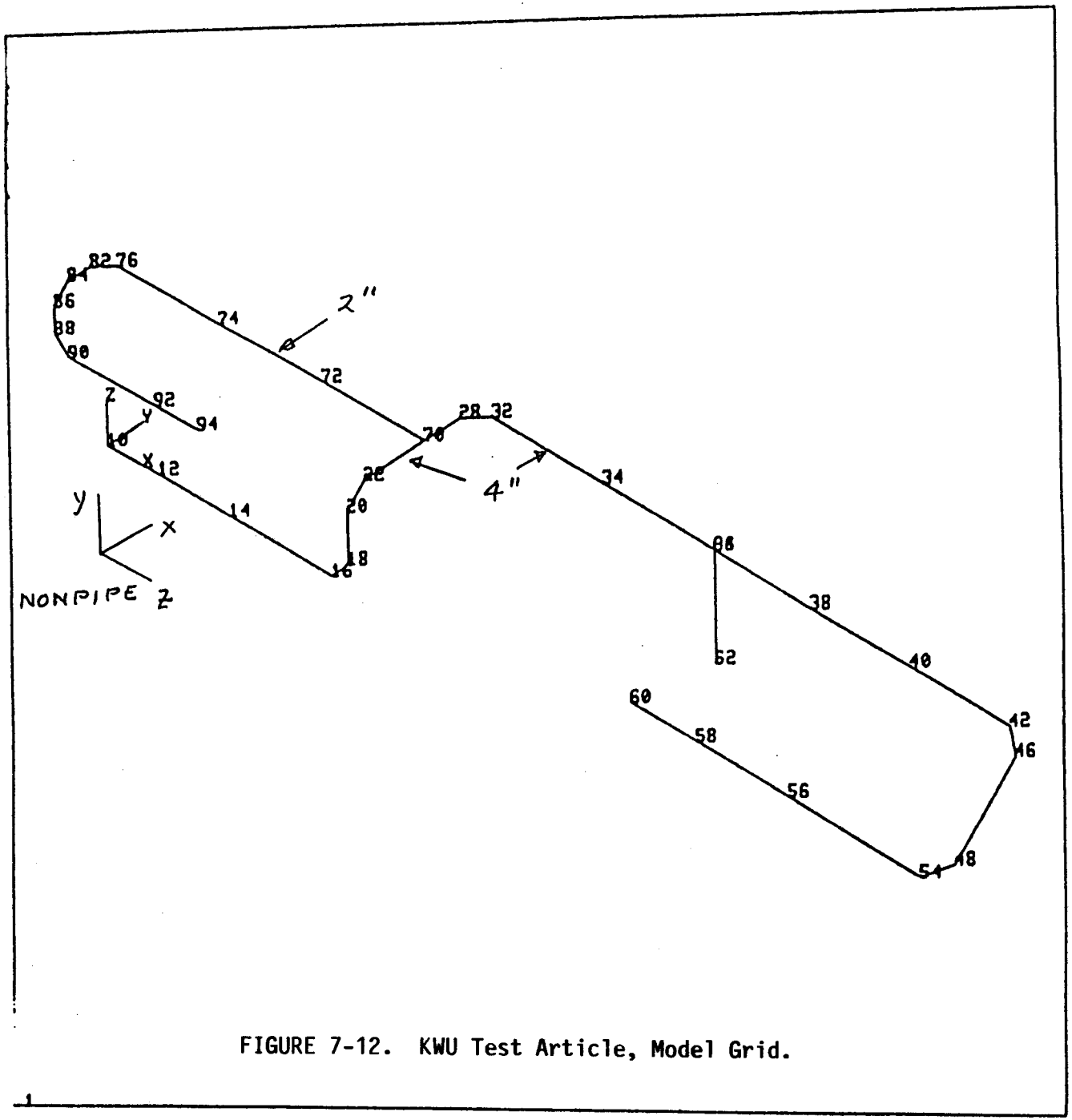

FIGURE 7-12. KWU Test Article, Model Grid.

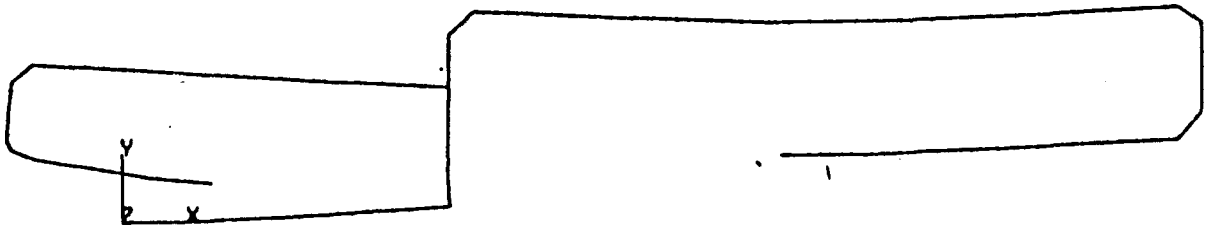

ANSYS
6/ 2/86
9.2753
PLOT NO. 6
POST1
STEP=1
ITER=3
FREQ=9.82
DISPLACEMENT

ORIG SCALING
ZV=1
DIST=172
XF=128
YF=23.5
ZF=11.5
DMAX=.199
DSCA=86.2

FIGURE 7-13. KWU Test Article, Mode 3 (Plan).

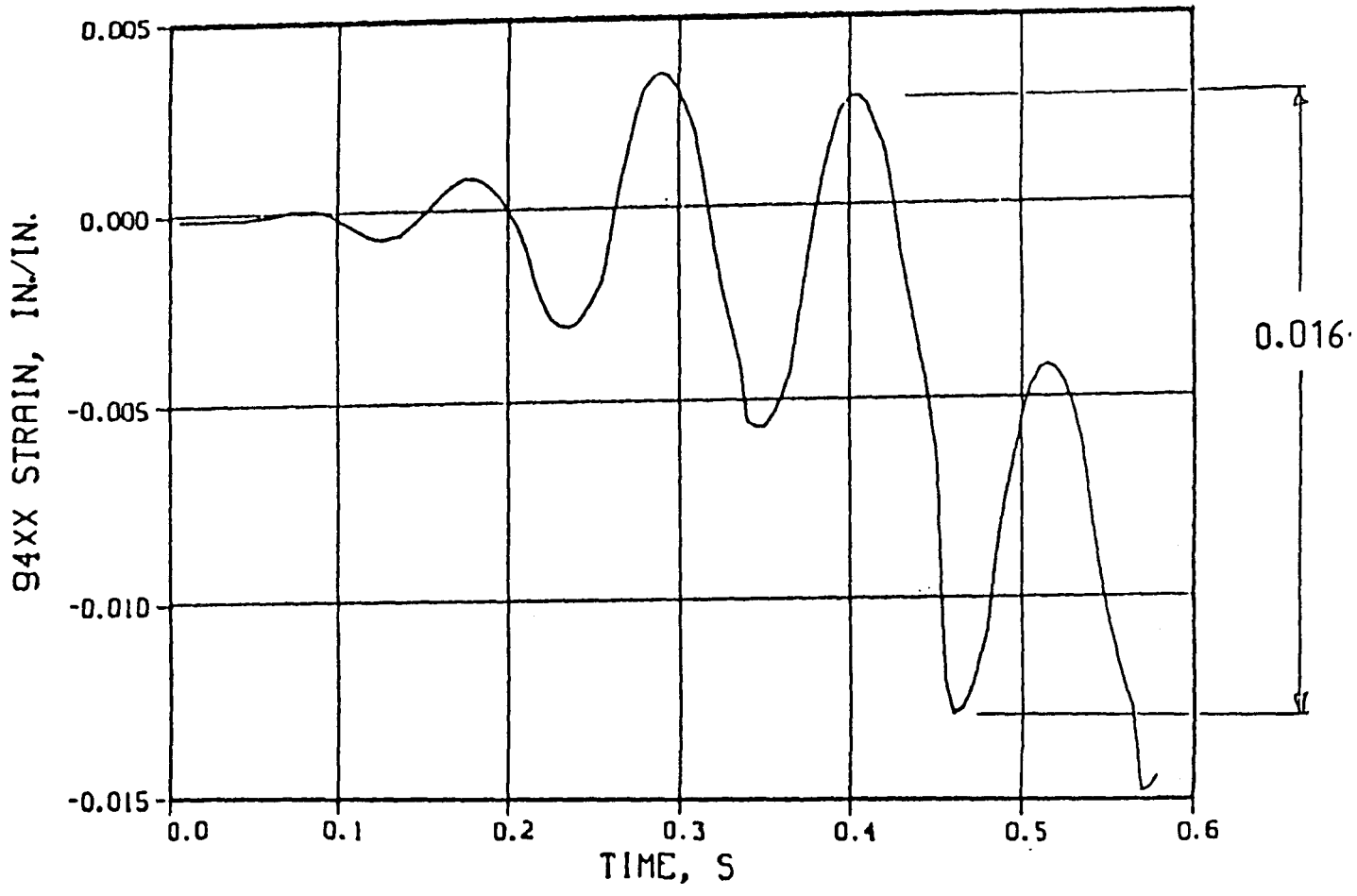

FIGURE 7-14. KWU Test Article, Branch Anchor Strains.

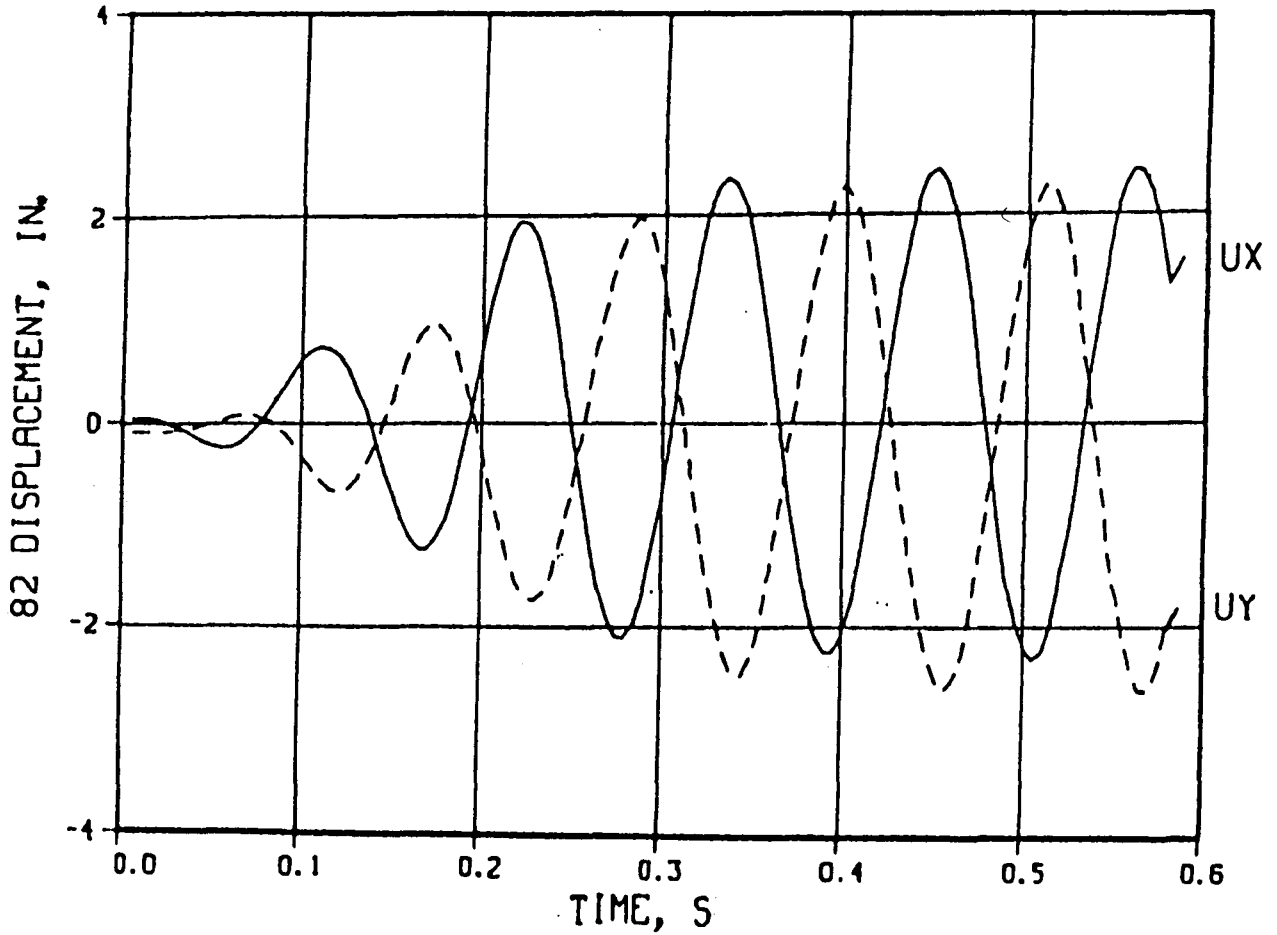

FIGURE 7-15. KWU Test Article, Node 82 Displacements.

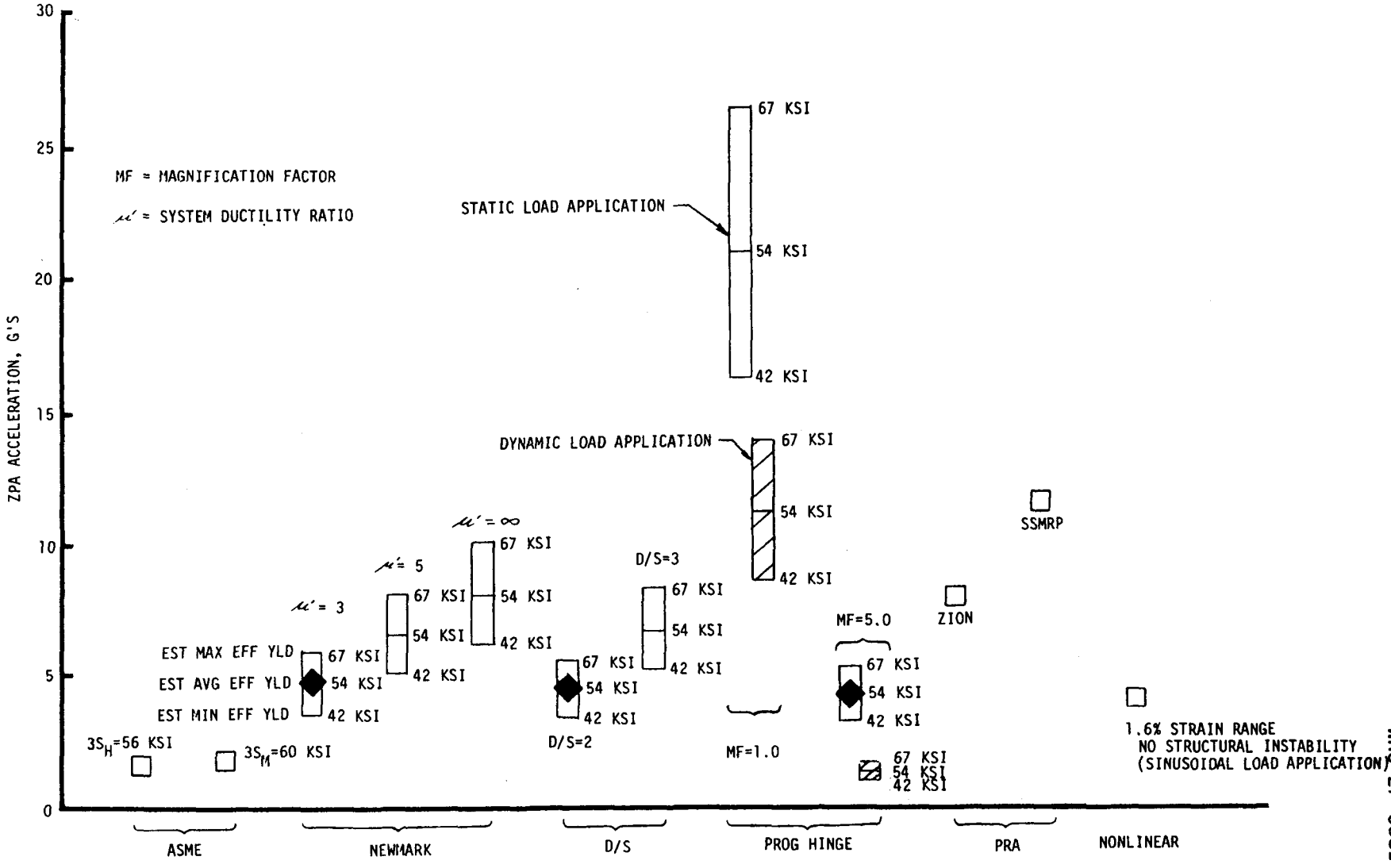

FIGURE 7-16. KWU Test Article, Summary of Failure Predictions.

8.0 ETEC THREE-INCH DIAMETER DEMONSTRATION TEST ARTICLE

A series of high-level dynamic tests were performed at ETEC on a three-inch diameter pipe configuration. Testing and accompanying analyses are described below.

8.1 TEST ARTICLE/STRUCTURAL MODEL

The ETEC three-inch diameter configuration (Figure 3-1) consisted of approximately 51 feet of three-inch diameter Schedule 40 piping. Pipe material was ASTM A-106, Grade B with minimum yield strength of 35 ksi and ultimate strength of 60 ksi. The 3 S_m for this material is 60 ksi, 3 S_N is 45 ksi. Long radius (1 1/2D) elbows were used. The test article had extensive strain gage and accelerometer instrumentation. A structural analytical model was developed and is shown in Figure 3-2.

8.2 TEST LOADING/FAILURE MODE

The dynamic loading of the ETEC three-inch diameter test article consisted of a time-history loading that represented a specific seismic response spectrum and by sinusoidal "burst" loading. The time-history loadings, which did not cause failure, were performed at three levels of ZPA: 5 g, 14 g, and 30 g. The sinusoidal burst tests consisted of (1) 10 cycles at 3.4 Hz, 4.7 Hz, and 6Hz (constant displacement) and (2) 6 Hz at 25 g constant acceleration. The base-line response spectrum loading is shown in Figure 3-3.

Failure of the test article occurred during the sinusoidal burst loading at 6 Hz at approximately 25 g load level. Failure took place in the crotch region of the tee when a crack developed, which is typical of fatigue failure associated with local peak strains and stress concentrations.

8.3 SIMPLIFIED ELASTIC AND ELASTO-PLASTIC ANALYSES

The simplified elastic and elasto-plastic methods described in Section 3.1 of this report have been applied to the configuration and loading environment used for the dynamic testing of the ETEC three-inch diameter test article. These are discussed below.

8.3.1 Linear Elastic Analyses

Linear elastic analyses have been performed using the PIPESD code for the structural model of Figure 8-2 under the response spectrum of Figure 8-3 with 5% damping. Stresses were calculated for the baseline spectrum and multiples thereof. The maximum stresses at several system locations have been plotted in Figure 8-4 with the stresses being the summation of dead weight and seismic test loading. On the abscissa, the equivalent ZPA is shown.

Figure 8-4 shows that the tee at Node 32, the straight section at Node 10 and the elbow at Node 18 have the maximum total stress. The ASME Code, Class 1, Level D allowable, 3 S_m (60 ksi), and the comparable ASME Code, Class 2 allowable ZPA loading for the system is 1.4 g for Class 1 allowables and 1.0 g for Class 2 allowables.

8.3.2 Newmark Plastic Spectra Method

As discussed in Section 3.1.2 of this report, the Newmark plastic spectra method uses a procedure that involves the construction of an elasto-plastic response spectra. The spectra are reduced by the factor $\sqrt{2u'-1}$, where u' is the system ductility ratio. This reduction is applied in the region of approximately 2 hertz to 8 hertz (for a Newmark-type spectrum). Figure 8-5 presents the test baseline spectrum and reduced spectra for several values of u'. Figure 8-5 shows that as the ductility ratio increases, the incremental change to the response spectrum becomes increasingly small. Analyses were performed using the spectra of Figure 8-5 for various values of u'.

Figure 8-6 presents the summation of the ETEC three-inch diameter test article dead weight plus seismic test loading stresses as a function of response spectra ZPA loading for a system ductility ratio of 10. The elbow at Node 18 is critical with the straight pipe at Node 10 also relatively highly stressed. Figure 3-7 presents the total stress at the Node 18 elbow for several system ductility ratios. Shown in Figure 8-8 is the sensitivity of the allowable load level to system ductility ratio. As might be expected from inspection of the spectra in Figure 3-5, the reduction in system response becomes less as higher system ductility ratios are approached.

8.3.3 Dynamic/Static Margin Ratio Method

As discussed in Section 3.1.3 of Reference 1, the D/S margin ratio method uses an elastic response spectrum analysis followed by a reduction of the stress results by means of a D/S factor. This method was used to assess the components of the pipe system under the proposed test loadings.

Figure 8-9 presents the summation of the ETEC three-inch diameter test article dead weight plus seismic test loading stresses as a function of response spectra ZPA loading for typical D/S ratios of 2, 3, and 4. The straight section at Node 10 and the elbow at Node 18 are seen to be nearly equally stressed.

8.3.4 System Ductility and Equivalent Yield Point

As discussed previously, the Newmark and D/S margin ratio methods utilized the concept of reduced system response as a result of inelastic action. This is based upon the premise that even a slight amount of inelastic action

reduces the response of the structure significantly because of nonlinear behavior. The inelastic action is accounted for in these methods by the introduction of parameters called the system ductility ratio and the equivalent yield point strength.

The ETEC three-inch diameter test article was fabricated from the same carbon steel material as the ETEC six-inch diameter test article, Reference 7. The configurations of the two systems are also highly similar. For these reasons, a system ductility ratio ($u' = 10$) was chosen for the three-inch diameter system that was equal to the one developed for the six-inch diameter system. The corresponding D/S margin ratio is approximately 4.

The equivalent yield point for ASTM A-106, Grade B carbon steel material was determined to be 53 ksi in Reference 1. A $\pm$25% on yield strength was assumed in order to estimate maximum and minimum yield points (66 ksi and 41 ksi).

8.3.5 Progressive Hinge Formation Method

As discussed in Section 8.1.4, the static progressive hinge formation method is based on an assessment of system stresses resulting from a static loading analysis which leads to a resulting collapse mechanism. An equivalent static loading was applied in the Z direction to the ETEC three-inch diameter pipe test article with resulting pipe stresses assessed against component capabilities. A second analysis was performed in which a constant dynamic load was applied in the Z direction. The purpose of applying the dynamic load was to permit excitation of out-of-plane modes that would not be affected by static loading.

Consistent with the ETEC six-inch diameter pipe system progressive hinge analysis, Section 6.0, the moment capability of the elbows included a factor of 1.5, which resulted from the Reference 20 comparison of limit moments on carbon steel elbows. Additionally, an examination of elbow moment-rotation plots for typical 4.5-inch elbow tests indicated moments at loss of load-carrying capacity are approximately 15% higher than moments at twice the angle at loss of linearity. The elbow moment collapse factor was therefore taken to be: 1.5 x 1.15 = 1.7. The 1.5 factor alone was used for straight pipe.

The analyses considered dead weight plus seismic test loading and indicated first hinge formation at straight pipe Node 10, with a second hinge forming at straight pipe Node 46. Additional hinges formed until a total of five

(Figure 8-10) produced an unstable system for the statically loaded system. A total of four hinges prior to system instability and a slightly different sequence of hinge formation was found in the analysis using constant dynamic input, with a final failure occurring at the tee (see Figure 8-11). The strength of the tee was assumed to be that of straight pipe, after incorporation of the appropriate stress intensification factors. The results of the progressive hinge analysis are shown in Table 8-1 for three levels of effective yield strength.

8.3.6 PRA-Type Methods

PRAs of the piping systems were made using the methods described in References 13 and 14. Reference 13, referred to by the author as the "Zion Method," determines the fragility of a piping system by estimating the median safety factor and logarithmic standard deviation. The latter are determined from analysis of a number of typical piping systems. Reference 14, the "SSMRP Method," is similar except that analysis of the specific piping system under consideration is utilized.

Both of these methods and their application to the test article are described in the following sections.

8.3.6.1 Test Article Fragility Using the "Zion Method"

This method considers the capacity of the piping, supports and anchors. In addition, equipment and structure response factors are considered. These are expressed in terms of a median safety factor, F, and logarithmic standard deviations of randomness, β_R, and uncertainty, β_U. A discussion of the various factors and their chosen values is presented in Section 6.6. A summary of the above factors is shown in Table 8-2. The factors used in predicting the fragility of the test article are shown in Table 8-3. The median acceleration based on a 0.2 g OBE is 21.97 x 0.2 or 4.39 g. Probability of failure curves for 0.05, 0.50 and 0.95 nonexceedence probabilities are shown in Figure 8-12.

8.3.6.2 Test Article Fragility Using the "SSMRP Method"

Reference 6 describes a probabilistic computational procedure for the seismic risk assessment of nuclear power plants. In this procedure, seismic input, soil-structure interaction, structure response, subsystem response and fragilities are considered on a probabilistic basis. Volume 7 of Reference 14 describes the methods used in determining fragilities.

The analytical approach for assessment of the ETEC three-inch diameter test article was identical to that described in Reference 1. The results show a

median acceleration of 5.25 g with β_R = 0.17 and β_U = 0.30. Probability of failure curves for 0.05, 0.50, and 0.95 nonexceedence probabilities are shown in Figure 8-13.

8.4 NONLINEAR TRANSIENT DYNAMIC INELASTIC ANALYSIS

NONPIPE transient analysis modelling proceeds in a similar fashion as the ETEC 6-inch and WHC 1-inch systems, modelling. A major difference occurs in the elbow limiting moment. Figure 8-14 relates the M_{y2} moment to the classic straight pipe limit moment M_{LS} for various lambda parameters Rt/r^2. The solid curve used for NONPIPE transient analysis is an average through two previous trilinear fits, and it follows the trend given in Reference 9. Elbow strains are recovered from end rotations using:

$$\epsilon = \frac{r_o}{\frac{\pi}{2} R} \cdot \frac{C_2}{k} \Delta\theta$$

where:

r_o = Pipe outside radius
R = Bend radius
k = Flexibility factor = 1.65/b
b = Rt/r^2
C_2 = Stress intensification = $1.95/b^{2/3}$
$\Delta\theta$ = SRSS of relative end rotation components.

Remaining modelling details are summarized in Table 8-4, while Figure 8-15 gives the grid prior to refinement.

Two transient runs at 12 g and 30 g ZPA were run by scaling the 0.55-s record shown in Figure 8-16. Results are summarized in Table 8-5; no sign of collapse is noted. Strain ranges to 14% occurred at two of the excitation tables, but magnifications are low. A significant increase in deformation occurs in the tee and elbow at the 30 g level compared to the 12 g level. The 12 g maximum strain range record is shown in Figure 8-17. Comparison with test strain values is limited by test records showing evidence of popped gages or other anomalies (Figures 8-18 and 8-19). Otherwise, comparison is generally reasonable. The 30 g strain range at Node 74 is an exception. It should be noted, however, that the test ZPA is 20 g in this case.

8.5 SUMMARY OF COLLAPSE FAILURE PREDICTIONS, ETEC THREE-INCH DIAMETER PIPE TEST

A summary of the pretest analysis results performed on the ETEC three-inch diameter test article are presented herein with test collapse levels predicted. Figure 8-20 (which is further discussed below) presents a summary of the analytical results for the NRC/ETEC test article using various simplified elastic methods. In all cases shown, the analytical results consider the summation of dead weight plus dynamic test load stresses. The estimates of most likely collapse loads for the various assessments are indicated in Figure 8-20 with a diamond (◆), which represents effective yield point (53 ksi) corresponding to an average material value. These results are also summarized in Table 2-1.

The limits discussed below for the Newmark, D/S, and static progressive hinge methods are 41 ksi, 53 ksi, and 66 ksi. These represent a minimum, average, and maximum expected effective yield point for carbon steel material.

Linear elastic analyses were performed on the pipe system for a baseline response spectra loading intended for the tests. The analyses were accomplished by scaling the spectra to obtain results for various base load levels. The allowable base input loading was found to be 1.4 g for an ASME Class 1, Level D limit ($3\ S_m$ = 60 ksi) and 1.0 g for an ASME Class 2, Level D limit ($3\ S_H$ = 45 ksi). This limit is shown on Figure 8-20 as "ASME."

The results of the Newmark analysis are presented in Figure 8-20 for system ductility ratios of 5, 10, and infinity. A system ductility ratio of 10 has been previously estimated which, along with an average effective yield values of 53 ksi, results in a failure level of 10.2 g base acceleration.

The allowable limits based upon the D/S margin ratio method were calculated for D/S ratios of 2 and 4, with these shown in Figure 8-20. The D/S value to 4 corresponds to a system ductility of approximately 10. It is seen in Figure 8-20 that an effective yield point of 53 ksi and a D/S value to 4 gives a predicted base acceleration limit of 10.0 g.

The results of the static progressive hinge method are shown in Figure 8-20 for yield values of 41, 53, and 66 ksi. An average effective yield stress of 53 ksi gives a predicted failure level of approximately 19 g and 23 g, respectively, for the static and dynamic analyses using the progressive hinge method. It should be noted that this represents the acceleration of the pipe itself and is related to the base input acceleration by the magnification factor. If one assumes a magnification factor of 2 (as suggested by Reference 4 and also by the results of the WHC one-inch high level tests), the predicted based acceleration at failure would be approximately 9.5 g and 11.5 g for the assumed yield point of 53 ksi.

The PRA-type fragility estimates gave collapse loads, at 50% probability and 50% nonexceedence, of 4.4 g for the "Zion" method and 5.2 g for the SSMRP method. These are shown in Figure 8-20.

The nonlinear transient analysis showed no indication of system collapse at a 30 g load level. Maximum calculated strain range (shown in Figure 8-20) at this load level was 14%.

8.6 FATIGUE CALCULATIONS

As previously discussed in Section 8.2, failure of the ETEC three-inch diameter test article involved crack development caused by fatigue in the region of the tee (Node 32, Figure 8-2). The fatigue failure was the result of cumulative loading cycles over the entire series of test loadings.

PIPESD dynamic elastic analyses were made for all loading conditions to determine stress levels in the tee region. Stress ranges were then calculated using a stress intensification factor (C_2K_2) for the tee of 2.6, and incremental fatigue damage was determined. These calculations are summarized in Table 8-6. It should be noted that the allowable cycles (N_f) shown in Table 8-6 represent average data rather than minimum values. As can be seen, fatigue damage based on elastic analyses is 0.81. Since failure is represented by unity, the calculations indicate that the fatigue failure of the test article should not have been unexpected.

TABLE 8-1

ETEC THREE-INCH DIAMETER TEST ARTICLE, PREDICTED

HINGE FORMATION LOAD LEVELS, PROGRESSIVE HINGE METHOD

Yield Stress (KSI)	Static Load Application		Dynamic Load Application	
	Collapse (G)	No. of Hinges	Collapse (G)	No. of Hinges
41	14.8	5	17.5	4
53	19.2	5	22.8	4
66	24.0	5	28.5	4

TABLE 8-2

FRAGILITY PARAMETERS FOR CLASS 2 PIPING
(ZION METHOD)

FACTORS	MEDIAN SAFETY FACTOR	RANDOMNESS β_R	UNCERTAINTY β_U
CAPACITY FACTOR			
PIPING -			
Strength - Thick Wall	8.04	0	0.36
- Thin Wall	4.39	0	0.36
Inelastic Energy Absorption	2.24	0.16	0.16
Three Hinge Factor	1.22	0	0.10
SUPPORTS			
Strength	3.26	0	0.29
Inelastic Energy Absorption	1.50	0.16	0.16
ANCHOR (WEDGE)			
Strength	5.70	0	0.30
Inelastic Energy Absorption	1.50	0.15	0.15
EQUIPMENT RESPONSE FACTOR			
Qulaification Method	1.00	0	0
Spectral Shape	1.39	0.20	0.13
Modeling	1.00	0	0.15
Damping	1.34	0.03	0.17
Mode Combination	1.00	0.15	0
Earthquake Component Combination	1.00	0.12	0.10
STRUCTURAL RESPONSE FACTOR	1.11	0.25	0.18

TABLE 8-3

FRAGILITY PARAMETERS FOR ETEC THREE-INCH DIAMETER TEST ARTICLE
(ZION METHOD)

FACTORS	MEDIAN SAFETY FACTOR	RANDOMNESS β_R	UNCERTAINTY β_U
CAPACITY FACTOR			
PIPING			
Strength	8.04	0	0.36
Inelastic Energy Absorption	2.24	0.16	0.16
Three Hinge Factor	1.22	0	0.10
EQUIPMENT RESPONSE FACTOR			
Qualification Method	1.00	0	0
Spectral Shape	1.00	0	0
Modeling	1.00	0	0.15
Damping	1.00	0.03	0.17
Mode Combination	1.00	0.15	0
Earthquake Component Combination	1.00	0	0
STRUCTURAL RESPONSE FACTOR	1.00	0	0
TOTAL	21.97	0.22	0.47

TABLE 8-4

TRANSIENT ANALYSIS MODELING SUMMARY

SYSTEM	HEDL	ETEC 6"	ETEC 3"	KWU
PIPE SIZE, IN.	1	6/3	3	4/2
NMBR ANALYSES	5	7	2	1
Sy, ksi	40	44	55	48/57
PIPE O. D., IN.	1.3	6.6/3.5	3.5	4.5/2.4
PIPE WALL, IN.	0.13	0.280.22	0.22	0.170.11
MIN ELMT LENGTH, IN.	1.0	4.0	2.2	2.1
LOCATION, NODE	20	10	10,46,74	94
MIN. Δt, MS	0.5	0.1	0.1	0.1
DURATION, S	1.75	0.55	0.55	0.58
α-β DAMPING, MIN, %	10	5	5	5
NMBR DOF's	408	336	252	276
NMBR ELMTS	67	55	41	44
NODAL DIFF	2	2	2	2

TABLE 8-5

TRANSIENT ANALYSIS SUMMARY
ETEC THREE-INCH DIAMETER TEST ARTICLE

ANALYSIS ZPA, g	NODE	LOCATION	LABEL	ANALYSIS VALUE	TEST VALUE	TEST ZPA, g
12	10	Table 3	$\Delta\varepsilon$, %	7.1	2.5[1]	12
	46	1		3.7	2.8	
	74	2		1.7	0.6	
30	10	Table 3	$\Delta\varepsilon$, %	14	2.5[1]	20
	46	1		8.5	6.9[2]	
	74	2		14	0.6	
12	30-32	Tee-run	$\Delta\varepsilon$[3], %	0.56		
30				3.8		
12	32-50	Tee-br		0.42		
30				0.45		
12	58	Magnification		1.79		
30				1.33		
12	16-18	Elbow	ε_{max},%	0.94		
30				5.2		

NOTES: 1) Short record (popped gage)

2) Capped record

3) Straight pipe, no intensification

TABLE 8-6

THREE-INCH DIAMETER ETEC PIPE TEE, $C_2K_2 = 2.6$

FATIGUE ANALYSIS BASED ON ELASTIC ANALYSIS

TESTS: (NO INTERNAL PRESSURE)

1. Seismic Motion - 5 G's ZPA, 15 Seconds Duration
2. Seismic Motion - 14 G's
3. Seismic Motion - 30 G's
4. Sinusoidal, 6" Disp. @ 3.4 Hz, 10 cycles, 7.1 G
5. Sinusoidal, 6" Disp. @ 4.7 Hz, 10 cycles, 13.5 G
6. Sinusoidal, 6" Disp. @ 6.0 Hz, 10 cycles, 22 G
7. Sinusoidal, 25 G's @ 6.0 Hz, 10 cycles,

STRESS RANGES CALCULATED $f_1 = 4.2$, $f_2 = 7.1$, $f_3 = 9$ hz

Test	S_a, ksi		N		N_f	N/N_f	$\Sigma N/N_f$
1	299	**	10	*	10^3	0.01	.01
2	836		10		110	.09	.10
3	1793		10		20	.50	.60
4	234		10		1500	.015	.615
5	447		10		400	.025	.64
6	726		10		120	.083	.72
7	825		10		110	.09	.81

*Assumed effective cycles per 15-second shake test (based on other analyses of same seismic motion used in test).

**From response spectra analyses of pipe, 5% damping, W/O any SCF for plasticity.

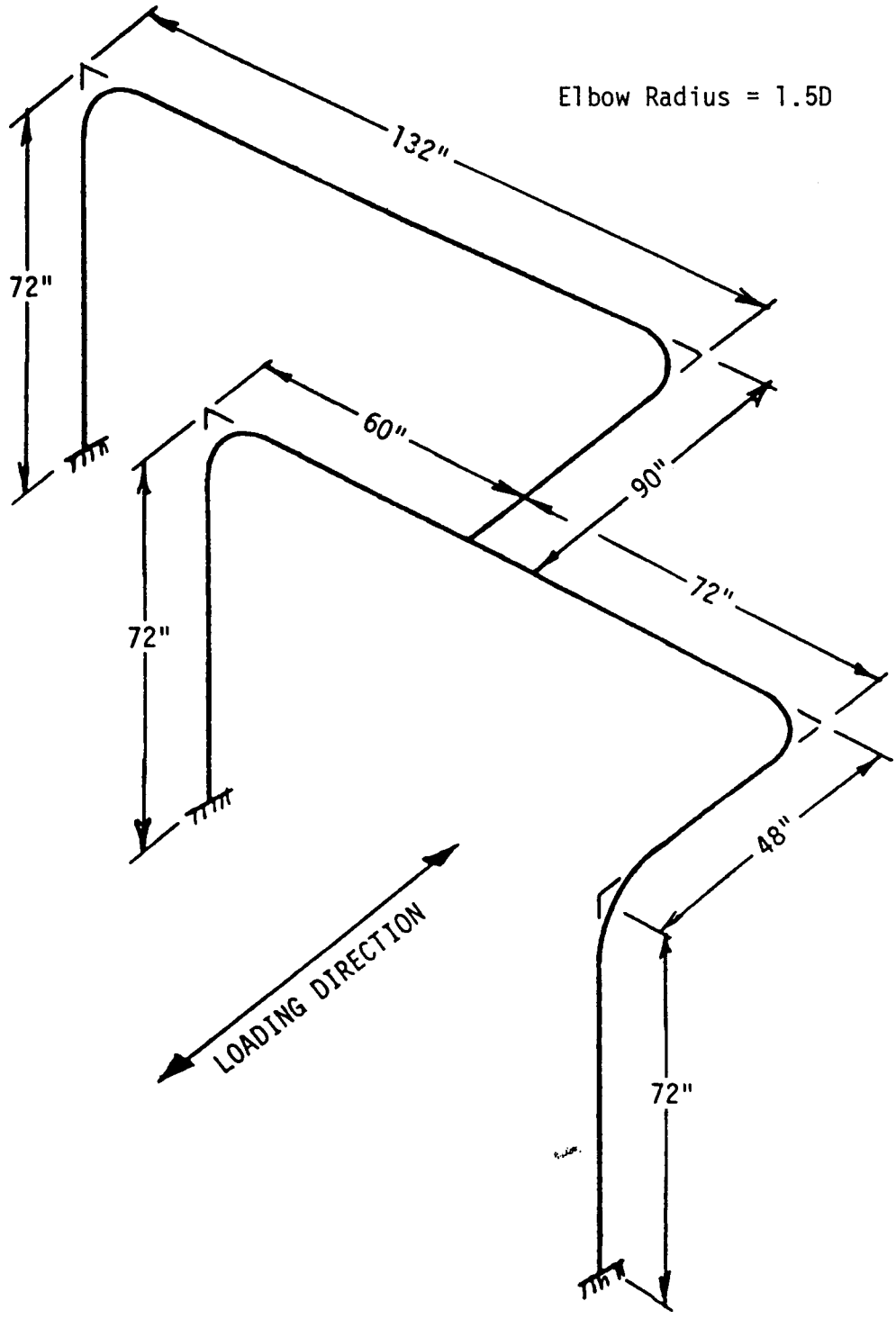

FIGURE 8-1. ETEC three-Inch Diameter Test Article.

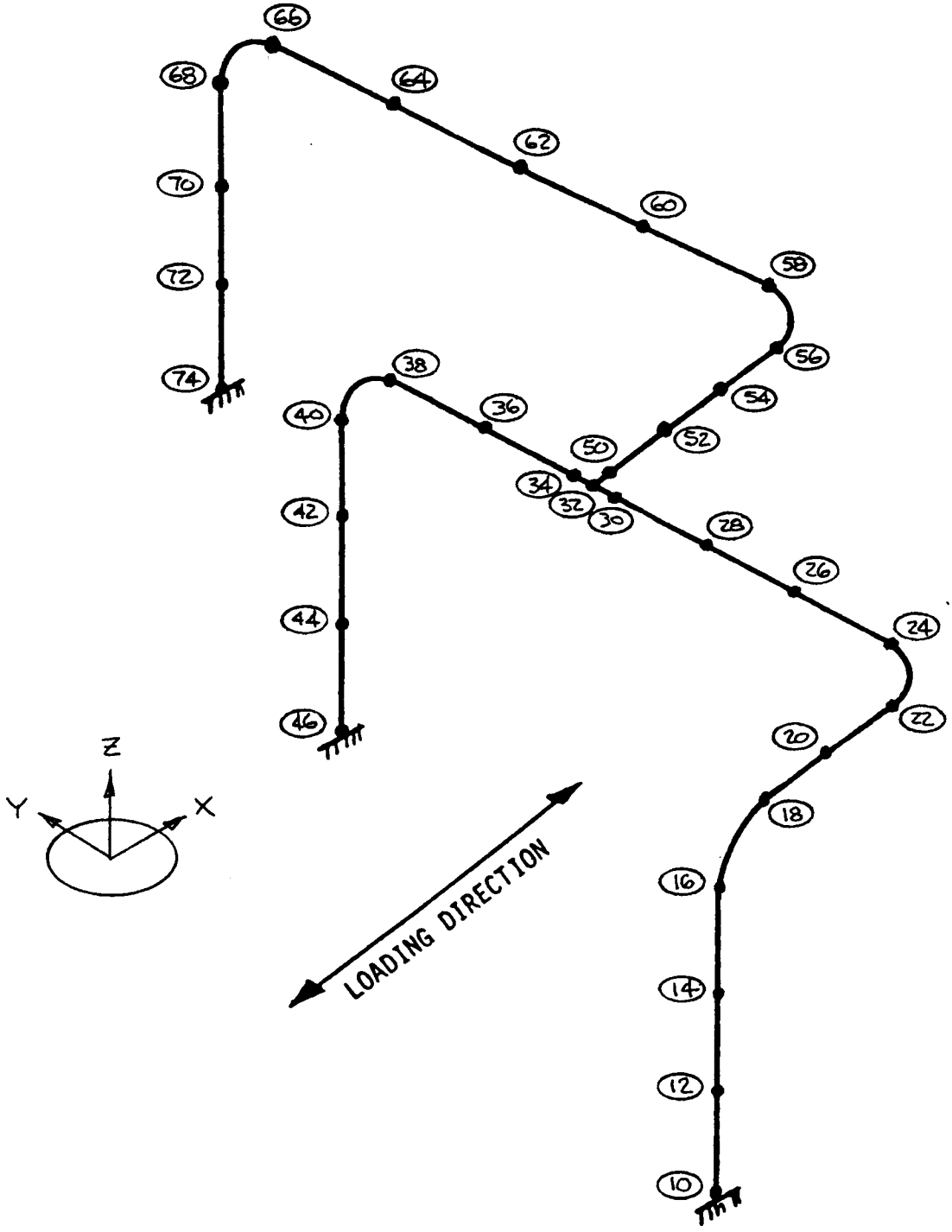

FIGURE 8-2. ETEC Three-Inch Diameter Test Article, Analytical Model.

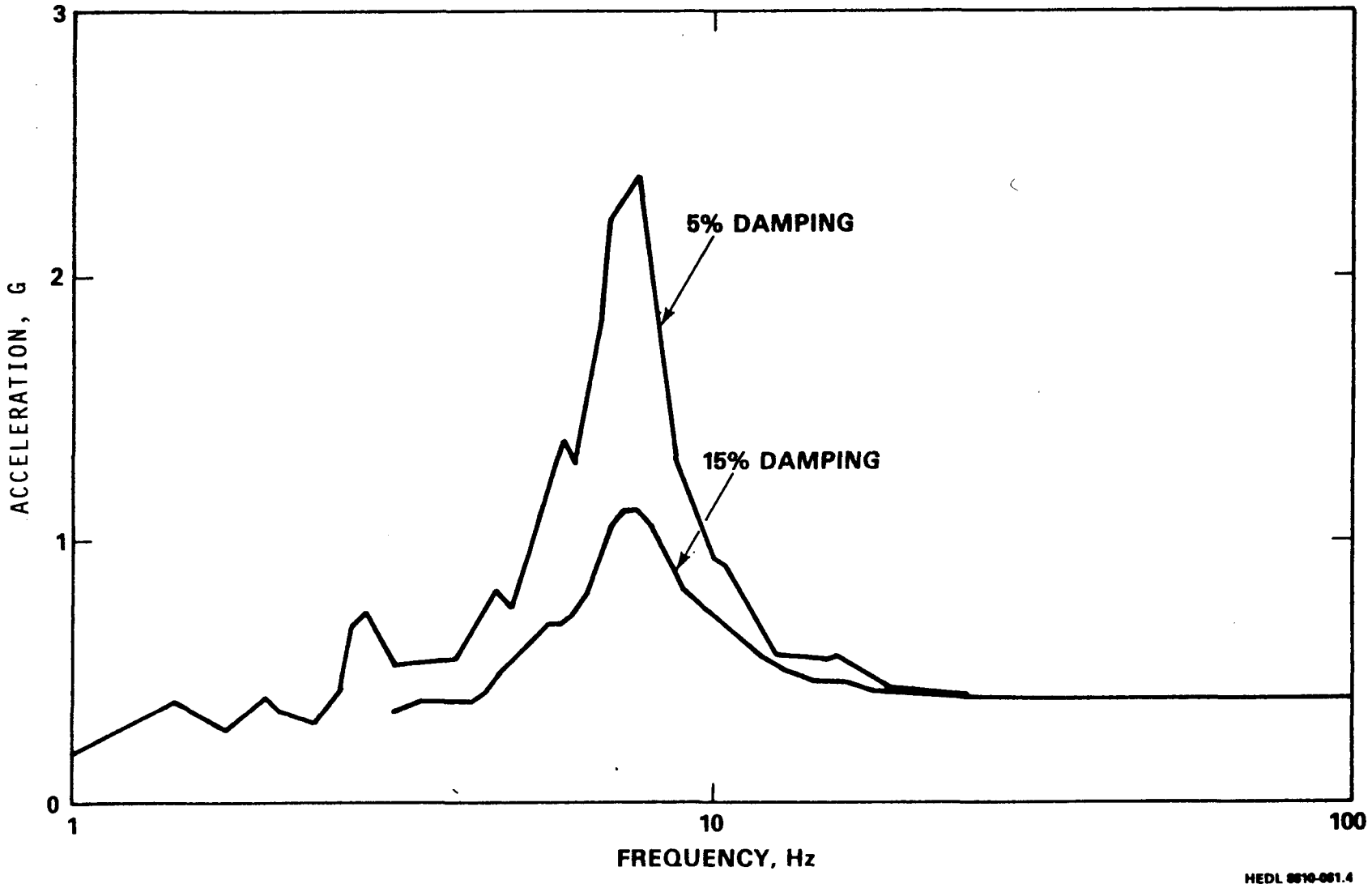

FIGURE 8-3. ETEC Three-Inch Diameter Test Article, Baseline Response Spectrum.

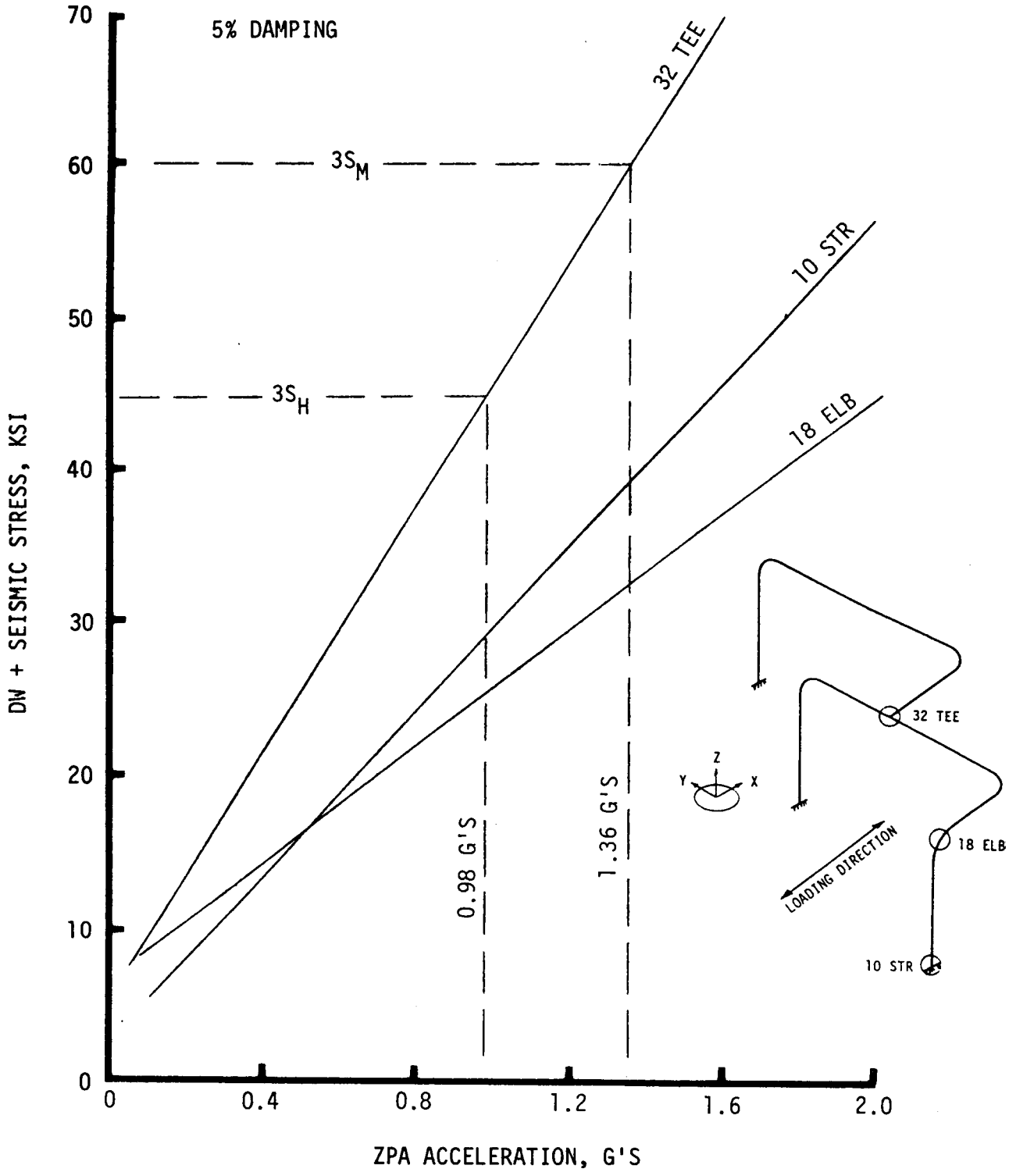

FIGURE 8-4. ETEC Three-Inch Diameter Test Article, Elastic Analysis.

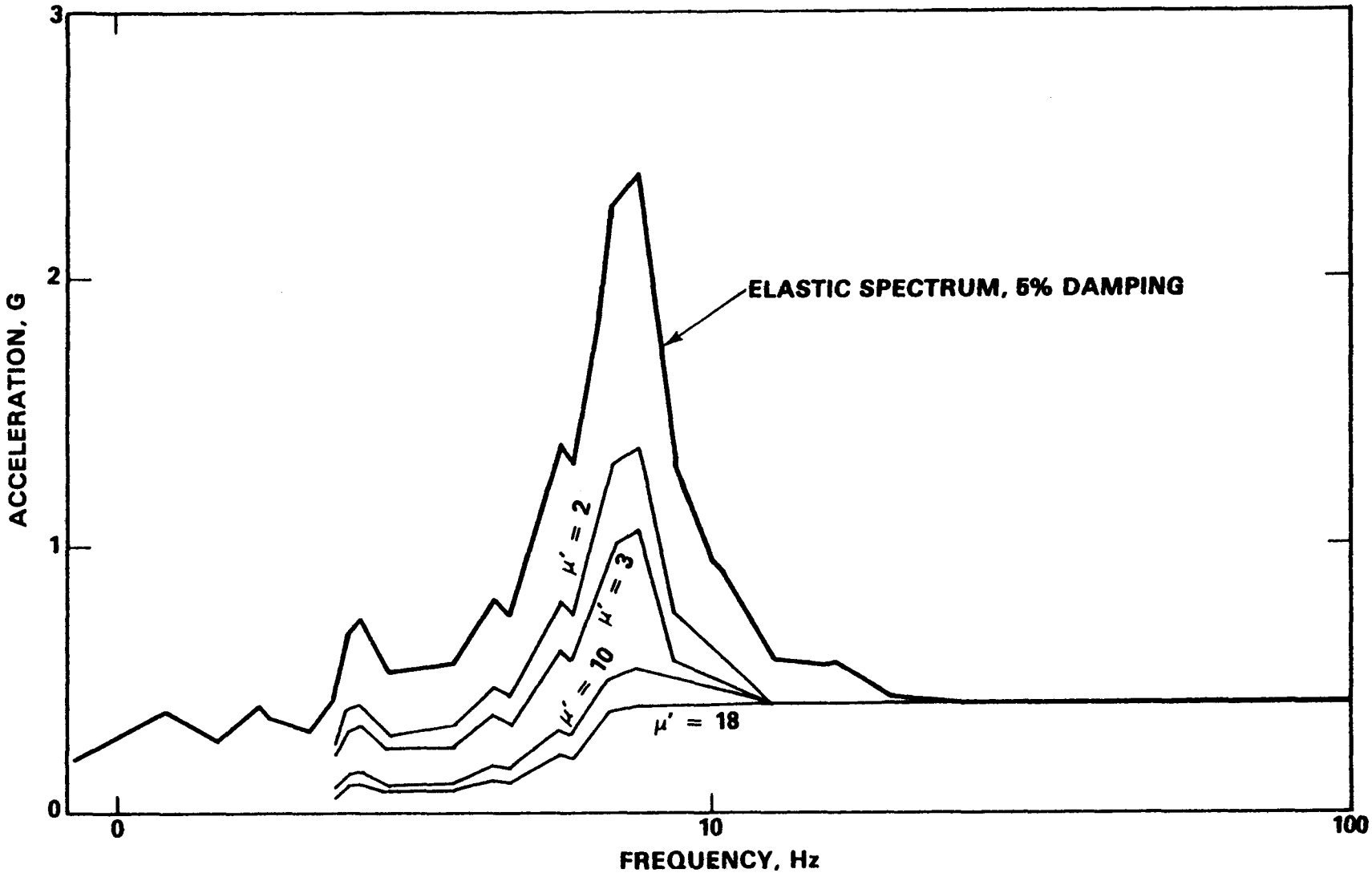

FIGURE 8-5. ETEC Three-Inch Diameter Test Article, Elasto-Plastic Response Spectrum, Newmark Method.

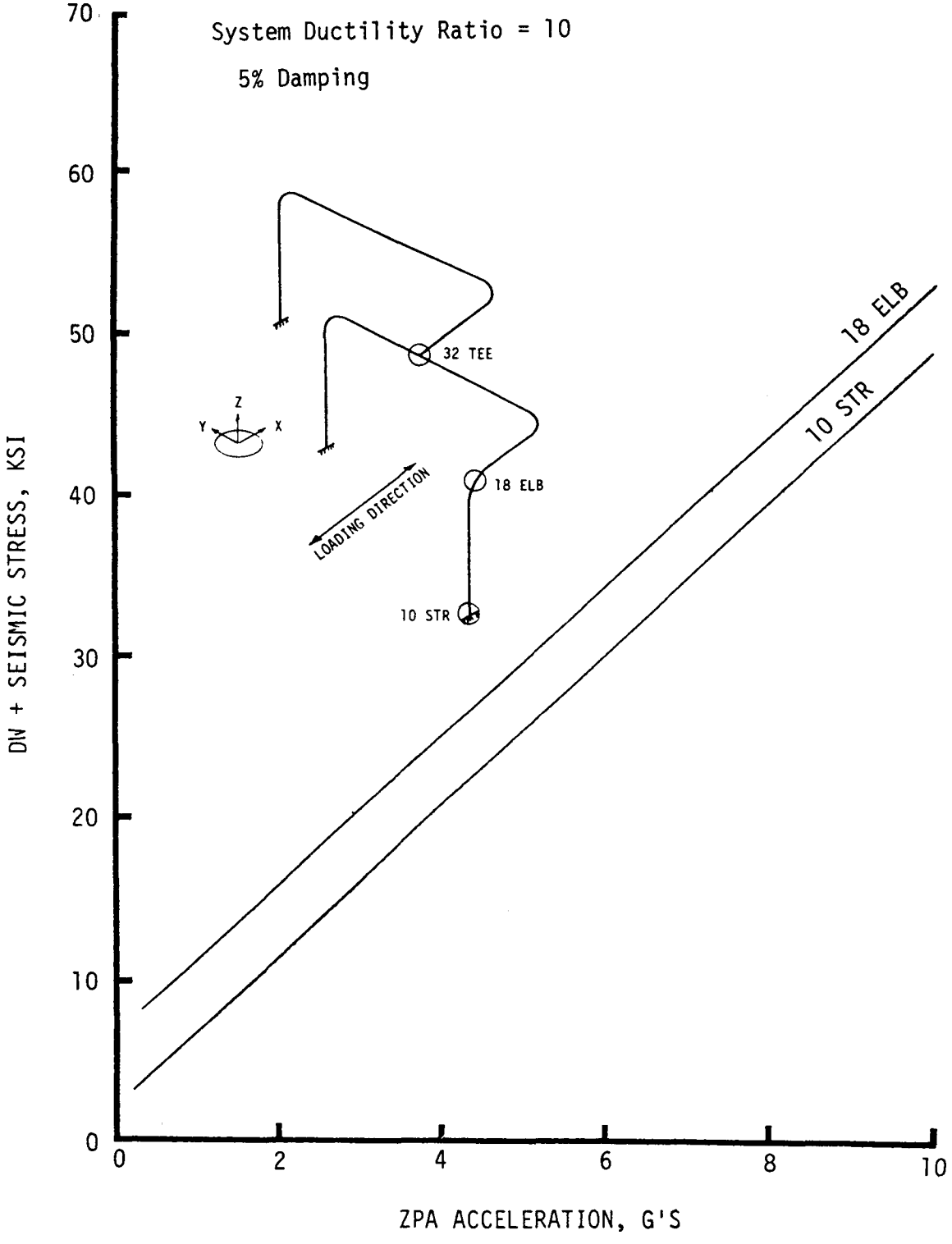

FIGURE 8-6. ETEC Three-Inch Diameter Test Article, Newmark Method.

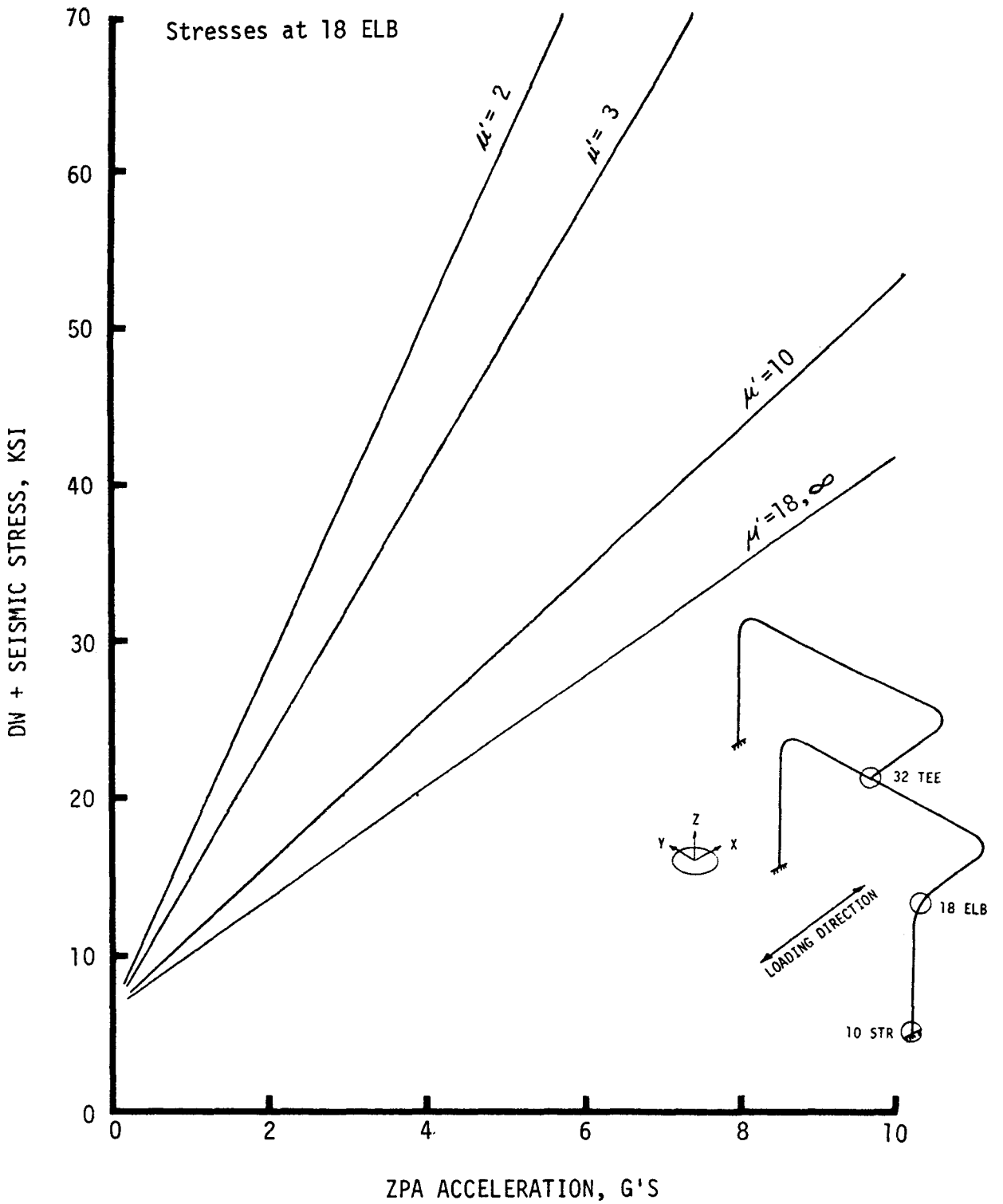

FIGURE 8-7. ETEC Three-Inch Diameter Test Article, Newmark Method, Elbow Stresses.

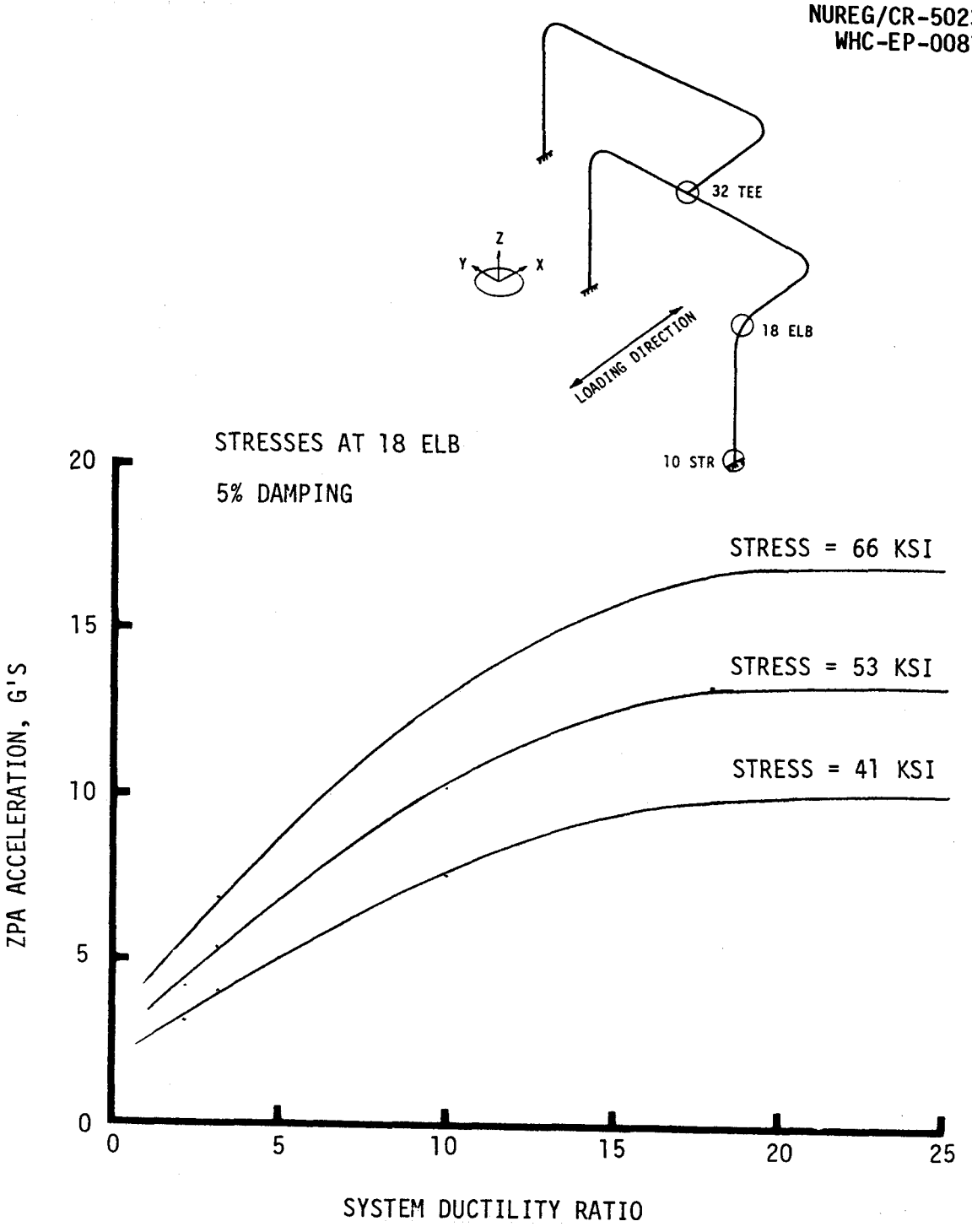

FIGURE 8-8. ETEC Three-Inch Diameter Test Article, Effect of Changing System Ductility Ratio.

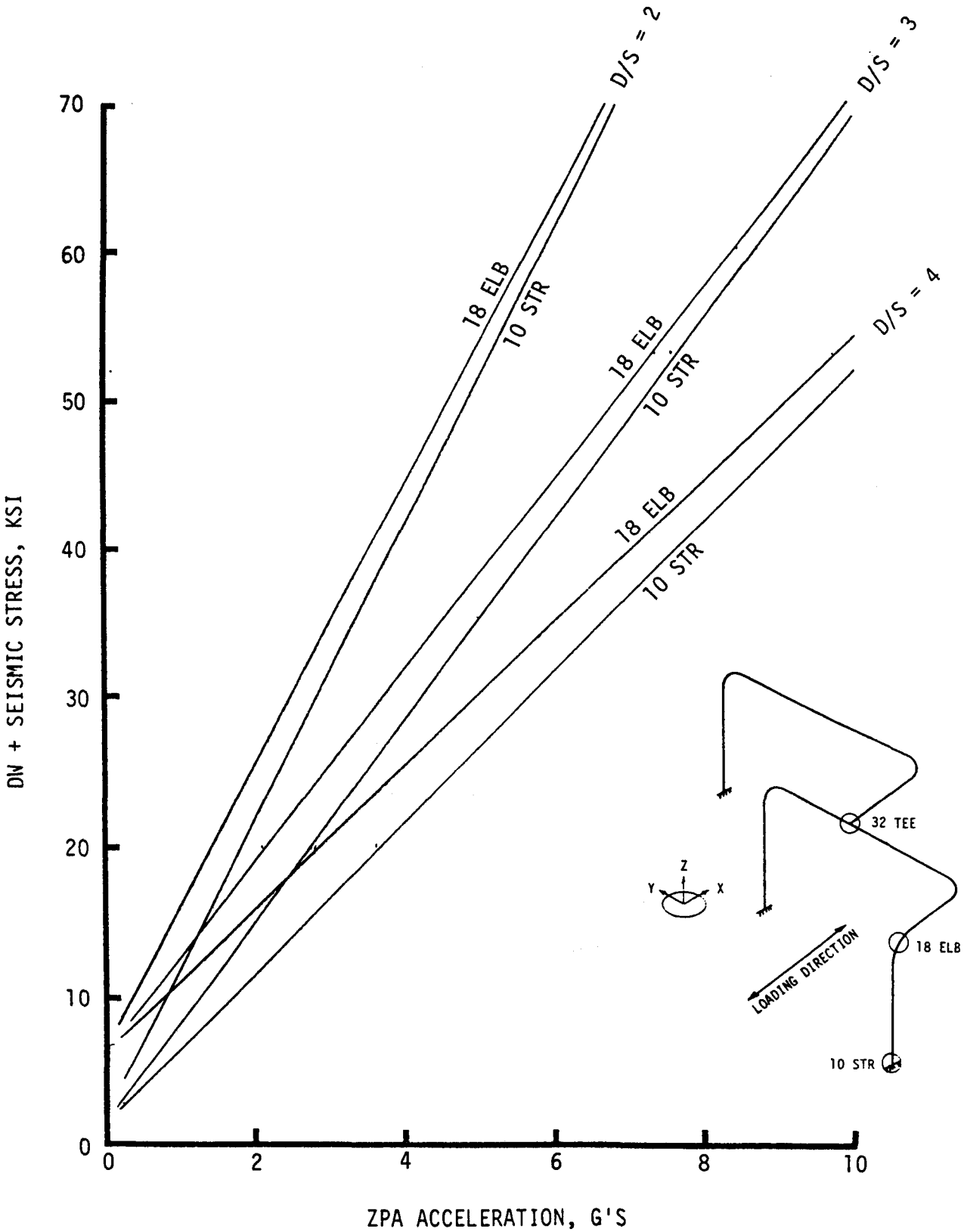

FIGURE 8-9. ETEC Three-Inch Diameter Test Article, D/S Method.

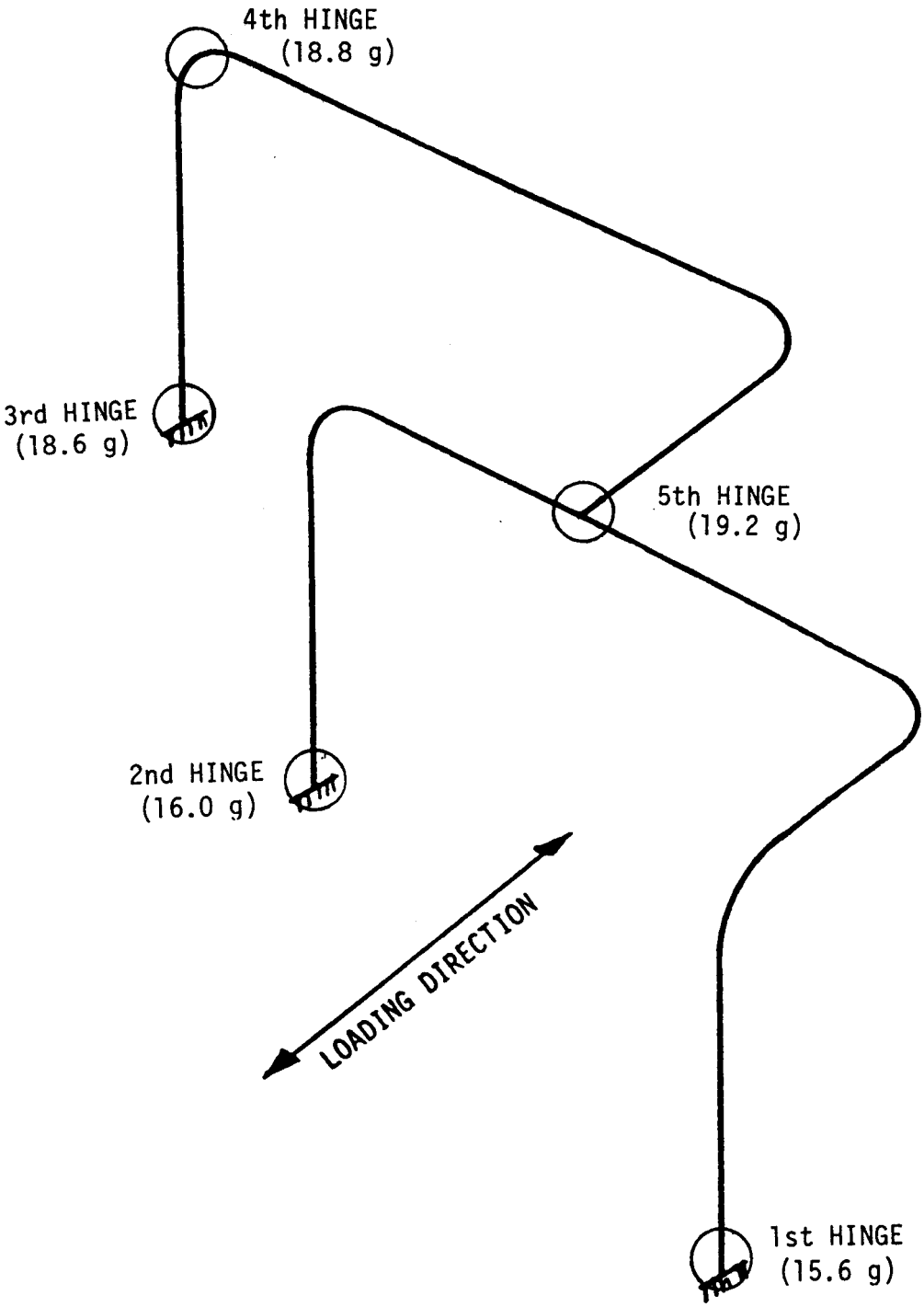

FIGURE 8-10. ETEC Three-Inch Diameter Test Article, Progressive Hinge Method, Static Load Application.

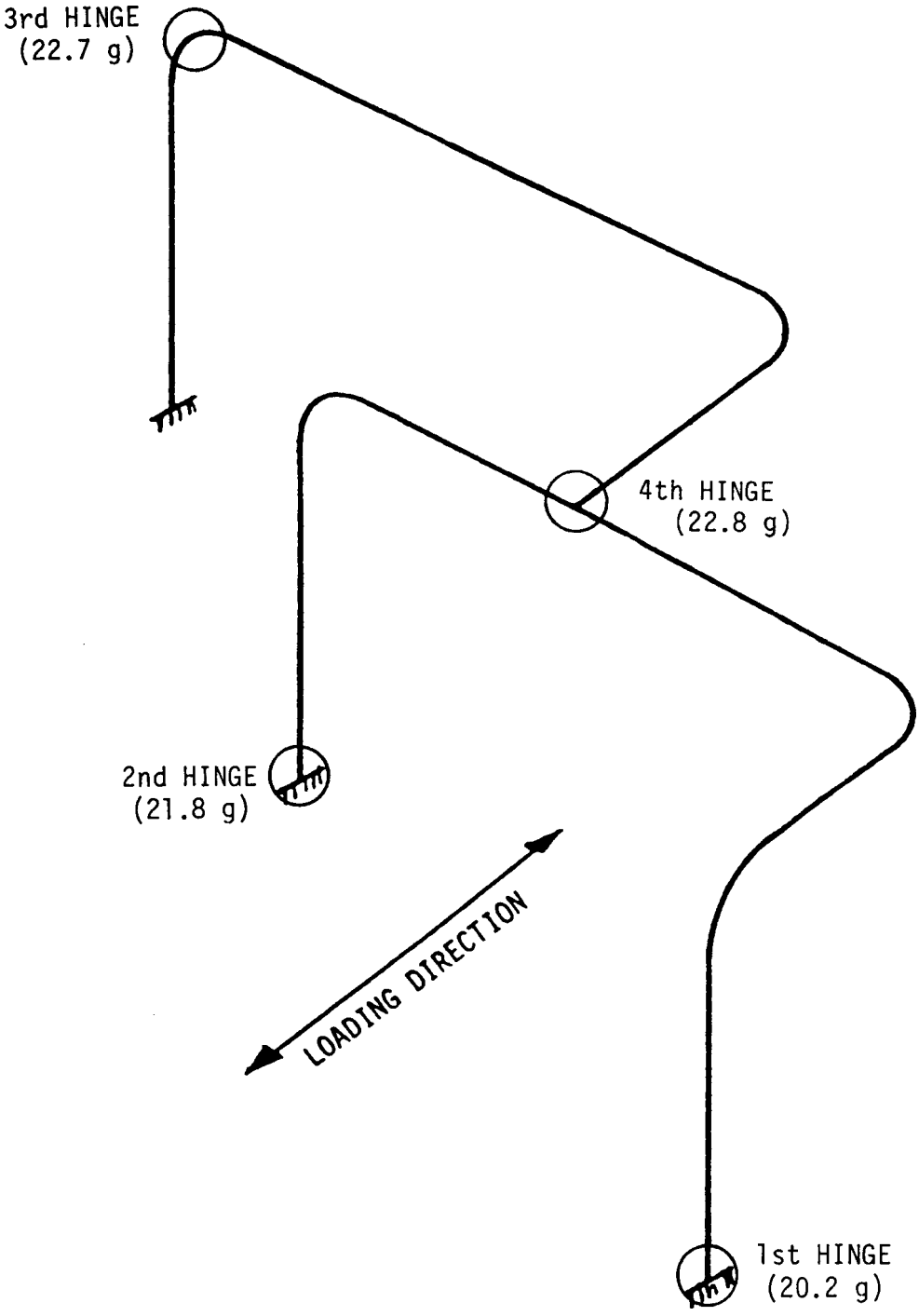

FIGURE 8-11. ETEC Three-Inch Diameter Test Article, Progressive Hinge Method, Dynamic Load Application.

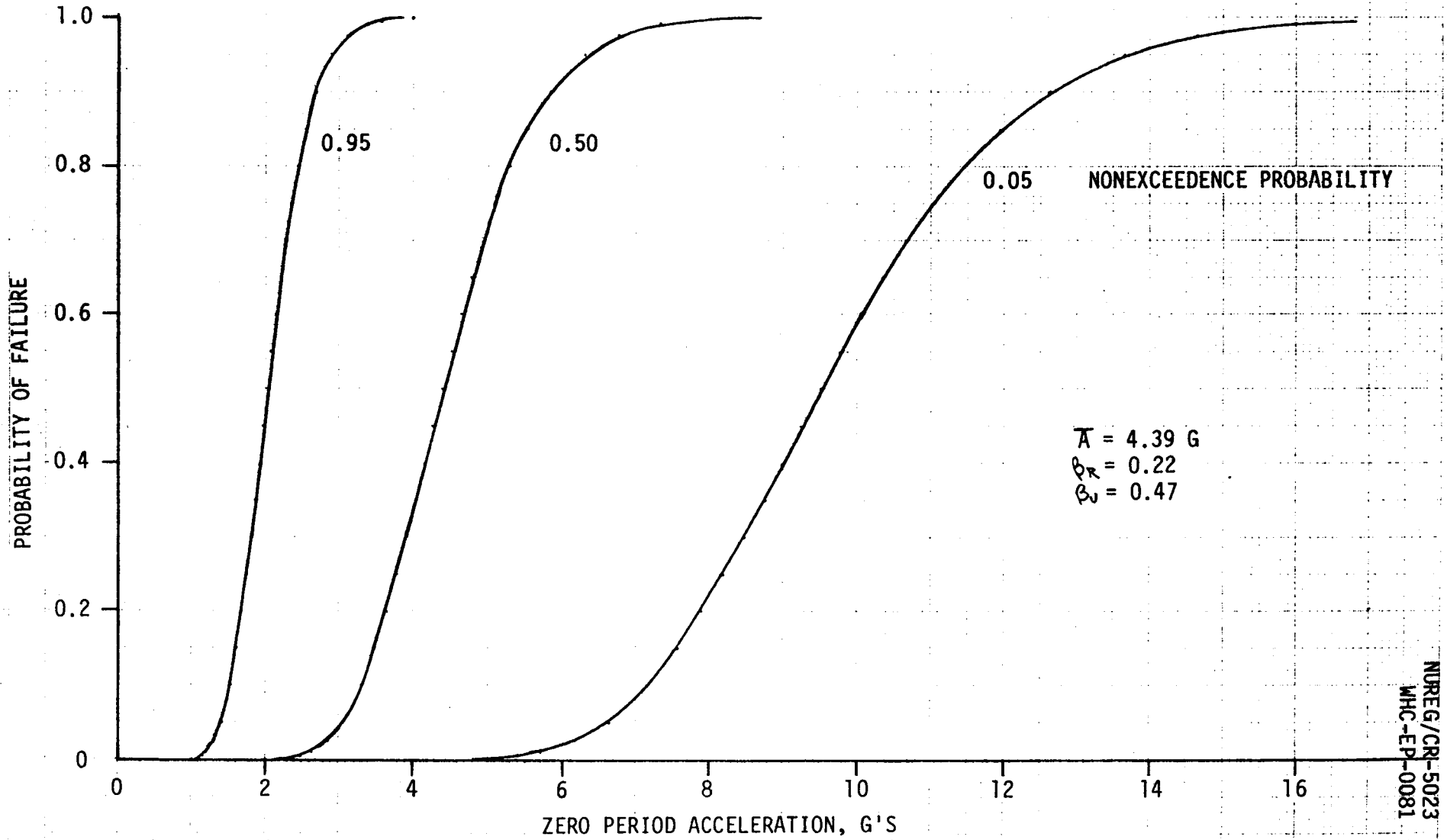

FIGURE 8-12. ETEC Three-Inch Diameter Test Article, Seismic Fragility by the "Zion Method."

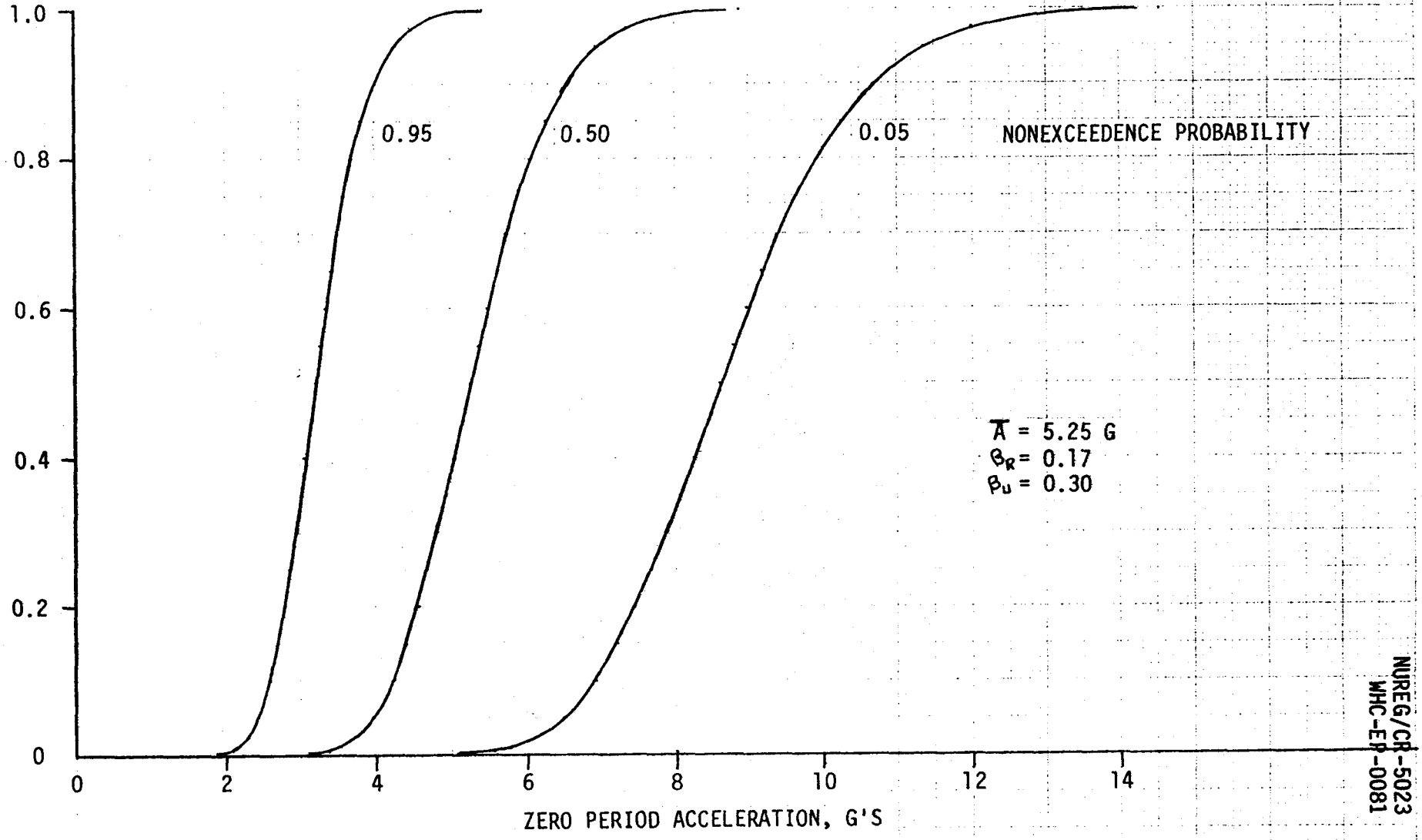

FIGURE 8-13. ETEC Three-Inch Diameter Test Article, Seismic Fragility by the "SSMRP Method."

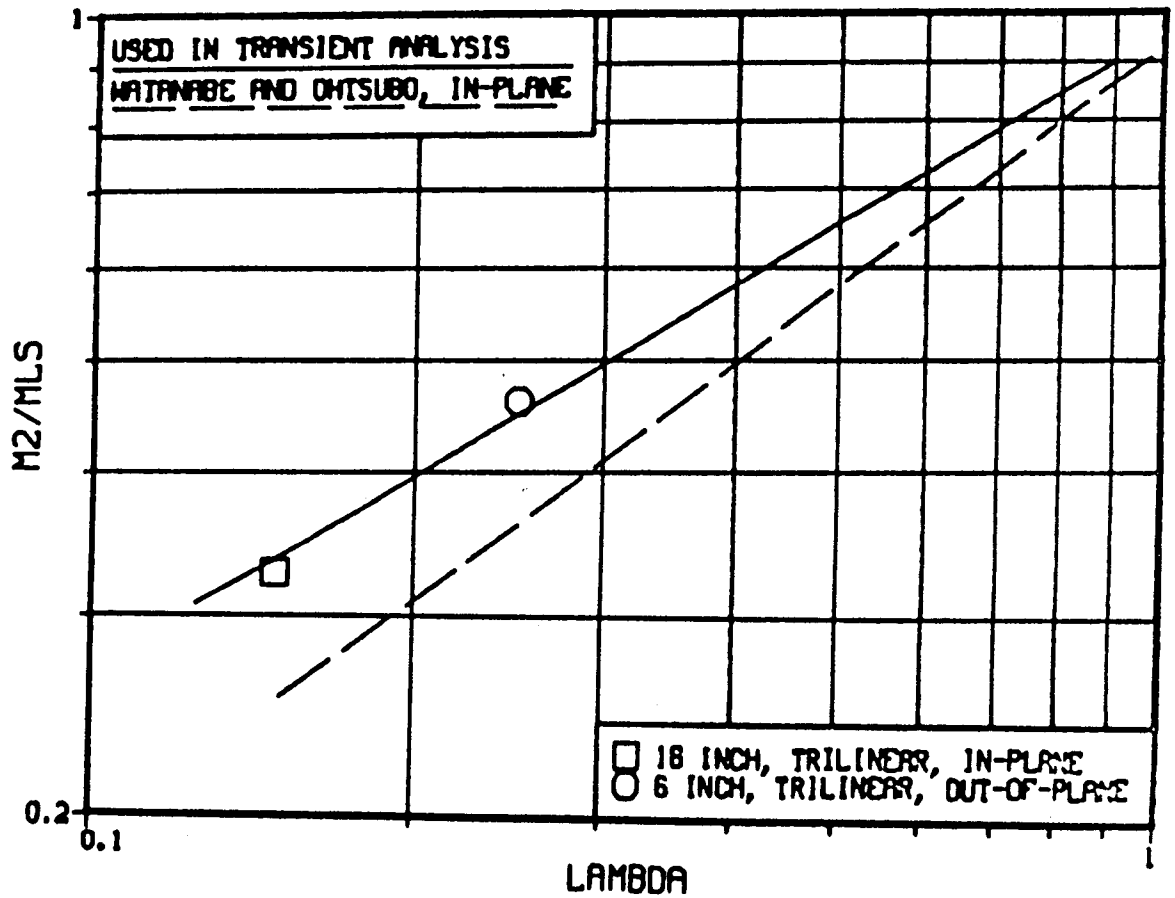

FIGURE 8-14. ETEC Three-Inch Diameter Test Article, Elbow Limiting Moments.

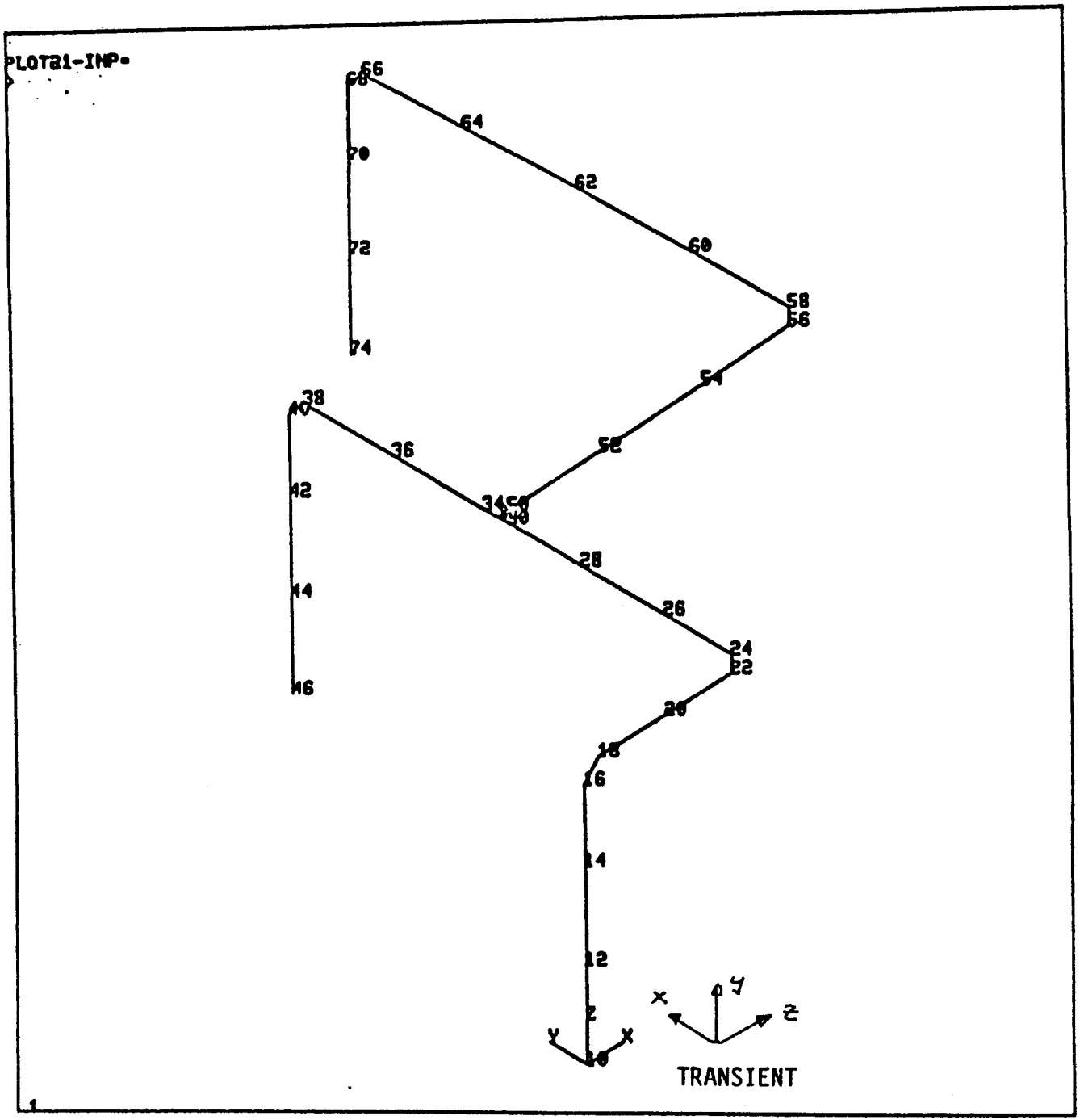

FIGURE 8-15. ETEC Three-Inch Diameter Test Article, Model Grid.

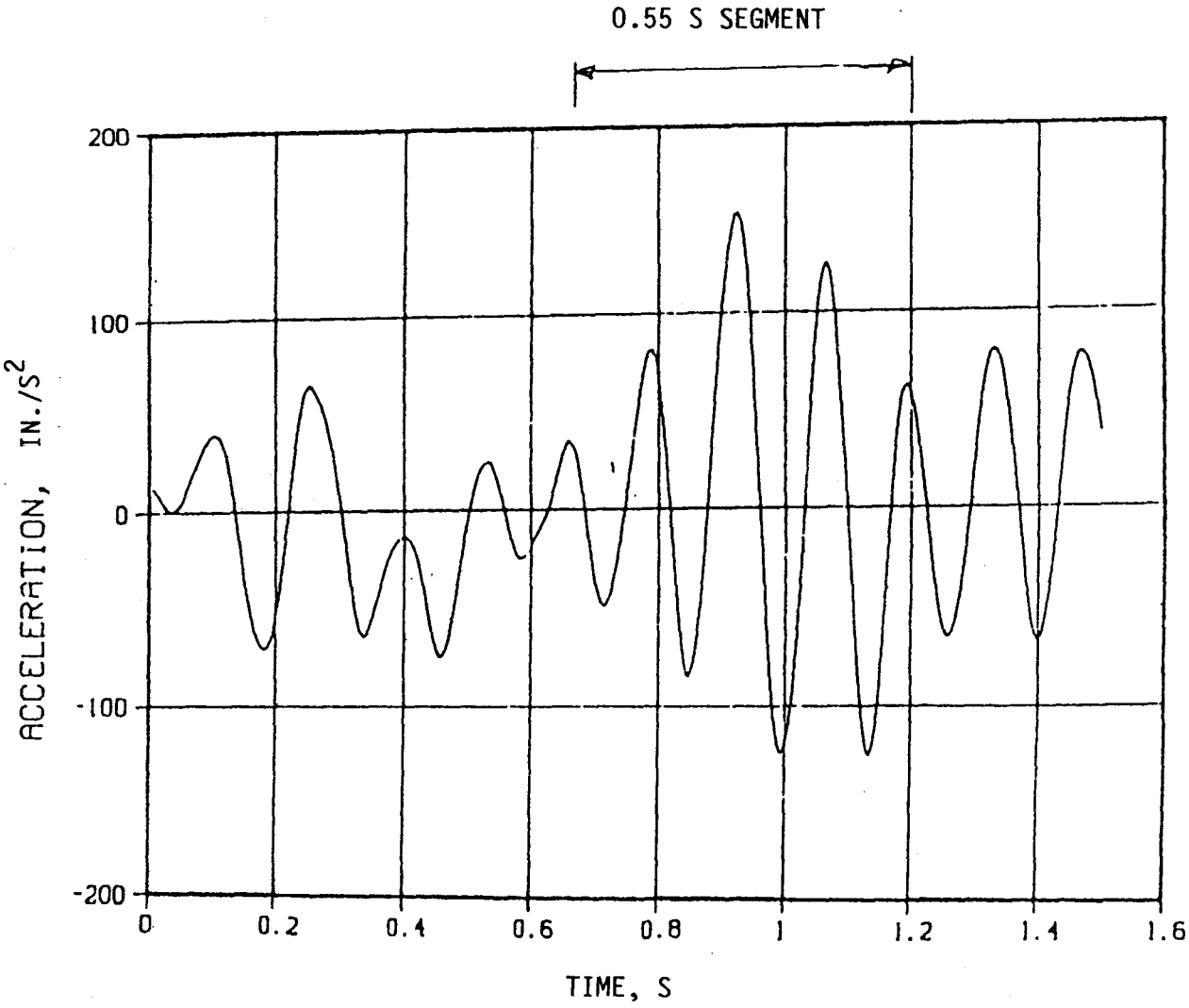

FIGURE 8-16. ETEC Three-Inch Diameter Test Article, Nominal 1.5 Second Segment.

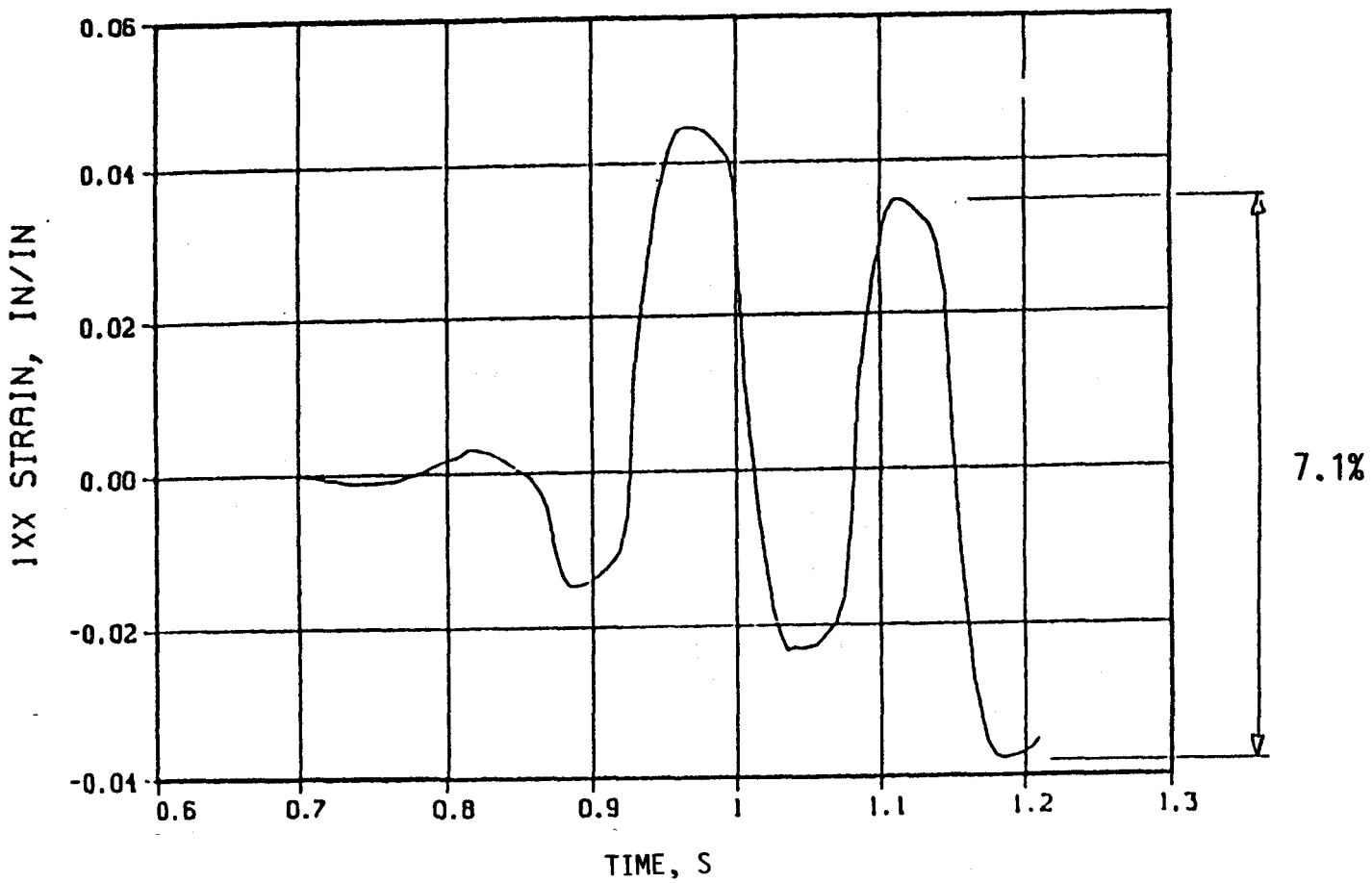

FIGURE 8-17. ETEC Three-Inch Diameter Test Article, Maximum Strain Range.

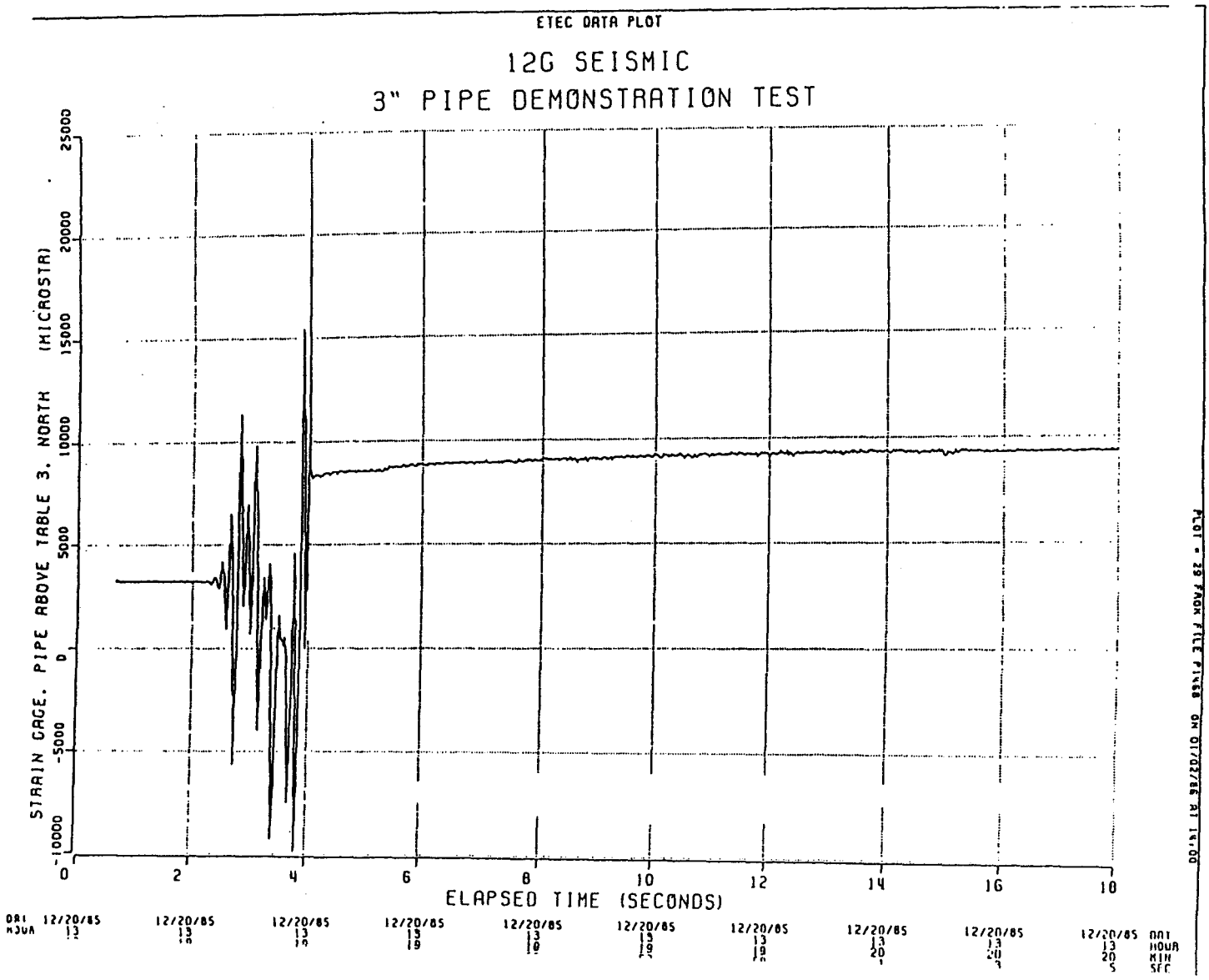

FIGURE 8-18. ETEC Three-Inch Diameter Test Article. Short Test Period.

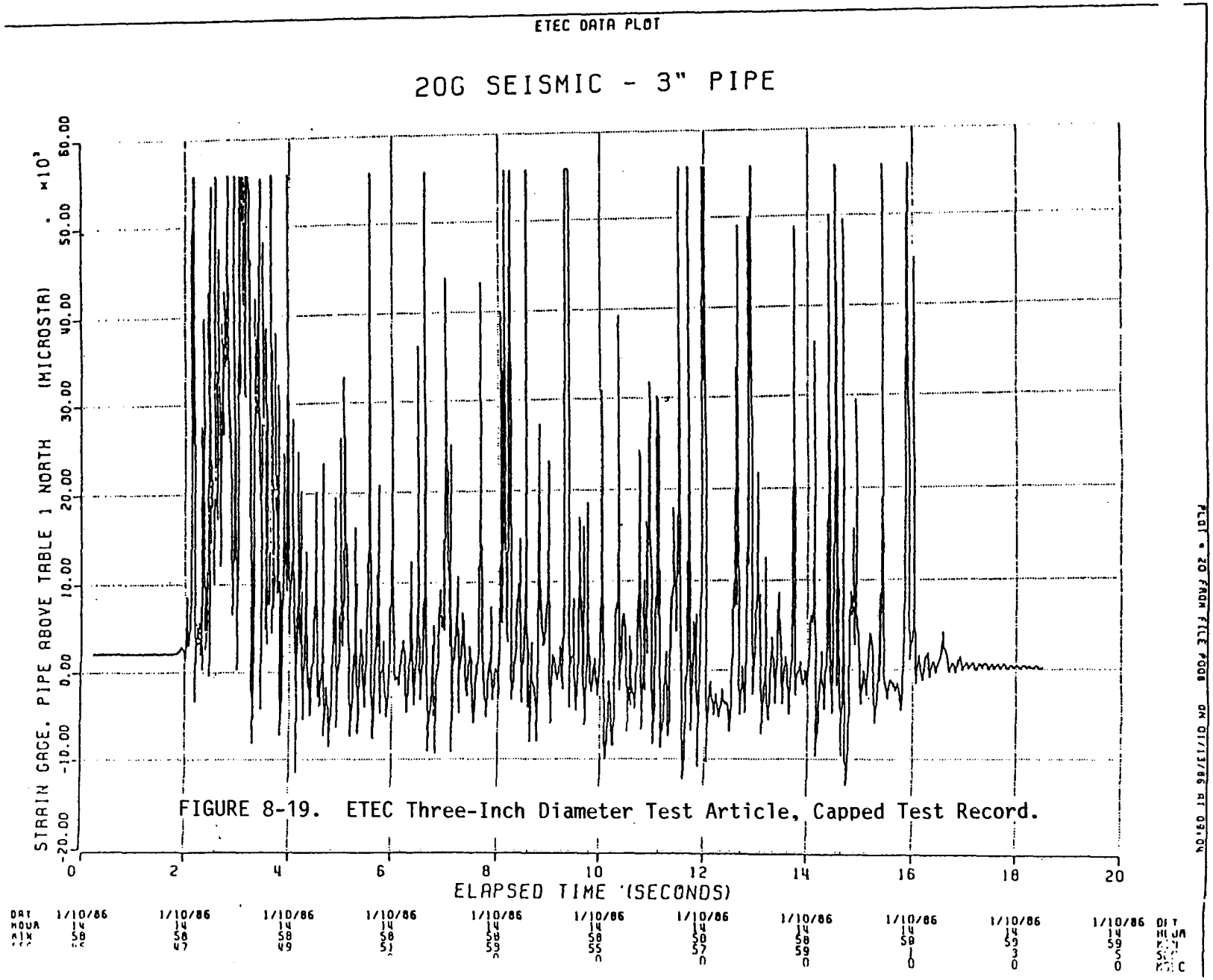

FIGURE 8-19. ETEC Three-Inch Diameter Test Article, Capped Test Record.

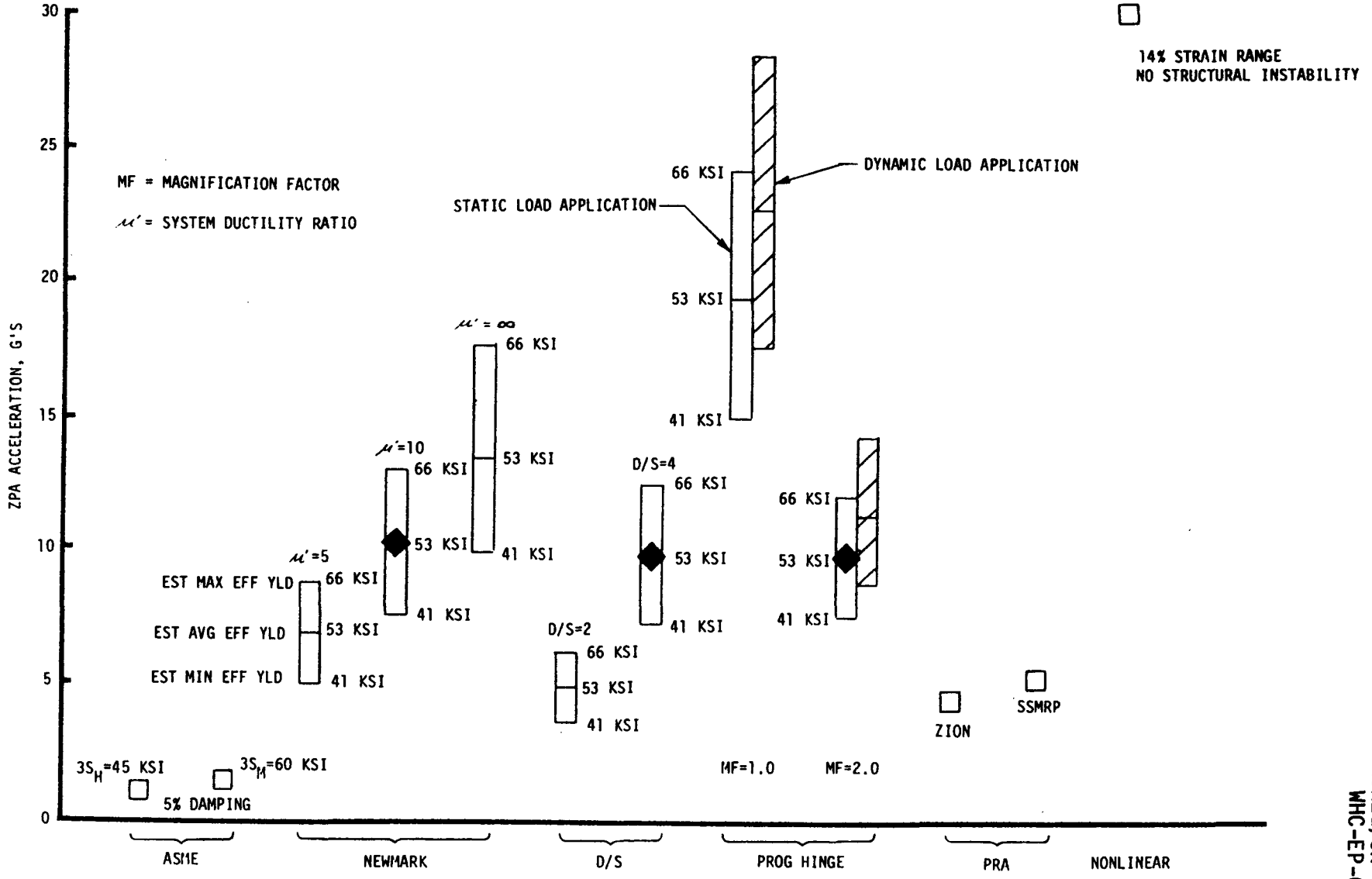

FIGURE 8-20. ETEC Three-Inch Diameter Test Article, Summary of Failure Predictions.

9.0 SIMPLIFIED PREDICTION METHOD FOR DAMPING CAUSED BY PLASTIC HINGES AND SNUBBERS

Simplified methods for predicting equivalent viscous damping are used to assess damping contributions caused by piping inelastic plastic hinge action and support snubbers. These increments are compared to experimental findings from shake and snap-back tests of several pipe systems. Good correlations were found confirming the usefulness of the simplified methods.

9.1 USE OF DATA FOR TECHNOLOGY ADVANCEMENTS AND RULE MAKING

Nuclear power plant piping designs of the last decade have incorporated many seismic restraints and snubbers to ensure adequacy to withstand earthquakes. The design methods have conservatively utilized very low damping values. In the past few years much experimental damping data of piping responding elastically has been gathered. This led to new proposals by industrial groups, such as the Pressure Vessel Research Council (PVRC), for higher design damping allowables. The ASME adopted an interim Code Case N-411.

Interest in high-level inelastic response and tests-to-failure have resulted in USA research programs sponsored by the U.S. Department of Energy (DOE), reported by Lindquist et al. (Reference 6); the U.S. Electric Power Research Institute (EPRI), reported by English (Reference 30), and Jaquay, Larson and Tang (Reference 31); and the U.S. Nuclear Regulatory Commission (NRC), reported by Chen, DeVita, and Onesto (Reference 7), Severud et al. (Reference 32), Guzy (Reference 33), Anderson et al. (Reference 34), and Weiner (Reference 35).

In West Germany, KWU and INTERATOM have sponsored work on high-level inelastic pipe response tests and analysis methods; refer to Haas et al. (Reference 8), Peters and Busch (Reference 36), and Weiner, Peters, and Busch (Reference 37).

The effective equivalent damping associated with the inelastic response is also of interest for use in simplified analyses. Numerous equivalent viscous damping determination methods have been studied by Hadjian (Reference 38), and others. Hadjian pointed out the differences that are found depending upon the assumptions regarding the structure equivalent stiffness of elasto-plastic systems. Bohm, Tagart and Wallach (Reference 39), emphasized the need for considering inelastic damping data. Accordingly, more correlations of test data to prediction model data are desired to clarify this technology.

9.2 SIMPLIFIED ANALYTICAL METHODS

The methods described herein provide simple techniques for calculating the total modal equivalent viscous damping coefficient. It is determined as the sum of damping because of (a) plastic hinges, (b) snubbers, and the pipe system exclusive of (a) and (b).

The equivalent viscous damping coefficient, ζ , for the piping system is approximated by:

$$\zeta = \Delta W/[4\pi(KE)] = \Delta W/[2\pi\sum_{i}^{n}(m_i\ x_i)]\ \omega_N^2 \qquad (1)$$

where, ΔW = energy loss per cycle and KE = maximum kinetic energy or strain energy of the system, m_i = i^{th} mass, x_i = max. amplitude of i^{th} mass, and $_N$ = circular frequency of mode N. The energy loss, ΔW, is made up of those losses due to plastic hinges, snubbers, and the other damping sources.

The plastic hinge energy loss, ΔW_p, is approximated by

$$\Delta W_p = 4 \sum_{i=1}^{K} \left[M_{pi} \left(\theta_{mi} - \theta_{yi} \right) \right] \qquad (2)$$

where, K = number of plastic hinges in system, M_{pi} = effective limit moment of plastic hinge i, 0_{mi} = maximum angle amplitude hinge i rotates through, and 0_{yi} = angle amplitude to initiate plastic hinge i yielding.

The snubber energy loss, ΔW_S, is approximated by:

$$\Delta W_S = \pi \sum_{j=i}^{L} \left[C_j\ \omega_N\ X_{Mj}^2 \right] \qquad (3)$$

where, C_j = damping coefficient of snubber j, ω_N = circular frequency of mode N, and X_{Mj} = maximum displacement of snubber j.

It is noted that in applying Eq. (1) and (2), quasistatic elastic-plastic system deformation solutions for increased modal acceleration loads are employed to evaluate the system displacements and angles and equivalent system stiffness and maximum kinetic or strain energy. This approach follows some of the concepts given by Peters and Busch (Reference 36). The procedure

in this reference uses a modal force field which is applied statically and increased until significant plastic deformation is incurred (quasistatic analysis). Elasto-plastic parameters, dependent on the strain level, are obtained for a simple two-bar substitute which is subjected to the seismic excitation appropriate for the piping system. The method used herein avoids the transient analysis of a substitute. Instead, effective values of system ductility, damping and frequency shift are obtained from the quasistatic analysis, and linear response spectrum techniques are applied iteratively. Given a mode ϕ, let $F_0 = K\phi$ be the corresponding vector of modal forces. Define

$F = \alpha F_0$ = Quasistatic forces applied to the piping system

α = Scale factor

X = Displacement vector corresponding to force F

$F_y = \alpha_y F_0$ = Forces producing 0.2% offset yield

ε = Maximum strain, function of

X_y = Displacements corresponding to F_y

M = Diagonal mass matrix.

Following (Reference 36), the corrected energy dissipation per cycle is

$$H = 2W$$

where

$$W = Q - (F \cdot X_y + (F - F_y) \cdot X)/2$$

$$Q = \int F \cdot dX$$

Q is the work done by the forces. In Figure 9-1a, the solid curve OAB represents the quasistatic analysis, and the parallelogram ABCD is H. With Figures 9-1b and 9-1c, the effective frequency and damping are defined by

$$\omega^2 = f \cdot x \,/\, x \cdot Mx \qquad 2\pi Z = H \,/\, f \cdot x$$

where

$$x = \tfrac{1}{2}(X + X_y) \qquad f = \tfrac{1}{2}(F + F_y)$$

$$f \cdot x = \tfrac{1}{4}(\alpha + \alpha_y)(F_0 \cdot X + F_0 \cdot X_y)$$

$$x \cdot Mx = \tfrac{1}{4}(X \cdot MX + 2X \cdot MX_y + X_y \cdot MX_y)$$

The system ductility (Reference 10) and strain range are

$$\mu = \tfrac{1}{2}(1 + \Sigma m\ \delta / \Sigma\ m\delta_y)$$

$$d\varepsilon = \varepsilon + \varepsilon_y$$

where m is a nodal mass, δ is a nodal displacement magnitude and the summation extends over the structural nodes.

9.3 PLASTIC HINGE DAMPING CORRELATIONS

The four piping systems of Figure 9-2 were shake-tested to high-level inelastic response. Table 9-1 provides correlations of calculated damping increments because of plastic hinges to total system damping levels estimated from the test response. Figures 9-3 and 9-4 show the quasistatic effective damping for the four systems as a function of response strain range and test input level ZPA.

Figure 9-5 illustrates the dependence of system ductility on the configuration. For a given strain range, the WHC one-inch case shows the greatest system ductility. This is explained by a nearly constant bending moment between the critical support and the elbow towards the region of maximum displacement. Such a distribution avoids a concentration of strain. Plots of frequency shift and damping show similar spreads among the configurations. These terms are plotted against system ductility in Figures 9-6 and 9-7. The relative lack of variation among curves in these two plots underscores the importance of the system ductility parameter in simplified analysis. For the larger system ductilities, these curves compare fairly well with the geometric equivalent simple oscillator results of Hadijian (Reference 38). The lower values at the lower ductilities are attributed to system hardening. The ETEC 3 in. shows less frequency shift and damping than the other systems. Again, this is a system hardening effect. In the progressive hinge analyses, this system proved to be the slowest in forming a mechanism. It has a tripod appearance with the three legs built in at the base. The WHC 1-inch and ETEC 6-inch systems look more like simple bents with out-of-plane excitation, and one would expect them to have the least system hardening. The branch in the KWU configuration looks like a bent with the excitation directed 45 deg to its plane.

9.4 SNUBBER AND SUPPORT DAMPING INCREMENTS

The small bore piping systems of Figures 9-8 and 9-9 and the large bore 16-inch diameter system of Figure 9-10 serve as benchmark data. Comparisons of test and calculated damping values follow.

The small bore, 1 inch to 3 inch diameter piping with heavy insulation was tested and total system damping in the 5 to 12% range was found. Snubber damping increments calculated for this piping were only in the 1 to 2% range as shown in Tables 9-2, 9-3, and 9-4. The damping caused by insulation and other system damping effects dominate these small bore piping damping values. However, for the larger bore piping with many snubbers, the snubber damping is more significant. The 16-inch diameter insulated stainless steel pipe system of Figure 9-10 was tested. Table 9-5 shows the damping calculation for the 1000 lb. pull location of Figure 9-10. Figure 9-11 shows the effects of load level and the total system damping per test relative to the calculated snubber damping. Note that the snubbers are calculated to contribute about half of the total system damping. In this case, the test elicitation was low and the maximum pipe stresses were about half that required for yielding.

9.5 DAMPING CONTRIBUTIONS CAUSED BY PLASTIC HINGES, SNUBBERS, AND REST OF PIPE SYSTEM

Regarding the WHC 1-inch diameter system (Table 9-1), the high-level test, (2.5 g's ZPA) of this small bore, heavily insulated pipe system with one mechanical snubber, experimentally revealed dynamic magnifications equivalent to 40 to 50% damping. At low levels the piping system was elastic and the equivalent damping was about 10%. The calculated equivalent increment of damping for one plastic hinge was 16% and with two hinges it was 29%. The single mechanical snubber provided only 1% damping. Thus, under high-level shaking, the insulation and plastic hinge damping are the major sources of damping for this insulated pipe system.

For the ETEC 6-inch and 3-inch diameter uninsulated pipe systems, which did not have any snubbers, the plastic hinge damping contributions of up to 20 to 30% were calculated. These levels compare reasonably with the test-deduced level of 13 to 22% (Reference 7).

9.6 CONCLUSIONS

A number of correlations of the calculated damping values per the above methods have been made with piping experimental findings. These comparisons of calculated and experimental data of numerous piping systems at multiple levels of response were presented. Good correlations were found. The simple methods provide a useful tool in assessing the extent plasticity and snubbers add to piping system damping during high-level inelastic response.

SYSTEM	PIPE DIAM(S).	MATERIAL	EXCITATION TYPE	MAX BASE INPUT, G'S	MAX.STRAIN RANGE, % ESTIMATE	ESTIMATED SYSTEM TEST DAMPING, %	CALCULATED PLASTIC HINGE EQUIVALENT VISCOUS DAMPING, %
HEDL 1 in. f_1 = 2 H_z Ref. 6	1 in.(25.4 mm)	304 S S	Sinusoidal 12-18 Cycles at 2 H_z	2.5	2.5 Ref. 6	40-50 Ref. 32	29
ETEC 6 in. f_1 = 5 H_z Ref. 7	6 in./3 in.	SA 106B	Seismic Sinusoidal 10 Cycles at 4 H_z	30 ZPA 18	4 4-8 Ref. 35	13-22 19 Ref. 35	18 (Mode 1) 20 (Mode 2) 16
ETEC 3 in. f_1 = 5 H_z	3 in.	SA 106B	Seismic Seismic	14 ZPA 30 ZPA	8 14	* *	30 (Mode 1) 16 (Mode 2) 36 (Mode 1) 22 (Mode 2)
KWU 4/2 in. Ref. 8	4 in./2 in.	Aust. S S	Harmonic at 8.9 H_z	4	1.8	*	5 (Mode 3)

*NO DATA AVAILABLE OR PUBLISHED YET.

TABLE 9-1. Pipe Damping During Shake Test High Level Inelastic Response.

NUREG/CR-5023
WHC-EP-0081

TABLE 9-2

ONE-INCH DIA INSULATED PIPE SNUBBER DAMPING FOR SNAPBACK TEST, FIGURE 9-8

(PULL AT H-6Z OF 90 LB)

SIMPLIFIED ANALYSIS OF SNUBBER DAMPING INCREMENT				TEST DATA	
NODE NO.	SNUBBER TYPE	INITIAL MAX LOAD, LB *	SNUBBER ENERGY LOSS/CYCLE E_s, IN.-LB		f_1 = 4.5 H_z
H-1	PSA-1/4	29	0.8	PULL LOAD LB	DAMPING AVE, %
H-2	-1/2	72	1.0		
H-3	-1/4	63	1.5	30	5
H-4	-3	144	0.5	60	6-7
H-5	-3	178	0.6	90	7
H-8	-1/4	156	3.0		

E_S = 7.4 IN.-LB

$$2\pi\ \omega_N^2 \sum (m_i\ x_i^2) = 2\pi\ (2\pi \times 4.5)^2 (0.149) = 748$$

$$\zeta_{SN} = \frac{7.4}{748} = 0.010, \text{ SAY } 1\% \text{ FOR 90-LB PULL AND SNAPBACK}$$

*BASED ON STATIC ANALYSIS AND MAGNIFICATION FACTOR OF 2.0 FOR SUDDEN SNAPBACK.

TABLE 9-3

ONE-INCH DIA INSULATED PIPE SNUBBER DAMPING FOR SNAPBACK TEST, FIGURE 9-8

(PULL AT H-7Z OF 70 LB)

SIMPLIFIED ANALYSIS OF SNUBBER DAMPING INCREMENT				TEST DATA	
NODE NO.	SNUBBER TYPE	INITIAL MAX LOAD, LB*	SNUBBER ENERGY LOSS/CYCLE E_s, IN LB	f = 10 H_z	
				PULL LOAD, LB	DAMPING AVE, %
H-1	PSA-1/4	1.4	____		
H-2	-1/2	0.7	____	24	7.7
H-3	-1/4	5.6	____	47	9.0
H-4	-3	66	0.2	70	9.6
H-5	-3	35	0.1		
H-6	-1/4	102	1.0		
H-8	-1/4	160	2.0		

E_S = 3.3 IN.LB

$$2\pi\,\omega_N^2 \sum (m_i\, x_i^2) = 2\pi\,(2\pi \times 10)^2\,(0.0067) = 166$$

$$\xi_{SN} = \frac{3.3}{166} = 0.020, \text{ SAY 2\% FOR 70 LB PULL AND SNAPBACK}$$

*BASED ON STATIC ANALYSIS AND MAGNIFICATION FACTOR OF 2.0 FOR SUDDEN SNAPBACK.

TABLE 9-4

DAMPING OF 1-INCH DIA INSULATED PIPING WITH AND WITHOUT SNUBBER, FIGURE 9-9

PIPE SYSTEM PER FIGURE 6-2 SUPPORTS PER TEST	PULL LOAD, LB	PREDICTED SNUBBER DAMPING, %	SYSTEM TEST DATA ζ, %	f_1, H_3
ONE SNUBBER, REST RIGID STRUTS	17	—	11-12	9.0
	34	—	9-10	9.0
	50	1	8-11	9.0
ALL RIGID STRUTS	17	—	4-6	10.5
	34	—	6	10.1
	50	—	5-7	9.8

TABLE 9-5

16-INCH DIA PIPING SNUBBER DAMPING ESTIMATE FOR SNAPBACK TEST, FIGURE 9-10

For 1000 lb Pull at H-7, For First Mode, $f_1 = 5\ H_3$; $\omega = 31.4$ Rad/S

NODE NO	SNUBBER TYPE	INITIAL MAX LOAD, LB*	DAMPING COEF. C, LB-S/IN.	SNUBBER INITIAL MAX DISPL., X, IN.	SNUBBER ENERGY LOSS/CYCLE $E_s = \pi C \omega X^2$
H-2	PSA-3	20	20	0.000	0
H-3	-3L	85	85	0.002	2
H-4	-3L	90	90	0.002	2
H-5	TWO-1L	2@795	2(2000)=4000	0.014	56
H-6	TWO-3	2@60	2(60) =120	0.001	1
H-9	TWO-3	2@650	2(700) =1400	0.013	24
H=11	TWO-1L	2@215	2(1000)=2000	0.007	10
H-12	-3	11	10	0	0
H-14	-3	30	30	0	0
H-15	-10	30	30	0	0
					$\sum \pi C_i \omega_N X_M^2 = 95$

$$2\pi\omega_N^2 \sum (m_i x_i^2) = 2\pi(2\pi \cdot 5)^2 (0.389) = 2400.;\ \zeta_{SN} = \frac{95}{2400} = 0.04, \text{ Say } 4\%.$$

*BASED ON STATIC ANALYSIS AND MAG. FACTOR = 2.0 FOR SUDDEN SNAPBACK.

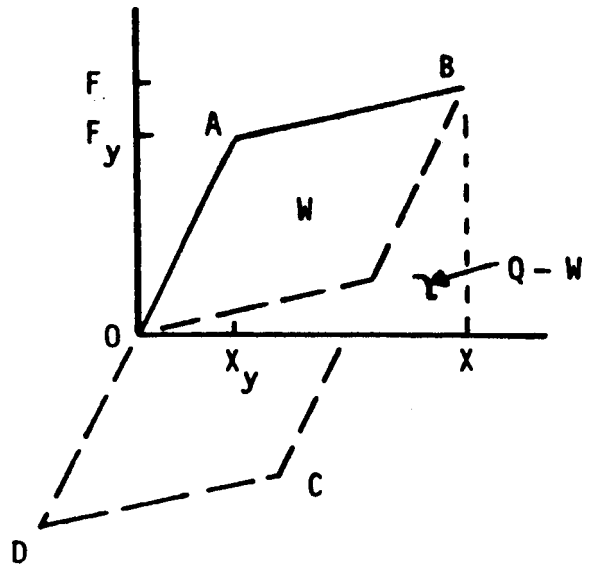

(a) H - SCHEMATIC

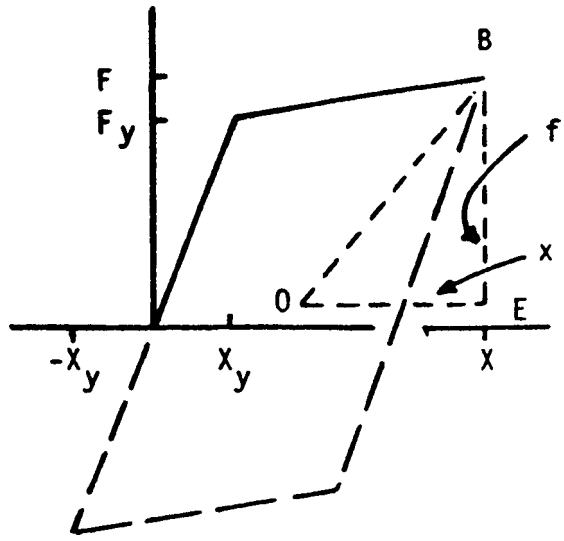

(b) ω - SCHEMATIC

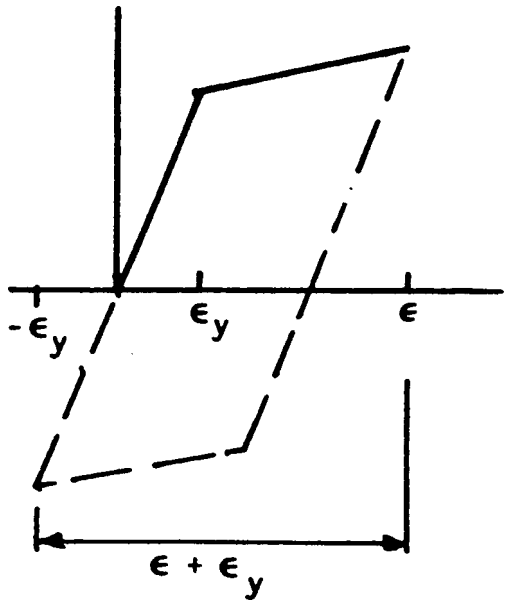

(c) $\Delta\epsilon$ - SCHEMATIC

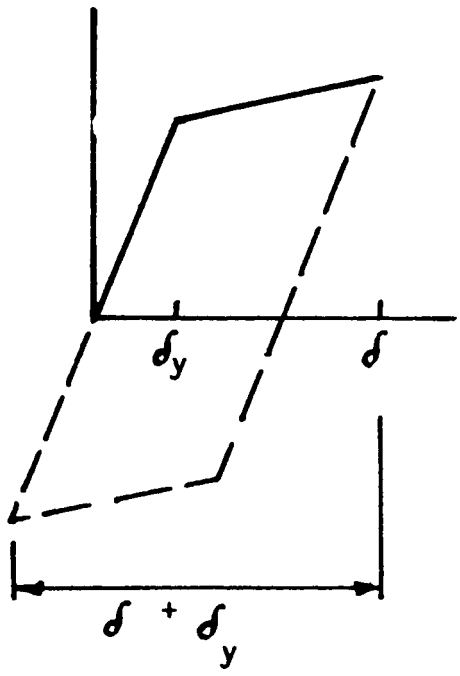

(d) μ - SCHEMATIC

FIGURE 9-1. Quasistatic Parameter Schematics.

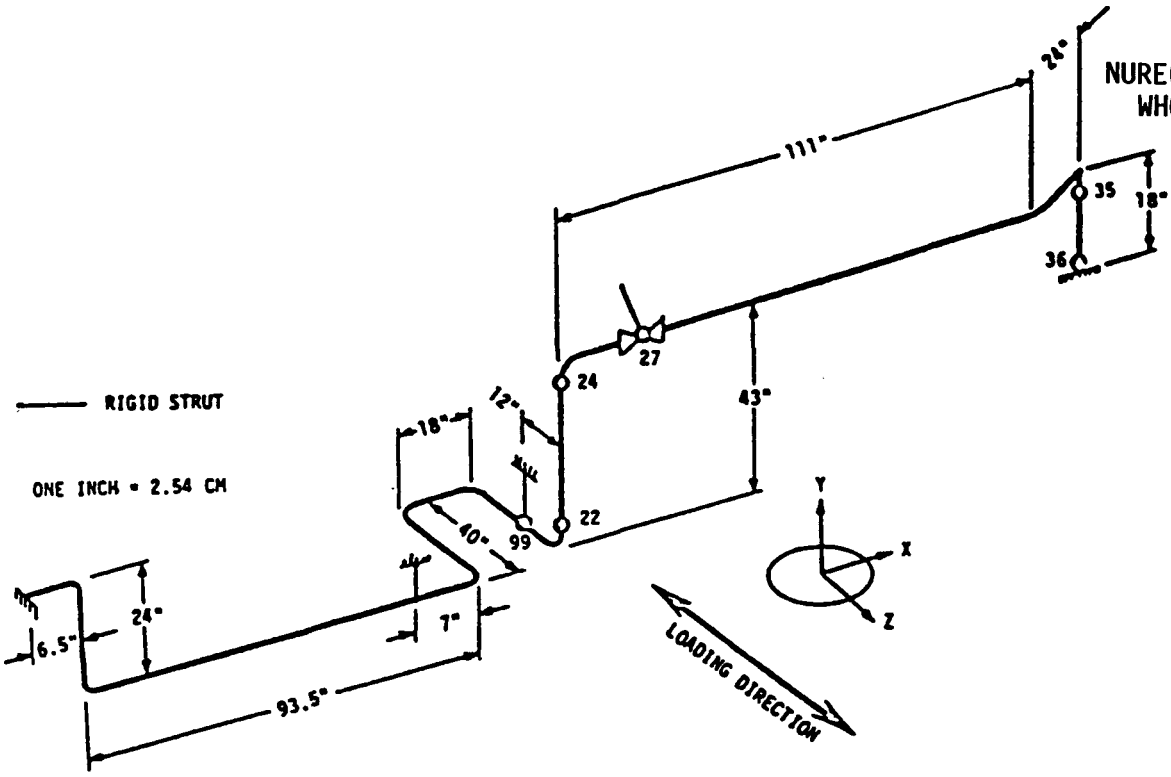

(a) HEAVILY INSULATED SMALL BORE (1" DIAMETER) STAINLESS STEEL PIPE SYSTEM

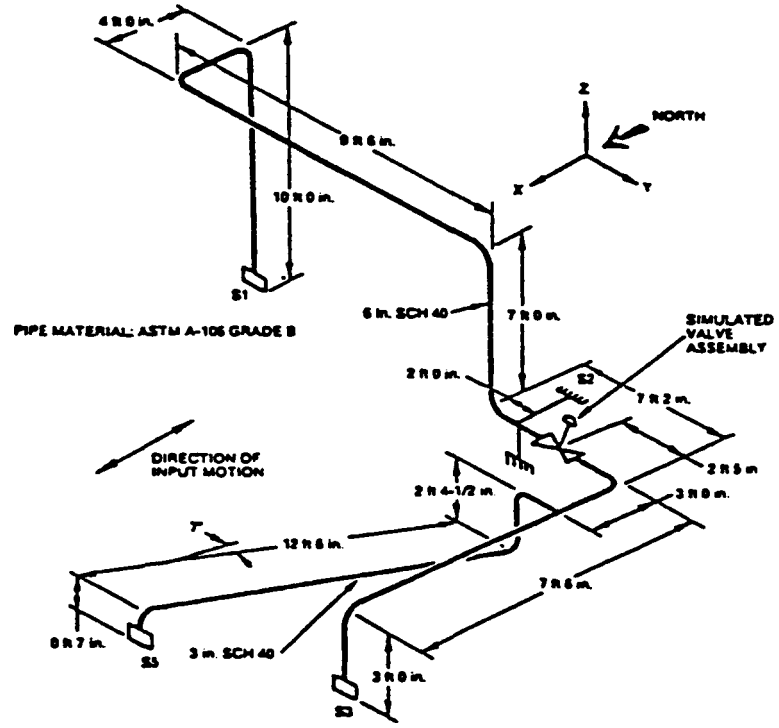

(b) UNINSULATED MILD STEEL (6" DIAMETER) PIPE SYSTEM

FIGURE 9-2. Piping Systems Tested to High-Level Inelastic Response.

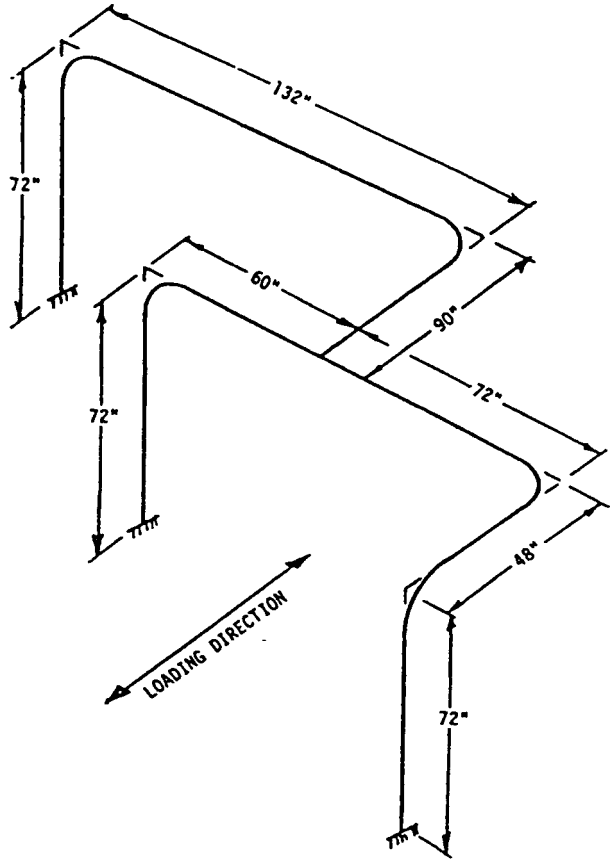

(c) UNINSULATED.MILD STEEL (3" DIAMETER) PIPE SYSTEM

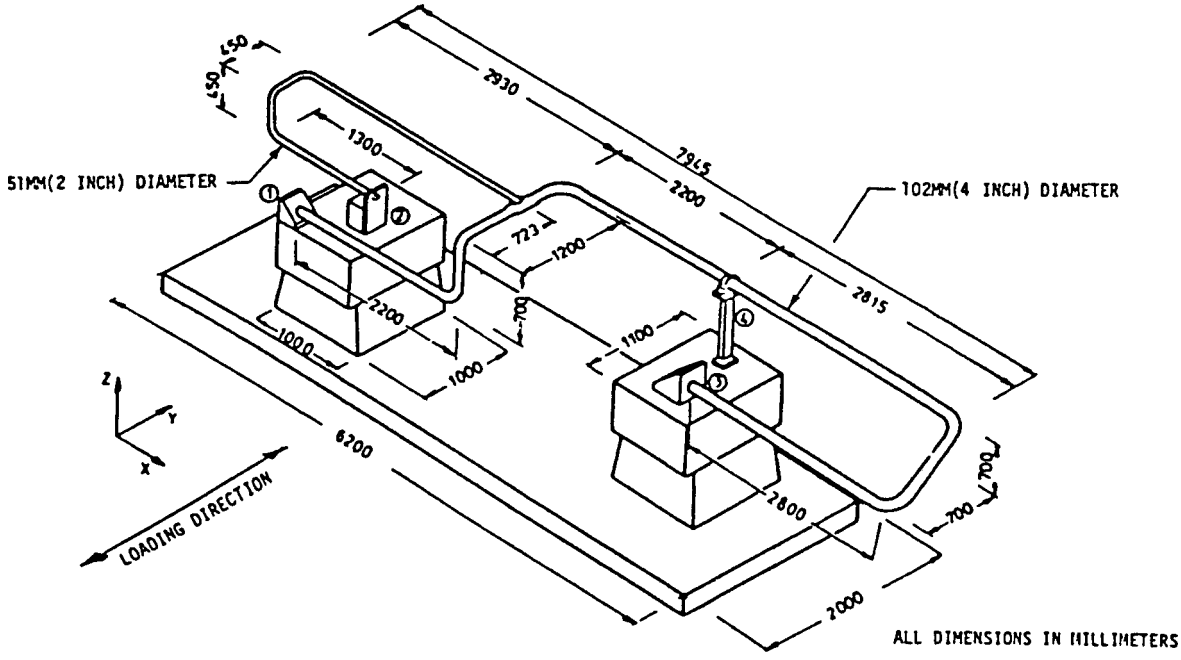

(d) UNINSULATED STAINLESS STEEL (4" AND 2" DIAMETER) PIPE SYSTEM

FIGURE 9-2. Continued.

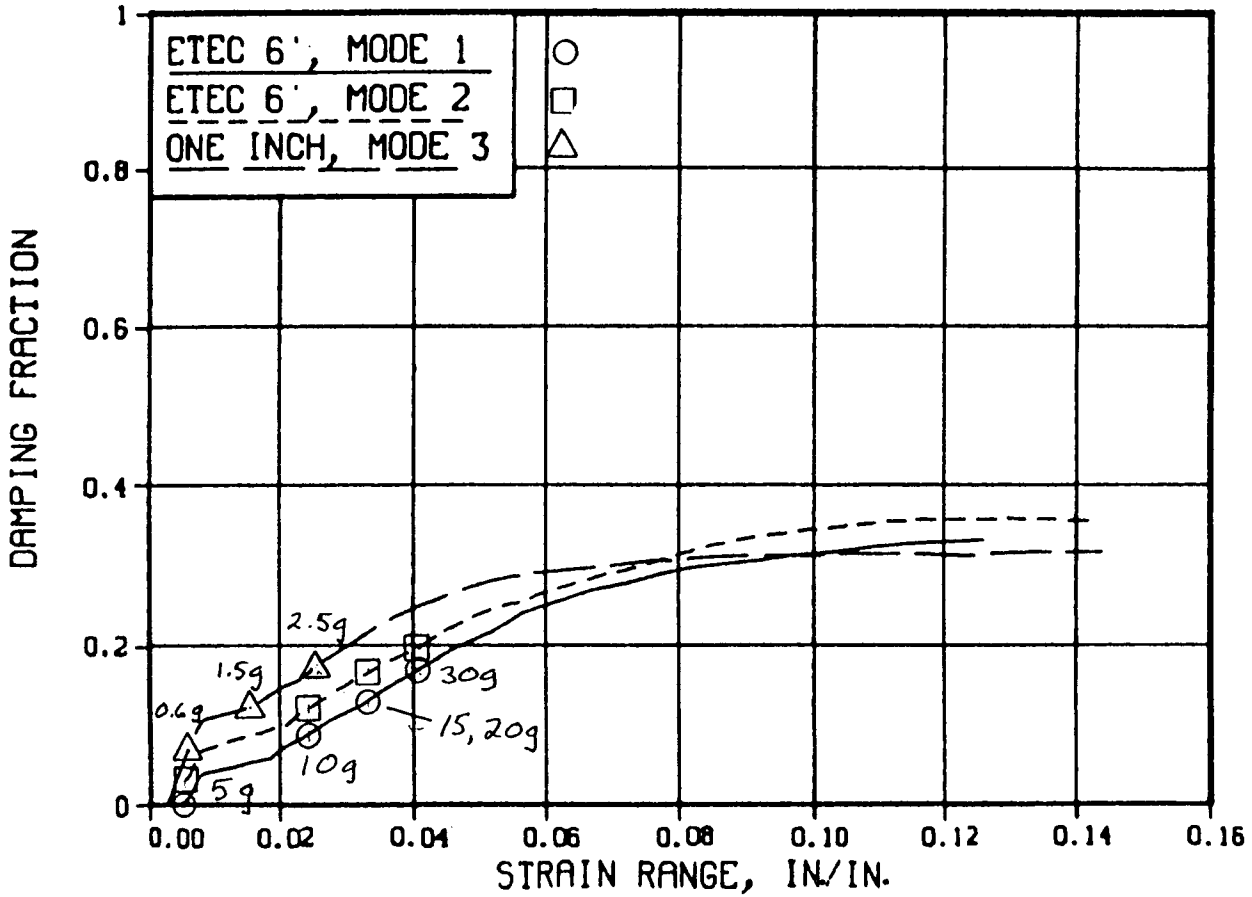

FIGURE 9-3. Quasistatic (Sym) Effective Damping.

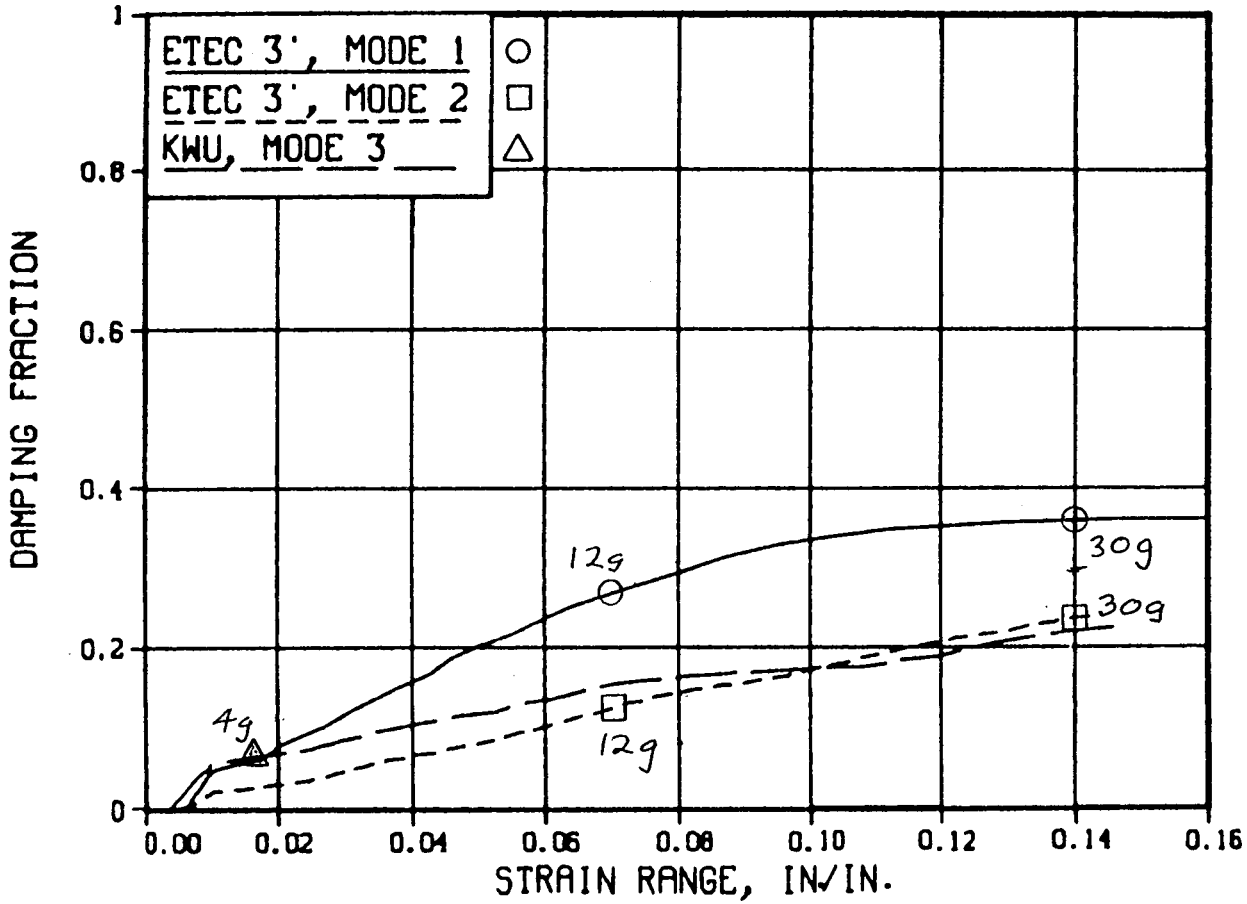

FIGURE 9-4. Quasistatic (Sym) Effective Damping.

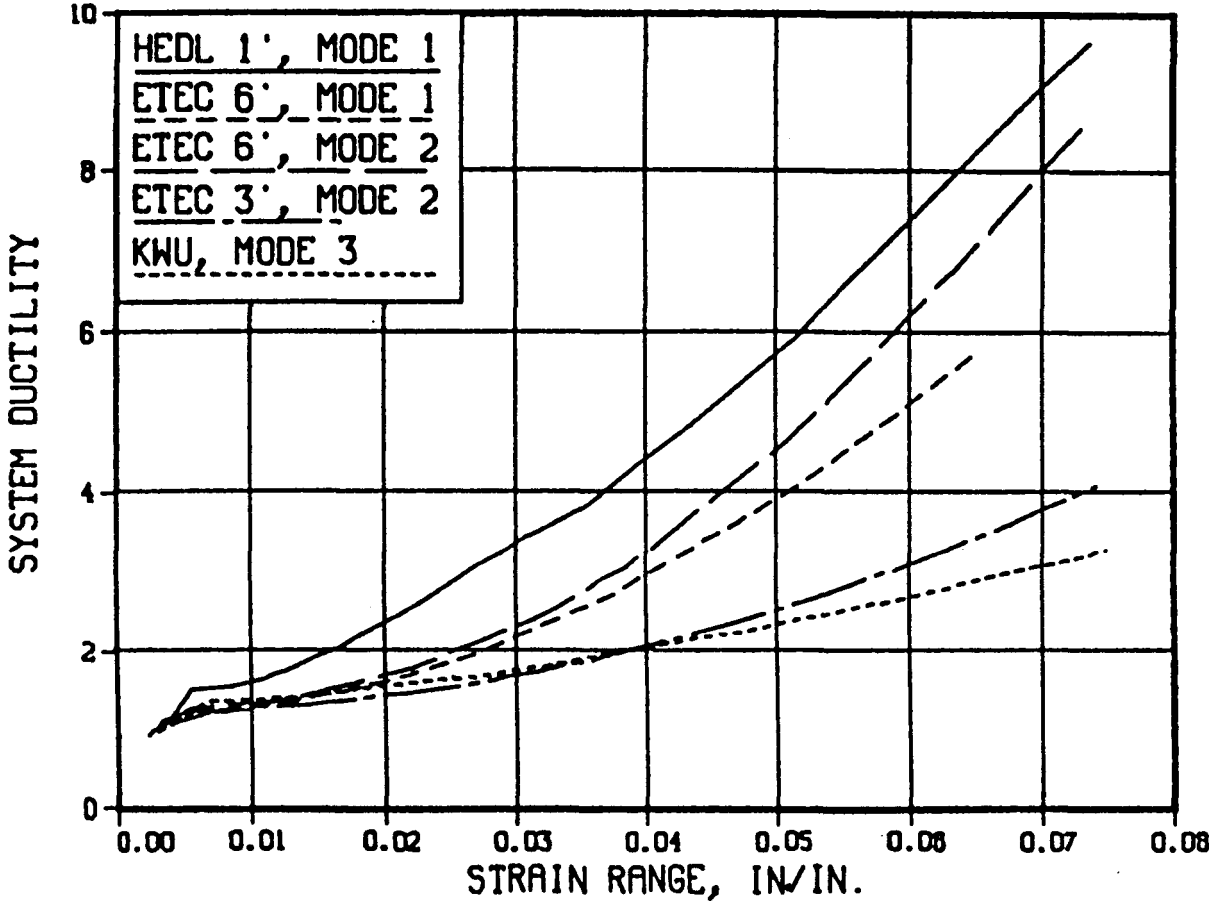

FIGURE 9-5. Quasistatic System Ductility.

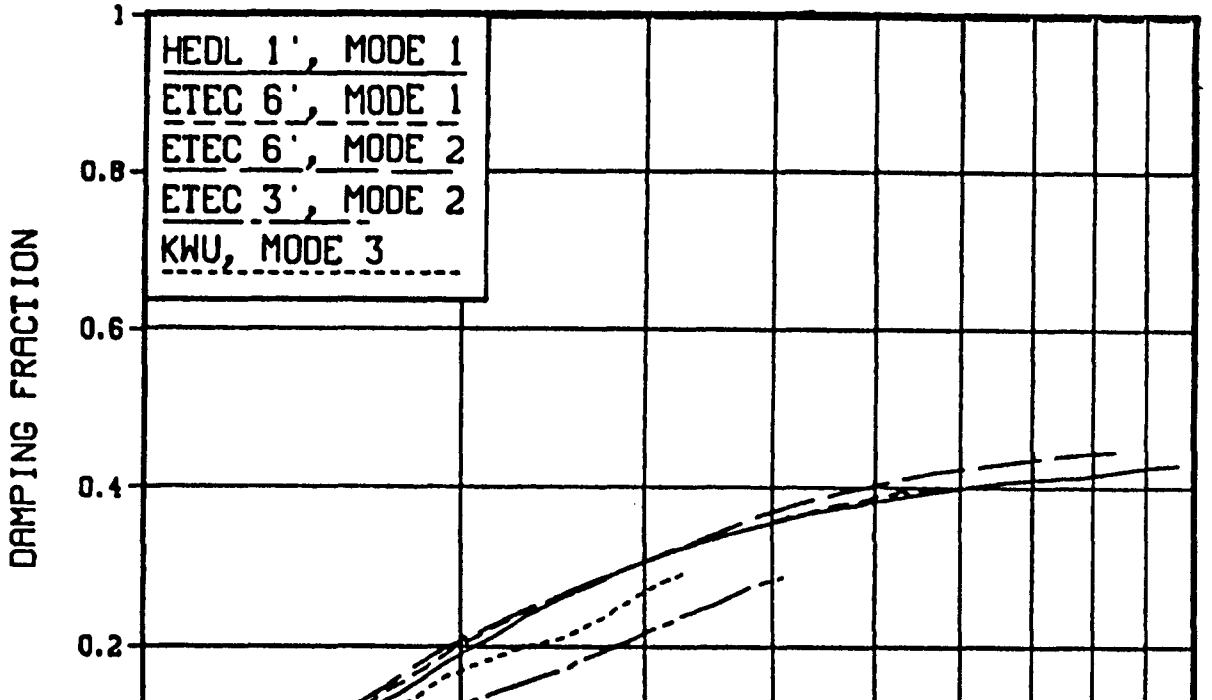

FIGURE 9-6. Quasistatic Effective Damping.

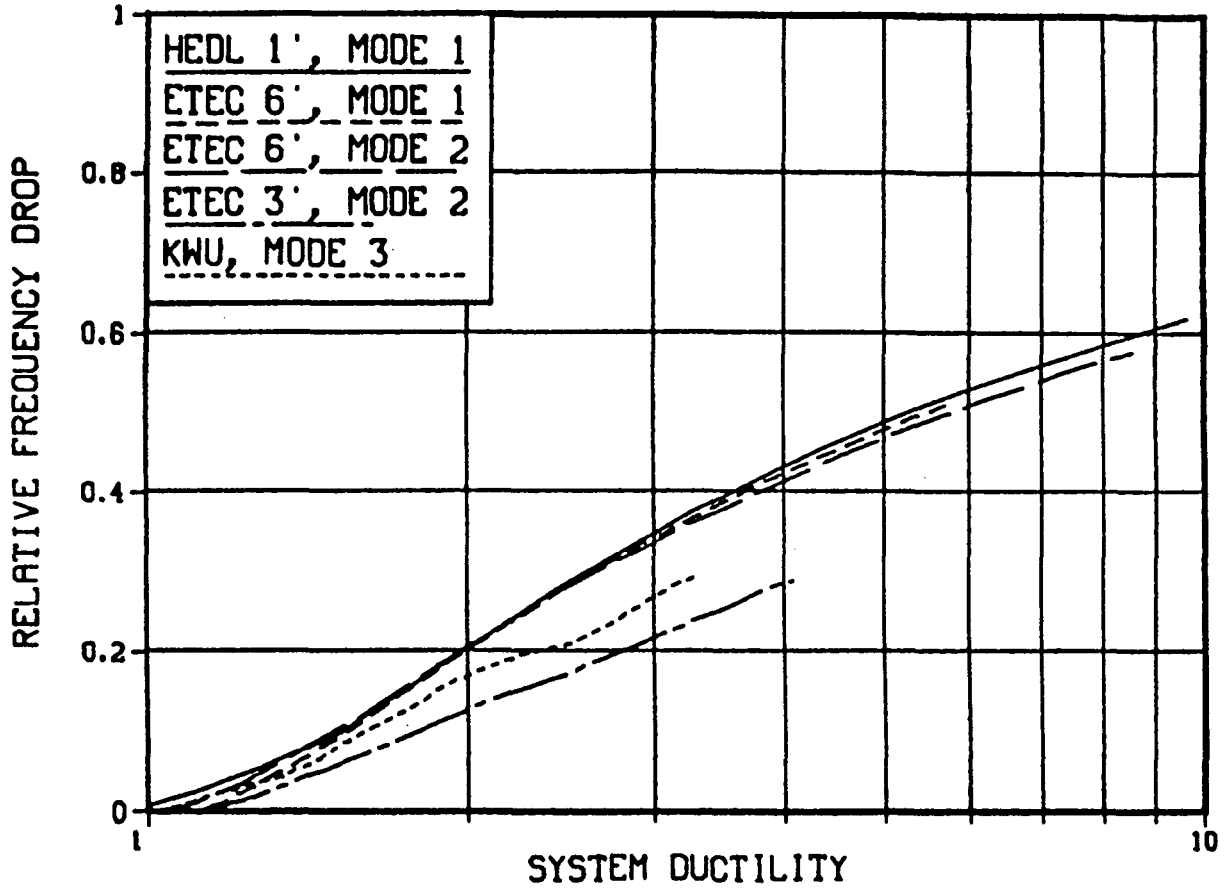

FIGURE 9-7. Quasistatic Frequency Shift.

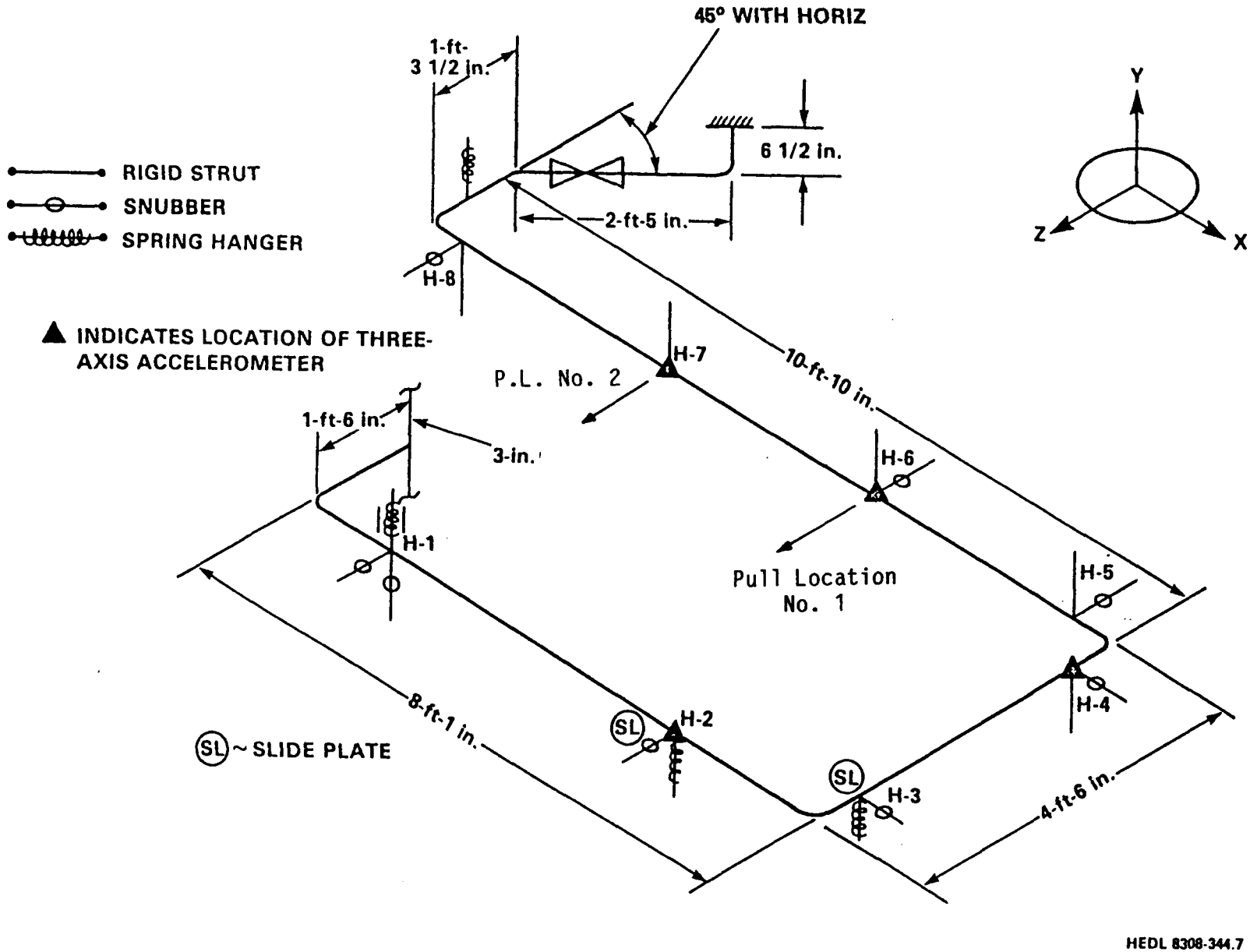

FIGURE 9-8. Insulated 1-inch Diameter Pipe System and Accelerometer Locations for Snapback Damping Tests.

NUREG/CR-5023
WHC-EP-0081

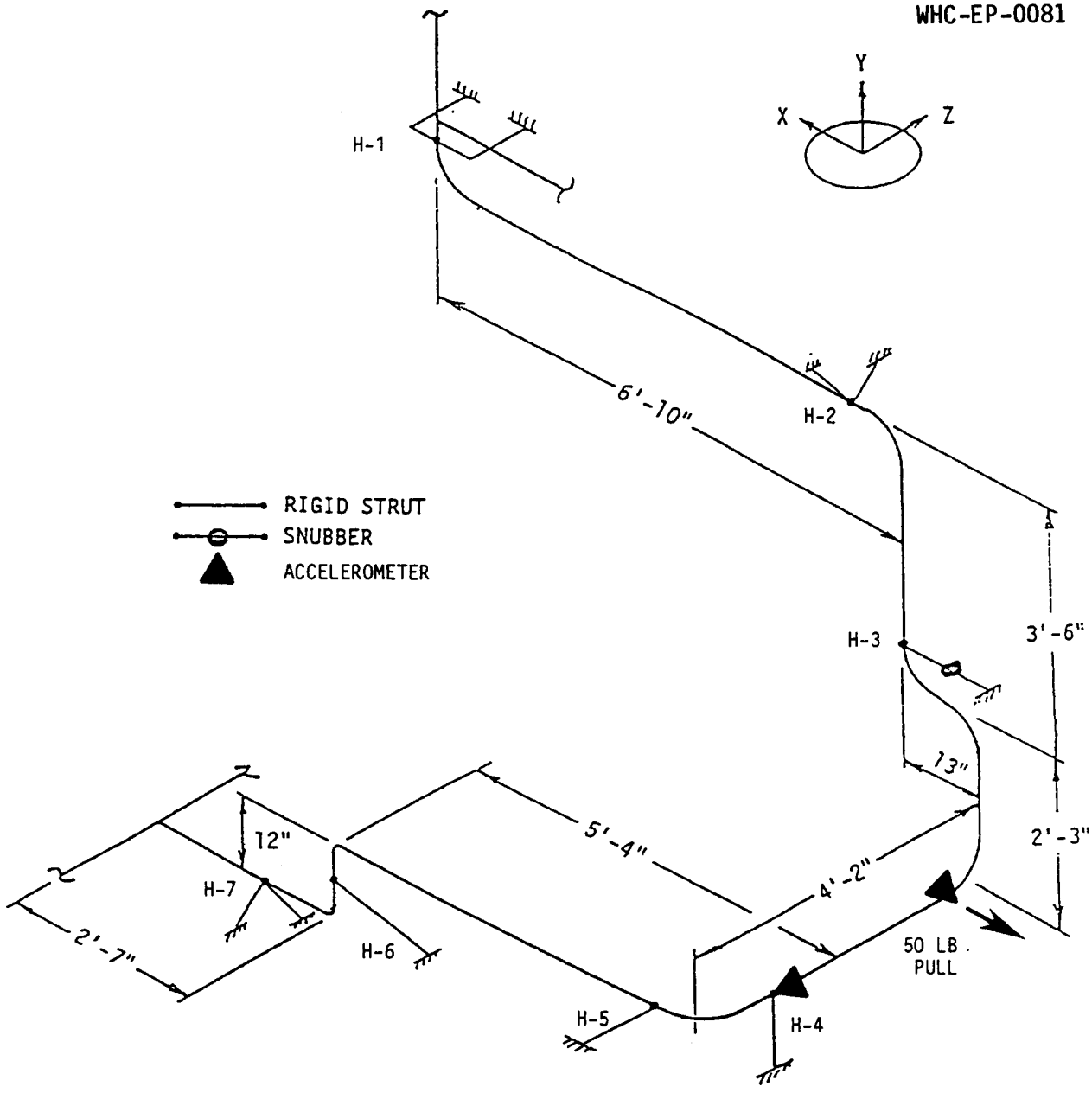

FIGURE 9-9. Snapback Test of 1-inch Diameter Pipe System with Snubber at H-3 and then with all Rigid Struts.

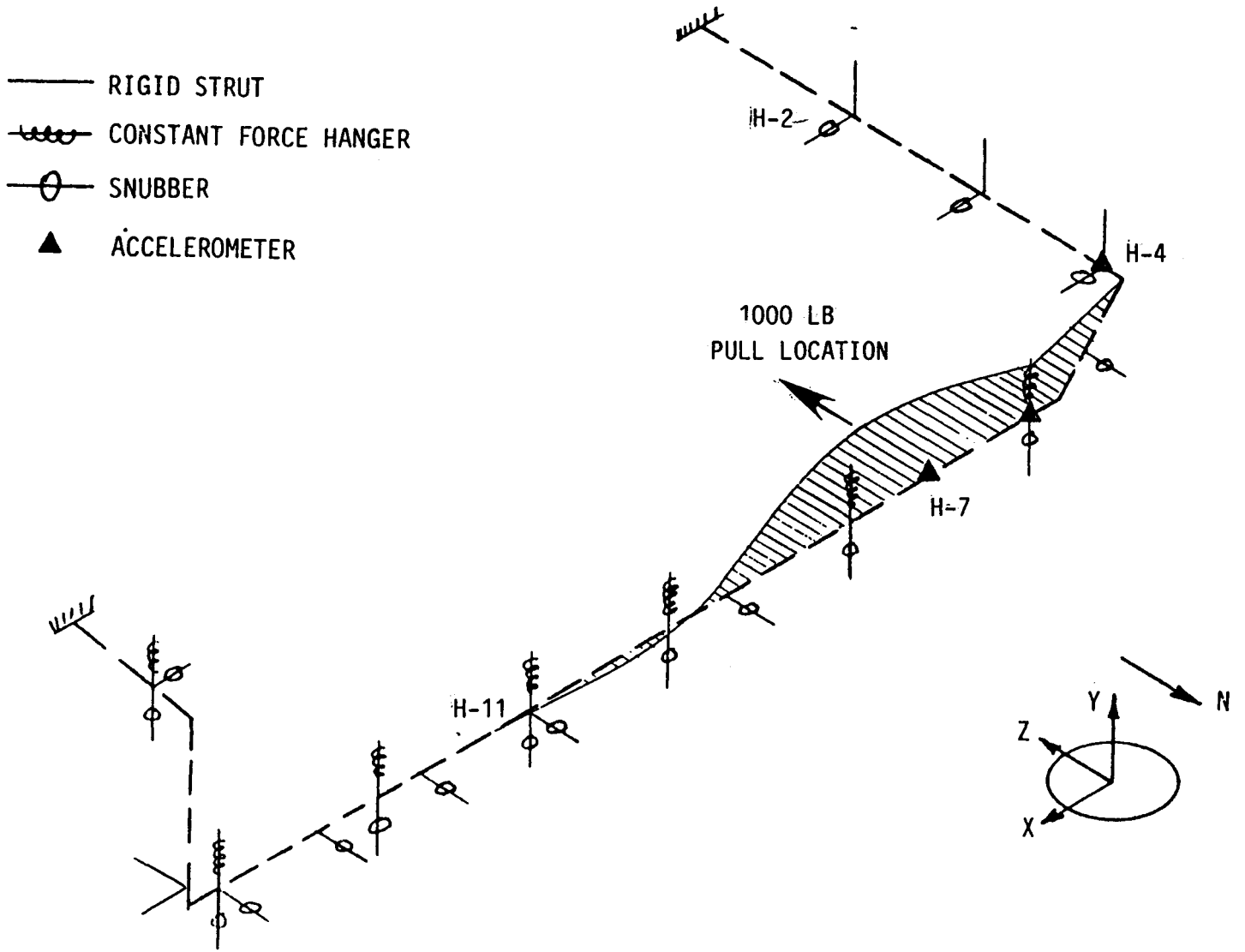

FIGURE 9-10. Piping Mode Shapes, Pull at H-7 for 16-inch Diameter Insulated Stainless Steel Piping System, First Mode, f - 5.0 H.

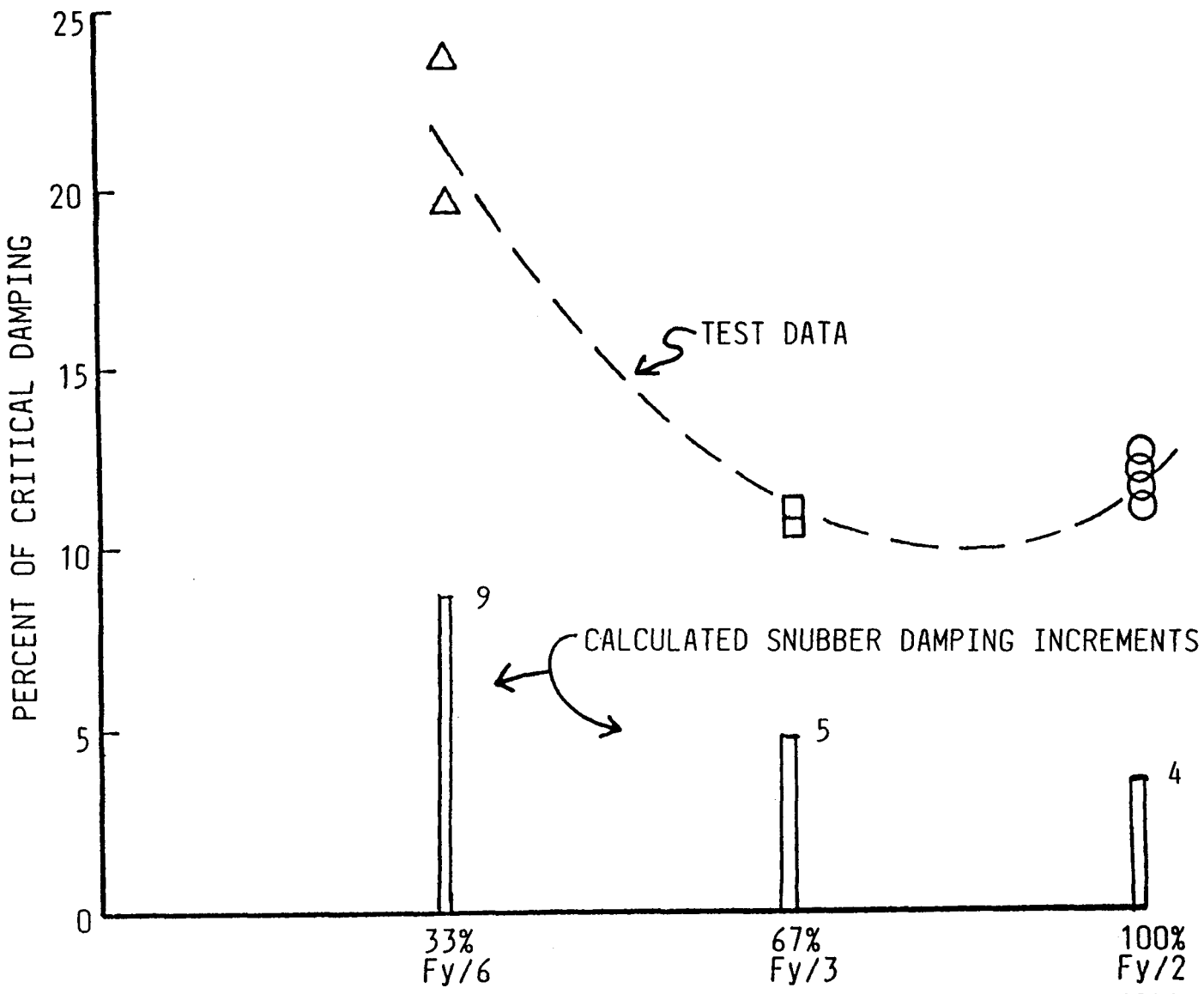

FIGURE 9-11. Effect of Load Level on Damping, Pull at H-7, Accelerometer H-7Z.

10.0 POST-TEST ANALYSIS METHODS IMPROVEMENTS

All the simplified pseudo-linear-elastic analyses performed prior to the tests gave response predictions that underestimated the test findings and the abilities of the piping systems to withstand the very high seismic loads without collapse. To better understand the reasons for the underpredictions, the methods were examined for conservatisms and inaccuracies. This resulted in the following observations.

10.1 USE OF DYNAMIC YIELD STRENGTH

The static values of yield strength, rather than dynamic values, were used in the pretest analyses. For the rate of dynamic loads applied, a dynamic increase factor of about 1.20, per Reference 42, is appropriate.

10.2 DYNAMIC SPECTRA LOADING FOR PROGRESSIVE HINGE METHOD

The static progressive hinge formation method involves application of static G loads separately in each of three global orthogonal directions and then combining the three responses. This process for loading in one direction does not very well simulate the dynamic inertia loads that can be in three directions simultaneously due to structural cross-coupling. An improved approach would be to apply a flat G load spectra with response-spectra analysis for each of the three global directions. This would permit the structural cross-coupling and model participation typical of dynamic analysis to be accounted for. Analyses of the four piping systems with the spectra approach produced the findings of Table 10-1 and Table 10-2.

As shown in Table 10-1, the progressive hinge dynamic load capacities of piping systems usually are greater than that predicted using the static analysis. However, note that the opposite is true for the KWU system. This system has significant cross-coupling of horizontal and vertical motion in the mode that governs the hinge formation. Moreover, the ETEC 3-inch diameter system analyses revealed different locations for the hinges. The dynamic analysis indicated a hinge at the location of the tee that actually ruptured in test. The static analysis did not indicate a hinge at the tee.

10.3 ITERATIVE QUASISTATIC SIMPLIFIED METHOD

The Newmark modified spectra, D/S ratio, and the progressive hinge methods all need a way of determining the appropriate system ductility or damping value that is consistent with the extent of inelastic deformation. Campbell et al. (Reference 10) provided an approximate method described in Section 3.2.1. The method uses the displacements obtained from a static inelastic response analysis to determine the system ductility index for a given

response level. Since the damping and system ductility index are nonlinear functions of response, the calculation of response of a given pipe system is thus a nonlinear process. Moreover, response and its associated dynamic magnification are also related to the shifts of model frequencies as the nonlinear stiffness changes with response level. Accordingly, it is desirable for predicting high-level response to account for both the energy loss (damping and ductility) and the frequency shifts as a function of response level. This has been done in quasistatic analyses of the four pipe system responses described in Section 9.3.

The quasistatic analysis used the same models as the transient analyses without gravity. Static analysis was achieved with very large time steps, usually 30 to 50 in number. Typically, two to three tries were required as the systems are load controlled. For each mode considered, a table (see Table 10-3) of frequency, damping, strain range and system ductility versus scale factor was prepared by postprocessing the NONPIPE output using formulas of Section 9.2. Simplified analysis for a given seismic excitation then proceed interactively as follows:

1. Assume a system ductility or scale factor.
2. Lookup frequency, damping and strain range. Add $\alpha\beta$damping.
3. Calculate displacement response δ at a typical node.
4. Revise the system ductility $\mu = \delta/\delta_y$, where δ_y is the modal displacement at yield. Go to 2.

The calculation of response for the given seismic excitation is based on the calculated linear response spectrum corresponding to the transient analysis time history. Steady response was used for harmonic excitation. Modes are combined by the CQC method (Reference 43) with seismic excitation and by combining phased signals with harmonic analysis.

Typical trends of strain versus excitation level are described in Figure 6-33 with the maximum strains incurred by the ETEC 6-in. system in transient and static analyses. The static loading is an increasing uniform inertial load in the direction of excitation. Each of the data markers for dynamic response in the plot represents the maximum strain incurred during a seismic time history. At low levels the transient/static response ratio is roughly the dynamic amplification with 5% damping. At higher levels, the static response increases suddenly while the transient response continues increasing at roughly the same rate. Transient hinges form in the straight and elbow sections at 5 g and 14 g, respectively. There is no significant change in response at these points. It is interesting to note how the elbow fails to maintain the larger transient response at higher levels. Linear response spectrum analysis shows the highest stress in the elbow.

A similar display for the WHC 1-inch system is given in Figure 10-2. Now a significant increase in maximum strain occurs after the formation of the first dynamic hinge at 0.6 g, but it is not as severe as the static case. The piping system had a relatively high (25% S_y) deadweight loading. Testing (Reference 6) showed an increase of permanent deformation from test to test which was induced by the deadweight loading. Transient analysis results agreed with these permanent deformations. Figure 10-3 shows the strain record at the point of maximum strain in the case of the 1.5 g base excitation. There is a shift in the average strain taking place in two cycles followed by steady cyclic response. This shift is largely responsible for the strain increase observed in Figure 10-2, and it reflects the test-to-test permanent deformations that are induced by deadweight loading. Still, this increase is not nearly as drastic in the static case. Note that the transient/static slope ratio at low excitation levels is 5:1, and roughly the opposite holds at the high excitations.

Magnifications for the four piping systems are shown in Figure 10-4. Values here are based on comparing the analysis displacement response of a characteristic point with the linear static response at the same maximum base acceleration. At low levels, e.g., 0.35 g in the WHC 1-inch system, the theoretical magnification value of five (corresponding to 10% damping) is almost achieved. At higher levels of excitation the magnification settles to values between one and two. The large magnification for the KWU system reflects limited plastic deformation because the transient analysis had only one short element exceeding the collapse moment.

Phase angles were obtained from transient analysis by comparing displacement response peaks with those of the base. Values are shown in Figure 8 alongside the WHC 1-inch and KWU magnifications. They relate to the magnifications in the way expected for linear response of compliant structures. The ETEC systems both involve seismic excitation. They do not show large magnifications at the lower load levels.

Generally, the magnifications based on simplified quasistatic analysis are lower than the transient values. The first two modes were included in each system except the KWU system which used modes three and five. Selection was based on the first two dominant modes in terms of producing strain. Had only one mode been chosen, results would not have changed much except for the ETEC 6-inch system. A single mode here would have produced about 30% less magnification.

Strain ranges obtained from analyses and tests are presented in Figure 10-5. The range is defined as the largest monotonic excursion of strain in the response record, except steady response values were used in the WHC 1-in. system. Each system includes a linear response spectrum point corresponding

to twice the 0.2% offset yield (about 3S). Test results are also shown. Overall, the four sources show the same general trend. There is no sudden increase in strain suggesting dynamic collapse. Relative to the linear response spectrum points there is a tendency for the nonlinear considerations to show greater strains once yielding becomes significant. The notable exception is the WHC 1-in. system which might be explained by the relatively large system ductility of Figure 9-5. Strain range in the WHC 1-in. system increases nearly proportionally with load level, and this is taking place in spite of the strongly decreasing magnification. This suggests that the plastic strain concentration effect (Reference 44) at a hinge is an important aspect in describing strain response in seismic excitation.

10.4 CONCLUSIONS

It is concluded that a dynamic increase factor on the material static yield strength and use of a dynamic spectra load in the progressive hinge method provide more accurate prediction methods. Analysis improvements, such as iterative quasistatic methods herein described, also provide improvements to methods for predicting inelastic strain response to high-level seismic excitation. Even with these improvements utilized, the simplified methods significantly underpredict (Table 10-4) the collapse capacities of the tested systems.

TABLE 10-1

COMPARISON OF STATIC AND DYNAMIC PROGRESSIVE HINGE PIPE SYSTEM LOAD CAPACITIES*

PIPE SYSTEM	STATIC ANALYSIS RESULTS	DYNAMIC SPECTRA ANALYSIS RESULTS
HEDL 1"	2.5 G's - 1st Hinge 2.7 G's - 2nd	2.8 - 1st 3.2 - 2nd
ETEC 6"	15.4 - 1st 16.2 - 2nd	19.1 - 1st 19.5 - 2nd
ETEC 3"	15.9 - 1st 16.4 - 2nd 19.5 - 3rd 20.4 - 4th 21.0 - 5th 21.2 - 6th	20.2 - 1st 21.8 - 2nd 22.7 - 3rd 22.8 - 4th
KWU 4/2"	13.3 - 1st 15.2 - 2nd	9.8 - 1st 11.2 - 2nd

* Both static and dynamic values based on static yield strengths. A dynamic increase factor of 1.2 could be applied to the above capacities per the discussion in Section 10.0.

TABLE 10-2

SUMMARY OF POST-TEST* ANALYTICAL PREDICTIONS AND TEST FINDINGS

ANALYTIC METHOD	HEDL 1-IN. DIA. PIPING	KWU 2-IN./4-IN. DIA. PIPING	ETEC 3-IN. DIA. PIPING	ETEC 6-IN. Dia. Piping
A. ASME CLASS 1, $3S_M$ LEVEL D, G'S	0.36 SINE	1.9 ZPA	1.4 ZPA	2.0 ZPA
B. ASME CLASS 2, $3S_H$, G'S	0.34	1.7	1.0	1.4
C. NEWMARK METHOD, G'S	1.9	5.8	12.2	12.0
D. DYNAMIC/STATIC MARGIN RATIO, G'S	1.9	5.4	12.0	11.7
E. PROGRESSIVE HINGE, SPECTRA LOAD, G'S				
() = DYN. MAGNIF. FACTOR	2.1 (1.8)	2.7 (5.0)	13.7 (2.0)	11.6 (2.0)
	3.8 (1.0)	13.4 (1.0)	27.4 (1.0)	23.1 (1.0)
F. PRA-TYPE FRAGILITY				
ZION METHOD, G'S	--	7.8	4.4	4.4
SSMRP METHOD, G'S	--	11.5	5.2	8.8
G. NONLINEAR INELASTIC DYNAMIC				
LOAD LEVEL, G'S	2.5	4.0 SINE	30.0	30.0
STRAIN RANGE, PERCENT	2.5	1.6	14.0	4.1
TEST FINDINGS				
A. MAX. BASE INPUT, G'S	2.8 SINE, 2 H_Z	4.0 SINE, 8.9 H_Z	30.0 ZPA	30.0 ZPA
	0.5 ZPA	5.5 ZPA	25.0 SINE, 6 H_Z	18.7 SINE, 5H_Z
B. NO FAILURES FOR ALL ZPA'S				
C. FAILURE MODE	RATCHETING-GROSS DEFORMATION	NONE	FATIGUE	RATCHET/FATIGUE OR DUCTILITY EXHAUSTION OR WALL THINNING AND DUCTILE OVERLOAD

*See Table 2-1 for Pre-Test Analytical Predictions.

NUREG/CR-5023
WHC-EP-0081

TABLE 10-3

TYPICAL LOAD-DEPENDENT DAMPING, FREQUENCY SHIFT, STRAIN RANGE AND SYSTEM DUCTILITY INDEX

```
ONE-SIDED QUASISTATIC MODAL PROCESSOR

ETEC 6 IN  MODE 1 OMP, STRAIN AT 10

YIELD STRAIN =  .1564E-02
MASS SCALE =  .2588E-02
LOAD STEPS =  35
STRAIN SCALE =  3.810
 1 FILES STRAIN COLUMNS =  2
LOAD SCALES =
 8.400      8.700      9.000      9.300      9.600
 9.700      9.800      9.900     10.00      10.10
10.20      10.30      10.40      10.50      10.60
10.80      11.00      11.20      11.40      11.60
11.80      12.00      12.20      12.40      12.60
12.80      13.00      13.20      13.40      13.60
13.80      14.00      14.20      14.40      14.60

YIELD -   FREQ =  4.902       M*D =  6.743       M*X*X =  16.33

STP  SCALE   DAMP    1 - F/FO  SYS-DUCT   EPS-RNG   M*X*X       FX          Q
 1   8.40  1.37E-14 -7.11E-15  1.07E+00  3.34E-03  2.12E+01  2.39E+03  1.00E+04
 2   8.70  1.98E-04  1.50E-04  1.09E+00  3.41E-03  2.27E+01  2.48E+03  1.08E+04
 3   9.00  1.74E-03  1.48E-03  1.11E+00  4.15E-03  2.45E+01  2.57E+03  1.16E+04
 4   9.30  7.96E-03  6.51E-03  1.15E+00  4.58E-03  2.72E+01  2.71E+03  1.29E+04
 5   9.60  1.52E-02  1.26E-02  1.18E+00  5.00E-03  3.02E+01  2.85E+03  1.42E+04
 6   9.70  1.86E-02  1.54E-02  1.19E+00  5.14E-03  3.15E+01  2.91E+03  1.48E+04
 7   9.80  2.22E-02  1.88E-02  1.21E+00  5.28E-03  3.28E+01  2.97E+03  1.54E+04
 8   9.90  2.50E-02  2.13E-02  1.22E+00  5.43E-03  3.41E+01  3.03E+03  1.60E+04
 9  10.00  2.88E-02  2.40E-02  1.24E+00  5.57E-03  3.54E+01  3.09E+03  1.65E+04
10  10.10  3.44E-02  2.96E-02  1.26E+00  8.13E-03  3.75E+01  3.18E+03  1.74E+04
11  10.20  3.87E-02  3.35E-02  1.27E+00  9.53E-03  3.92E+01  3.25E+03  1.81E+04
12  10.30  4.34E-02  3.78E-02  1.29E+00  1.88E-02  4.11E+01  3.32E+03  1.89E+04
13  10.40  5.22E-02  4.59E-02  1.32E+00  1.15E-02  4.42E+01  3.44E+03  2.02E+04
14  10.50  5.95E-02  5.24E-02  1.35E+00  1.25E-02  4.70E+01  3.55E+03  2.13E+04
15  10.60  6.69E-02  5.97E-02  1.38E+00  1.36E-02  5.02E+01  3.66E+03  2.25E+04
16  10.80  8.36E-02  7.58E-02  1.44E+00  1.55E-02  5.77E+01  3.92E+03  2.52E+04
17  11.00  1.00E-01  9.23E-02  1.51E+00  1.76E-02  6.64E+01  4.20E+03  2.83E+04
18  11.20  1.19E-01  1.11E-01  1.59E+00  1.93E-02  7.74E+01  4.52E+03  3.19E+04
19  11.40  1.46E-01  1.39E-01  1.70E+00  2.19E-02  9.53E+01  5.00E+03  3.73E+04
20  11.60  1.76E-01  1.71E-01  1.85E+00  2.47E-02  1.21E+02  5.61E+03  4.43E+04
21  11.80  2.01E-01  2.00E-01  1.99E+00  2.75E-02  1.50E+02  6.22E+03  5.14E+04
22  12.00  2.28E-01  2.32E-01  2.17E+00  2.99E-02  1.88E+02  6.94E+03  6.00E+04
23  12.20  2.58E-01  2.60E-01  2.35E+00  3.23E-02  2.33E+02  7.69E+03  6.89E+04
24  12.40  2.71E-01  2.88E-01  2.54E+00  3.51E-02  2.86E+02  8.48E+03  7.88E+04
25  12.60  2.87E-01  3.12E-01  2.73E+00  3.78E-02  3.44E+02  9.27E+03  8.86E+04
26  12.80  3.05E-01  3.37E-01  2.96E+00  4.01E-02  4.20E+02  1.02E+04  1.01E+05
27  13.00  3.19E-01  3.60E-01  3.18E+00  4.25E-02  5.03E+02  1.11E+04  1.12E+05
28  13.20  3.31E-01  3.88E-01  3.41E+00  4.49E-02  5.97E+02  1.21E+04  1.25E+05
29  13.40  3.41E-01  3.99E-01  3.64E+00  4.73E-02  6.99E+02  1.30E+04  1.38E+05
30  13.60  3.53E-01  4.18E-01  3.91E+00  5.00E-02  8.25E+02  1.42E+04  1.53E+05
31  13.80  3.65E-01  4.38E-01  4.22E+00  5.31E-02  9.82E+02  1.55E+04  1.71E+05
32  14.00  3.78E-01  4.59E-01  4.61E+00  5.61E-02  1.19E+03  1.71E+04  1.93E+05
33  14.20  3.87E-01  4.77E-01  4.97E+00  5.90E-02  1.41E+03  1.85E+04  2.14E+05
34  14.40  3.94E-01  4.94E-01  5.34E+00  6.18E-02  1.66E+03  2.01E+04  2.36E+05
35  14.60  4.02E-01  5.09E-01  5.72E+00  6.48E-02  1.92E+03  2.16E+04  2.58E+05
READY.
```

TABLE 10-4

HIGH-LEVEL PIPING RESPONSE AND FAILURE
RATIOS OF ANALYTIC CAPACITY TO TEST MAX. BASE INPUT ACCELERATION

	ASME CL. 1	PLASTIC SPECTRA	PROG. HINGE-STATIC	PROG. HINGE-DYN.	HINGES TO STATIC COLLAPSE	INELASTIC MAX STRAIN RANGE	TEST FAILURE MODE
HEDL 1" DIA.	0.13	0.68	1.15	1.36	2	2.5%	R-GD
KWU 2"-4"	0.34	1.04	6.3	3.3	2	1.6%	NONE
ETEC 3"	0.05	0.41	0.76	0.91	6	14.0%	F
ETEC 6"	0.07	0.40	0.65	0.77	2	4.0%	R-F or R-DE or R-DR

R-GD = RATCHET-GROSS DEFORMATION
F = FATIGUE
R-F = RATCHET-FATIGUE
R-DE = RATCHET-DUCTILITY EXHAUSTION
R-DR = RATCHET-DUCTILE RUPTURE

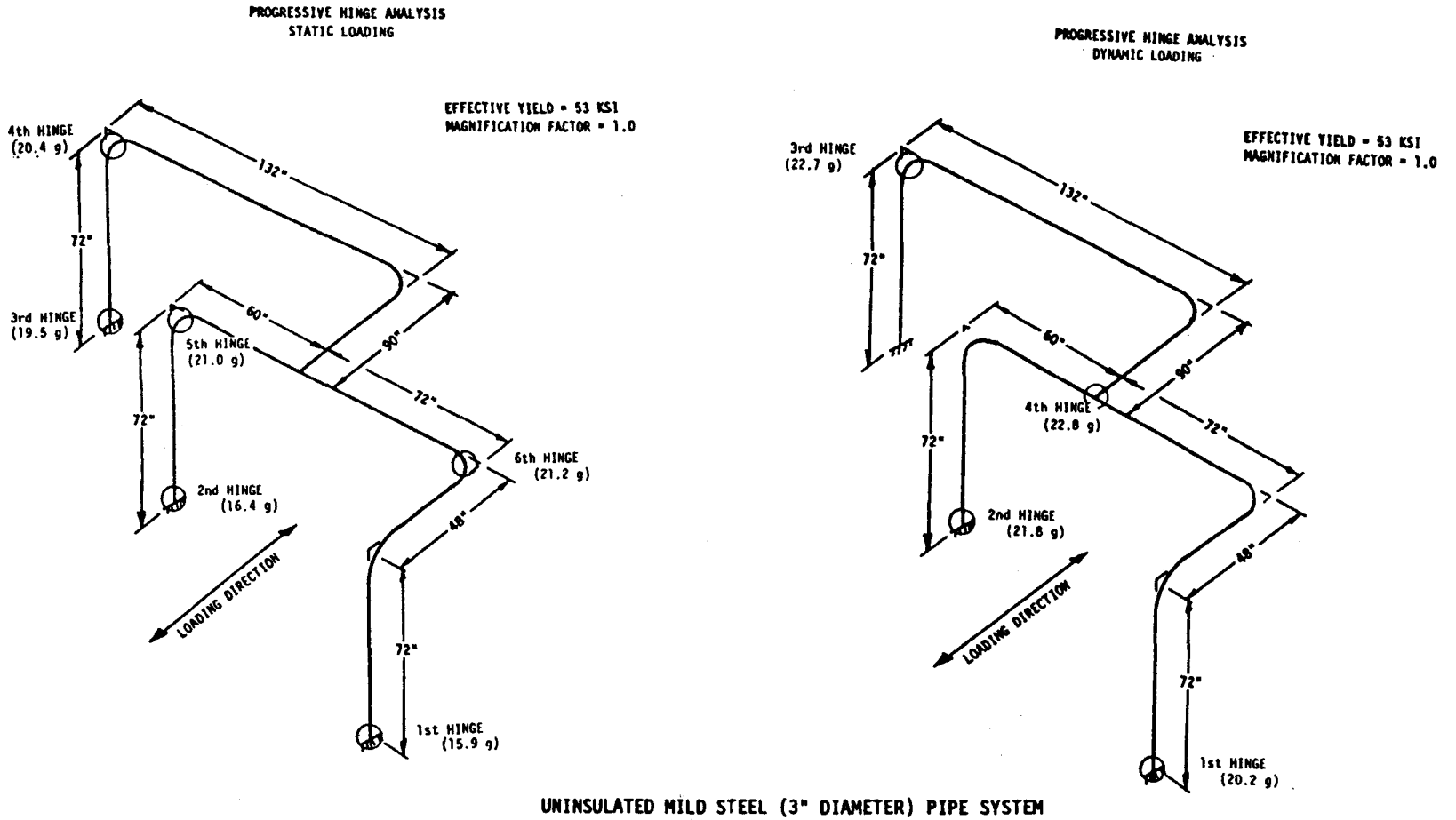

FIGURE 10-1. Comparison of Static and Flat Spectra Response Analyses for Progressive Hinge System Capacity Assessments.

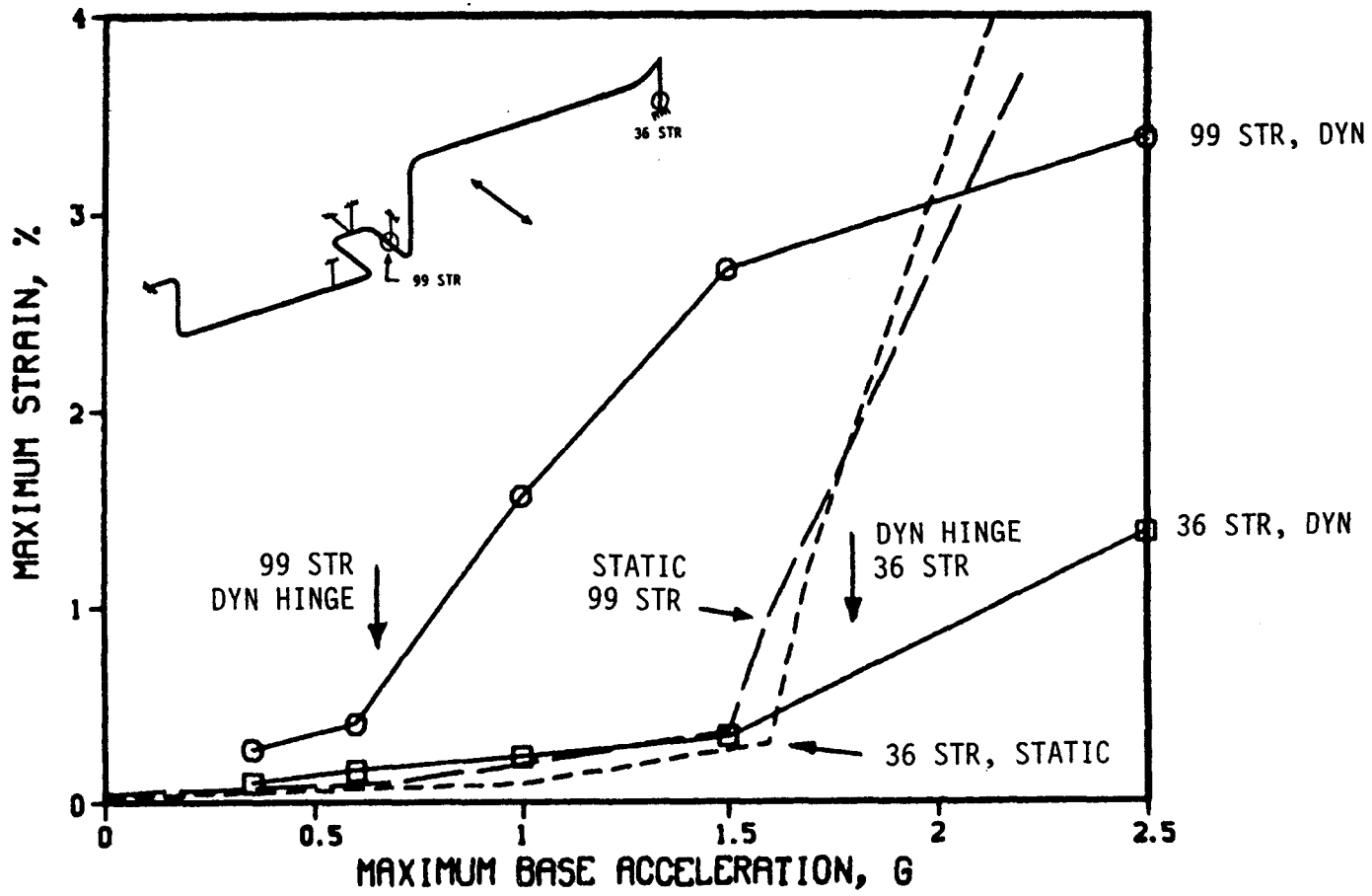

FIGURE 10-2. WHC 1-in. Transient-Static Strain Comparison.

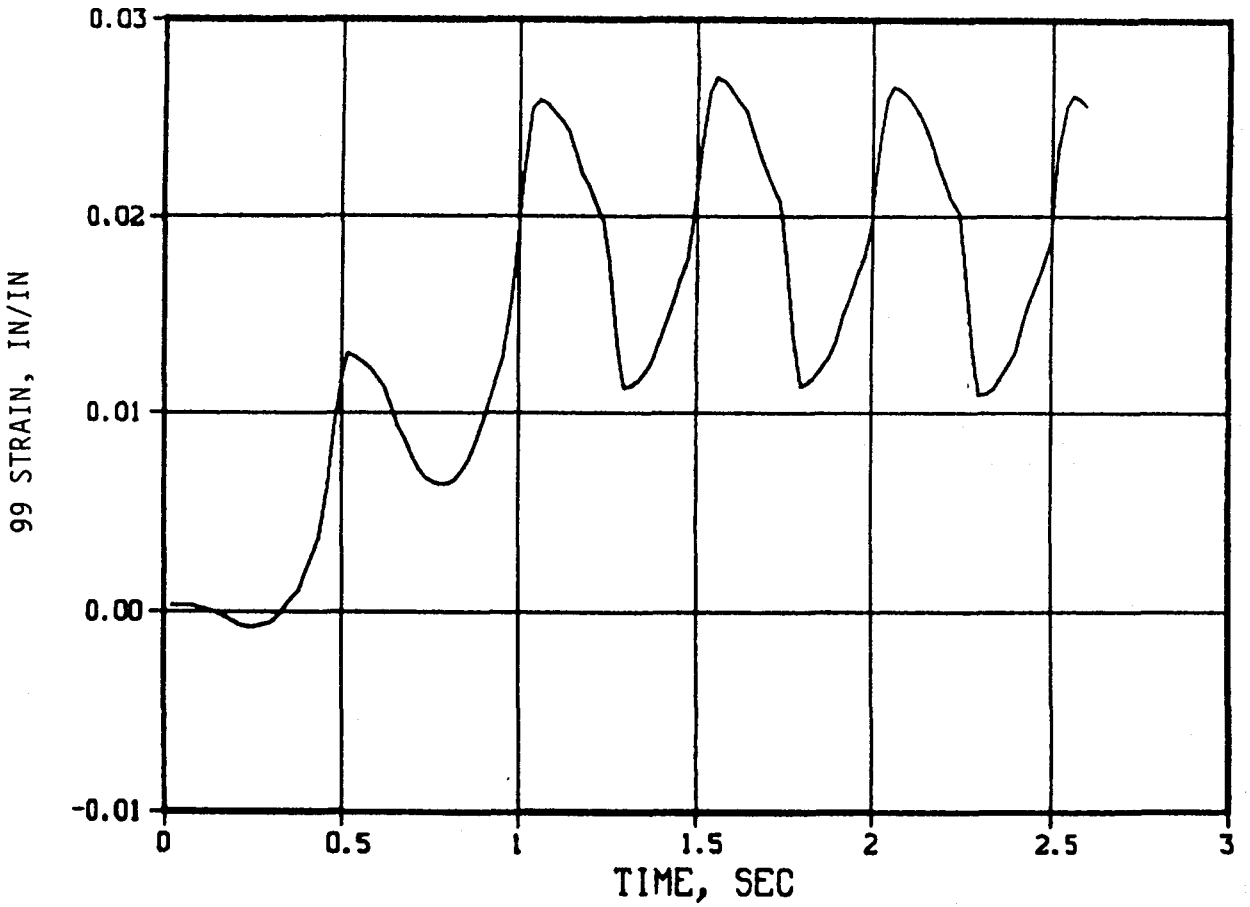

FIGURE 10-3. WHC 1-in. 1.5 g Maximum Strain Record.

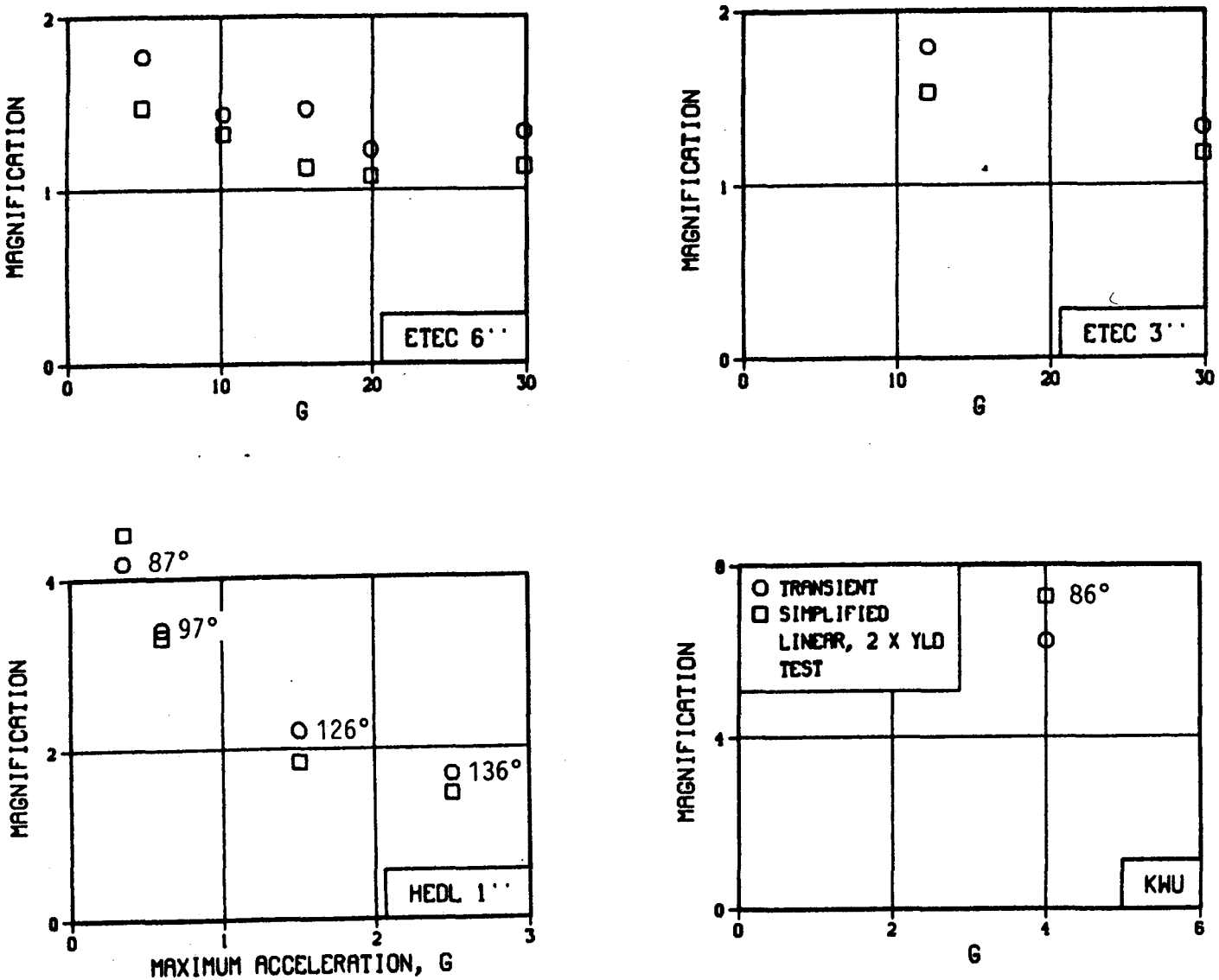

FIGURE 10-4. Magnifications.

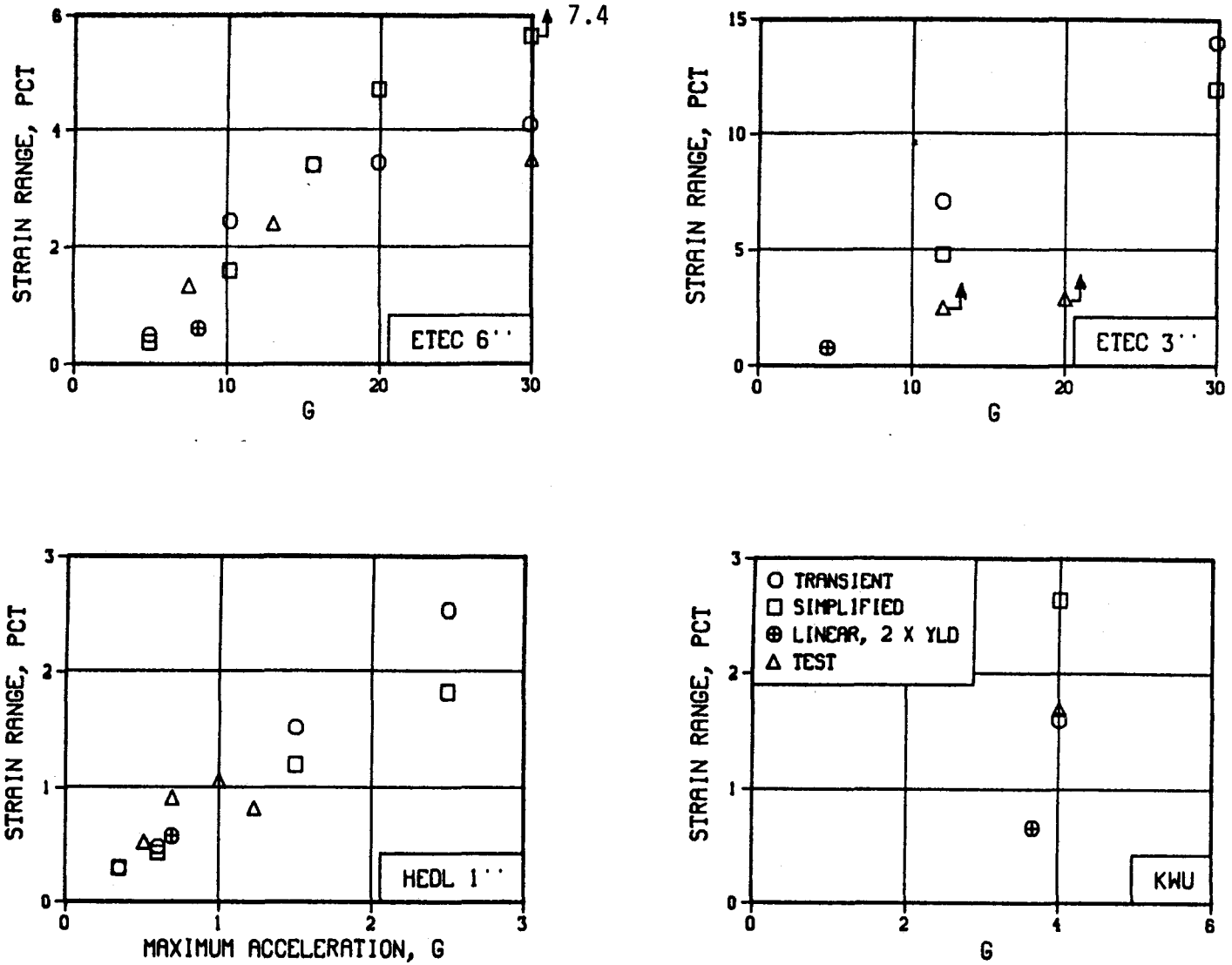

FIGURE 10-5. Strain Ranges.

11.0 CONCLUSIONS AND RECOMMENDATIONS

1. Pretest failure predictions of the NRC/ETEC seismic fragility demonstration test, using a number of pseudo-linear-elastic methods, all underestimated the ability of the pipe system to withstand very high seismic loads without collapse. The Newmark and D/S ratio methods indicated collapse at about 10 g's. The progressive hinge method gave collapse at 8 to 16 g's depending on use of a dynamic magnification factor of 2 or 1, respectively. The seismic PRA-type fragility average estimate was 4.4 and 8.8 g's for the Zion and SSMRP methods. The test actually withstood 30 g's without collapse.

2. Pretest inelastic transient dynamic analyses using the NONPIPE program correctly predicted no collapse load up to the limit of the analyses: 2.8 g's, 30 g's, 30 g's and 5.5 g's ZPA for the WHC one-inch diameter test system, ETEC six-inch diameter system, ETEC three-inch diameter system, and KWU four-inch/two-inch diameter systems, respectively. The analyses predicted a maximum strain range that correlated very well with strain gage data from these tests.

3. The reduction of dynamic magnification with increasing plastic response of the piping under high-level shaking is a major factor in limiting response well below current elastic response spectra predictions. Current ASME Class 1 and 2 methods, intended to protect against collapse, gave allowable shake levels of 2.0 and 1.4 g's, respectively. These are one order of magnitude below that withstood by the demonstration test.

4. The reduction of dynamic amplification with plastic response is due conceptually to two factors: (1) internal energy dissipation resulting in higher damping and ductility ratios, and (2) resonant detuning because of system increased flexibility. Simplified plastic reduced spectra techniques such as herein used with the Newmark and the D/S ratio methods do not account for the second factor. This omission could partially explain the underpredictions by the simplified methods.

5. All of the simplified elastic failure prediction methods require that a characteristic parameter be established whether it be system ductility ratio, D/S factor, or magnification factor. More work is needed to develop methods and procedures to quantify these parameters to account for inelastic response.

6. Ductility ratios for the piping system (the ratio of the maximum displacement to that at effective yield) are much less than material ductility ratios at tensile failure. The appropriate ratios for the WHC stainless steel pipe and the ETEC carbon steel pipe systems were

in the 5 to 10 range. Higher system ductility ratios will not raise the collapse capacities predicted by the pseudo-linear elastic methods up to the 50 to 100% higher levels withstood experimentally.

7. The progressive hinge method predicts the sequence of plastic hinge formation and permits a visualization of the system collapse mechanism. The method gives results judged more useful than the Newmark plastic spectra or the Dynamic/Static ratio methods provided proper magnification factors are selected and dynamic spectra loading are utilized.

8. Accounting for plastic hinge energy dissipation and modal frequency shifts due to system inelastic action improves the simplified methods. Simple methods and quasistatic system analysis techniques were herein described to account for those effects.

9. Failure of the ETEC six-inch diameter pipe system did occur after extensive multiple high level seismic and sinusoidal burst tests. The failure mode involved local cracking and section rupture near one pipe leg support, where ratcheting produced a bulge in the pipe diameter. Post-test analyses herein reported indicate that the failure was by ratchet-fatigue and/or ductility exhaustion, or a ratchet wall thinning and ductile tensile overload.

10. Correlations of test and calculated high-level piping dynamic response show good promise for simplified inelastic prediction methods. More tests and correlations are needed to establish a reasonable data base and to develop reliable methods for establishing safe design. This includes establishing procedures for conservatively accounting for the inelastic energy absorption and dynamic response of the piping system and establishing code acceptance criteria such as allowable ductility ratios, allowable strain criteria, or static allowable stress or load criteria. This work is consistent with the NRC Piping Review Committee recommendations (Reference 40).

11. It is recommended that additional pipe systems, that have or will be tested to high levels, be analyzed with simplified inelastic methods for response and failure mode assessments. In particular, the piping components tested under the EPRI/NRC piping and fitting program at GE (Reference 30) and the NRC pipe tests (Reference 41) at HDR and Todatsu (NUPEC) should be used to develop the needed design methods and code limits.

12.0 REFERENCES

1. K. Blakely, P. Ibanez, and S. Griffith, Dynamic Behavior of Piping and Supports at High-Load Levels--Experimental Study of a Scaled System, ASME Paper, 82-WA/PVP-4, 1982.

2. L. K. Severud, D. A. Barta, and M. J. Anderson, "Small Bore Piping Seismic Test Findings," Special Applications in Piping Dynamic Analysis, ASME PVP, Vol. 67, 1982.

3. A. T. Onesto et al., "Six-Inch Diameter Pipe Seismic Fragility Test," Proceedings of the 14th Water Reactor Safety Information Meeting, Washington, D.C., December 1986.

4. G. M. Hulbert, G. A. Schott, and C. F. Heberling, II, "Experimental Damping Results for a Medium Diameter LMFBR Pipe System," ASME PVP, Vol. 86, June 1984, pp. 109-117.

5. G. E. Howard, W. B. Walton, and B. A. Johnson, "Laboratory Studies: Dynamic Response of Prototypical Piping Systems," Transactions of the 8th International Conference on Structural Mechanics in Reactor Technology, Brussels, Belgium, Paper K 15/2, Vol. K(b), 1985.

6. M. R. Lindquist, M. J. Anderson, L. K. Severud, and E. O. Weiner, "High- Level Dynamic Testing and Analytical Correlations for a Small Bore Piping System," Seismic Engineering for Piping Systems, Tanks, and Power Plant Equipment, ASME PVP, Vol. 108, 1986.

7. Section III of the ASME Boiler and Pressure Vessel Code, 1983 Edition.

8. E. Haas et al., "Experimental and Analytical Investigation of the Dynamic Response of a Branched Piping System Due to Elasto-Plastic Behavior," Transactions of the 8th SMIRT, Paper K 15/3, Brussels, Belgium, August 1985.

9. N. M. Newmark, "A Response Spectrum Approach for Inelastic Seismic Design of Nuclear Reactor Facilities," Transactions of the Third International Conference on Structural Mechanics in Reactor Technology, London, England, Paper K, 5/1, Vol. 4, Part K, 1975.

REFERENCES (CONT'D)

10. R. D. Campbell, R. P. Kennedy, and R. D. Thrasher, Inelastic Response of Piping System Subjected to In-Structure Seismic Excitation, ASME Paper 83-PVP-50.

11. K. Jaquay, "A Simplified Limit Analysis Approach for Seismic Design of Ductile Piping System," Presentation at the ASME Winter Annual Meeting, New Orleans, LA, December 9-14, 1984.

12. "NONPIPE, A Computer Program for Nonlinear Analysis of Piping Systems- User Information Manual," Engineering Decision Analysis Co., Inc., Palo Alto, CA, September 30, 1983.

13. R. P. Kennedy and M. K. Ravindra, "Seismic Fragilities for Nuclear Power Plant Risk Studies," Nuclear Engineering and Design, Volume 79 (1984) No. 1, May 1984.

14. Seismic Safety Margins Research Program Phase I Final Report, U.S. Nuclear Regulatory Commission, NUREG CR-2015.

15. PIPESD and PIPESD/HEAT Pipe Static, Dynamic and Thermal Transient Analysis System-User Information Manual, 84000100, Control Data Corporation, Minneapolis, MN, 1982.

16. Combining Modal Responses and Spatial Components in Seismic Response Analysis, U.S. Nuclear Regulatory Commission Regulatory Guide 1.92.

17. Structural Analyses and Design of Nuclear Plant Facilities, ASCE Manual on Engineering Practice - No. 58, American Society of Civil Engineers, New York, NY, 1980.

18. ASME Boiler and Pressure Vessel Code, Section III, Division 1, Sub-Section NB, American Society of Mechanical Engineers, 1983 Edition.

19. C. W. Lin and G. J. Bohm, "Building and Equipment Seismic Response for PWR Plants," American Society of Mechanical Engineers Publication 76-WA/PVP-14, 1976.

20. M. Radomski and D. J. White, "Some Theoretical Considerations Relating to Strain Concentration in Elastic-Plastic Bending of Beams," Journal of Strain Analysis, 3 No. 4, 1968.

21. Letter, A. T. Onesto to M. J. Anderson, "Revised Seismic Input for NRC Demonstration Pipe Test Program," Rockwell International Correspondence 85ETEC-DRF-3162, September 10, 1985.

REFERENCES (CONT'D)

22. S. E. Moore and E. C. Rodabaugh, Background for the ASME Nuclear Code Simplified Method for Bounding Primary Loads in Piping Systems, American Society of Mechanical Engineers Paper PVP, Vol. 50, June 1981.

23. N. E. Dowling, "Fatigue Life Prediction for Complex Load Versus Time Histories," Pressure Vessels and Piping: Design Technology, 1982, A Decade of Progress, American Society of Mechanical Engineers, New York, NY, p. 487.

24. W. L. Greenstreet, "Experimental Study of Plastic Responses of Pipe Elbows," ORNL/NUREG-24, Oak Ridge National Laboratory, Oak Ridge, TN, February 1978.

25. L. H. Sobel, "The Southwell Method for Predicting Buckling Loads for Elbows," WARD-SD-94000-6, W ARD, Madison, PA, 1980.

26. Criteria of the ASME Boiler and Pressure Vessel Code for Design by Analysis in Sections III and VIII, Division 2, American Society of Mechanical Engineers, New York, NY, p. 16, Figure 9, 1969.

27. J. F. Harvey, Pressure Vessel Design, Van Nostrand Nuclear Science Series, New York, NY, pp. 194 and 195, 1963.

28. H. G. Edmunds and F. J. Beer, "Notes on Incremental Collapse in Pressure Vessels," Journal of Mechanical Engineers Science, Vol. 3, No. 3, 1961.

29. H. Ohtsubo and O. Watanabe, "Flexibility and Stress Failures of Pipe Bends - An Analysis by the Finite Ring Method," American Society of Mechanical Engineers Paper 76-PVP-40.

30. W. F. English, Piping and Fitting Dynamic Reliability Program First Semi-Annual Progress Report, May - October 1985, General Electric NEDC-31272, EPRI Contract RP-1543-15, November 1985.

31. K. R. Jaquay, J. E. Larson, and H. T. Tang, "A Simplified Method for Inelastic Piping Systems Seismic Response Prediction," presented at EPRI/NRC Joint Symposium on Current Issues Related to Nuclear Power Plant Structures, Equipment, and Piping, at North Carolina State University, December 10-12, 1986, Raleigh, NC.

REFERENCES (CONT'D)

32. L. K. Severud et al., "Nonlinear Piping Damping and Response Predictions," Proceedings of the 14th Water Reactor Safety Information Meeting, U.S. Nuclear Regulatory Commission, Washington, D.C., December 1986.

33. D. J. Guzy, "Piping and Fitting Dynamic Reliability Program," Proceedings of the 14th Water Reactor Safety Information Meeting, Washington, D.C., December 1986.

34. M. J. Anderson et al., "Analytical Methods and Experimental Correlations for Piping High Level Inelastic Seismic Response," presented at the American Society of Mechanical Engineers 5th National Congress on Pressure Vessels and Piping, San Diego, CA, June 1987.

35. E. O. Weiner, "Dynamic Magnification of Piping Systems with Inelastic Behavior," presented at the American Society of Mechanical Engineers 5th National Congress on Pressure Vessels and Piping, San Diego, CA, June 1987.

36. K. A. Peters and K. A. Busch, "Strain Estimation for Low Cycle Dynamic Loads," Res Mechanica, 19 (1986) 343-363, Elsevier Applied Science Publishers Ltd., England.

37. E. O. Weiner, K. A. Peters, and K. A. Busch, "Comparison of a Quasistatic Seismic Strain Range Method with Test and Detailed Transient Analysis," presented at the American Society of Mechanical Engineers 5th National Congress on Pressure Vessels and Piping, San Diego, CA, June 1987.

38. A. H. Hadjian, "A Re-Evaluation of Equivalent Linear Models for Simple Yielding Systems, Earthquake Engineering and Structural Dynamics," Vol. 10, 759-767 (1982).

39. G. J. Bohm, S. W. Tagart, Jr., and J. Wallach, "The ASME Code Design Needs for Damping in Piping Systems," Trans. of 8th SMIRT Conference, Brussels, Belgium, August 19-23, 1985, paper K 18/1.

40. Report of the U.S. Nuclear Regulatory Commission Piping Review Committee, U.S. NUREG-1061, Vol. 5, 1985.

41. Seismic Safety Research Program Plan, U.S. Nuclear Regulatory Commission NUREG-1147, pp. F-8 and F-12, 1985.

REFERENCES (CONT'D)

42. Structural Analysis and Design of Nuclear Plant Facilities, ASCE-Manuals and Reports on Engineering Practice - No. 58, American Society of Civil Engineers, New York, NY, pp. 314-317, 1980.

43. E. L. Wilson et al., "A Replacement for the SRSS Method in Seismic Analysis," Earthquake Engineering and Structural Dynamics, Univ. Calif., Berkeley, Vol. 9, n2, March 1981, p. 1887.

44. M. Radomski and D. J. White, "Some Theoretical Considerations Relating to Strain Concentration in Elastic-Plastic Bending of Beams," Journal of Strain Analysis, Vol. 3, n4, 1968.

ONSITE DISTRIBUTION

No. of Copies	Addressee	Mail Stop
24	Westinghouse Hanford Company	
	M. J. Anderson	L2-55
	M. R. Lindquist	L2-55
	W. J. McShane	L2-50
	K. V. Scott	HO-07
	L. K. Severud (13)	L2-57
	S. E. Wagner	L2-55
	E. O. Weiner	L2-57
	Central Files (2)	L8-04
	Documentation (2)	L8-15
	Microfilm Services	L8-15